NASA/TM–2019-220291

CASPEr-1, Part 6: Uncertainty Quantification, Factor Effects, and Outlier Analysis for an On-board Airplane Trajectory Prediction Function

Wilfredo Torres-Pomales
Langley Research Center, Hampton, Virginia

July 2019

NASA STI Program . . . in Profile

Since its founding, NASA has been dedicated to the advancement of aeronautics and space science. The NASA scientific and technical information (STI) program plays a key part in helping NASA maintain this important role.

The NASA STI program operates under the auspices of the Agency Chief Information Officer. It collects, organizes, provides for archiving, and disseminates NASA's STI. The NASA STI program provides access to the NTRS Registered and its public interface, the NASA Technical Reports Server, thus providing one of the largest collections of aeronautical and space science STI in the world. Results are published in both non-NASA channels and by NASA in the NASA STI Report Series, which includes the following report types:

- TECHNICAL PUBLICATION. Reports of completed research or a major significant phase of research that present the results of NASA Programs and include extensive data or theoretical analysis. Includes compilations of significant scientific and technical data and information deemed to be of continuing reference value. NASA counter-part of peer-reviewed formal professional papers but has less stringent limitations on manuscript length and extent of graphic presentations.

- TECHNICAL MEMORANDUM. Scientific and technical findings that are preliminary or of specialized interest, e.g., quick release reports, working papers, and bibliographies that contain minimal annotation. Does not contain extensive analysis.

- CONTRACTOR REPORT. Scientific and technical findings by NASA-sponsored contractors and grantees.

- CONFERENCE PUBLICATION. Collected papers from scientific and technical conferences, symposia, seminars, or other meetings sponsored or co-sponsored by NASA.

- SPECIAL PUBLICATION. Scientific, technical, or historical information from NASA programs, projects, and missions, often concerned with subjects having substantial public interest.

- TECHNICAL TRANSLATION. English-language translations of foreign scientific and technical material pertinent to NASA's mission.

Specialized services also include organizing and publishing research results, distributing specialized research announcements and feeds, providing information desk and personal search support, and enabling data exchange services.

For more information about the NASA STI program, see the following:

- Access the NASA STI program home page at http://www.sti.nasa.gov

- E-mail your question to help@sti.nasa.gov

- Phone the NASA STI Information Desk at 757-864-9658

- Write to:
  NASA STI Information Desk
  Mail Stop 148
  NASA Langley Research Center
  Hampton, VA 23681-2199

NASA/TM–2019-220291

CASPEr-1, Part 6: Uncertainty Quantification, Factor Effects, and Outlier Analysis for an On-board Airplane Trajectory Prediction Function

Wilfredo Torres-Pomales
Langley Research Center, Hampton, Virginia

National Aeronautics and
Space Administration

Langley Research Center
Hampton, Virginia 23681-2199

July 2019

Acknowledgments

The work presented in this report was supported by the Technologies for Airplane State Awareness (TASA) Project under the Airspace Operations and Safety Program (AOSP) of the Aeronautics Research Mission Directorate (ARMD). I would like to express my gratitude to Dr. Steve Young, who posed the challenge that motivated this work and has continued to support it with technical guidance and funding. Michael M. Madden and James R. Barnes were involved in the initial planning of CASPEr-1 and provided valuable guidance and information about the prediction functions, terminal area procedures, cockpit avionics, and the simulation infrastructure available to implement the test plan. Paul C. Sugden was in charge of implementing the test plan; his comments, questions, and suggestions were critical in refining the test plan and ensuring a successful implementation. Laura J. Smith and Yamira Santiago-Espada have contributed to the planning, data analysis, and the development of an assessment approach for airplane state and automation mode prediction functions.

Available from:

NASA STI Program / Mail Stop 148
NASA Langley Research Center
Hampton, VA 23681-2199
Fax: 757-864-6500

Abstract

This report presents data analysis results for a simulation-based approach named CASPEr (Characterization of Airplane State Prediction Error) to characterize the performance of onboard energy state and automation mode prediction functions for terminal area arrival and approach phases of flight over a wide range of conditions. In particular, the results include quantification of energy state (i.e., altitude and airspeed) prediction performance, models for prediction performance as a function of initial energy state (i.e., initial altitude, airspeed, and weight) and weather factors, and analysis of outlier prediction performance. Wind speed, wind direction, and wind gradient were found to be major factors in energy state prediction performance. Initial energy and gust intensity were also significant factors in airspeed prediction performance. Furthermore, the results suggest that errors in automation mode prediction may be a major contributor to outlier prediction performance.

Table of Contents

Acronyms and Abbreviations

4D	Four Dimensions
absMax	Maximum Absolute Value (same as maxAbs)
AFS	Auto-Flight System
AIME	Automation and Information Management Experiment
AP	Auto-Pilot
AT	Auto-Throttle
ATC	Air Traffic Control
CAS	Calibrated Airspeed
CASPEr	Characterization of Airplane State Prediction Error
CAST	Commercial Aviation Safety Team
CDU	Control Display Unit
DOE	Design Of Experiments
EICAS	Engine Indicating and Crew Alerting System
FAA	Federal Aviation Administration
FAF	Final Approach Fix
FMC	Flight Management Computer
FMS	Flight Management System
HITL	Human In The Loop
IAF	Initial Approach Fix
IAP	Instrument Approach Procedure
IAS	Indicated Airspeed
IC	Initial Conditions
IQR	Inter-Quartile Range
KMEM	Memphis International Airport
Kt	Knots (also kt)
LOC-I	Loss Of Control In-flight
maxAbs	Maximum Absolute Value
MCP	Mode Control Panel
MHP/PAE	Multiple Hypothesis Prediction function with Predictive Alerting
ND	Navigation Display
RMS	Root Mean Square
RMSE	Root-Mean-Square Error
RNAV	Area Navigation
RW	Runway (same as RWY)
RWY	Runway
SE	Safety Enhancement
STAR	Standard Terminal Arrival Route
TAS	True Airspeed
TFMS	Tactical Flight Management System
TOD	Top Of Descent
TP	Trajectory Prediction
TPS	Trajectory Prediction System
TRL	Technology Readiness Level
UQ	Uncertainty Quantification
VSD	Vertical Situation Display

1. Background

In 2010 the Commercial Aviation Safety Team (CAST) sponsored a study to analyze a set of loss of control in flight (LOC-I) accidents and incidents involving commercial transport airplanes in which the flight crew lost awareness of the airplane's state (i.e., attitude and energy) [1] [2]. This study identified recurring themes in the analyzed LOC-I events and suggested a number of wide ranging intervention strategies to mitigate the risks associated with the identified problems. Among the identified interventions were changes to current and future aircraft designs in areas such as flight envelope protection, improved alerting, automation design, and energy state management display and prediction systems. Subsequent analysis and assessment activities by CAST yielded a set of specific safety enhancement (SE) recommendations and detailed implementation plans [3] [4]. The SE recommendations included research and development (R&D) in technologies that address open issues in areas such as alerting, distraction, automation confusion, and system knowledge.

Motivated by safety recommendations from the Commercial Aviation Safety Team (CAST), NASA is developing onboard technologies for commercial transport airplanes as safety interventions to reduce the risk of loss of control in flight (LOC-I) events. The Automation and Information Management Experiment (AIME) is a series of R&D experiments intended to raise the technology readiness level (TRL) for selected new technologies, discover design characteristics requiring refinement, and assess their usability [5]. The technologies being evaluated include, among others, a Trajectory Prediction function (TP) [6] [7] and a Multiple Hypothesis Prediction function with Predictive Alerting (MHP/PAE) [8]. These predictive technologies are intended to enhance the situational awareness of the flight crew, in particular awareness of the airplane energy state and automation mode. These technologies provide information to the flight crew on the cockpit Navigation Display (ND), the Vertical Situation Display (VSD), the Engine Indicating and Crew Alerting System (EICAS), and a Synoptics display.

2. CASPEr-1

Considering that these state prediction and alerting technologies are currently at low to medium readiness level, the immediate focus should be on assessing the performance and integrity of the predictive functions over a wide range of conditions. Thus, the near-term problem of interest is the evaluation of performance for selected operational scenarios.

A simulation-based approach, called Characterization of Airplane State Prediction Error (CASPEr), was defined to evaluate the performance of the predictive functions. Figure 1 is a high-level graphic of

the concept. The approach leverages the high-fidelity simulation infrastructure developed for the AIME experiments, but it uses a software model of pilot behavior rather than a real pilot, thus eliminating some of the limitations and cost of human-in-the-lop (HITL) experiments. However, CASPEr is intended to complement rather than supplant HITL experiments as the Pilot Software Model cannot fully capture the complexity of real pilot behavior. CASPEr enables high observability and controllability of the test conditions, flexibility to configure and evolve the simulation capability as needed, and the possibility of faster-than-real-time simulations, which enables the collection of large amounts of performance data.

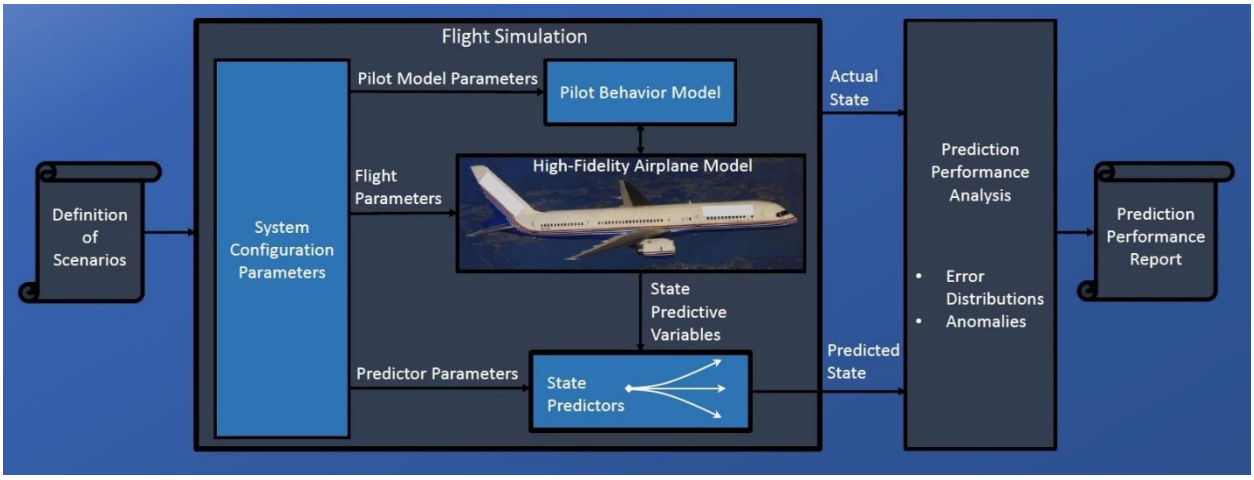

Figure 1: High-Level Graphic of CASPEr

CASPEr-1 is the first application of the CASPEr approach for performance evaluation of the predictive technologies with fully automated high-fidelity flight simulations. The test plan is given in Appendix A. The goal of CASPEr-1 is an initial performance evaluation of the predictive functions operating under different conditions. Only the TP airplane state prediction function was tested. The PAE function may be tested in future simulation experiments. All the flight operations were in the Memphis International Airport terminal airspace (code KMEM) flying published arrival routes (Standard Terminal Arrival Route, STAR) and instrument approaches (IAP) to selected runways. Airport information and instrument flight procedures for KMEM are publically available from the FAA [9].

Figure 2 is a breakdown of the test plan for CASPEr-1. The test was designed to enable observation and measurement of the effect of flight operation factors on the performance of the prediction functions. The test was structured into six parts, each consisting of variations of one or more factors relative to the conditions of a reference flight designated as the baseline. The chosen baseline flight was a descent on BLUZZ to runway 36C following the published trajectory restrictions for altitude and speed along the route, with normal initial airplane altitude, speed and weight, no wind, and with lateral and vertical navigation and speed controlled by the FMC. The procedure plates for BLUZZ and the approach to runway 36C are given in Section 4. All the flights in CASPEr-1 can be seen as controlled variations in

operational and environmental parameters relative to the baseline, including STAR, runway, airplane weight, wind speed, wind direction, wind gradient, gust speed, and gust gradient. Air temperature (standard, 59°F) and pilot delay (0 seconds) are constant in CASPEr-1.

As indicated in Figure 2, in Part 1 the controlled variables were the arrival route and the landing runway. In Part 2, the controlled variables were the airplane weight and the vertical and speed profiles. In Part 3, the wind speed, wind gradient, and gust intensity were varied. The FMC was always in control of the flights in Parts 1, 2, and 3. In Parts 4 and 5, there were pilot interventions in the operation of the automation to implement deviations from the programmed vertical and speed profiles. Specifically, Part 4 implemented altitude holds of various durations at a specified altitude, and Part 5 implemented a stepdown energy profile where the altitude and speed were reduced in a sequence of two or three steps of various durations. In Parts 1 to 5, the values of the flight operation factors were explicitly enumerated. In contrast, in Part 6, the values for the initial energy state (i.e., altitude, speed, and weight) and weather (i.e., wind speed, wind gradient, and gusts) were sampled from uniform random variable distributions with specified ranges.

This report describes the design and results for Part 6 of CASPEr-1.

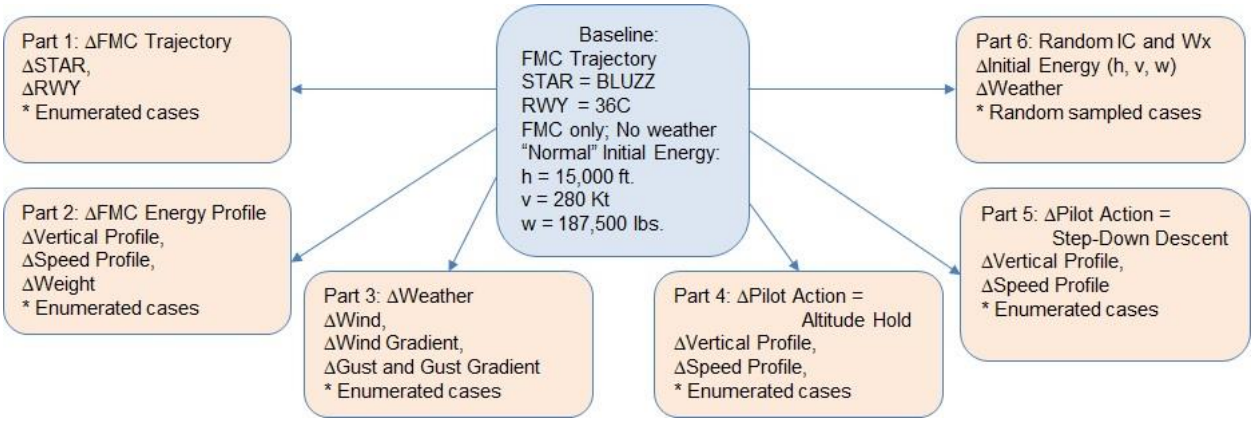

Figure 2: High-Level Decomposition of CASPEr-1

3. Experiment Design for Part 6

The main purpose of Part 6 of CASPEr-1 is to quantify (i.e., measure) the uncertainty of energy state predictions. Uncertainty in this context refers to error distribution (i.e., variability) for a given range of operating conditions. The flight path was BLUZZ to runway 36C, which is on a landing course of 358° (i.e., approximately straight north). Figure 3 is the KMEM airport diagram. Figure 4 is the RNAV arrival

chart for BLUZZ. Figure 5 is the RNAV IAP for runway 36C. The flight management computer (FMC) was in control of the flight, and the autoflight system (i.e., autopilot and autothrottle) was set to LNAV and VNAV modes to follow FMC commands. The simulated pilot controlled the deployment of flaps and the landing gear. The variable controlled factors were the initial airplane energy and the weather. Table 1 gives the value ranges and distributions for the variable parameters. The air temperature was set to the standard model (59^0F) and the pilot input delay was 0 seconds (i.e., no anticipation or delay). The quantified prediction performance is valid for these operational and environmental conditions.

Table 1: Variable Parameters in Part 6 of CASPEr-1

	Value Range		**Distribution**
	Min	**Max**	
Initial Energy Factors			
Altitude	14,000 ft.	16,000 ft.	Uniform
Airspeed	250 kt	310 kt	Uniform
Weight	150,000 lbs.	225,000 lbs.	Uniform
Weather Factors			
Wind Speed (Ground level)	0 kt	Up to 25 kt (see Figure 6)	Uniform
Wind Direction	0 deg	360 deg	Uniform
Wind Gradient	0 kt per 1,000 ft.	5.00 kt per 1,000 ft.	Uniform
Gust (Ground level)	0 kt RMS	2.00 kt RMS	Uniform
Gust Gradient	0 kt RMS per 1,000 ft.	0.27 kt per 1,000 ft.	Uniform

Table 2 gives the maximum allowable wind speeds for landing with the autoflight system engaged. This is an environmental constraint relation between wind speed and wind direction that must be satisfied in the execution of the test. To satisfy this constraint, the maximum wind speed was set according to the following rule:

- For wind direction θ within ±66 degrees of the landing direction, the maximum wind speed is $10/\cos(\theta)$ kt.
- Otherwise, the maximum wind speed is 25 kt.

This rule is illustrated in Figure 6.

Table 2: Maximum Allowable Wind Speed for Landing with Autoflight System

Wind Direction	**Maximum Wind Speed**
Headwind	25 kt
Crosswind	25 kt
Tailwind	10 kt

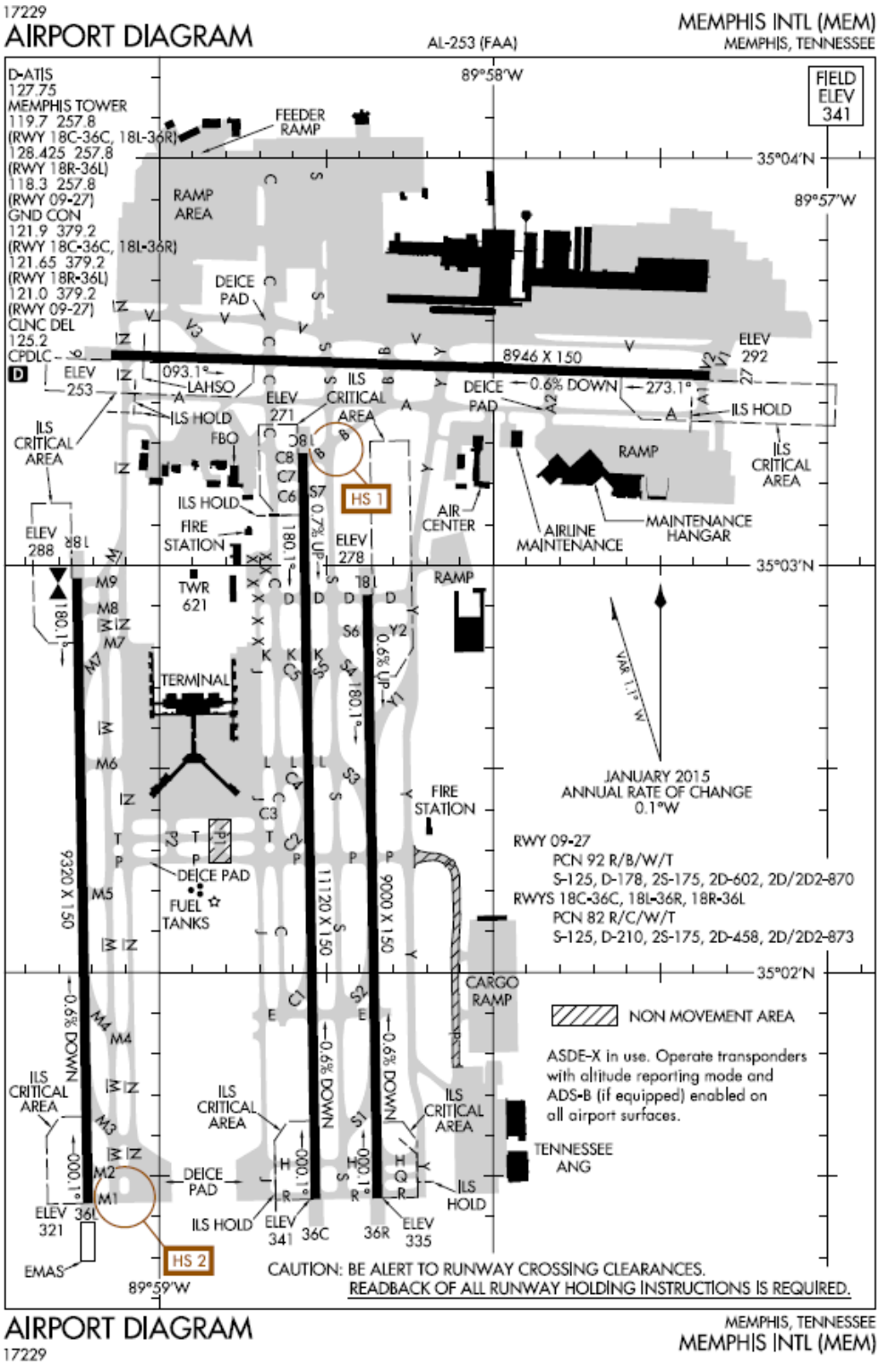

Figure 3: Airport Diagram for Memphis International Airport (KMEM)

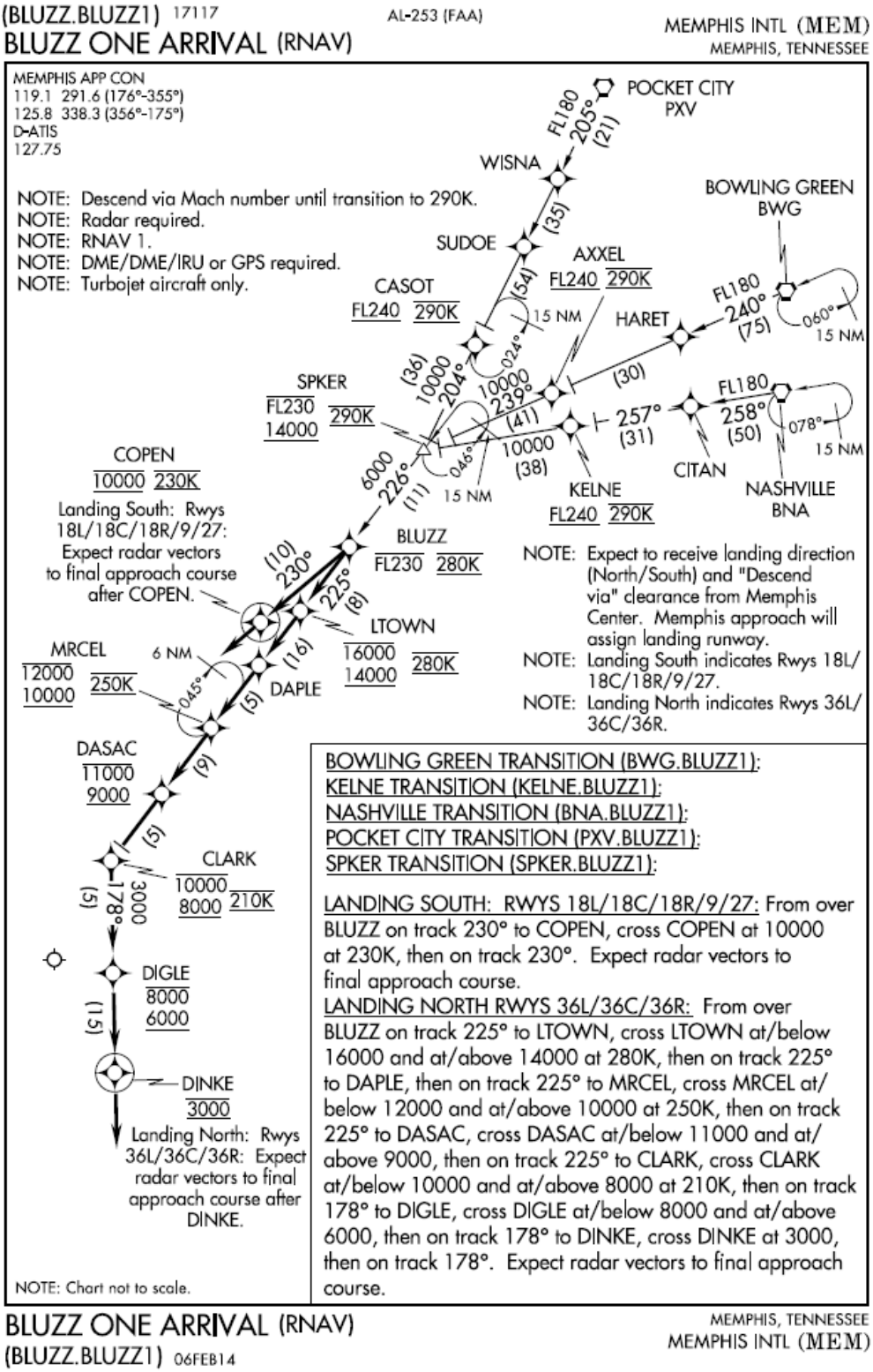

Figure 4: Standard Terminal Arrival Route BLUZZ at KMEM

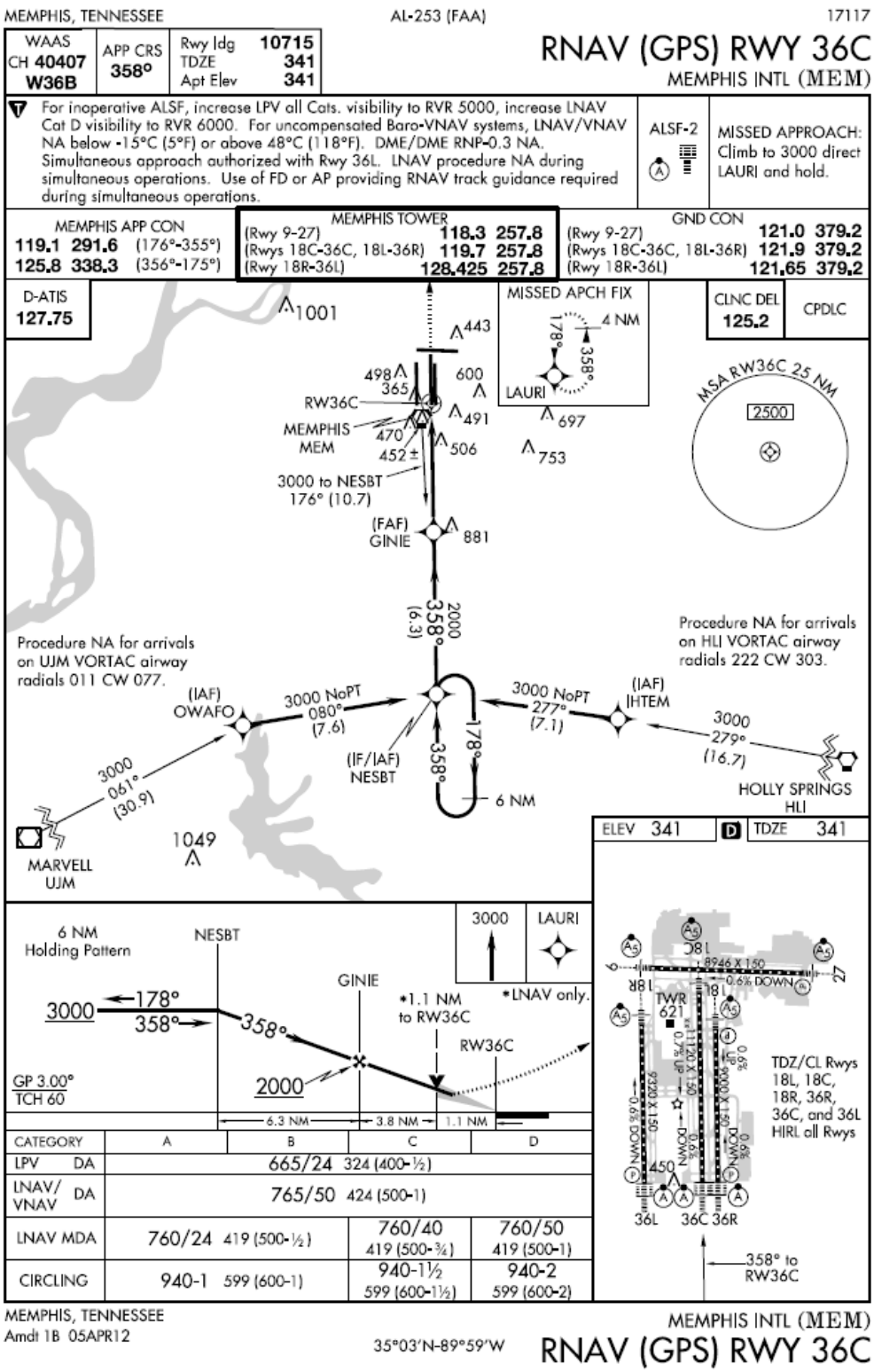

Figure 5: Approach Chart for Runway 36C at KMEM

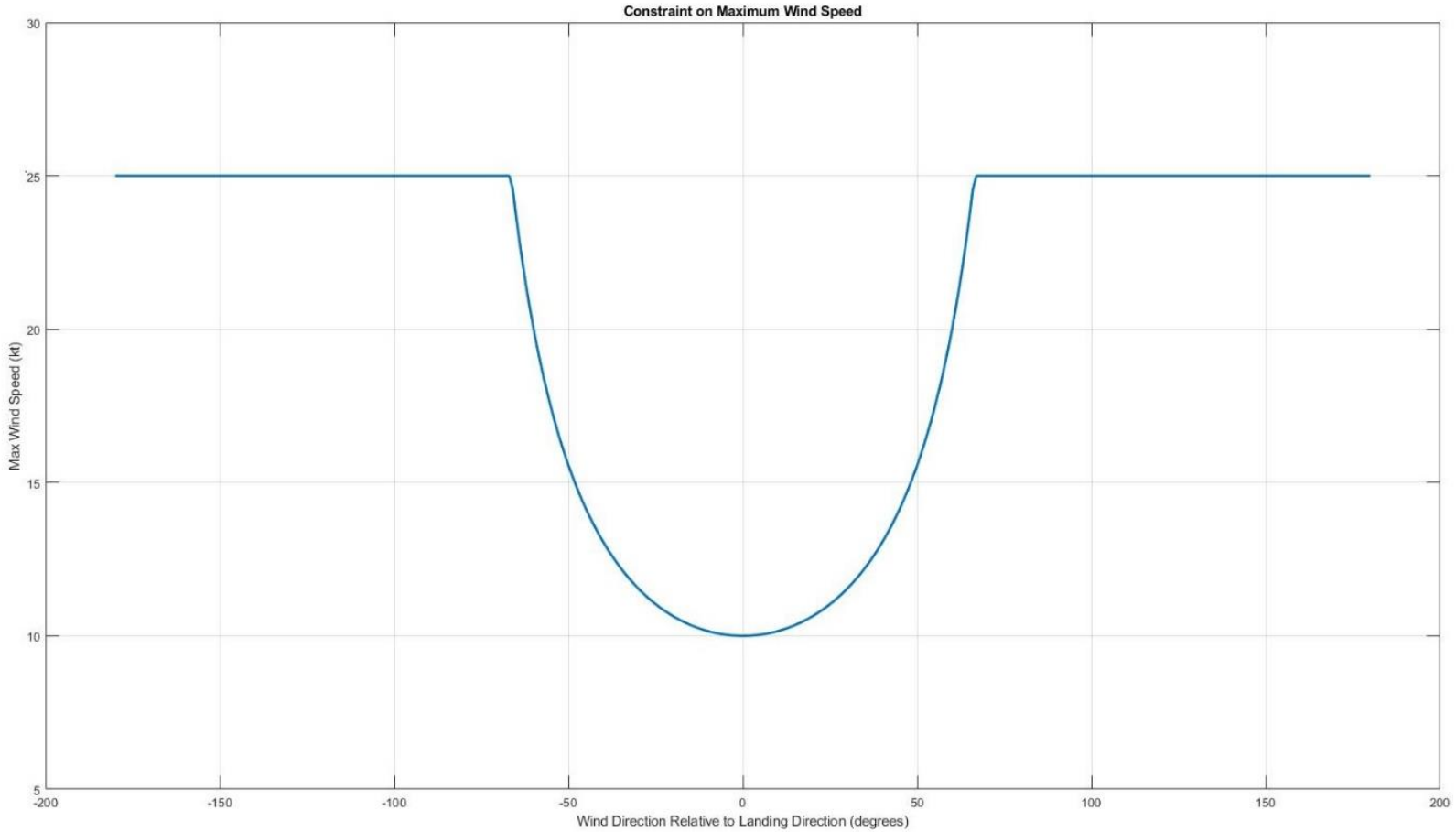

Figure 6: Maximum Wind Speed in Relation to Wind Direction

The approach to prediction performance quantification consists of two stages. In the first stage, a predetermined number of flights (denoted n) is flown with operational and environmental parameters set as described above. Each flight is an independent random trial (i.e., a test flight) that generates a sample of central tendency and dispersion measures for the airplane energy state prediction error. In the second stage, the sample measures of prediction error are aggregated and average measures with confidence intervals are computed. These averages and confidence intervals are the quantified uncertainty for airplane energy state prediction.

The number of flights (n) is determined by conceptualizing the test as an experiment for a binomial random process with the sample space Ω divided into two sets: set A with aggregate event probability p, and set B with aggregate event probability $1 - p$. The mean number of samples from set A in an experiment of n trials is np. Assuming that we want an average of 10 samples from set A and that the probability of set A is $p = 0.10$, the total number of trials is $n = 10/p = 100$. Therefore, for our uncertainty quantification experiment, we need at least 100 flights to ensure that, on average, we have 10 sample flights from any subset of operational and/or environmental conditions with total probability of 10%.

This is a practical approach to determine the number of flights given that there is no a-priori information about the relation between operating conditions and the performance of the prediction function, or about the output characteristics of the prediction function such as the probabilities of anomalous behavior. For this situation, in which there is nearly total ignorance about the process being examined (i.e., the prediction function for the given operating conditions), the experiment should be designed with emphasis on coverage of the range of operating conditions and having a sufficiently large sample to ascertain the major characteristics of the prediction performance distribution. Assuming that the prediction performance measures have a unimodal distribution shape, sets A and B above correspond to the tail(s) and the peak region of the distribution, respectively. This approach is also consistent with a prediction performance analysis that examines both error distributions and anomalies, as indicated in the CASPEr concept graphic in Figure 1. In this analysis, an anomaly is any behavior from the prediction function that is "inconsistent with or deviating from what is usual, normal, or expected; marked by incongruity or contradiction; inappropriate" [10] [11]. In this analysis, a distribution outlier is considered an anomaly.

The data analysis consists of three parts. The first part is uncertainty quantification of prediction performance as statistical measures of prediction error distributions. The second part of the analysis is modeling of the prediction performance as polynomial functions of the controlled factors as a means to measure the relative effect of individual factors on performance. The first two parts of the analysis also generate sets of flights with outlier prediction performance. These outliers are examined in the third part

of the analysis to identify performance characteristics and hypothesize about possible causes of outlier performance.

4. Prediction Performance Metrics

The purpose of CASPEr-1 is to analyze and evaluate the performance of the TP function, which is intended to enhance safety by supporting flight crew awareness of the airplane energy state and automation mode. However, CASPEr is not intended as a means to diagnose the performance of the prediction function, which would require a more granular decomposition of operational factors and deep insight into the input-output relations and internal behavior of the prediction function. Instead, the interest is in the relation between the flight operation factors and the performance of the prediction function. Since the automation is used to guide and control the airplane, there is a causal relation from the automation (mode, targets, and constraints) to the airplane energy state. Based on this, the airplane state of main interest in CASPEr-1 is the translational state (e.g., altitude and speed). The automation mode is of secondary interest as a means to understand and explain observed translational state predictions. The rotational state of the airplane (e.g., roll and pitch) is not considered in the analysis of prediction performance.

The translational state variables of the airplane include the horizontal position given in terms of latitude and longitude, and the energy state given in terms of altitude, airspeed, and total energy. The unit of measure for latitude and longitude is degrees (deg or ^{o}); for altitude the unit is feet (ft); airspeed is measured in knots (kt). The predicted airspeed is the indicated airspeed V_{IAS}, which is the speed indicated by the pressure-based speed measuring instruments on the airplane and is used in communications between pilots and air traffic controllers [12]. The calibrated airspeed V_{CAS} is the airspeed corrected for instrument and altitude measurement errors. The true airspeed V_{TAS} is the actual speed of the airplane relative to undisturbed air. V_{CAS} and V_{TAS} are related by a complex mathematical relation with parameters of air density, pressure, and temperature. In the simulation environment used for CASPEr, V_{IAS} and V_{CAS} are equal since instrument and altitude measurement errors are not modeled.

The total translational energy of the airplane (denoted E_{Total}) is equal to the potential energy (E_P) plus the kinetic energy (E_K):

$$E_{Total} = E_P + E_K = m_a g h + m v_{TAS}^2/2$$

where m_a denotes the mass of the airplane, g denotes the gravitational acceleration (in m/s^2), h denotes the altitude (in m), and v_{TAS} denotes the true airspeed (in m/s) [13]. The specific energy, or energy height, of the airplane is given by:

$$H_e = E_{Total}/w = h + v_{TAS}^2/2g$$

where w = mg, the weight of the airplane. H_e is an altitude-equivalent measure of energy and it has units of distance, given in meters or converted to feet. The energy height is used here as a single measure of energy that combines both altitude and airspeed.

From a computing perspective, the prediction function provides a real-time service to other entities that depend on its output. These entities are either computing functions or the flight crew. This service consists of a sequence of (service) items, each characterized by a value (or content) and a time of generation [14], which are required to satisfy specified real-time timing constraints such as the update rate (or update period). The behavior of the prediction function is its sequence of outputs in time [15].

For CASPEr-1, the update rate for the TP prediction function is 1 Hz. The output of interest at time t (i.e., the service item at time t) consists of the predicted values of airplane state variables for look-ahead times τ ranging from 0 to 299 seconds (i.e., almost 5 minutes). Let $x_{Pred}(t, \tau)$ denote the predicted value of state variable x generated at time t for look-ahead time τ, i.e., the predicted value of the state for time $t + \tau$. Since the predicted airplane state variables are real-valued, we can measure prediction performance based on the following simple definitions of absolute and relative prediction errors at time t for look-ahead τ:

$$e_{Pred,Abs}(t, \tau) = x_{Pred}(t, \tau) - x_{Obs}(t + \tau)$$

$$e_{Pred,Rel}(t, \tau) = [x_{Pred}(t, \tau) - x_{Obs}(t + \tau)]/x_{Obs}(t + \tau)$$

where x_{Pred} and x_{Obs} denote predicted and observed state values, respectively. Notice that for each observed state variable x at real-time T, i.e., $x_{Obs}(T)$, the prediction function generates 300 predictions starting with the predicted state value at time $t = T - 299$ (i.e., $\tau = 299$) until time $t = T$ (i.e., $\tau = 0$) when the output is an estimate of the current state.

A simulated test flight generates a sequence of prediction errors for each airplane state variable which are auto-correlated, rather than independent random samples, as these errors are based on predictive models of a physical system (i.e., the airplane). This implies that the prediction performance analysis should not be based on statistical measures intended for independent sample sets if such measures could be misleading. Instead the prediction errors are viewed as time-sampled signals or time series and

conventional measures for signal characteristics are applied. Let L denote the number of outputs (i.e., service items) generated by the prediction function during a simulated flight, where each service item consists of a vector of 300 prediction values (one for each look-ahead time) for each predicted state variable. As an example, for a simulated flight of 15 minutes, there are 15 min x 60 sec/min x 300 predictions/sec = 270,000 prediction error data values for each predicted state variable. Conventional measures of central tendency (e.g., mean and median) and dispersion (e.g., standard deviation, root-mean-square-error RMSE, inter-quartile range, min-max range) are applied to these large error data sets. Plots and other data visualizations are also used to generate observations about the performance and behavior of the prediction function.

The three main prediction performance measures used in this analysis are the median, RMS, and maxAbs for the absolute and relative prediction error during a flight. The median absolute error for one flight and look-ahead τ is given by:

$$\text{Median}(\tau) = \text{median}\{e_{Pred,Abs}(t, \tau), \text{ for all } 0 \le t \le t_{end}\}$$

where t_{end} is the time at the end of the flight. The RMS absolute error for one flight and look-ahead τ is:

$$\text{RMS}(\tau) = \sqrt{\left[\sum_{t=0}^{tend} e_{Pred\_Abs}^{2}(t, \tau)\right]/m}$$

with $m = t_{end} + 1$ is the number of data points. The maxAbs absolute error measure of prediction performance is the maximum absolute value of the absolute prediction error in a flight. The maxAbs for one flight and look-ahead τ is:

$$\text{maxAbs}(\tau) = \max\{| e_{Pred,Abs}(t, \tau) |, \text{ for all } 0 \le t \le t_{end}\}.$$

5. Flight Trials

Figure 7 to Figure 12 show the airplane state data for all the test flights in Part 6 of CASPEr-1. The complete set of test points is given in Appendix B. As seen in Figure 7, all the flights followed the same lateral path on BLUZZ to runway 36C. The path followed on the final turn from waypoint DINKE at the end of the STAR to waypoint NESBT at the beginning of the approach depends on the airspeed of the airplane when it reaches DINKE.

Figure 8 shows the altitude and airspeed in relation to distance to the runway. The distance to the runway is computed by the FMC. Notice that the initial altitude is between 14,000 and 16,000 ft. and the

initial airspeed is between 250 and 310 kt. Also notice that if the initial altitude or airspeed is lower than the lower limit of the next waypoint, the airplane does not increase its energy state and instead it waits until it passes a waypoint with a lower limit than its current state. In addition, notice that the altitude at DINKE is 3,000 ft. and the turn from DINKE to NESBT is at a constant altitude.

Figure 9 shows the relation between altitude and airspeed for all test flights. All the flights proceed from the top right corner to the bottom left corner of the plot. The initial altitude and airspeed points are contained in the dashed box between 14,000 to 16,000 ft. and between 250 and 310 kt. The black dots mark the approximate location of the waypoints and are for visual reference only. The airplane steps down in energy until it reached CLARK, then it descends at around 210 kt until DINKE, where it turns at constant altitude and airspeed until it reached NESBT. After NESBT, the airplane reaches the final landing airspeed in one or two steps down.

Figure 10 shows the scatter plot of test points for wind speed and wind direction. The effect of the constraint on maximum wind speed as a function of wind direction is clearly visible.

Figure 11 shows that the landing airspeed is a function of the airplane weight with a 0.993 correlation coefficient.

Figure 12 shows that the landing airspeed is not a function of the wind speed, with a 0.035 correlation coefficient.

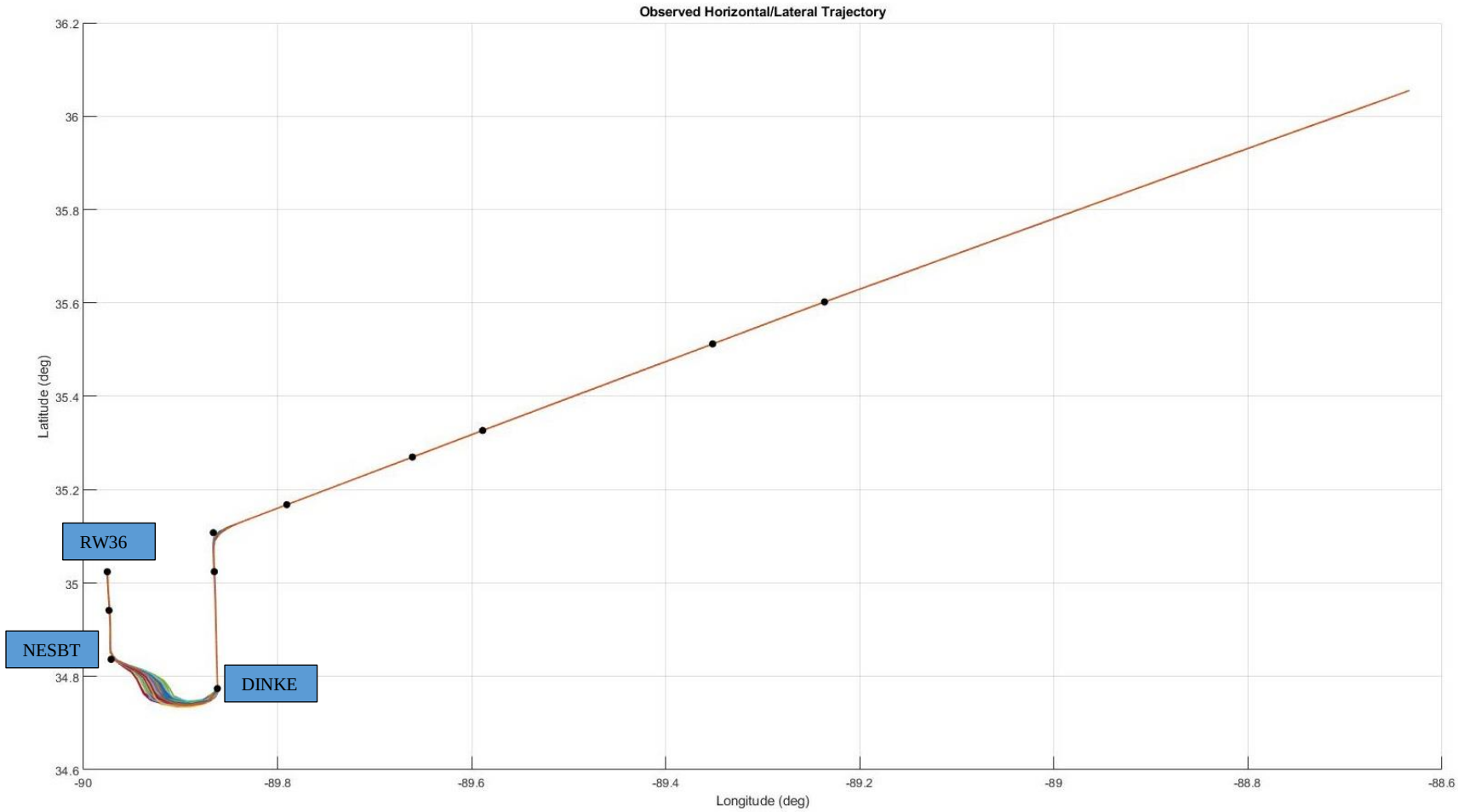

Figure 7: Lateral Path for All Test Flights on Arrival Route BLUZZ to Runway 36C

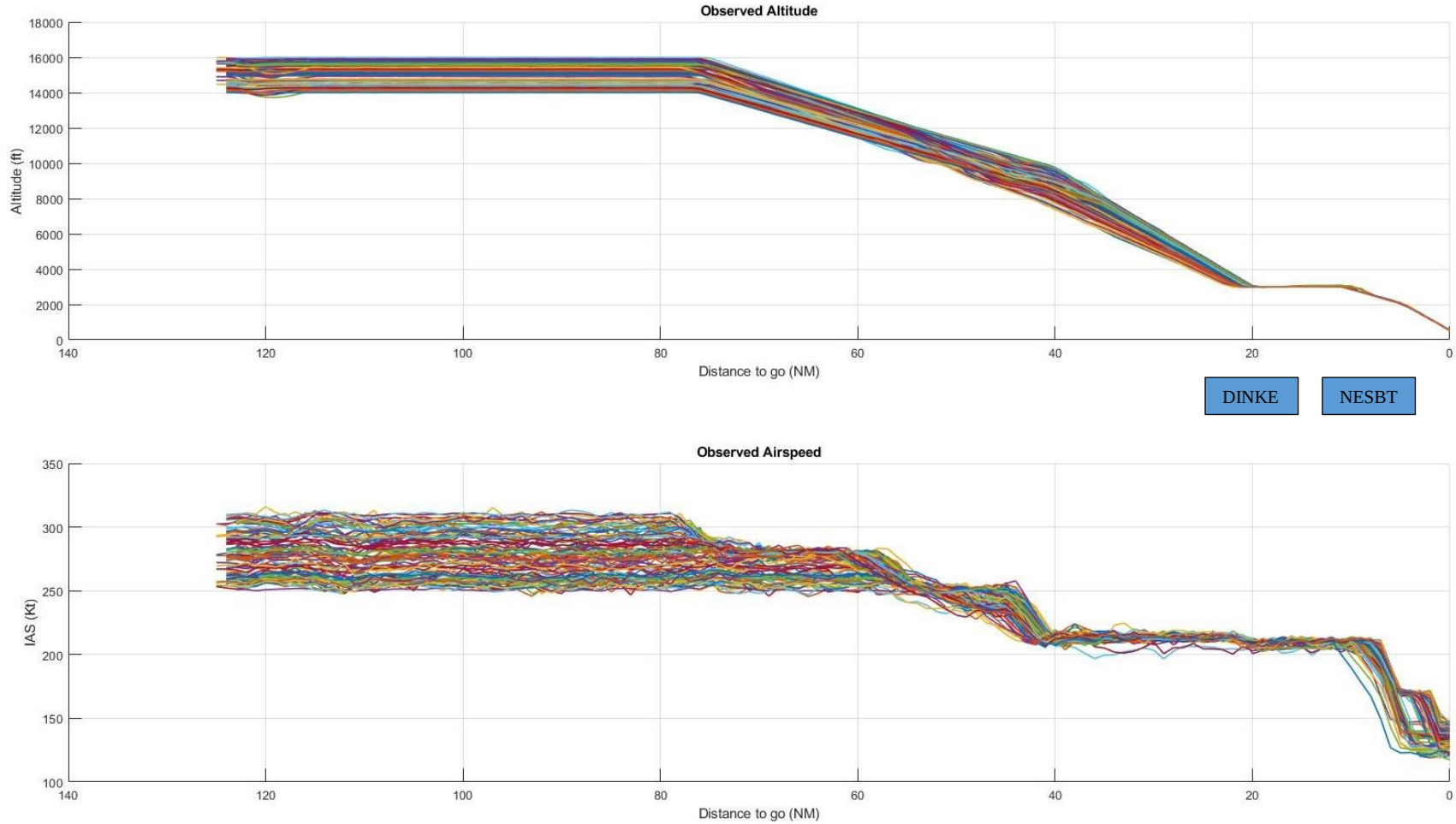

Figure 8: All Test Flights: Altitude and Airspeed in Relation to Distance to Runway

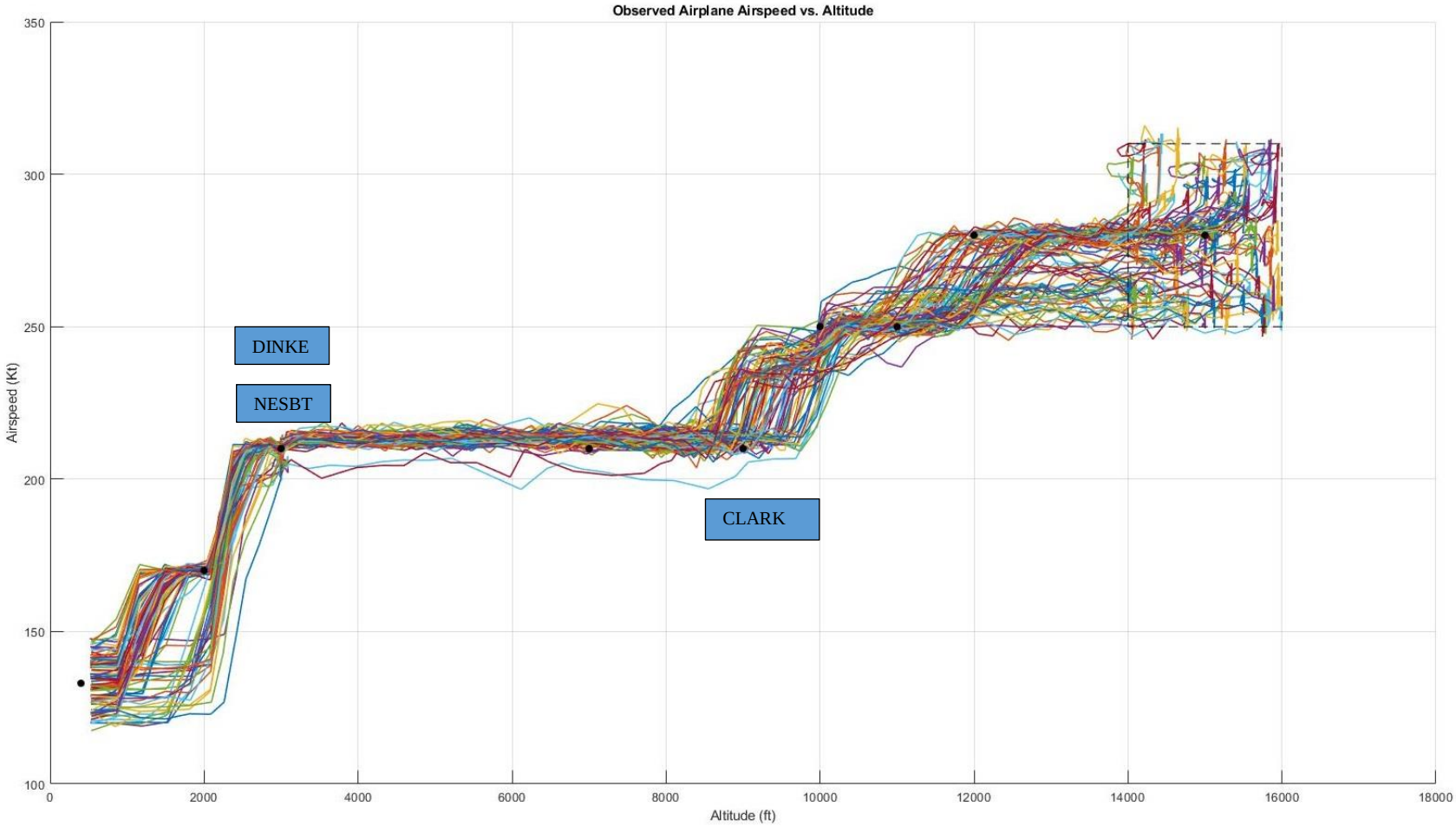

Figure 9: All Test Flights: Altitude vs. Airspeed

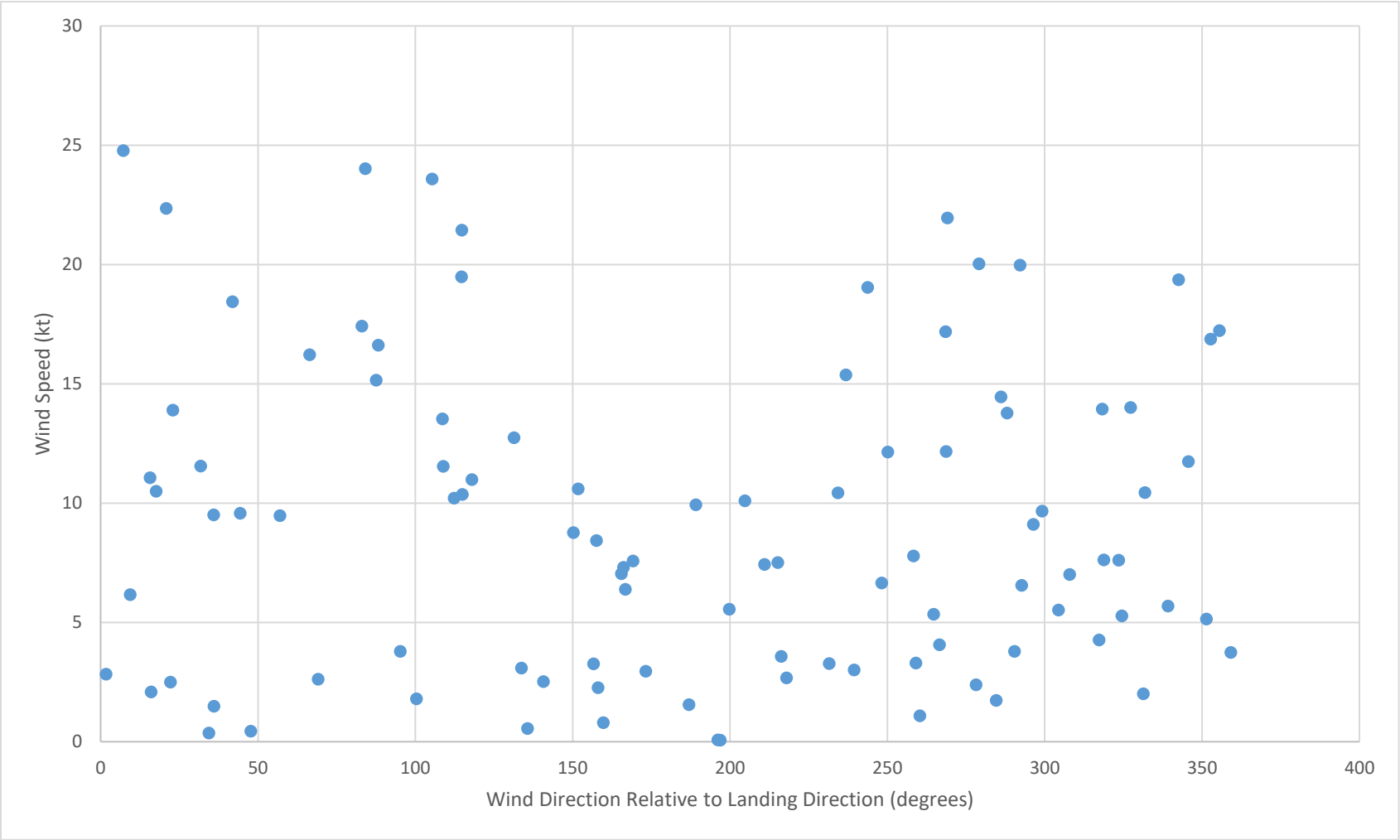

Figure 10: Test Points for Wind Speed and Wind Direction

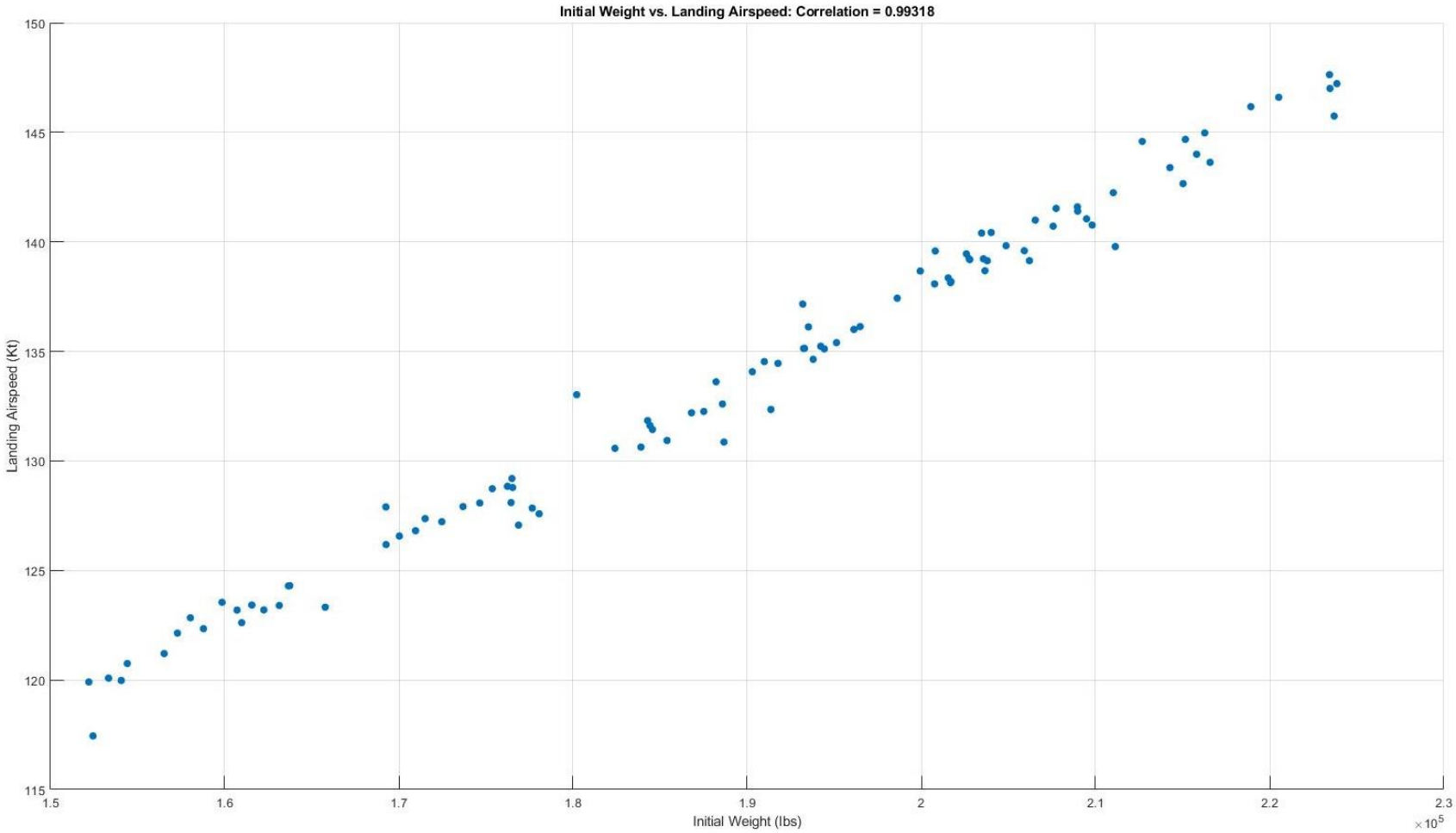

Figure 11: All Test Flights: Landing Airspeed vs. Airplane Weight

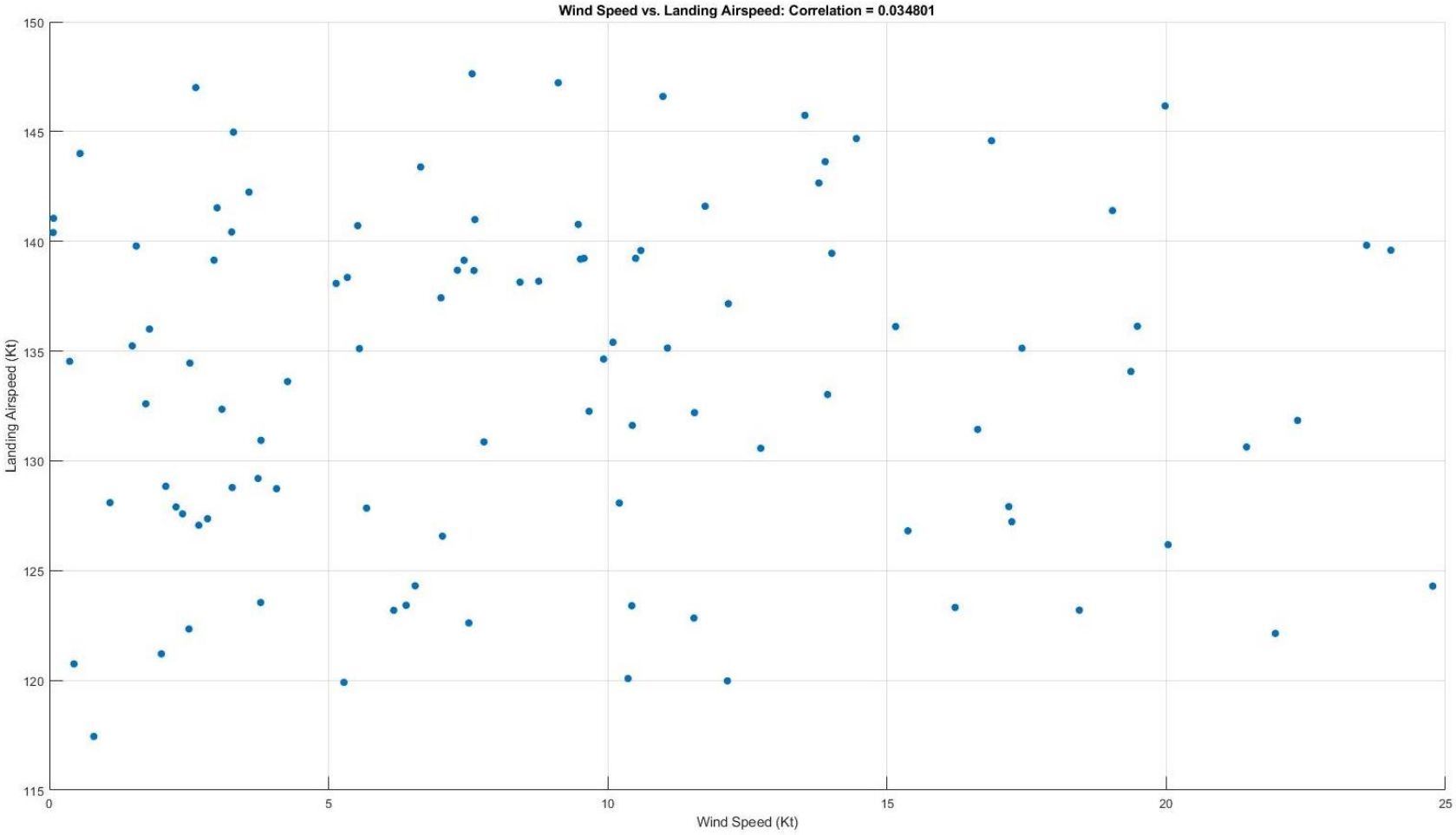

Figure 12: All Test Flights: Landing Speed vs. Wind Speed

6. Typical Prediction Performance

This section examines typical prediction performance for one of the test flights, specifically test point 43. Table 3 gives the factor values for this flight. Relative to the factor ranges given in Table 1, the altitude and airspeed are mid-range; the weight is heavy; the wind speed at low altitude is low and the wind gradient is midrange; the runway approach is with a tailwind (i.e., ~180 degrees from the landing direction); the gust strength at low altitude is high, and the gust gradient is low.

Table 3: Initial Airplane Energy and Weather Factor Values for Test Flight 43

	Initial Airplane Energy			**Weather**				
ID	**Altitude (ft)**	**IAS (kt)**	**Weight (lbs)**	**Wind Speed (kt, Ground Level)**	**Wind Direction (deg)**	**Wind Gradient (kt / 1,000 ft)**	**Gust (kt RMS, Ground Level)**	**Gust Gradient (kt RMS / 1,000 ft)**
43	14,586.90	275.36	211,138.00	1.55	186.97	3.06	1.93	0.10

Figure 13 shows observed (i.e., actual airplane state) and predicted altitude vs. airspeed for test point 43. The look-ahead time τ is for intervals of 1-minute (i.e., 60 seconds). The predictions track well the observed profile. Recall that the airplane makes a turn at constant altitude and airspeed between waypoints DINKE and NESBT, which is why these waypoints coincide on this plot. The prediction error seems to be worse in the interval between CLARK and DINKE.

Figure 14 shows the observed and predicted time histories for altitude, airspeed, and energy height. At these scales, the predictions track the observed state very closely, with the most visible persistent error being in the airspeed prediction between CLARK and DINKE. Figure 15 shows the absolute error for the full duration of the flight. The altitude prediction error is between -400 ft. and 300 ft., and the airspeed prediction error is between -20 kt and 20 kt. Figure 16 shows the relative prediction error, which emphasizes the error at low altitude, airspeed, and energy. Notice that the relative error is highest during the approach phase of the flight after passing the NESBT waypoint.

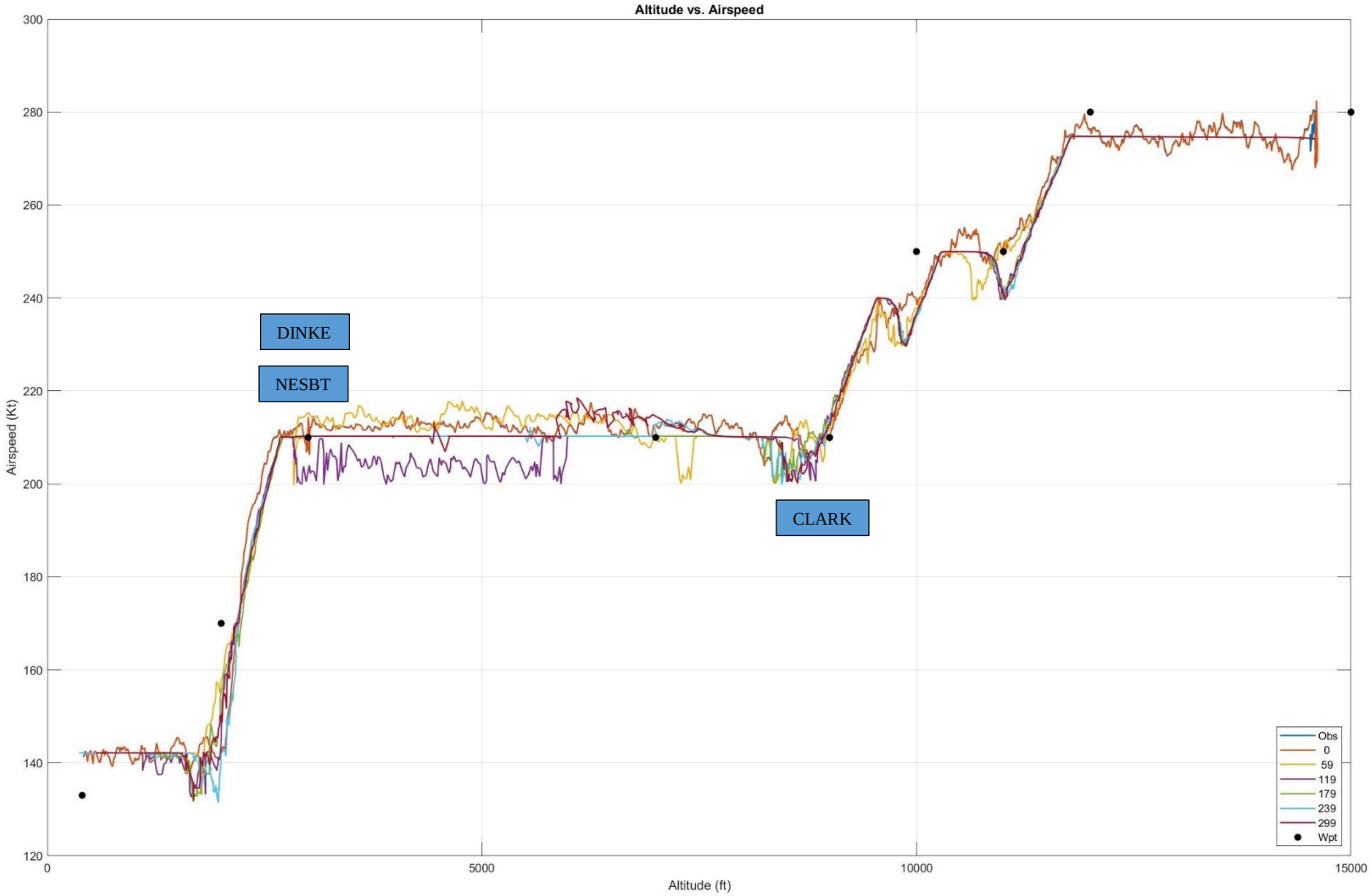

Figure 13: Test Flight 43: Altitude vs. Airspeed Observed and Predicted At 1-Minute Look-ahead Intervals

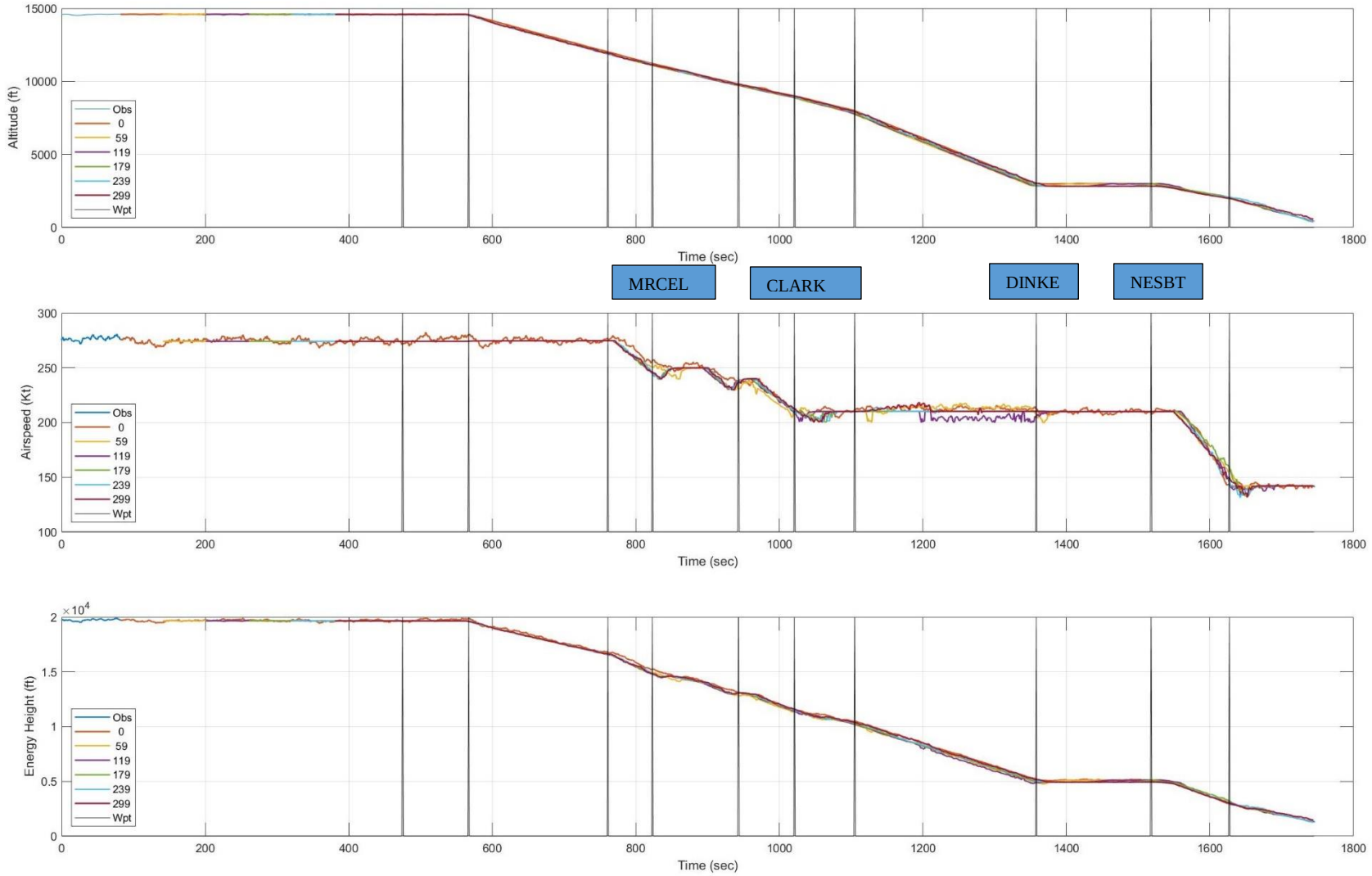

Figure 14: Test Flight 43: Altitude, Airspeed, and Energy Height Observed and Predicted At 1-Minute Look-ahead Intervals

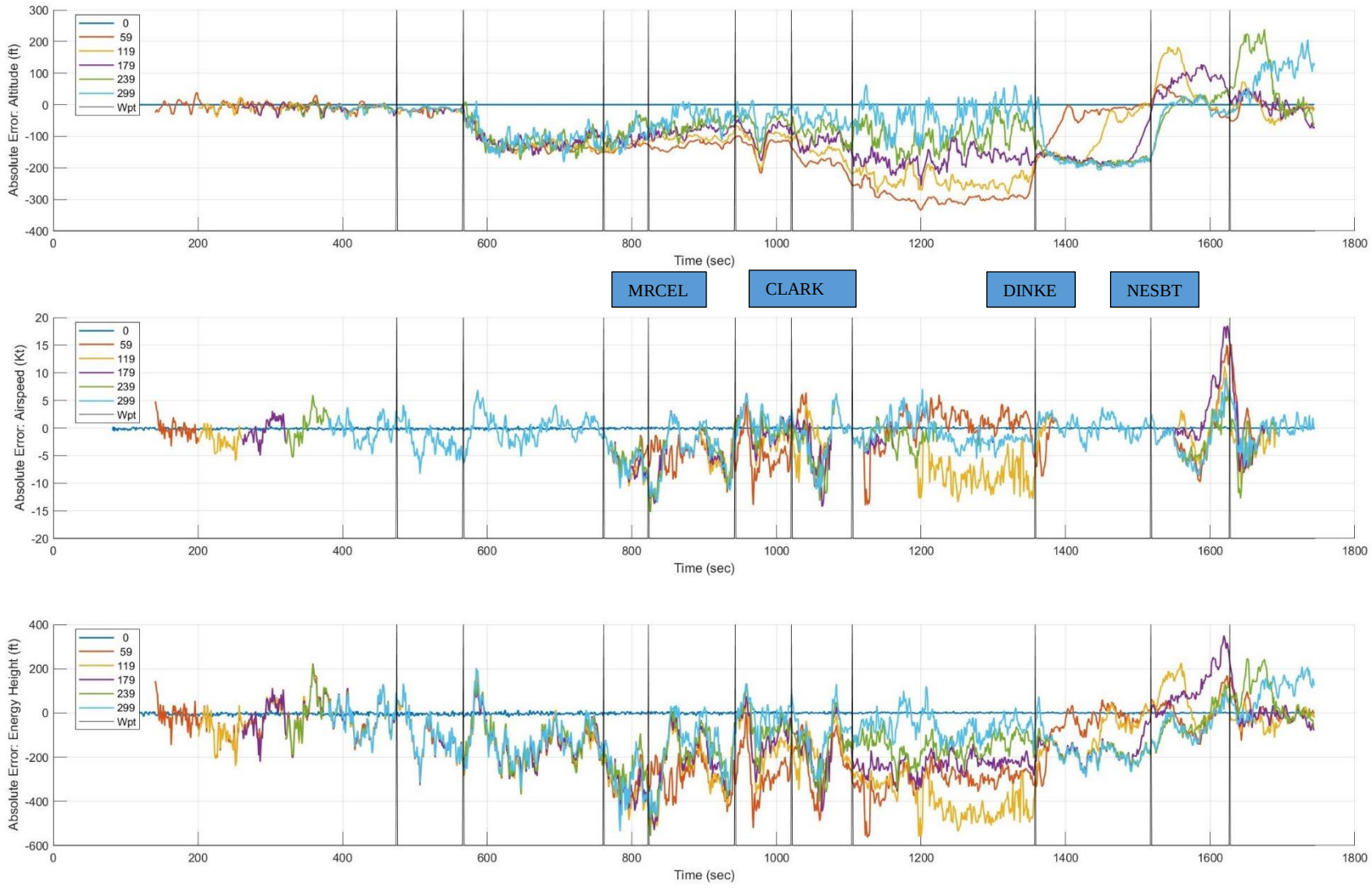

Figure 15: Test Flight 43: Absolute Error for Altitude, Airspeed, and Energy Height Prediction At 1-Minute Look-ahead Intervals

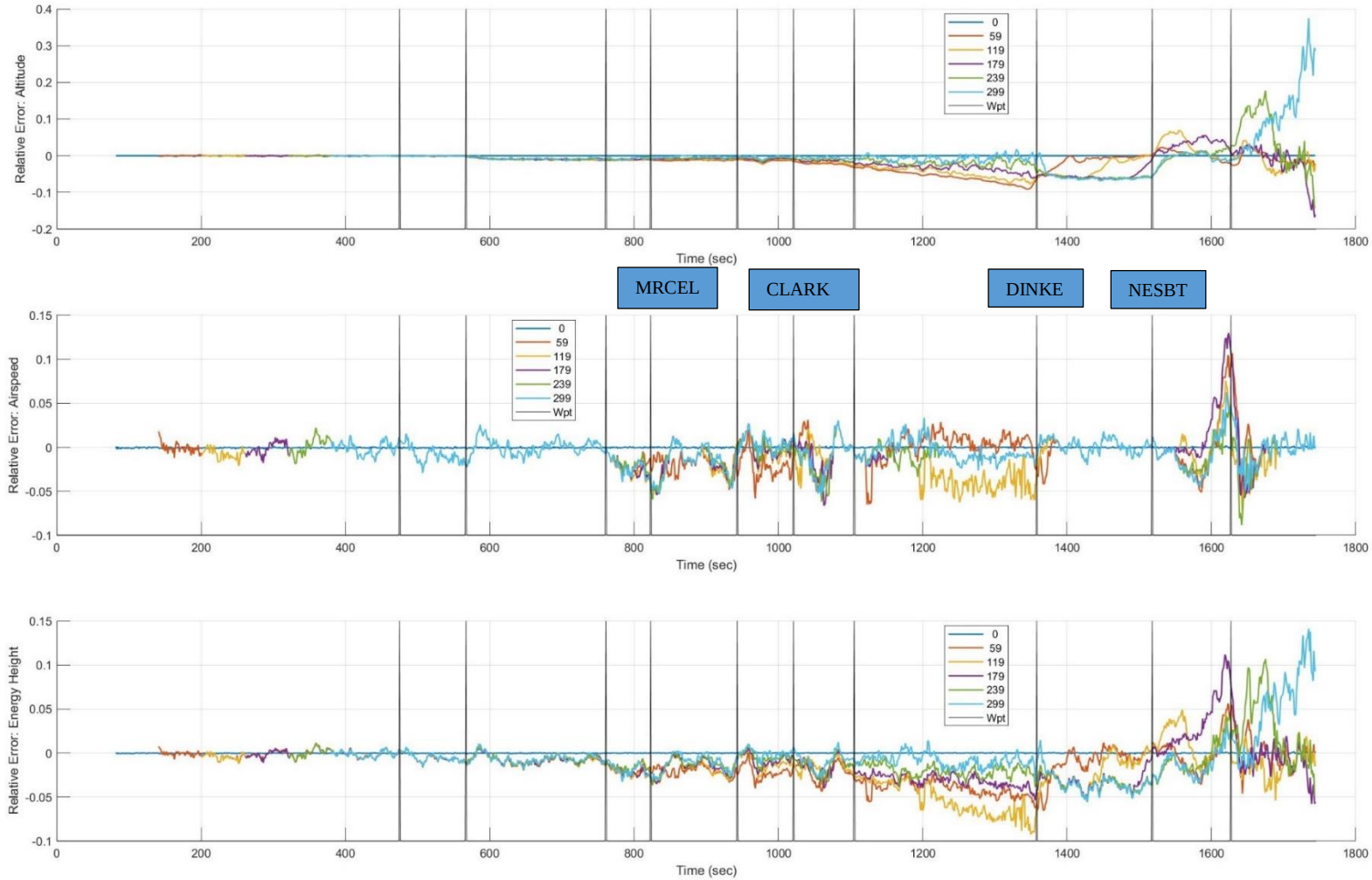

Figure 16: Test Flight 43: Relative Error for Altitude, Airspeed, and Energy Height Prediction At 1-Minute Look-ahead Intervals

Figure 17 and Figure 18 show the heatmaps for absolute error of energy prediction for predicted time $t + \tau$ and for time of prediction t (i.e., the time at which the prediction was made). The red rounded squares mark regions of interest. In red square 1, notice the pattern of somewhat evenly spaced vertical lines in colors ranging from gray to light green, corresponding to energy height error up to around 300 ft. Comparing the time axis with Figure 14, we see that the airplane was flying at constant altitude during this part of the flight. A possible explanation for this error pattern is that the predictor does not account for the effects of future gusts at around the predicted time $t + \tau$, which can cause small oscillations in the airplane altitude and airspeed and, therefore, small cyclic errors in the predictions.

The vertical green, yellow, and red band in red square 2 is an indication that this part of the flight is relatively more difficult to predict for any look-ahead time τ from 0 to 299 seconds. This is an indication that the waypoint spatial pattern and restrictions are a factor in the accuracy of the predictions.

In the region marked by red square 3, the prediction error peaks for look-ahead time τ between around 50 and 150 seconds. This is counterintuitive, as one would expect the error to grow monotonically with τ. Notice in Figure 17 that the red and yellow features have a combination of vertical and forward slant, and in Figure 18 these feature are a combination of backward and vertical slant. This is an indication that both the time at which predictions were made t and the time being predicted $t + \tau$ are significant factors in the prediction error in this region. One possible explanation for the prediction error in this region is an error in the predicted automation mode for some τ during this time interval.

Figure 19 shows the summary statistics for the altitude prediction absolute error as a function of look-ahead time τ. The median and mean statistics vary between 0 and -100 ft. The maximum inter-quartile range and RMS errors for altitude prediction are around 150 ft. The absolute-value error is largest between look-ahead τ of 25 and 150 seconds, which matches the observations for the heatmaps in Figure 17 and Figure 18.

Figure 20 shows summary statistics for airspeed prediction error. The median and mean error is very close to zero for the full range of look-ahead time τ. The RMS error is around 5 kt and the maximum absolute-value of the error is less than 25 kt. The noisy oscillation in the Max, Min, Range, and AbsMax curves is probably related to the effect of gusts on the speed on the airplane and unmodeled weather and airplane dynamics in the prediction function.

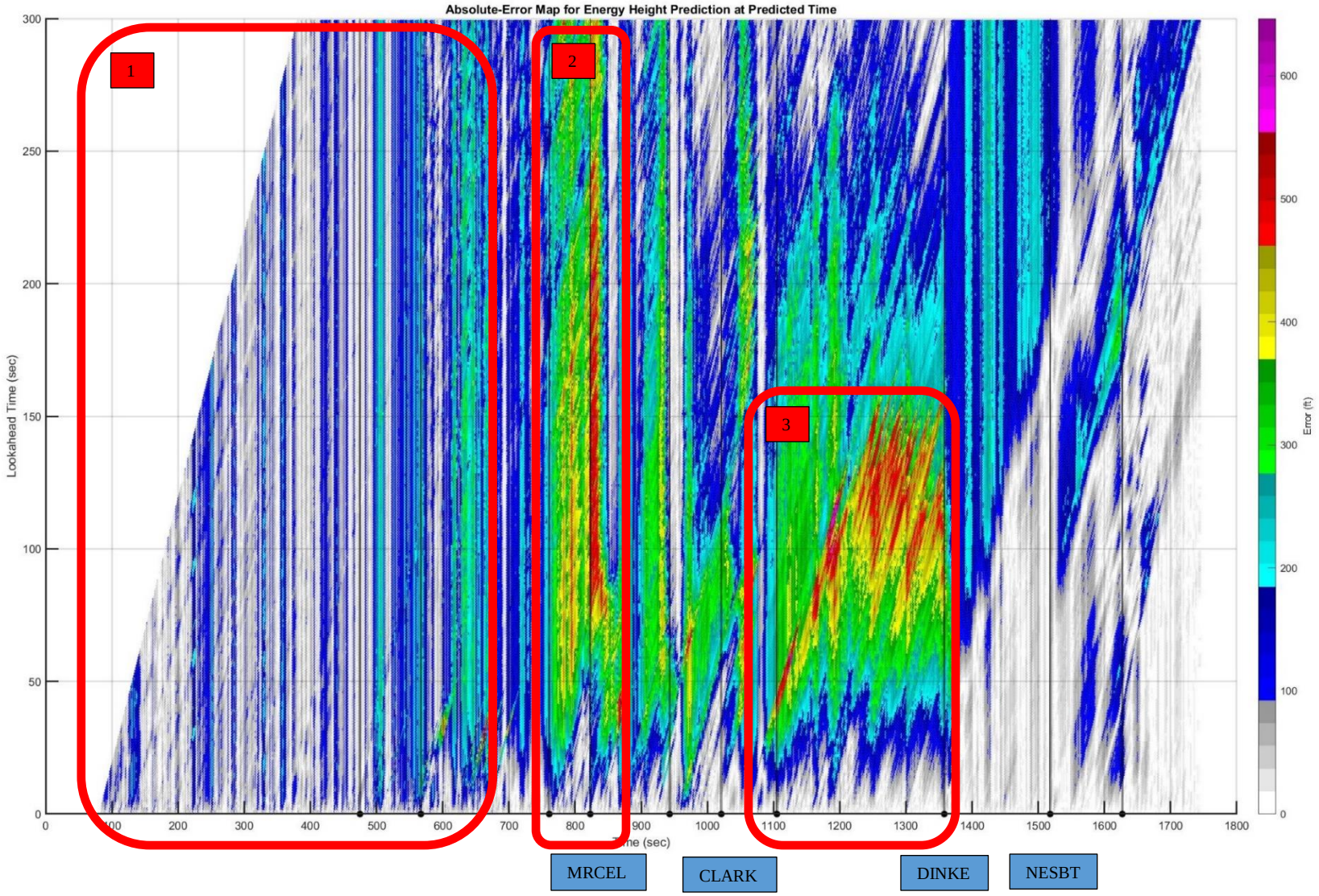

Figure 17: Test Flight 43: Heatmap of Absolute Error for Energy Height Prediction at Predicted Time $t + \tau$

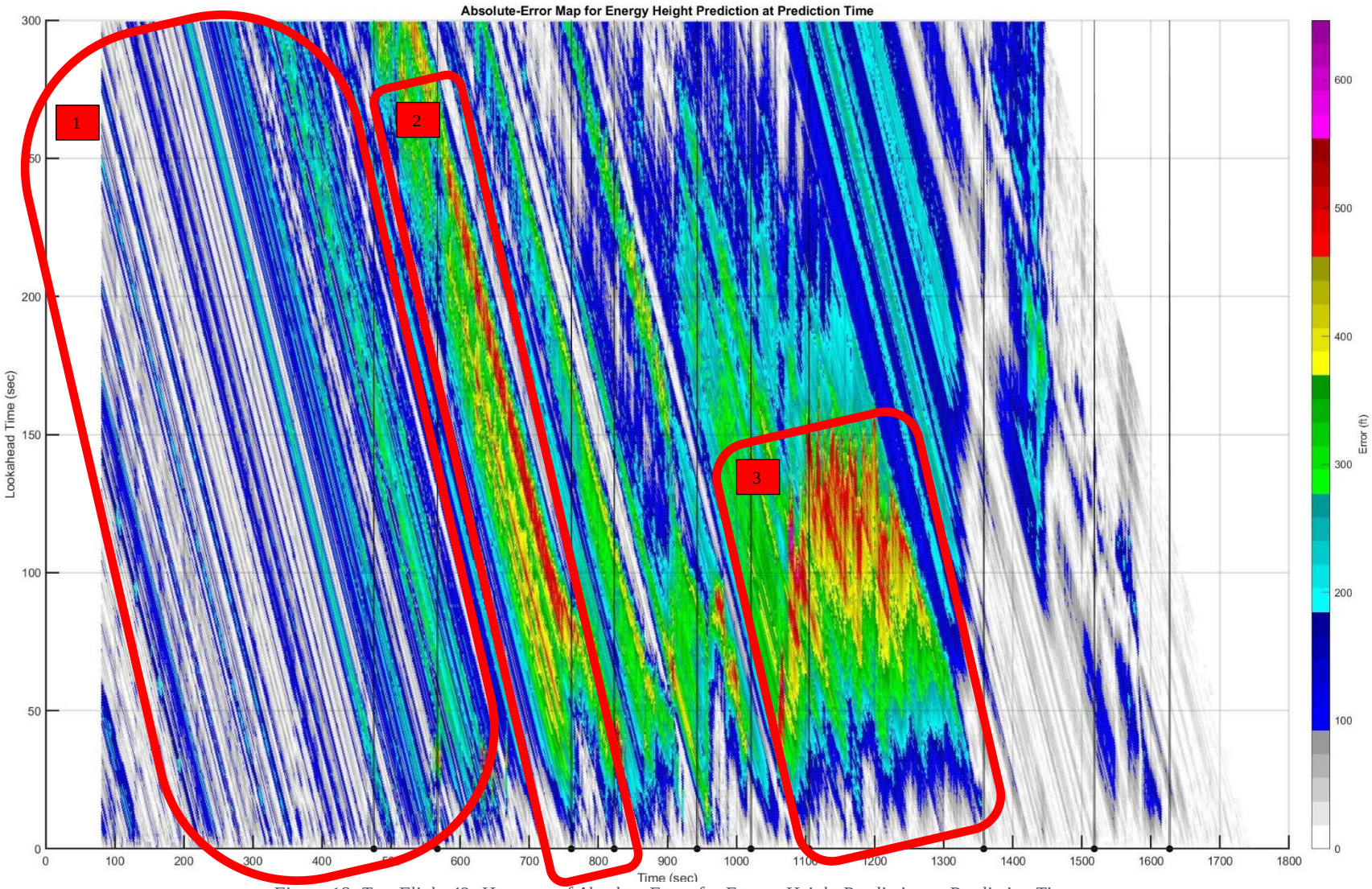

Figure 18: Test Flight 43: Heatmap of Absolute Error for Energy Height Prediction at Prediction Time t

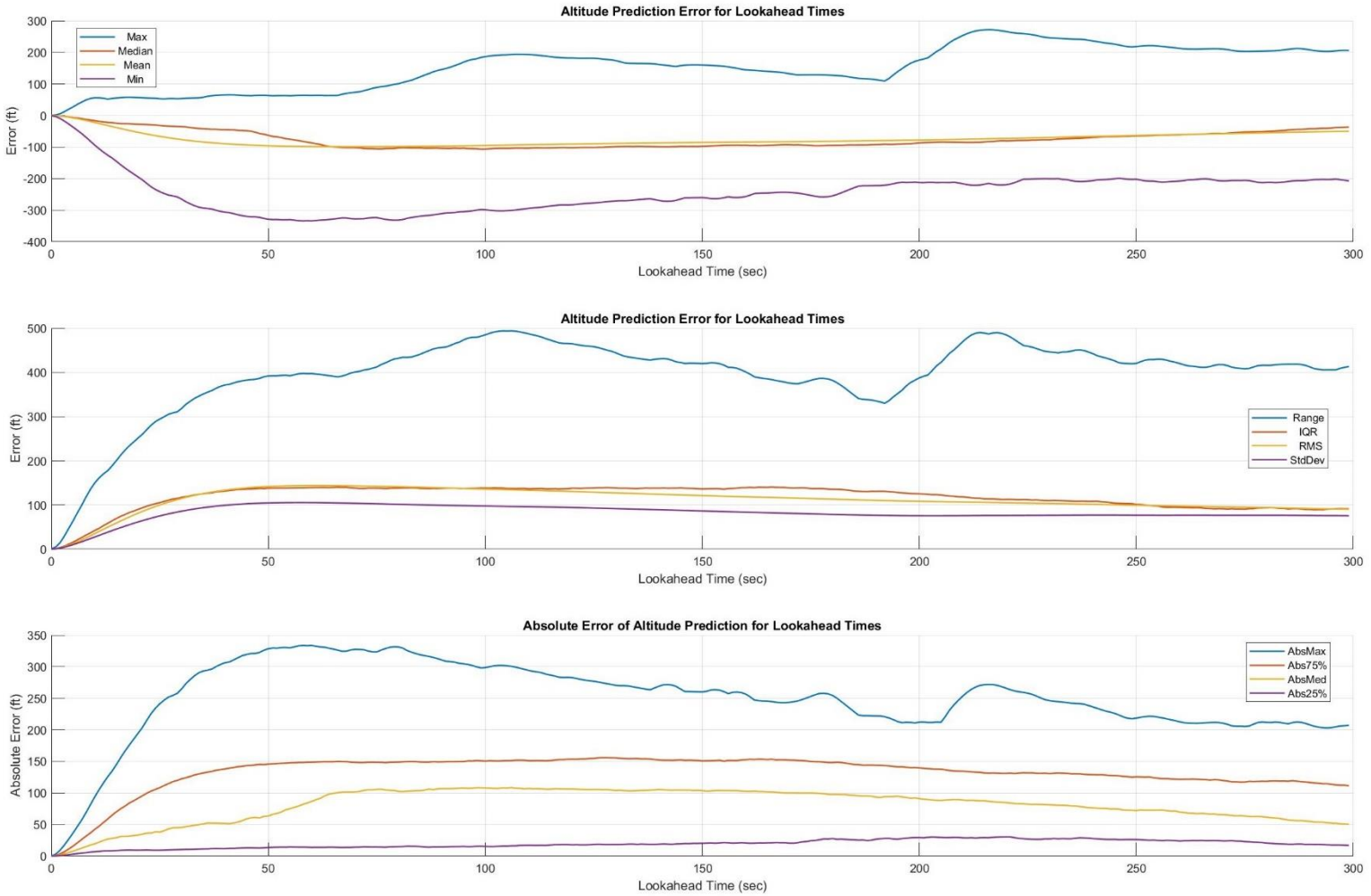

Figure 19: Test Flight 43: Absolute Error Statistics for Predicted Altitude as a Function of Look-ahead Time τ

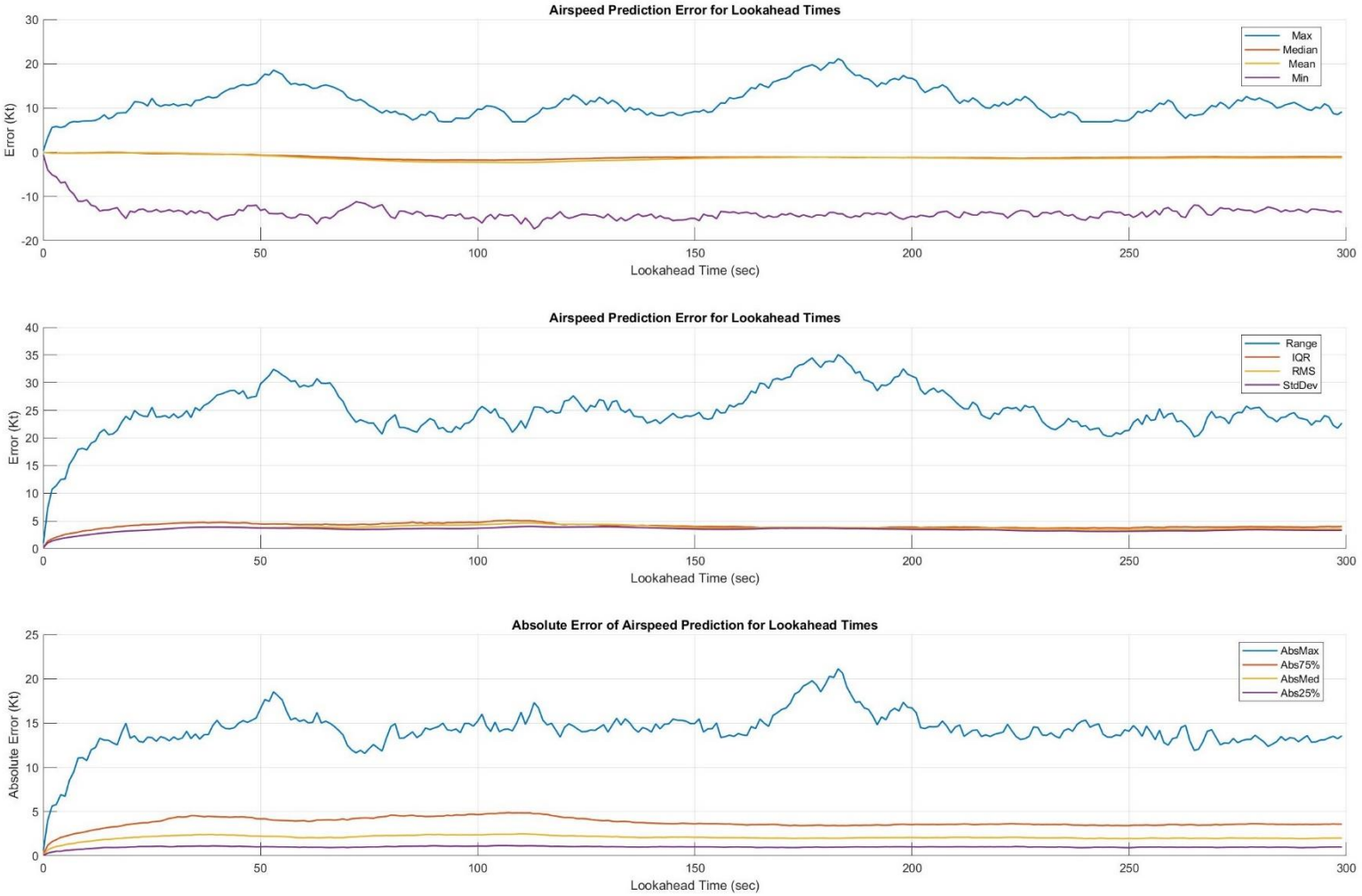

Figure 20: Test Flight 43: Absolute Error Statistics for Predicted Airspeed as a Function of Look-ahead Time τ

7. Prediction Uncertainty Quantification

This section quantifies the uncertainty (i.e., measures the variability) in altitude and airspeed prediction and identifies anomalous outlier behavior for further analysis in a later section of this report. As stated earlier, anomalous behavior is "inconsistent with or deviating from what is usual, normal, or expected; marked by incongruity or contradiction; inappropriate" [10] [11]. Altitude prediction is examined first, followed by airspeed prediction.

7.1. Altitude Prediction

Figure 21 to Figure 28 show the main results for the quantification of altitude prediction uncertainty. Figure 21 and Figure 22 show the median and RMS absolute error as a function of look-ahead time τ for the 100 test flights. Both figures consist of a main group (or set) of curves containing the majority of the flights and one or more curves that deviate from the main group.

Figure 23 and Figure 24 quantify the distributions of the median and RMS absolute error in terms of quartiles. In Figure 23, the combined middle two quartiles (i.e., from 25% to 75%) is smaller than the first (0% to 25%) and fourth (76% to 100%) quartiles, especially for look-ahead time larger than 200 seconds. In Figure 24, the distribution is more evenly distributed, except for look-ahead time larger than 150 seconds where the fourth quartile (75% to 100%) grows quickly.

Figure 25 to Figure 26 give the sample average over all 100 flights and the 95% confidence interval for the mean of the median of the absolute error and the relative error, respectively. The sample average X_{bar} for measure X (e.g., median or RMS) as a function of τ is given by:

$$X_{bar}(\tau) = [\Sigma_{i=0..99} X_i(\tau)]/n,$$

where $X_i(\tau)$ is the measure for the i-th flight and look-ahead τ. Variable n is equal to the number of samples (i.e., 100). The sample variance is given by:

$$S^2(\tau) = \{\Sigma_{i=0..99} [X_i(\tau) - X_{bar}(\tau)]^2\}/n$$

The half-width for the 100(1-α)% confidence interval is given by:

$$HW(\tau) = t_{n-1,1-\alpha/2} \sqrt{[S^2(\tau)/n]},$$

where $t_{n-1,1-\alpha/2}$ is the upper 1-α/2 critical point for the t distribution with n-1 degrees of freedom [16]. The confidence interval for the mean of measure X is given by:

$$CI = X_{bar}(\tau) \pm HW(\tau)$$

Notice in Figure 25 and Figure 26 that the mean of the median error increases relatively quickly for look-ahead time between 0 and 100 seconds, and then the medians increase much more slowly or decrease. This is a counterintuitive result that deserves a closer examination in a future study to understand the causes and implications. Also, notice that the confidence intervals increase slowly as the look-ahead time increases.

Figure 27 and Figure 28 show the sample averages and confidence intervals for the mean of the RMS absolute error and relative error for the altitude prediction. The most salient feature in both plots is the change in slope at around look-ahead of 50 seconds. The curve for RMS absolute error more or less stabilizes thereafter, but the curve for RMS relative error continues to increase with the look-ahead time. Here again, in both cases, the confidence interval becomes wider as the look-ahead time increases. This means that the variability of the RMS error (i.e., second order variability) increases with the look-ahead time.

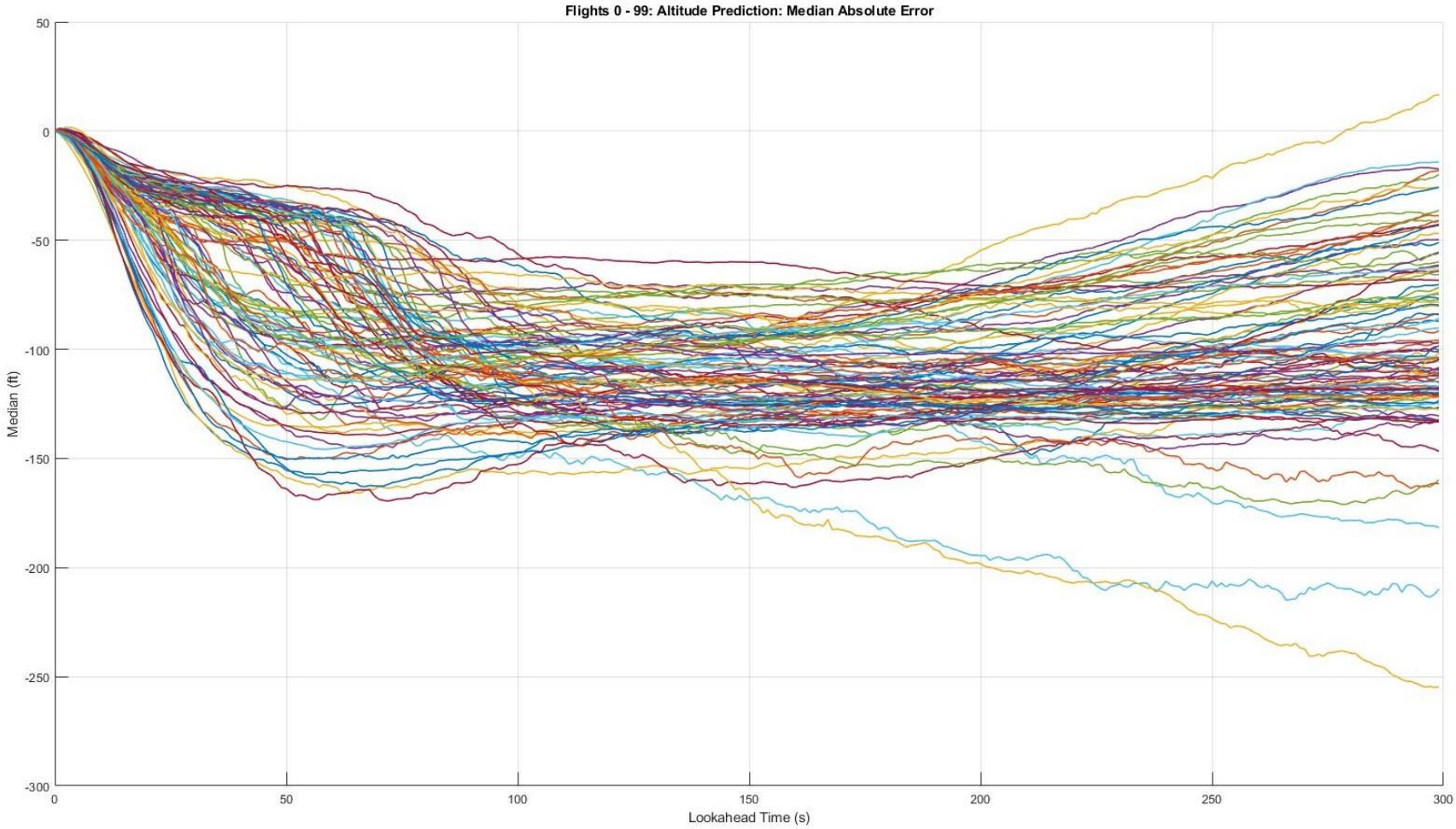

Figure 21: Flights 0 - 99: Median Absolute Error of Altitude Prediction as a Function of Look-Ahead Time

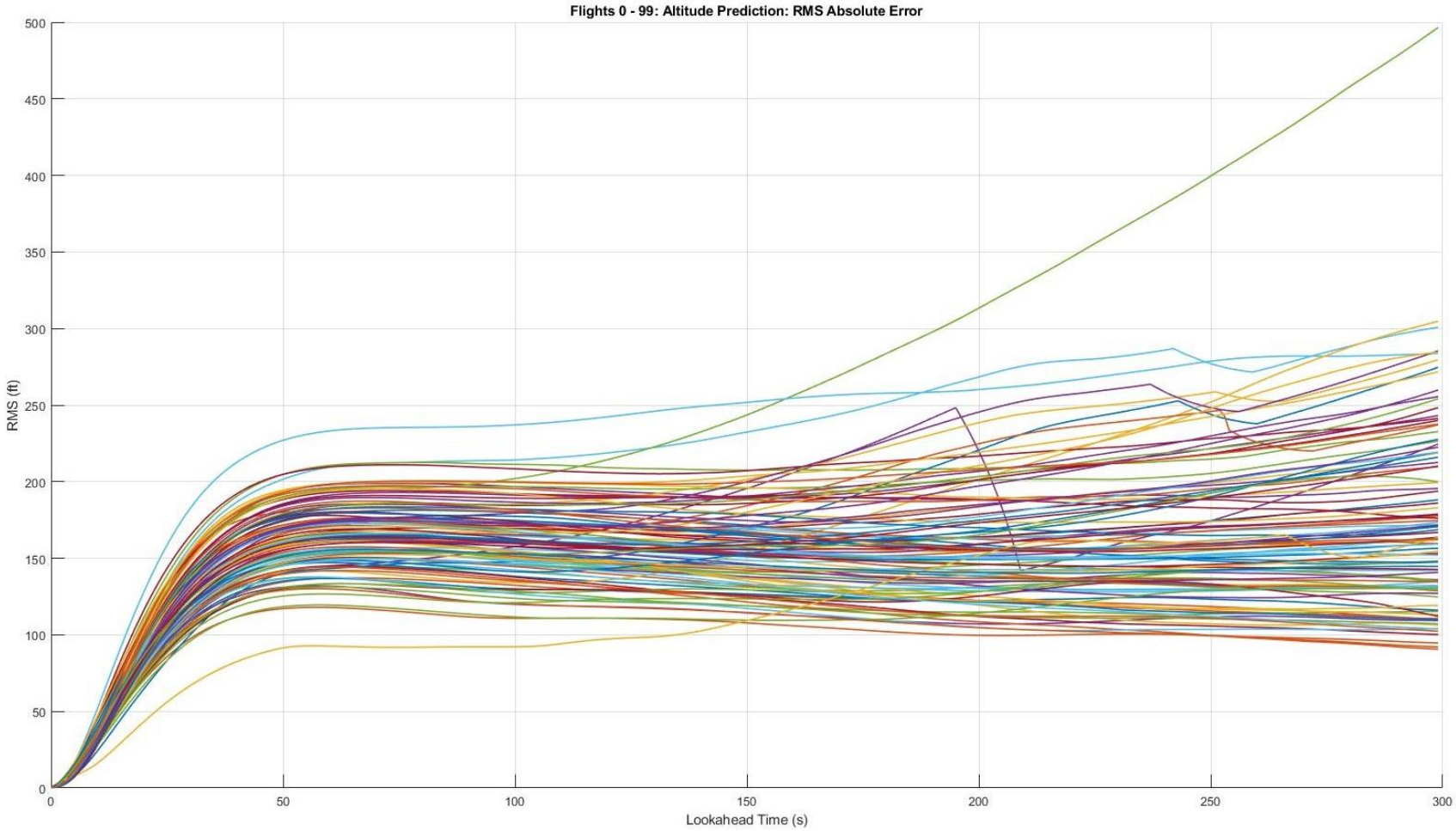

Figure 22: Flights 0 - 99: RMS Absolute Error of Altitude Prediction as a Function of Look-Ahead Time

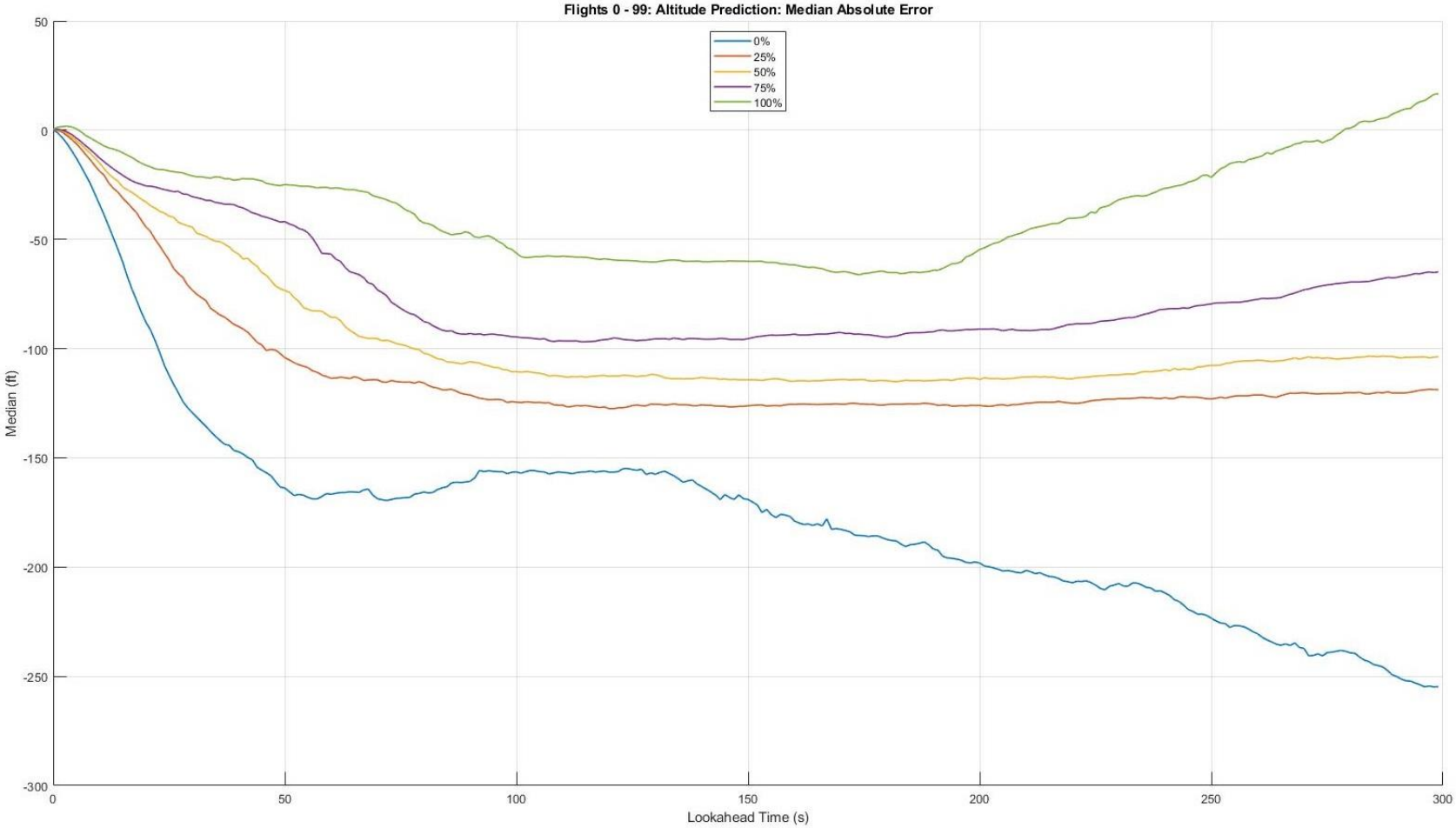

Figure 23: Flights 0 - 99: Quartiles of Median Absolute Error for Altitude Prediction as a Function of Look-Ahead Time

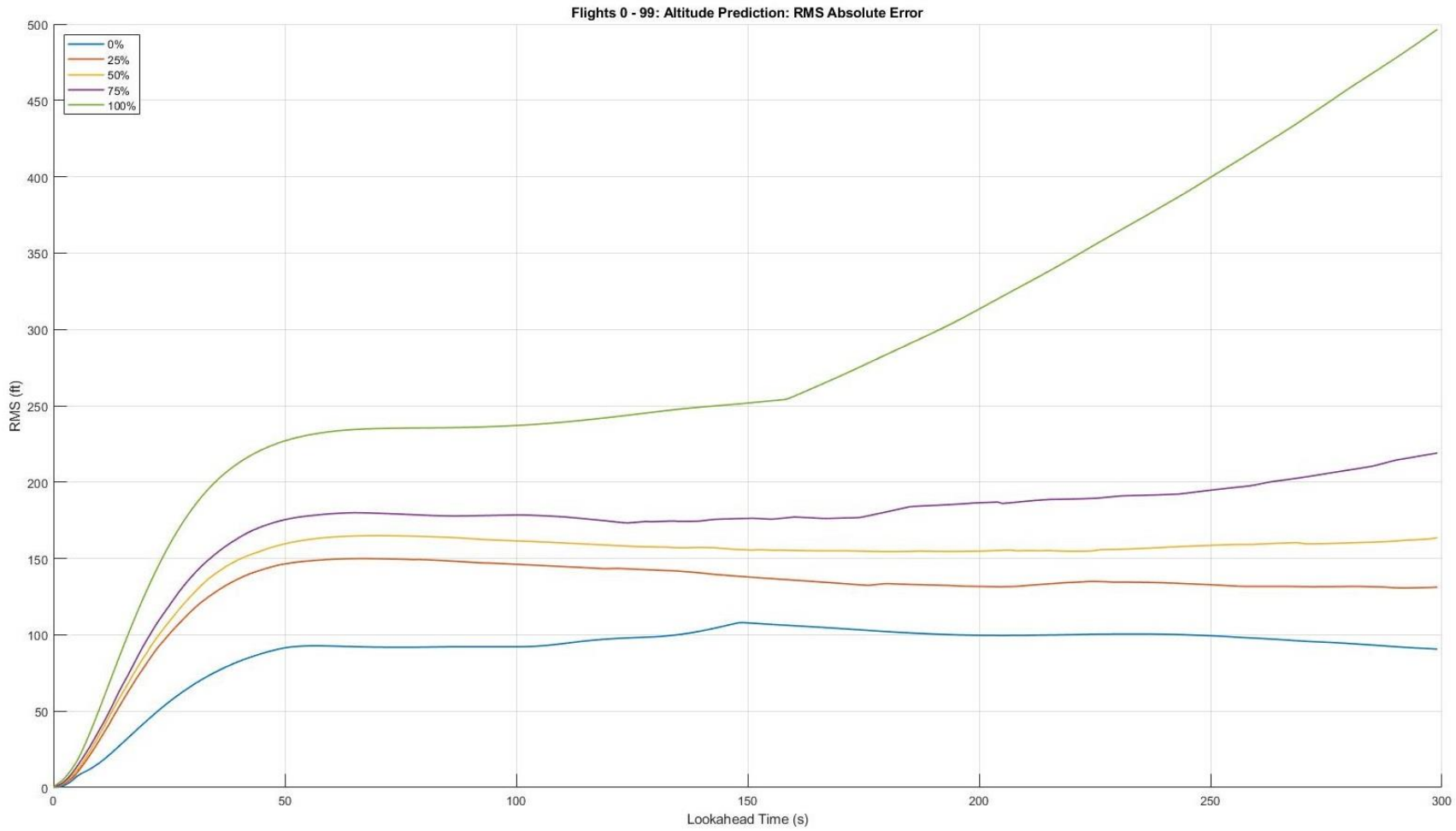

Figure 24: Flights 0 - 99: Quartiles of RMS Absolute Error for Altitude Prediction as a Function of Look-Ahead Time

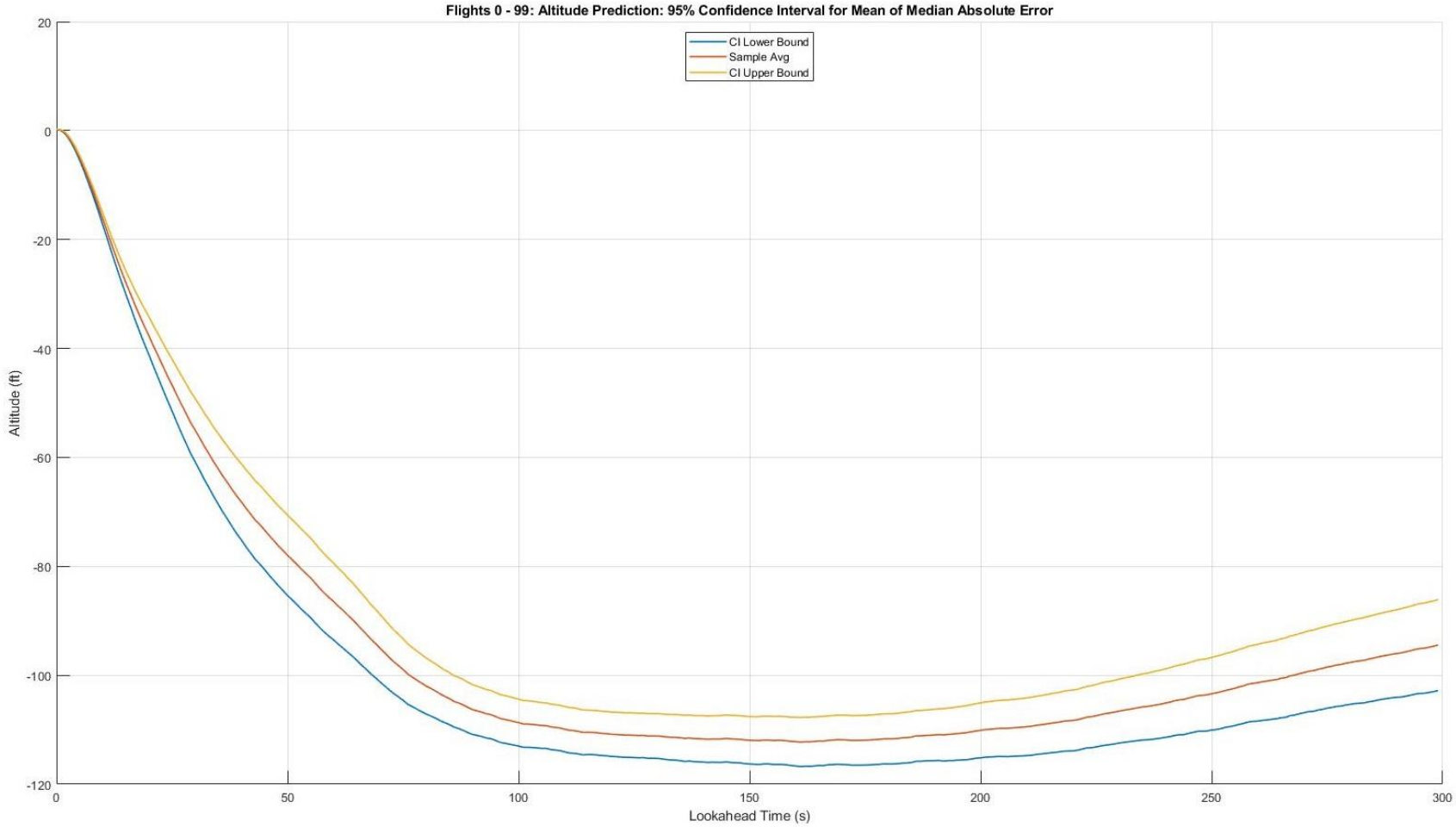

Figure 25: Mean Median Absolute Error of Altitude Prediction: Sample Average and 95% Confidence Interval as a Function of Look-Ahead Time

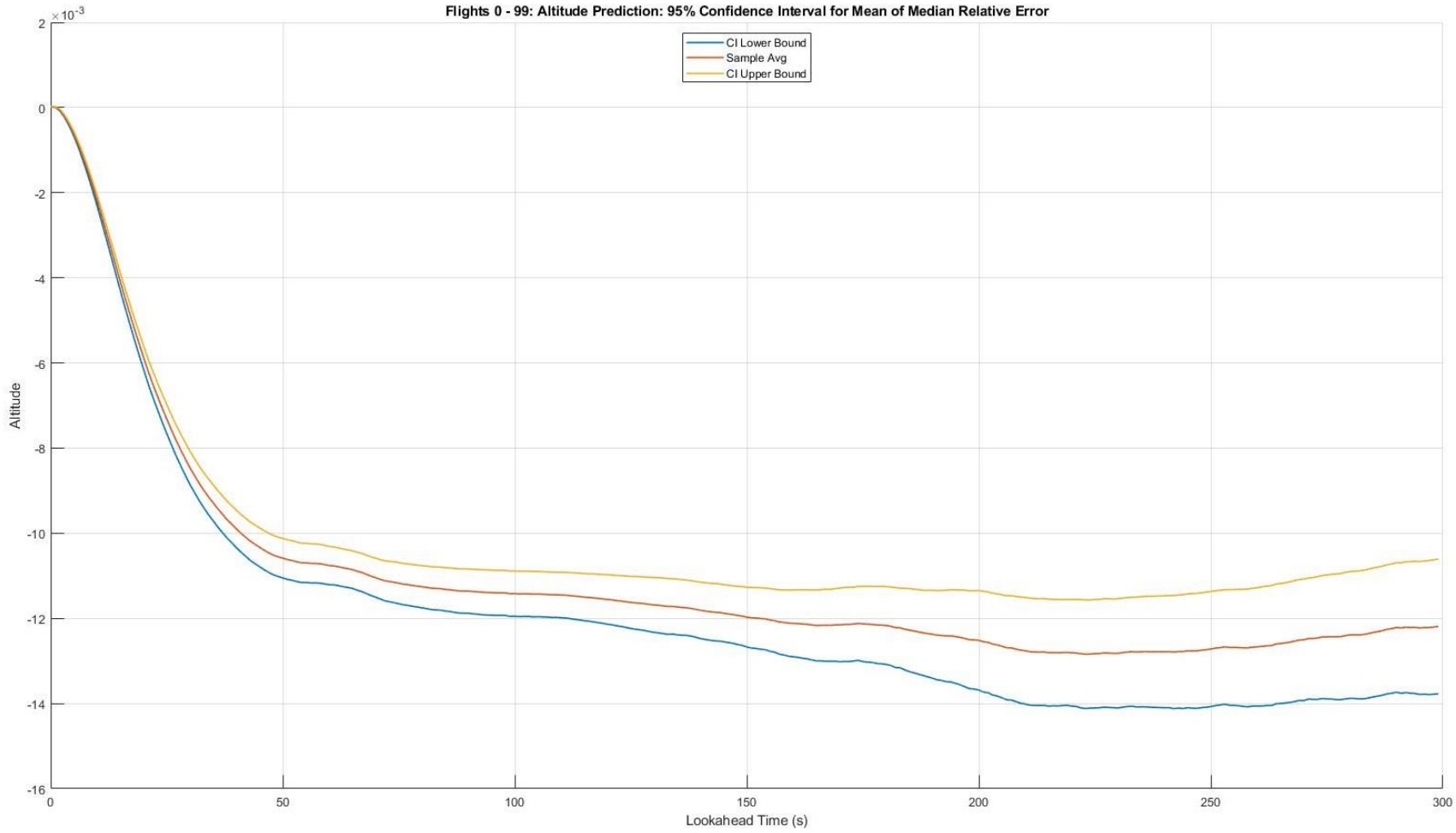

Figure 26: Mean Median Relative Error of Altitude Prediction: Sample Average and 95% Confidence Interval as a Function of Look-Ahead Time

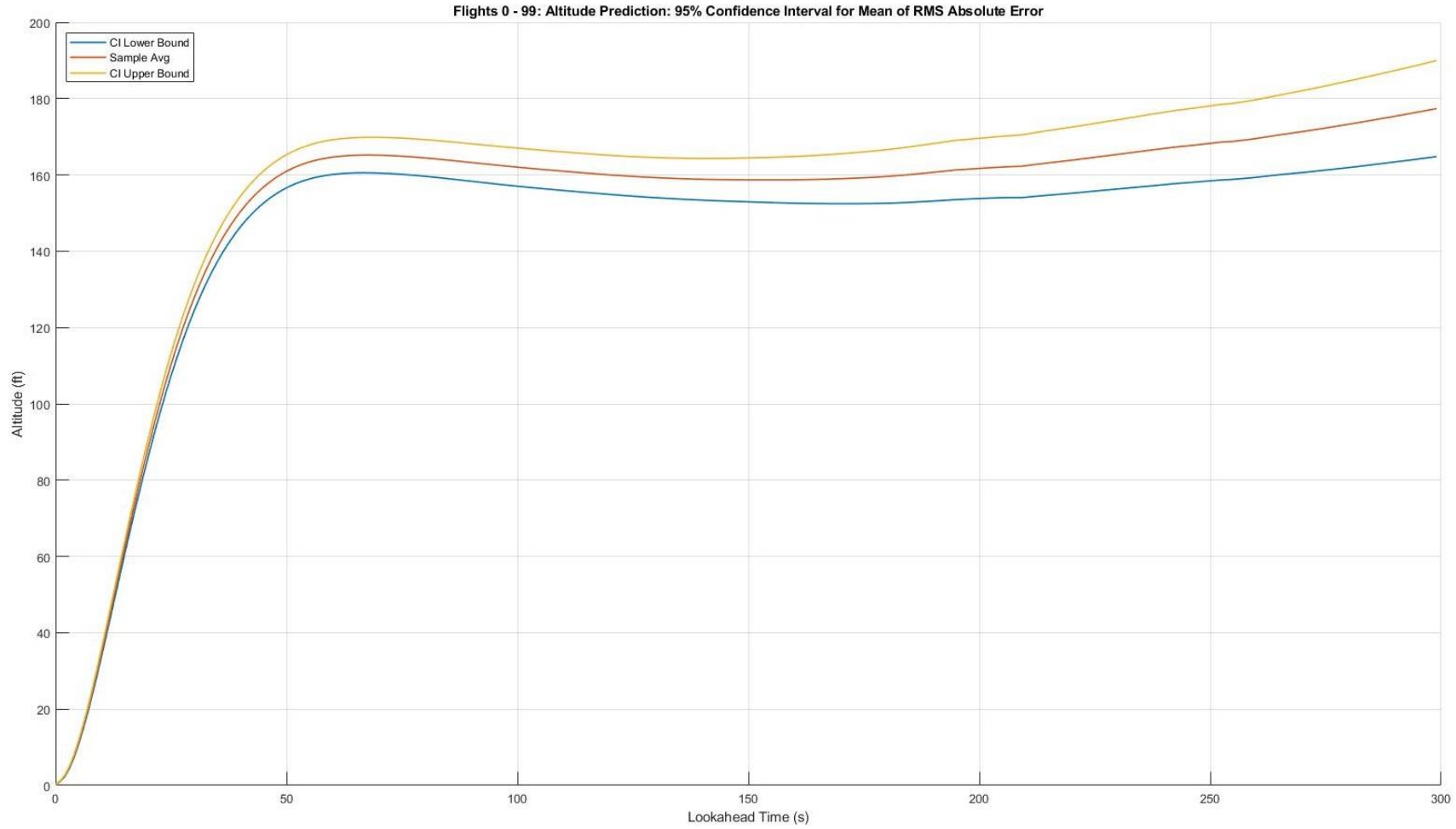

Figure 27: Mean RMS Absolute Error of Altitude Prediction: Sample Average and 95% Confidence Interval as a Function of Look-Ahead Time

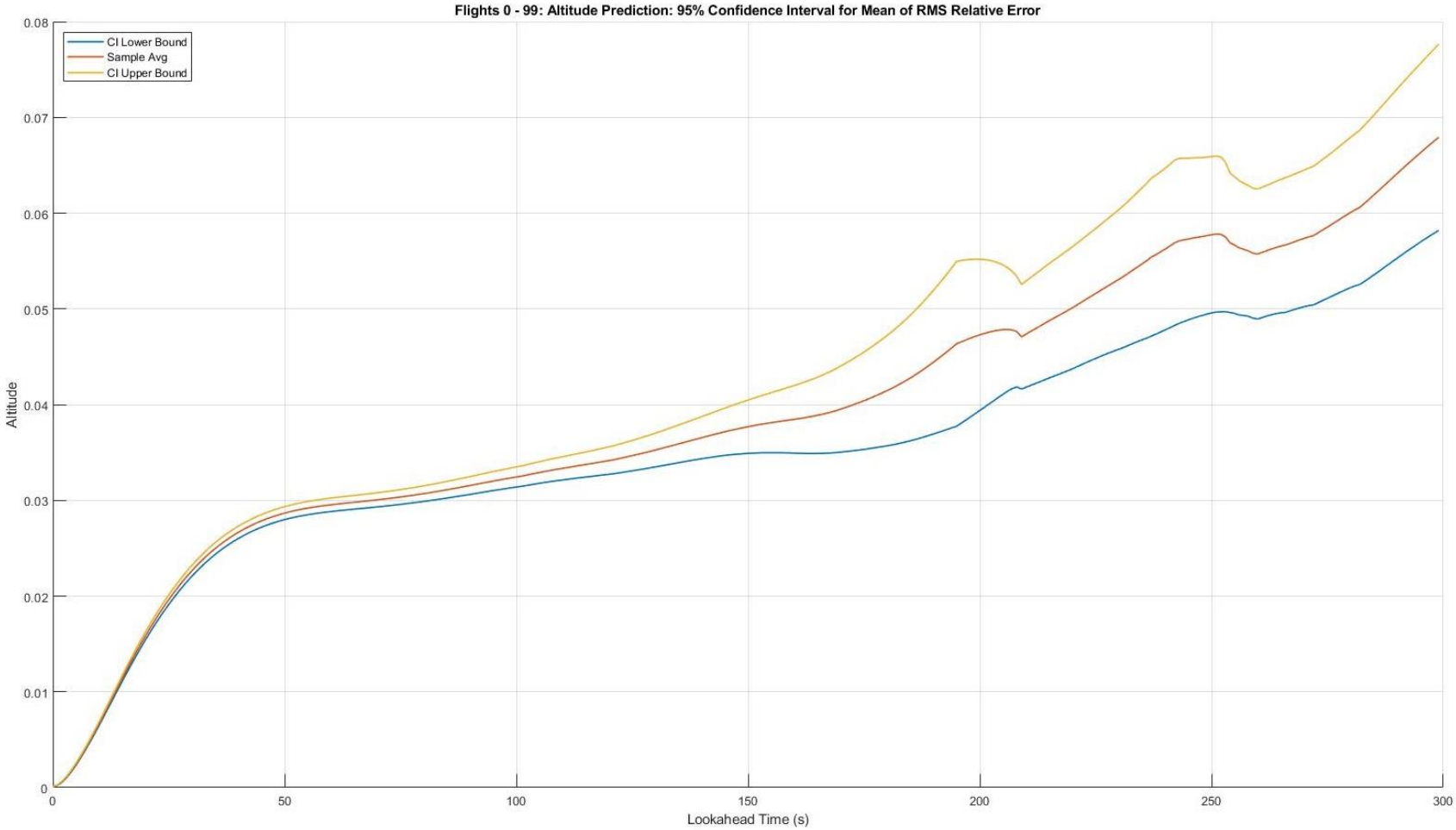

Figure 28: Mean RMS Relative Error of Altitude Prediction: Sample Average and 95% Confidence Interval as a Function of Look-Ahead Time

7.2. Airspeed Prediction

Figure 29 to Figure 36 show the main results for the quantification of airspeed prediction uncertainty. Figure 29 and Figure 30 show the median and RMS absolute error as a function of look-ahead time τ for the 100 test flights. For the median in Figure 29, notice that the distribution is fairly symmetric in the range ±5 kt, and also that most of the curves are negative across the full range of the look-ahead time. In Figure 30, one salient feature is how the RMS increases quickly until around look-ahead time of about 35 second and then stabilizes for almost every flight. The other salient feature in Figure 30 are the four outliers with large peaks at look-ahead time of about 70 seconds. Also notice the performance curve that clearly separates itself from the rest starting at look-ahead time of about 240 seconds and reaching a value of 15 kt for look-ahead time of 300 seconds.

Figure 31 and Figure 32 quantify the distributions of the median and RMS absolute error in terms of quartiles. In Figure 31, notice how the inter-quartile range (the range between 25% and 75%) is much smaller than the first quartile (from 0% to 25%) and the fourth quartile (from 75% to 100%) across the range of the look-ahead time. This is an indication that the majority of the flights have very similar prediction performance with respect to central tendency. In Figure 32, the range of the first three quartiles combined (from 0% to 75%) is smaller than the range of the fourth quartile (75% to 100%). This suggests the presence of prediction performance outliers.

Figure 33 to Figure 36 give the sample average over all 100 flights and the 95% confidence interval for the mean of the median and the RMS for both the absolute error and the relative error. Comparing Figure 33 and Figure 34 for the median, notice that the shapes of the curves are very similar, which is an indication that the bias component of the prediction error at lower airspeed is not more significant than at higher airspeed; otherwise the curves for the relative error would be clearly different than the curves for the absolute error because that the relative error emphasizes prediction error for smaller observed airspeed values. Also notice that the width of the confidence intervals increases up to a look-ahead time of 100 seconds and remains approximately constant from then on. Comparing Figure 35 and Figure 36, the shapes of the curves are again very similar, which is an indication that the dispersion error at lower airspeeds is not more significant than the error at higher airspeed. In addition, notice that the width of the confidence intervals is largest in the look-ahead range from about 35 seconds to 180 seconds, and from then on it seems to stabilize. This is an interesting characteristic that may be worth a closer examination in a future study to gain insight into the factors that influence the performance of the prediction function.

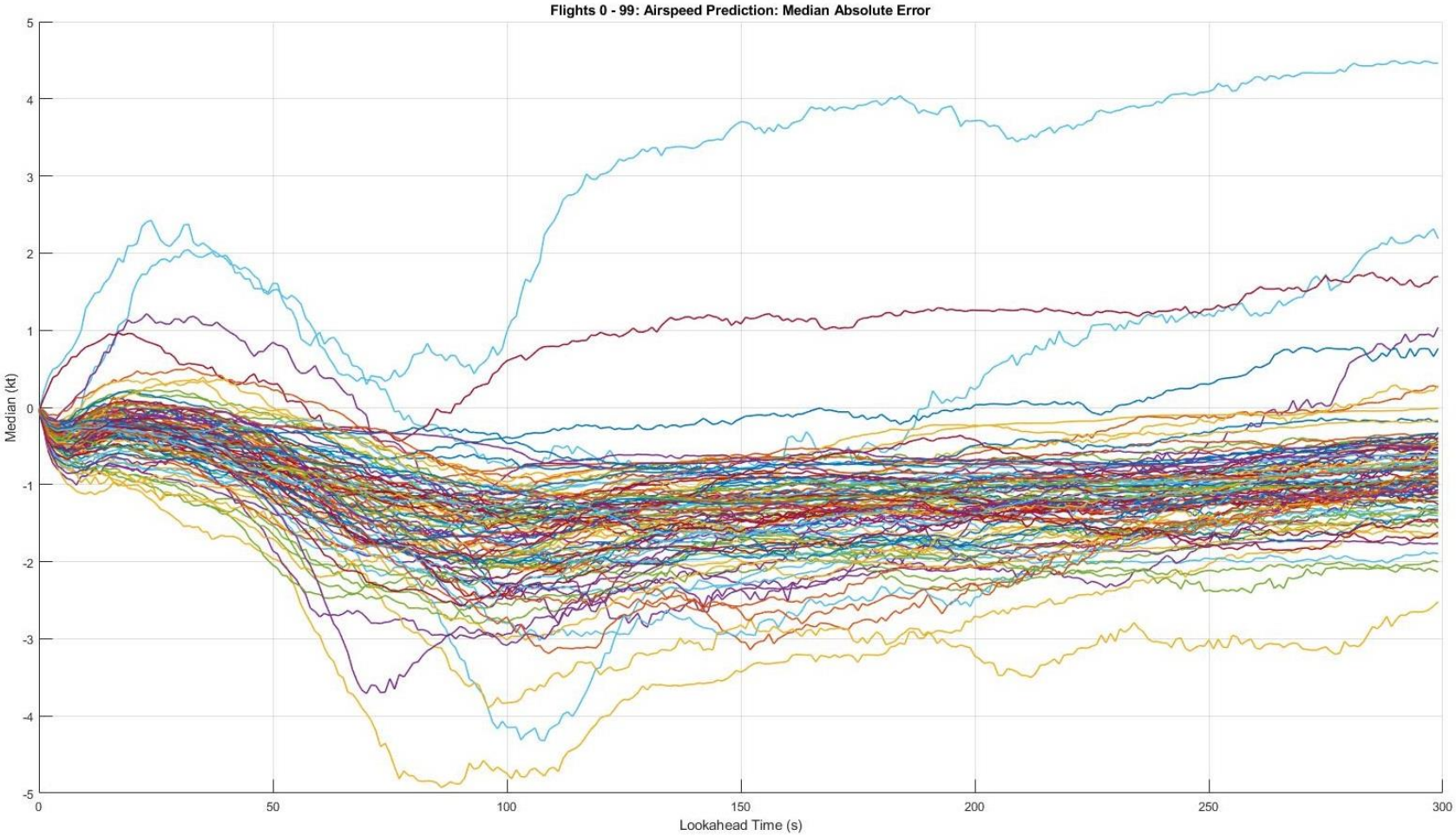

Figure 29: Flights 0 - 99: Median Absolute Error of Airspeed Prediction as a Function of Look-Ahead Time

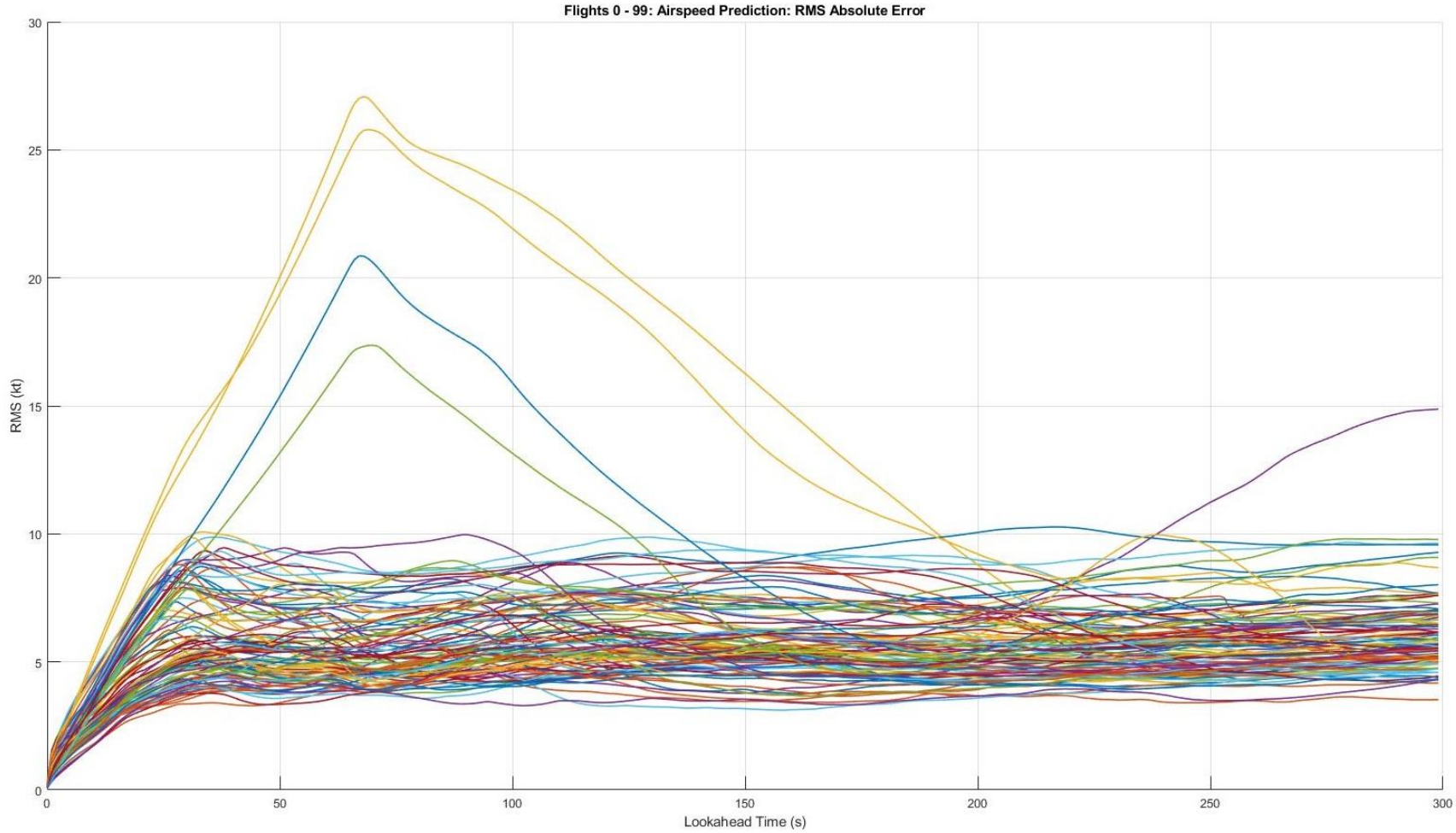

Figure 30: Flights 0 - 99: RMS Absolute Error of Airspeed Prediction as a Function of Look-Ahead Time

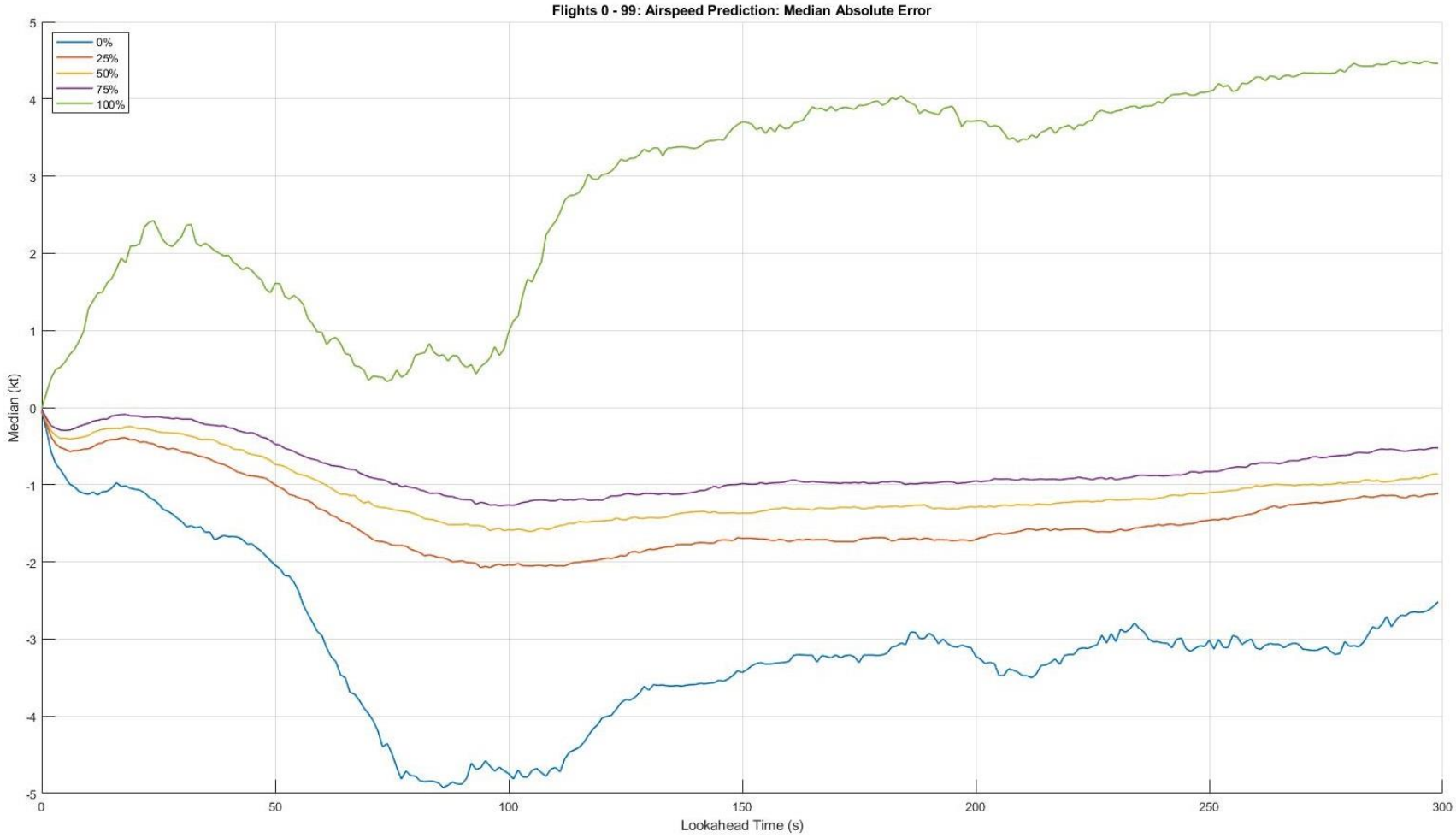

Figure 31: Flights 0 - 99: Quartiles of Median Absolute Error for Airspeed Prediction as a Function of Look-Ahead Time

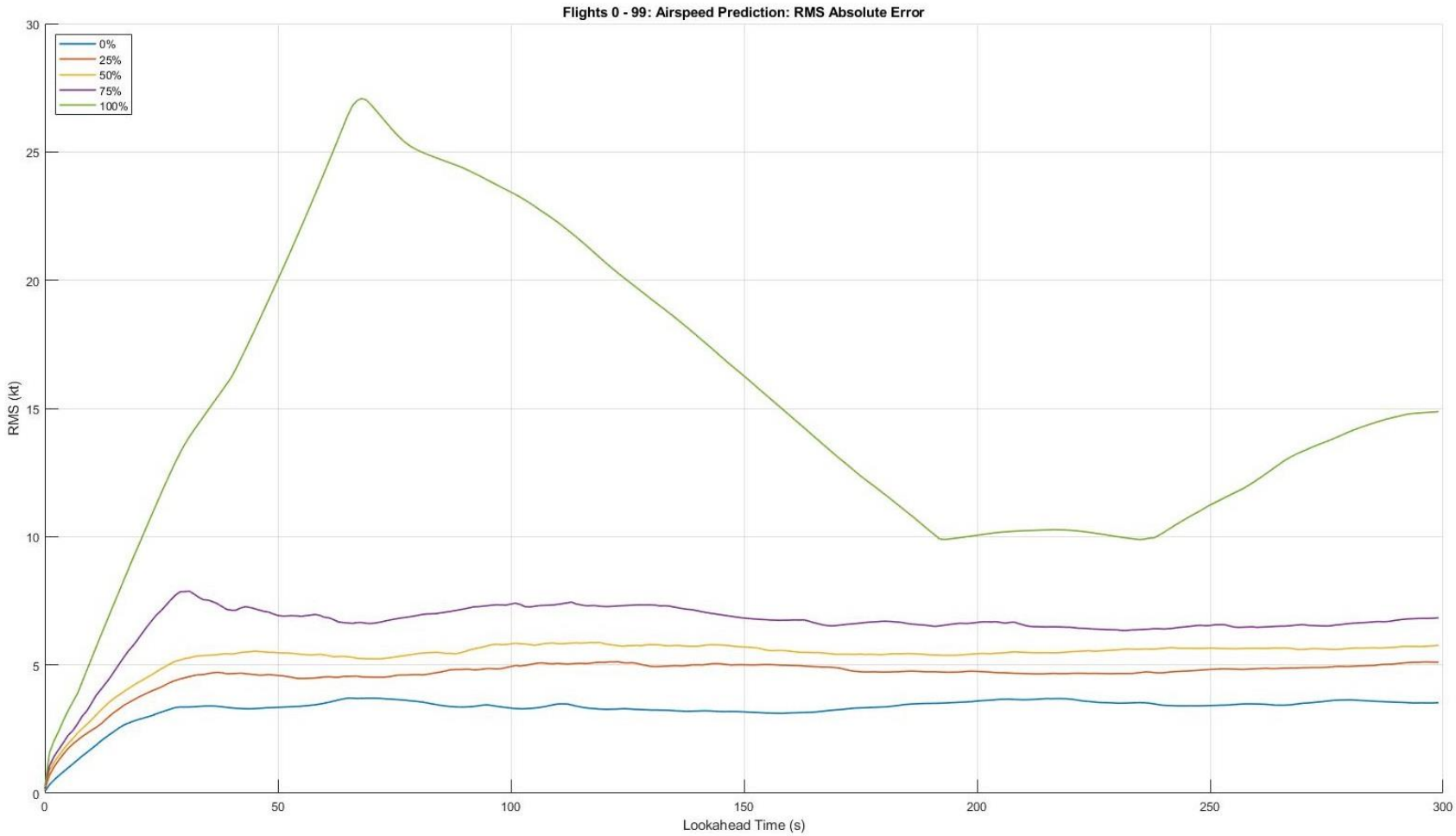

Figure 32: Flights 0 - 99: Quartiles of RMS Absolute Error for Airspeed Prediction as a Function of Look-Ahead Time

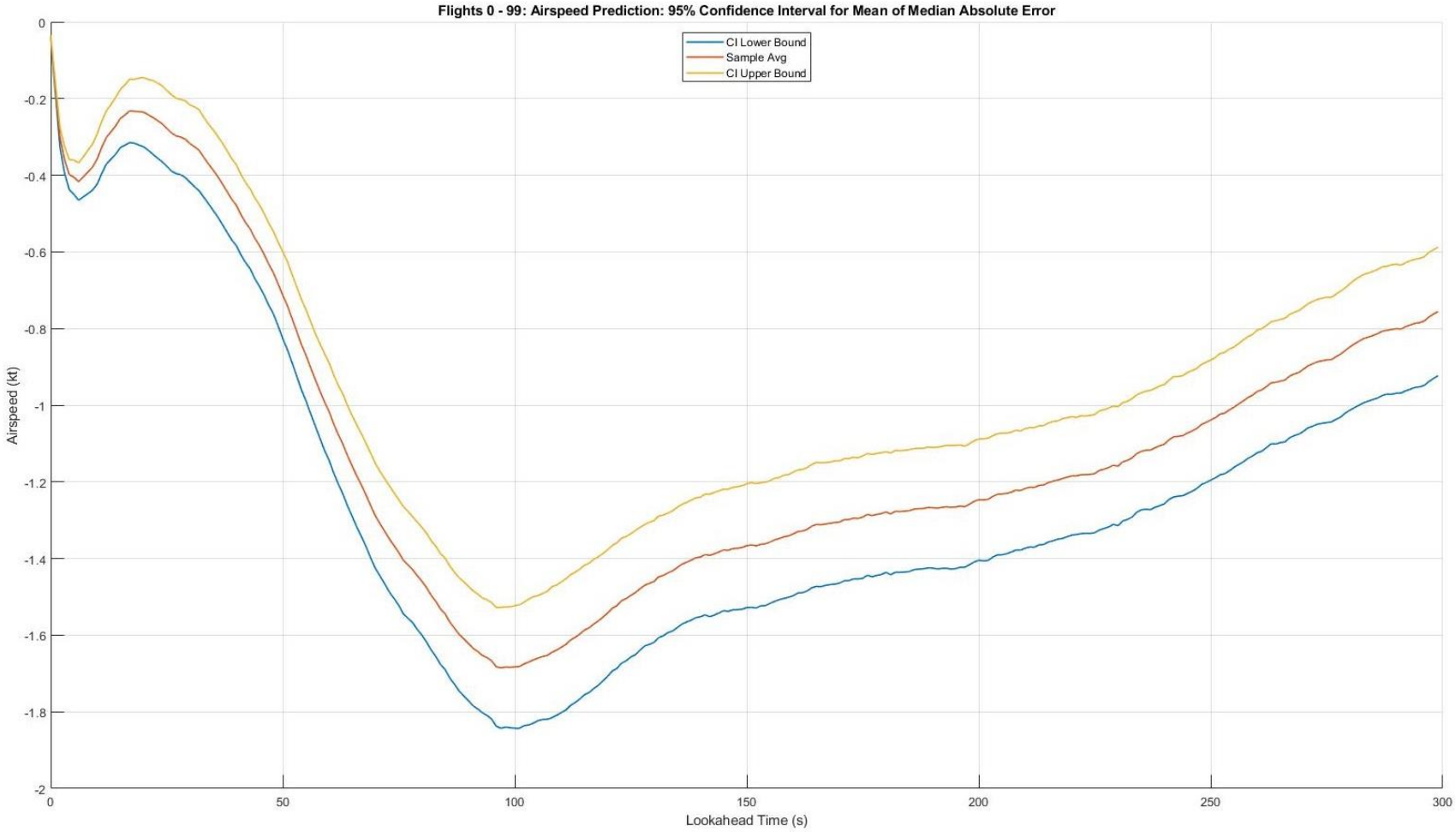

Figure 33: Mean Median Absolute Error of Airspeed Prediction: Sample Average and 95% Confidence Interval as a Function of Look-Ahead Time

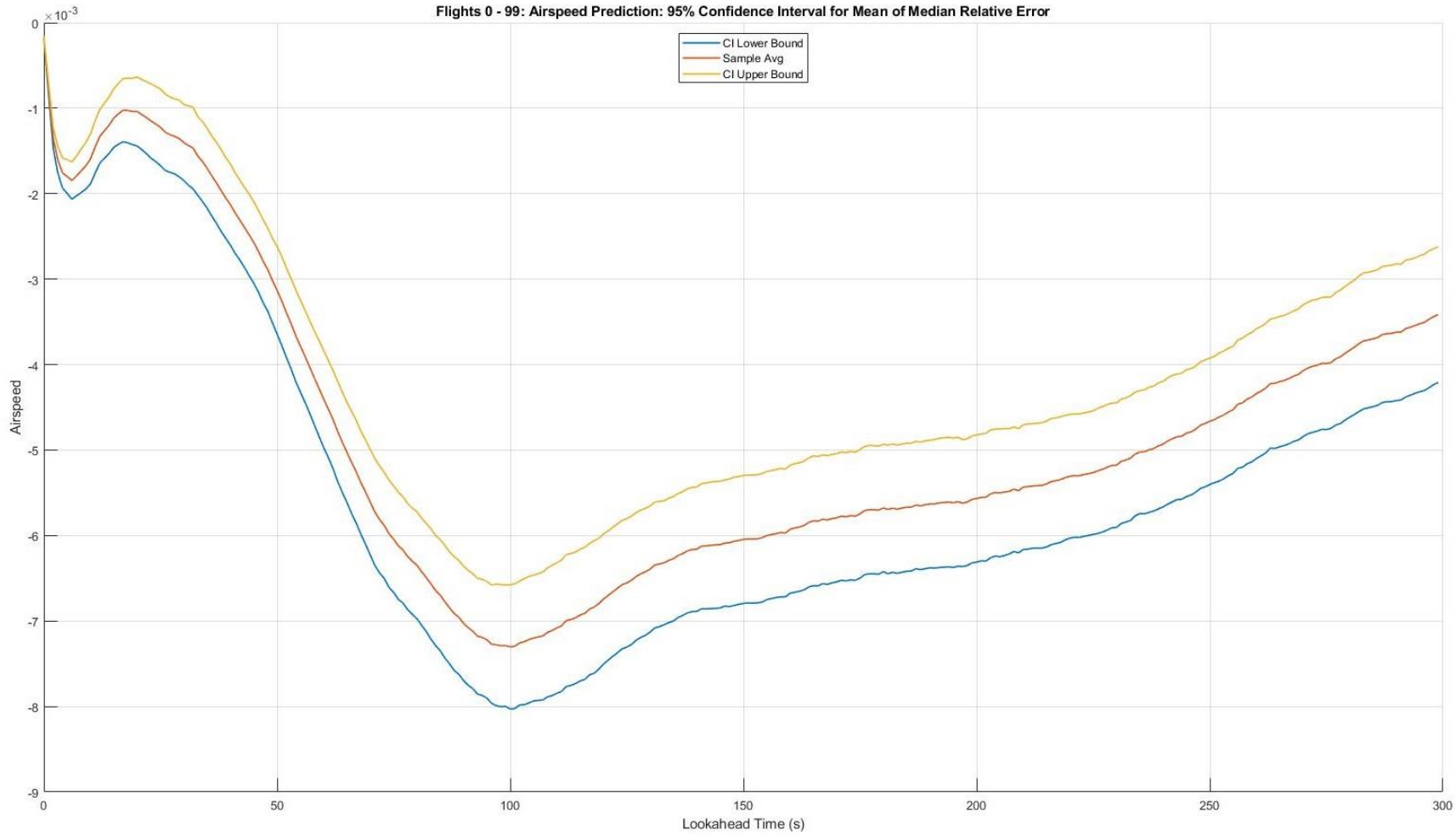

Figure 34: Mean Median Relative Error of Airspeed Prediction: Sample Average and 95% Confidence Interval as a Function of Look-Ahead Time

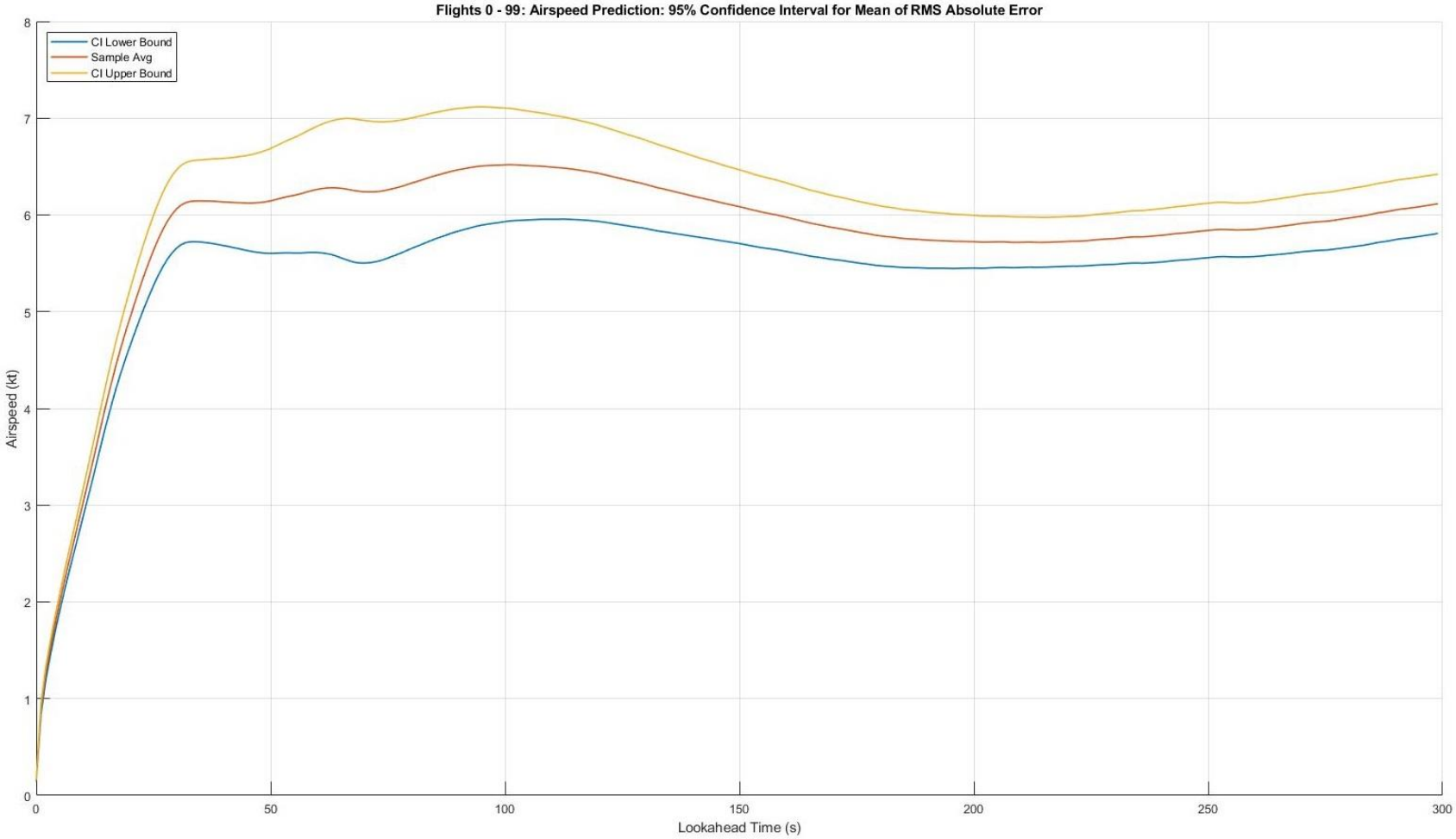

Figure 35: Mean RMS Absolute Error of Airspeed Prediction: Sample Average and 95% Confidence Interval as a Function of Look-Ahead Time

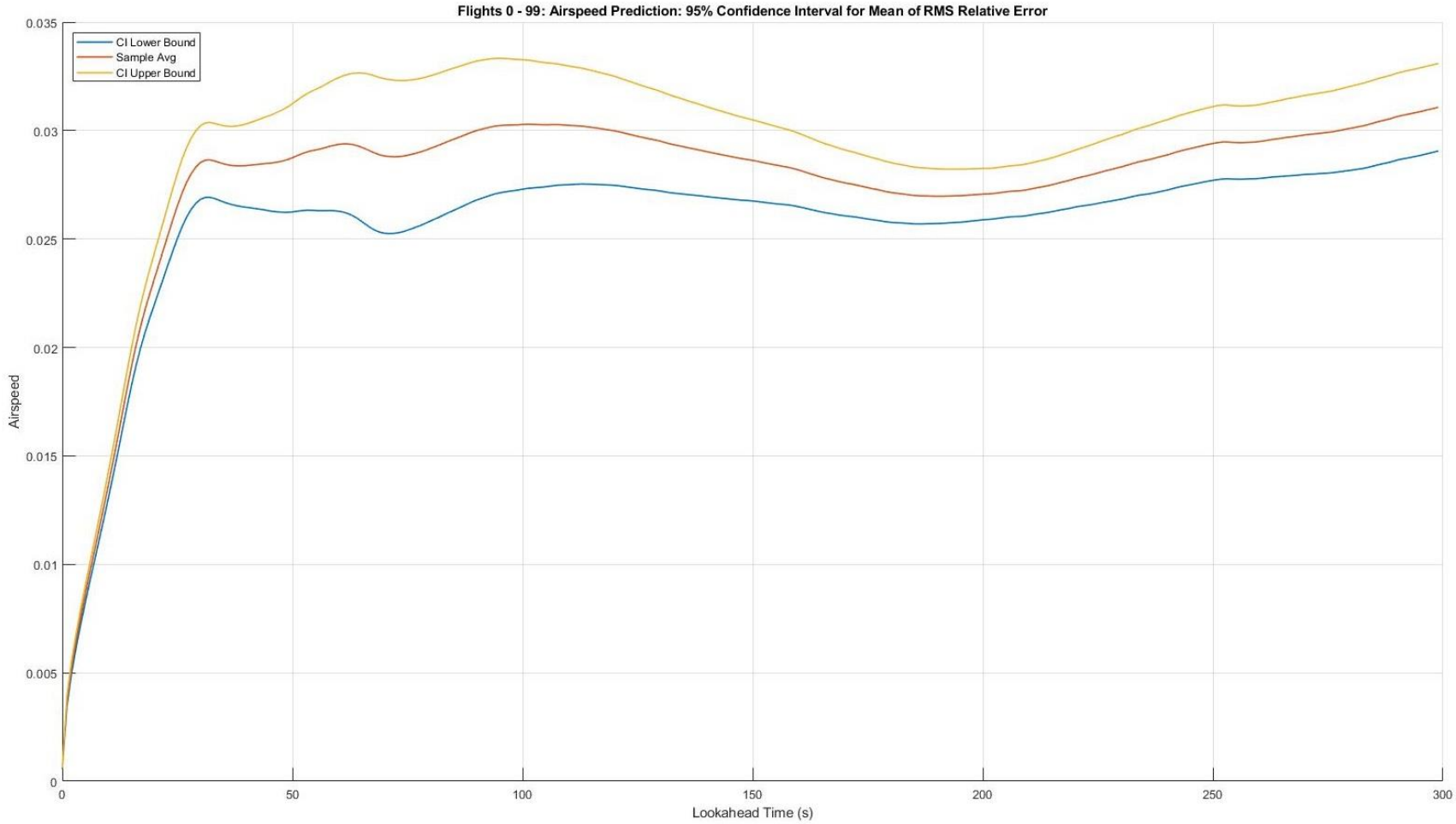

Figure 36: Mean RMS Relative Error of Airspeed Prediction: Sample Average and 95% Confidence Interval as a Function of Look-Ahead Time

7.3. Prediction Performance Outliers

The next part of the uncertainty quantification analysis is to identify outliers for altitude and airspeed prediction performance. Two major considerations for this are that there are no precise objective criteria to identify outliers or anomalous predictions, and that the number of flights with prediction performance that stands out from the rest can be too large to conduct a detailed analysis. Figure 37 is an example of this situation. The red circle marks a set of about eleven flights that could be labeled as outliers for this particular performance measure. Other performance measures may have a different set of outliers.

A three-part approach was chosen to identify outliers based on the curves of prediction performance measures. The first part was to limit the search and identification of outliers to the RMS and maxAbs plots for both absolute and relative error. This is a reasonable choice considering that the distribution and confidence intervals for the median error are very small compared to the RMS and maxAbs.

For the second part of the approach, the outliers were identified by visual inspection of the RMS and maxAbs plots. Figure 37 is an example. This identification resulted in the eight groups of outliers listed in Table 4. Appendix C gives the prediction performance curves that were identified as candidate outliers. Notice that many of the outliers listed in Table 4 are repeated in different rows. This is an indication that the performance of the predictor for those outlier flights was fundamentally different than for the other flights.

Table 4: Identified Outliers for Prediction Performance Measures of Error Dispersion

Performance Measures			**Outliers**
Altitude Prediction	RMS	Absolute Error	11
		Relative Error	3, 5, 16, 23, 35, 36, 66, 79, 86, 91, 95
	maxAbs	Absolute Error	3, 5, 11, 35, 36, 66
		Relative Error	3, 5, 16, 23, 35, 36, 66, 86
Airspeed Prediction	RMS	Absolute Error	3, 23, 79, 91, 95
		Relative Error	3, 23, 79, 91, 95
	maxAbs	Absolute Error	3, 23, 36, 79, 91, 95
		Relative Error	3, 23, 36, 79, 86, 91, 95

The third part of the approach was to combine these outliers into a single group:

Prediction Performance Outliers: {3, 5, 11, 16, 23, 35, 36, 66, 79, 86, 91, 95}

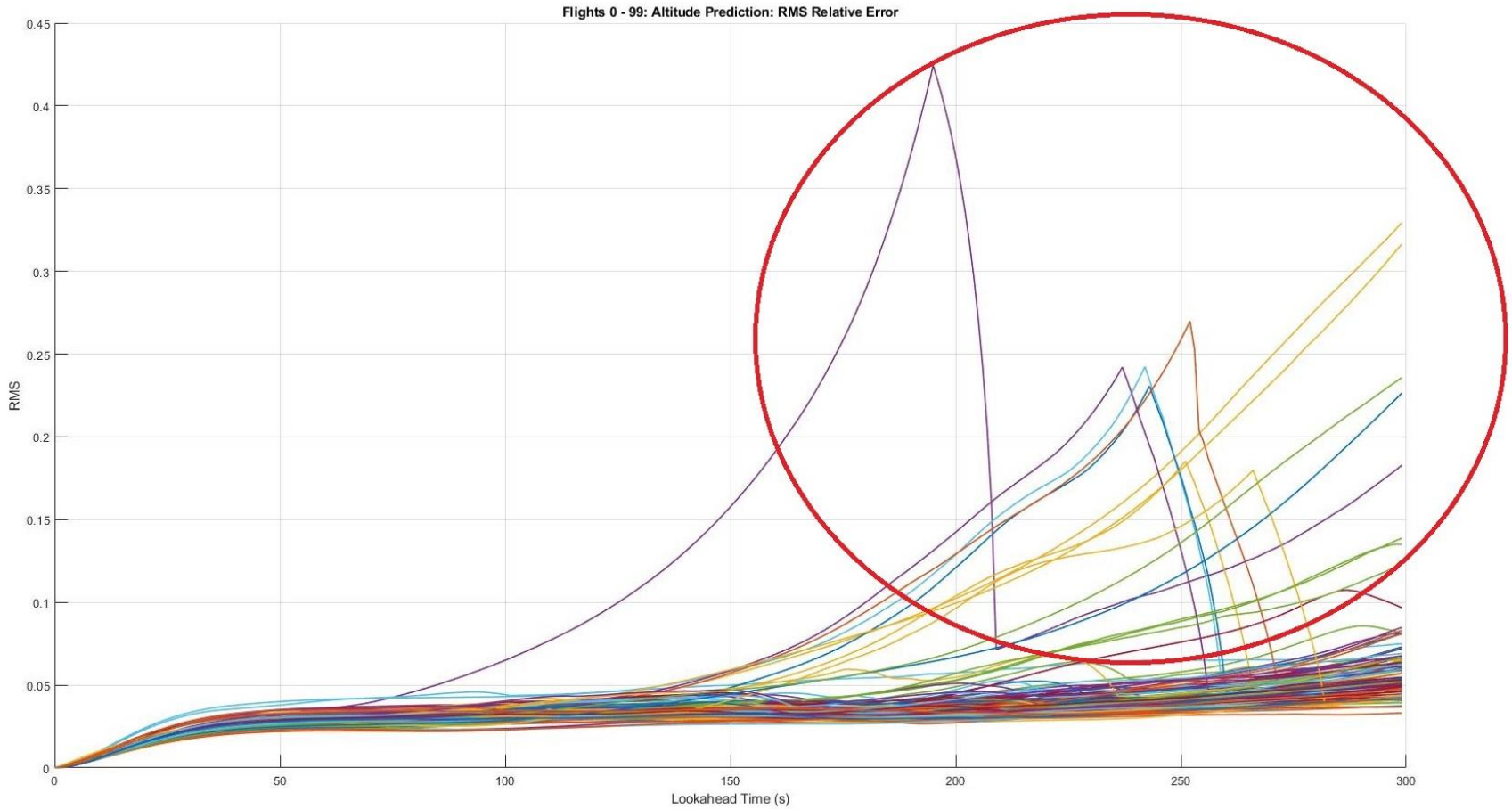

Figure 37: Flights 0 - 99: Outliers for RMS Relative Error of Altitude Prediction as a Function of Look-Ahead Time

8. Factor Analysis

The purpose of this analysis is to determine the relative effect of the controlled factors on prediction performance. This is accomplished by modeling the relation between controlled factors and prediction performance measures in terms of polynomial functions and applying regression analysis to fit the polynomials to the data. An iterative exploration process is used in which polynomial functions are postulated, refined, and evaluated until there is reasonable evidence that the best model has likely been achieved, for a given amount of invested effort. The considerations in the application of this approach are that it introduces subjectivity in the development and assessment of the model, and that the polynomial regression analysis provides an approximation function whose output is only statistically correlated to the actual data. The polynomial model fitted by regression analysis is an arbitrary black-box model, not a causal model of the mechanisms by which the controlled factors determine prediction performance. Nevertheless, this modeling approach is useful for the purpose of evaluating the relative importance of the controlled factors on the performance of the predictor.

The modeling polynomials considered were primarily first, second, and quadratic order, both with and without two-way interaction terms. The following list gives the general form of these polynomials for n independent variables X_1 to X_n and one dependent variable Y. These polynomials can model increasingly complex relations. Also, if the independent variables are scaled to the range of ±1, the a and b coefficients capture the weight (i.e., importance) of the variables and their interactions.

- First-order polynomial:

  $Y = P_1(X) = a_0 + a_1X_1 + .. + a_nX_n$

- First-order polynomial plus two-way interaction terms:

  $Y = P_{1i}(X) = P_1(X) + a_{1,2}X_1X_2 + .. + a_{1,n}X_1X_n + a_{2,3}X_2X_3 + .. + a_{1,n}X_1X_n + .. + a_{n-1,n}X_{n-1}X_n$

- Second-order polynomial:

  $Y = P_2(X) = P_{1i}(X) + a_{1,1}X_1^2 + .. + a_{n,n}X_n^2$

- Second-order polynomial plus quadratic two-way interaction terms:

  $Y = P_{2i}(X) = P_2(X) + b_{1,2}(X_1X_2)^2 + .. + b_{1,n}(X_1X_n)^2 + b_{2,3}(X_2X_3)^2 + .. + b_{1,n}(X_1X_n)^2 + .. + b_{n-1,n}(X_{n-1}X_n)^2$

The prediction performance measure chosen for this analysis was the integral of the RMS absolute error curve as a function of look-ahead time. For example, this is the integral of one of the curves in

Figure 22. Let RMS(τ) denote the RMS prediction performance for look-ahead τ, and let C_{RMS} denote the sum (i.e., the integral) of RMS(τ) for τ = 0 … 299. Then:

$$C_{RMS} = \Sigma_{\tau=1 \,..\, 299} \, RMS(\tau)$$

This cumulative measure does not have information about the effect of the look-ahead time, which is not a test variable, but it captures the overall effect of the controlled factors on prediction performance.

A total of six polynomial models were developed, including models for absolute and relative error of altitude, airspeed, and energy prediction. Two important concerns arose in the development of these models. One concern was that the wind speed and the wind direction are not entirely independent controlled variables since, as described in Section 3, the maximum wind speed must satisfy a constraint as a function of wind direction. The second concern was that the wind direction is specified as a linear variable in the range of 0 to 360, but this actually is a circular (or polar) variable such that the distance between angles θ_1 and θ_2 is $\min\{|\theta_1 - \theta_2|, |360^o + \theta_1 - \theta_2|\}$. Neither of these was explored in detail because the goal of the analysis is to derive qualitative insights from the models about the effect of the controlled variables on prediction performance. Future studies should examine these concerns more carefully.

8.1. Models for Absolute Prediction Error

Three polynomial models were developed for the cumulative RMS of the absolute prediction error, one each for altitude, airspeed, and energy.

8.1.1. Altitude

Table 5 gives the terms and coefficients of the model. This model has R-squared value of 0.75 and the output has a linear correlation coefficient ρ of 0.85 after removing the results for test flights 3, 11, 12, 27, and 79, which are considered outliers relative to this performance measure. Figure 38 shows the scatter plot of the actual prediction performance measure and the output of the model.

Generally, any term with a p-value smaller than 0.05 is considered a meaningful addition to the model. The p-value of the WindGradient term is larger than this, but the term was retained because removing it increases the R-squared value of the model. The R-squared value measures the fraction of the variability in the dependent variable that can be explained by the model.

The model in Table 5 indicates that wind direction is the single most important factor in prediction performance and that there is a strong interaction between wind speed and wind direction. The initial altitude is a significant factor, as well as wind gradient, gust intensity, and gust gradient. Overall, this

model says that altitude prediction performance is strongly dependent on weather factors, especially wind direction and wind speed.

Table 5: Terms and Coefficients of Polynomial Model for Cumulative RMS Absolute Error of Altitude Prediction

Terms	Coefficients	P-value
Intercept	38,774.08	3.52E-72
WindDir^2	20,266.05	2.16E-18
Altitude	7,013.84	3.34E-16
Gust * GustGradient	2,877.04	2.60E-02
WindGradient	1,327.30	6.98E-02
(Wind *WindDir)^2	-20,050.92	1.30E-06

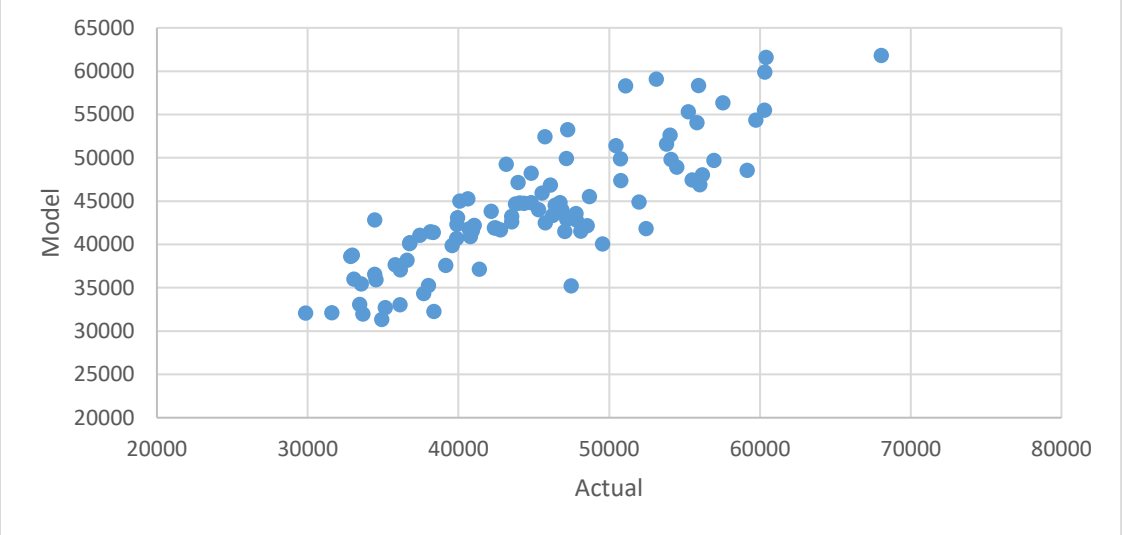

Figure 38: Scatter Plot of Actual and Modeled Cumulative RMS Absolute Error of Altitude Prediction ($\rho = 0.85$)

8.1.2. Airspeed

The terms and coefficients of the model are given in Table 6. This model has R-squared value of 0.77 and the output has a linear correlation coefficient ρ of 0.88 after removing the results for test flights 3, 16, 23, 25, 42, 66, 72, 79, 87, 91, and 95, which are considered outliers relative to this performance measure. Figure 39 shows the scatter plot of the actual prediction performance measure and the output of the model.

These results indicate that airspeed prediction performance is strongly dependent on the initial airspeed (based on large relative coefficients and quadratic term). Performance has quadratic dependencies on both wind gradient and wind direction. Initial altitude, wind speed, and gust intensity have the weakest effects on performance.

Table 6: Terms and Coefficients of Polynomial Model for Cumulative RMS Absolute Error of Airspeed Prediction

Terms	**Coefficients**	**P-value**
Intercept	1,499.26	4.74E-52
IAS	442.77	2.85E-24
IAS^2	302.53	3.39E-06
WindGradient^2	170.68	2.74E-03
WindDir^2	131.71	2.84E-02
Altitude	117.77	7.06E-05
Wind	96.47	4.44E-03
Gust	94.50	1.34E-03

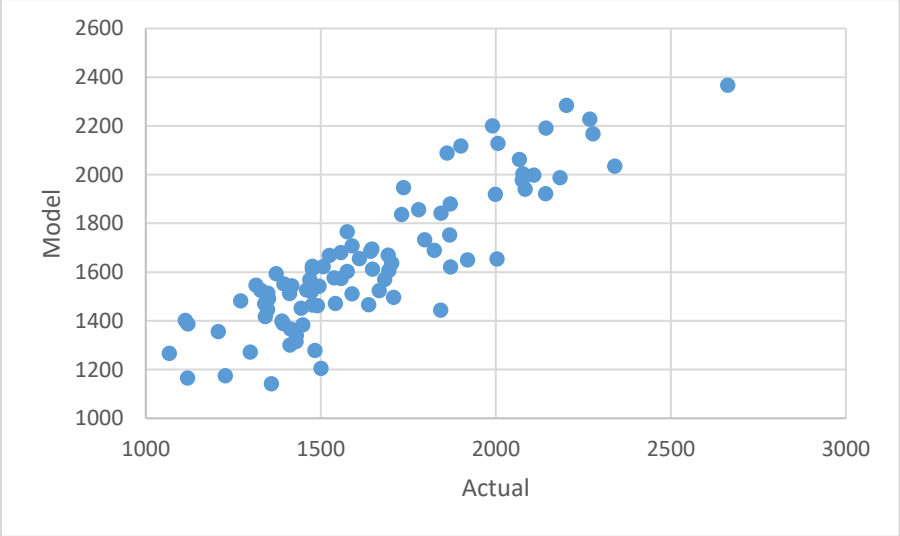

Figure 39: Scatter Plot of Actual and Modeled Cumulative RMS Absolute Error of Airspeed Prediction (ρ = 0.88)

8.1.3. Energy

The terms and coefficients of the model are given in Table 7. This model has R-squared value of 0.76 and the output has a linear correlation coefficient ρ of 0.87 after removing the results for test flights 3, 11, 22, 23, and 79, which are considered outliers relative to this performance measure. Figure 40 shows the scatter plot of the actual prediction performance measure and the output of the model.

Table 7: Terms and Coefficients of Polynomial Model for Cumulative RMS Absolute Error of Energy Prediction

Terms	Coefficients	P-value
Intercept	61,115.82	1.65E-68
WindDir^2	16,433.63	4.85E-13
IAS	12,726.35	6.77E-21
IAS^2	10,244.10	4.60E-06
Gust * GustGradient	3,551.31	4.84E-02
Altitude	2,607.23	8.18E-03
Gust	1,997.03	4.17E-02

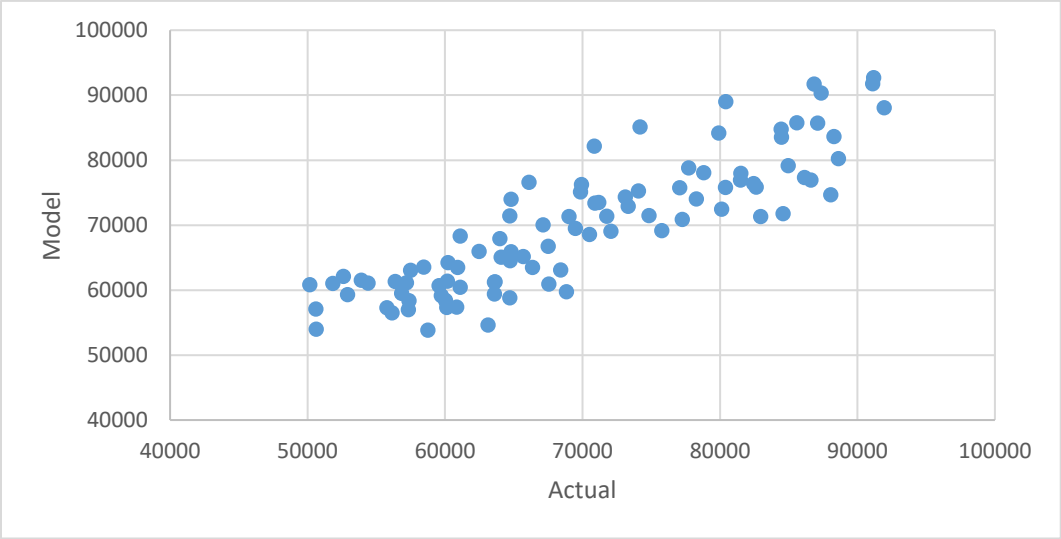

Figure 40: Scatter Plot of Actual and Modeled Cumulative RMS Absolute Error of Energy Prediction (ρ = 0.87)

Based on the model, energy prediction performance is most strongly dependent on wind direction and initial airspeed. This is consistent with the results for altitude and airspeed prediction performance. Energy prediction performance is dependent to a lesser extent on gust intensity, gust gradient, and initial

altitude. An interesting result is that, for this particular cumulative performance measure, energy prediction performance is not dependent on wind speed.

8.2. Models for Relative Prediction Error

Three polynomial models were developed for the cumulative RMS of the relative prediction error, one each for altitude, airspeed, and energy. These models for relative prediction error are much less effective than the models for absolute prediction error. The reason for this may be related to the fact that the relative error emphasizes the error at lower altitude and airspeed, while the RMS statistic is an average over the whole flight. The interaction of these could be causing a distortion in the cumulative performance measure that is not easily compensated for with the applied polynomial models. Another possible reason for the poor modeling accuracy is that there may be uncontrolled (and thus, unmodeled) factors that have a strong effect on the relative error of prediction performance. Large and discrete changes in predictions at low altitude and/or airspeed would be an example. This should be examined further in future studies.

8.2.1. Altitude

The terms and coefficients of the model are given in Table 8. This model has R-squared value of 0.40 and the output has a linear correlation coefficient ρ of 0.63 after removing the results for test flights 3, 5, 16, 23, 35, 36, 66, 79, 86, 91, and 95, which are considered outliers relative to this performance measure. Figure 41 shows the scatter plot of the actual prediction performance measure and the output of the model. Notice that all the weather factors are included in the model, in addition to the airplane weight. This is to be expected, as any effect of the initial altitude and airspeed is nulled by the time the airplane reaches DINKE at 3,000 ft. and 210 kt. However, the R-squared and correlation coefficient values make it clear that this is an incomplete model of prediction performance.

Table 8: Terms and Coefficients of Polynomial Model for Cumulative RMS Relative Error of Altitude Prediction

Terms	**Coefficients**	***P*-value**
Intercept	10.79	5.64E-76
Gust * GustGradient	1.11	4.82E-03
Wind	0.97	4.51E-03
WindGradient	0.63	4.37E-03
Weight	-0.71	1.42E-04
WindDir * WindGradient	-0.83	4.31E-02
WindDir	-0.87	2.05E-04

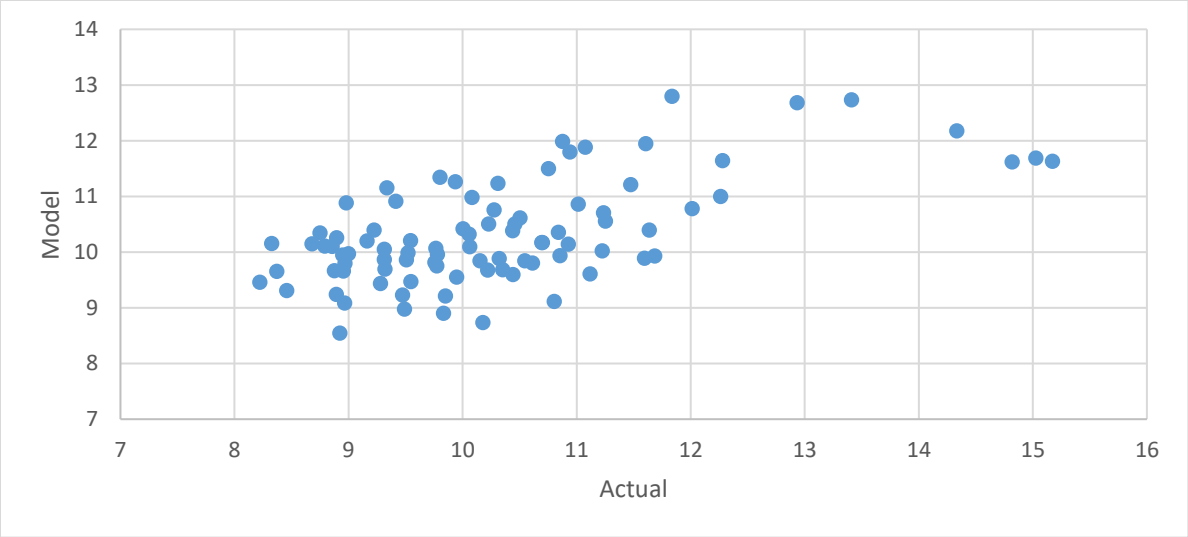

Figure 41: Scatter Plot of Actual and Modeled Cumulative RMS Relative Error of Altitude Prediction (ρ = 0.63)

8.2.2. Airspeed

Table 9 gives the terms and coefficients of the model. This model has R-squared value of 0.47 and the output has a linear correlation coefficient ρ of 0.68 after removing the results for test flights 3, 12, 23, 79, 86, 91, and 95, which are considered outliers relative to this performance measure. Figure 42 shows the scatter plot of the actual prediction performance measure and the output of the model.

Table 9: Terms and Coefficients of Polynomial Model for Cumulative RMS Relative Error of Airspeed Prediction

Terms	Coefficients	P-value
Intercept	7.71	2.21E-67
IAS	1.25	1.13E-10
Altitude	0.53	1.37E-03
Gust	0.43	8.13E-03
Weight	-0.37	5.72E-02
WindGradient^2	0.59	6.53E-02

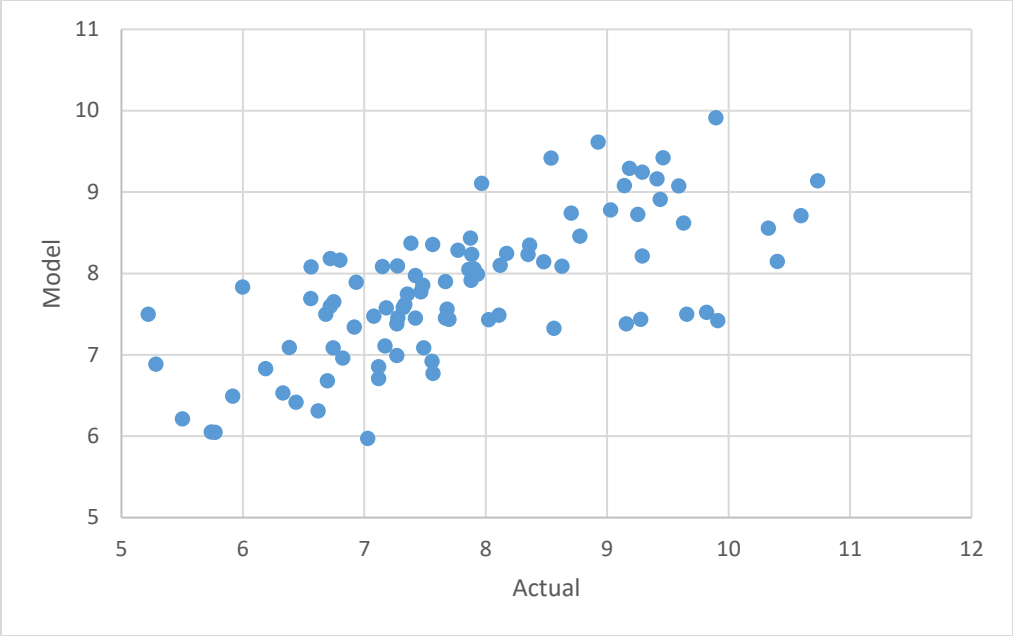

Figure 42: Scatter Plot of Actual and Modeled Cumulative RMS Relative Error of Airspeed Prediction ($\rho = 0.68$)

The strongest factors are the initial airspeed and the wind gradient, but notice that all three factors of the initial airplane energy are in the model. Gust intensity is a variable disturbance on airspeed throughout whole flight and, based on the observations in Section 6, its effect is probably not accounted for by the predictor.

8.2.3. Energy

The terms and coefficients of the model are given in Table 10. This model has R-squared value of 0.46 and the output has a linear correlation coefficient ρ of 0.68 after removing the results for test flights 3, 5, 16, 23, 32, 35, 36, 66, 79, 86, 91, and 95, which are considered outliers relative to this performance measure. Figure 43 shows the scatter plot of the actual prediction performance measure and the output of the model. Gust intensity and gust gradient have the strongest effect, but notice that weight has a negative effect on prediction error, probably because a heavier airplane is less sensitive to gusts. Wind and initial airspeed are strong factors in altitude and airspeed prediction errors, respectively, so it is to be expected that energy is strongly dependent on both. Wind direction and wind gradient are strong factors on altitude prediction error, so these, too, are expected to be significant factors on energy prediction performance.

Table 10: Terms and Coefficients of Polynomial Model for Cumulative RMS Relative Error of Energy Prediction

Terms	Coefficients	P-value
Intercept	9.32	1.67E-79
Gust * GustGradient	0.96	1.25E-03
Wind	0.86	2.42E-05
IAS	0.74	8.60E-06
WindGradient	0.15	3.38E-01
WindDir	-0.49	3.49E-03
Weight	-0.54	3.89E-03

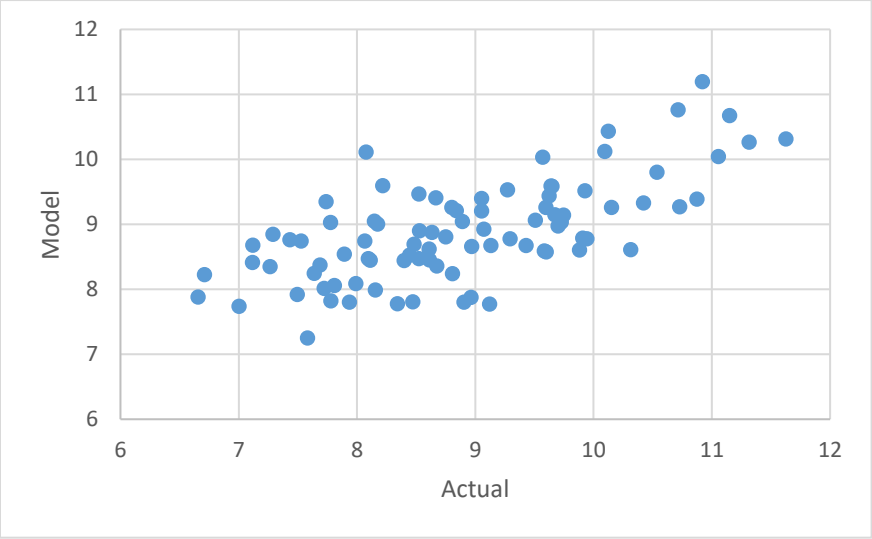

Figure 43: Scatter Plot of Actual and Modeled Cumulative RMS Relative Error of Energy Prediction (ρ = 0.68)

8.3. Prediction Performance Outliers

Table 11 lists the test flights with outlier prediction performance identified by polynomial regression modeling. Many of the outliers are listed multiple times. The outliers listed at least three times include the following:

Prediction Performance Outliers: {3, 16, 23, 66, 79, 86, 91, 95}

Notice that all of these are included in the outlier set identified in Section 7 based on visual inspection of altitude and airspeed prediction performance curves.

Table 11: Outliers Identified Based on Cumulative Measures of Prediction Performance

Cumulative RMS Performance Measures		Outliers
Absolute Error	Altitude	3, 11, 12, 27, 79
	Airspeed	3, 16, 23, 25, 42, 66, 72, 79, 87, 91, 95
	Energy	3, 11, 22, 23, 79
Relative Error	Altitude	3, 5, 16, 23, 35, 36, 66, 79, 86, 91, 95
	Airspeed	3, 12, 23, 79, 86, 91, 95
	Energy	3, 5, 16, 23, 32, 35, 36, 66, 79, 86, 91, 95

9. Outlier Analysis

The following group of twelve test flights were selected for which prediction performance was "out of family" or anomalous based on the results from uncertainty quantification and factor analysis with polynomial regression modeling.

Prediction Performance Outliers: {3, 5, 11, 16, 23, 35, 36, 66, 79, 86, 91, 95}

Figure 44 shows the altitude and airspeed as a function of distance to the runway for these test flights with outlier prediction performance. Figure 45 shows altitude vs. airspeed for the outlier flights.

Appendix D gives the prediction performance results for the outliers set. Appendix E provides additional prediction performance results for each of these outlier test flights.

Visual inspection of the plots in Appendix D yielded two interesting observations. First, comparing the RMS and maxAbs plots, it seems clear that the RMS plots smooth and simplify the performance curves, but the RMS also hides irregularities that can provide clues about structures (i.e., common relations) in the outlier set. Looking at Figure 46 and Figure 47, notice that the maxAbs curves are a lot more "noisy" (i.e., have a more local variability) than the RMS curves. This local variability in the maxAbs is probably an effect of wind gusts, which vary randomly over time during a flight. Notice also that many maxAbs curves have one or more large changes in amplitude over the range of the look-ahead time. These changes in amplitude suggest that prediction performance is probably being influenced by the waypoint structure of the flown trajectory and other factors (probably the controlled variable factors) that determine the differences in performance.

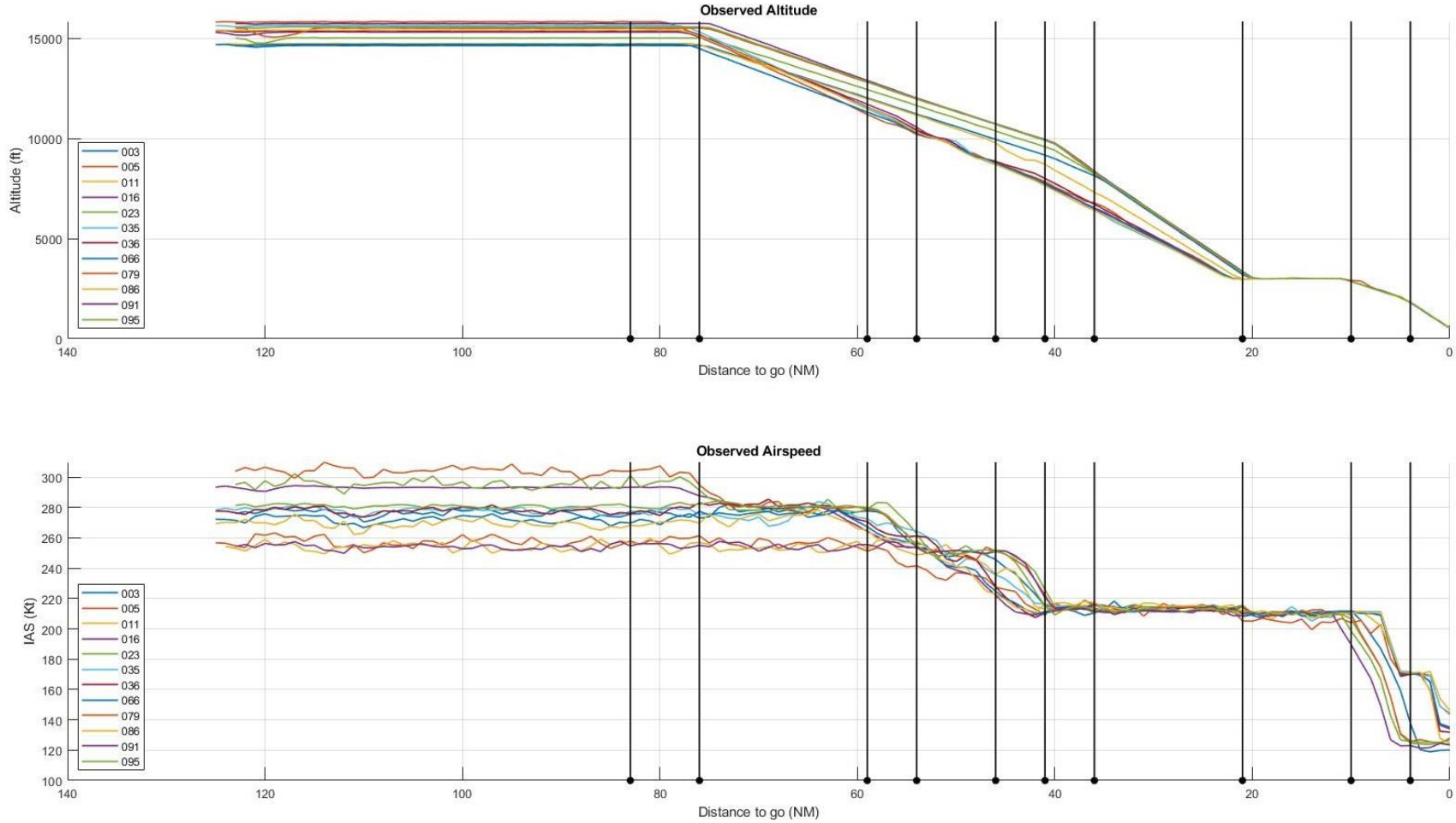

Figure 44: Outlier Test Flights: Altitude and Airspeed as a Function of Distance to Runway

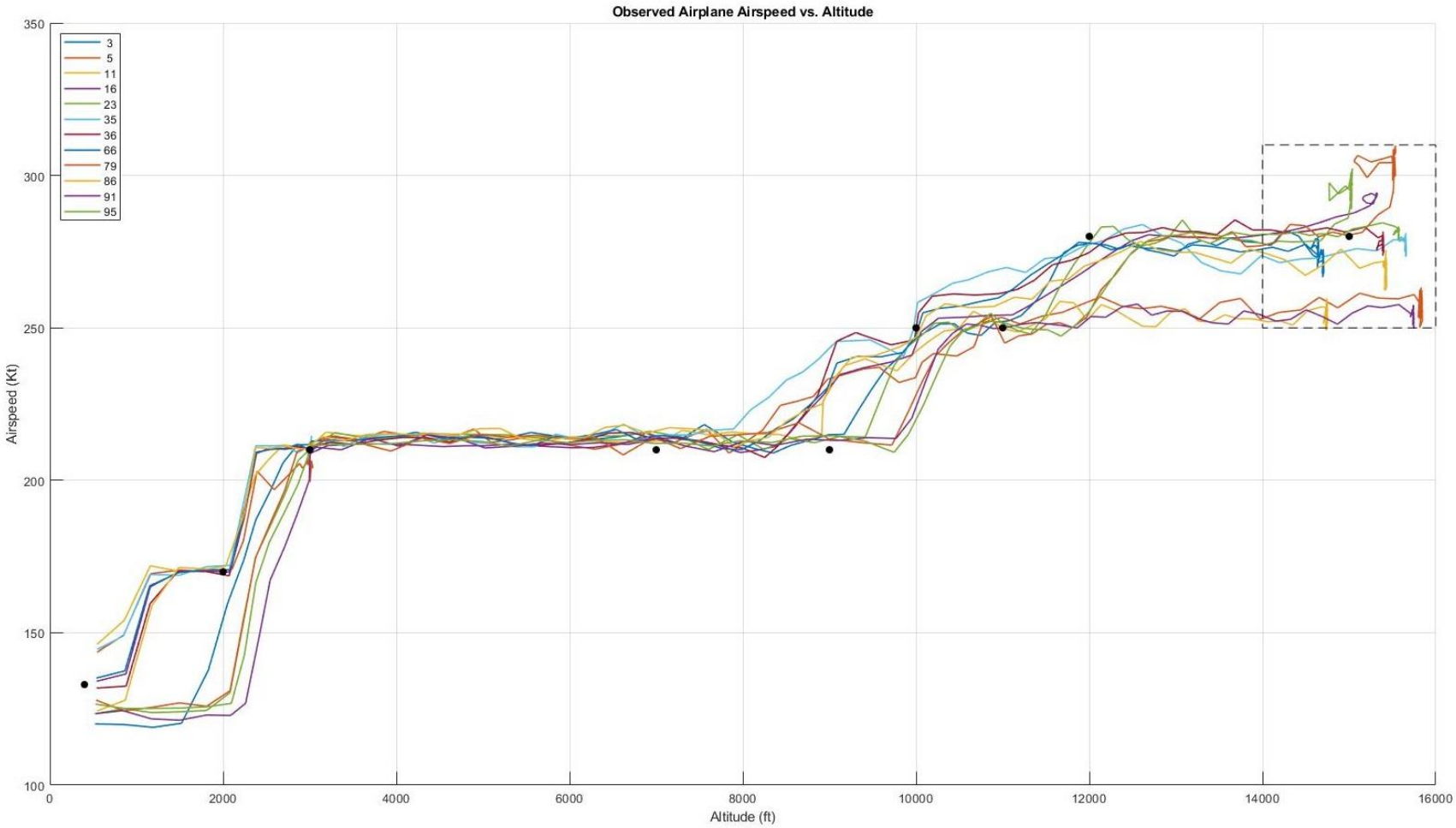

Figure 45: Outlier Test Flights: Altitude vs. Airspeed

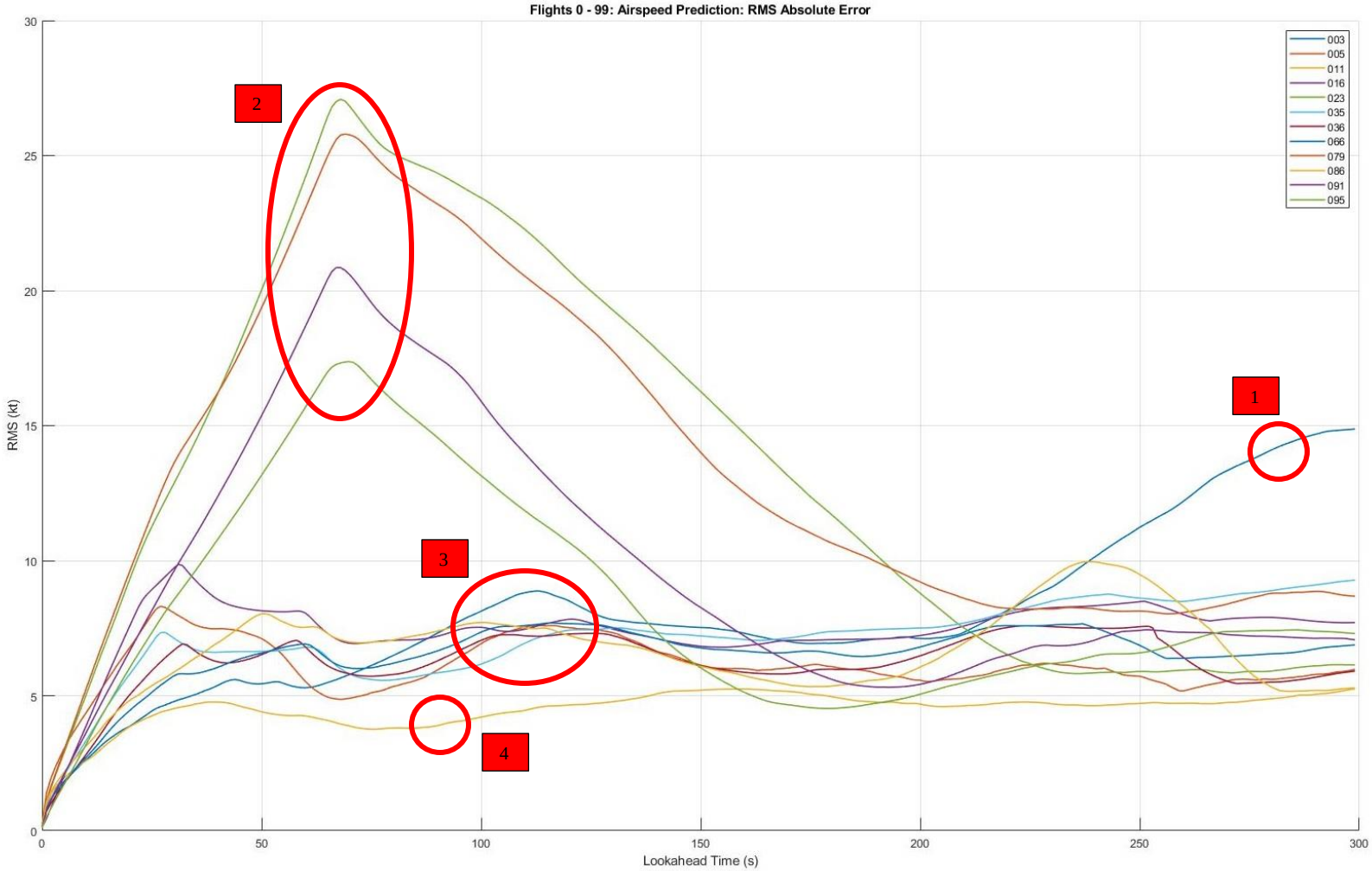

Figure 46: Outlier Test Flights: RMS Absolute Error of Airspeed Prediction as a Function of Look-Ahead Time

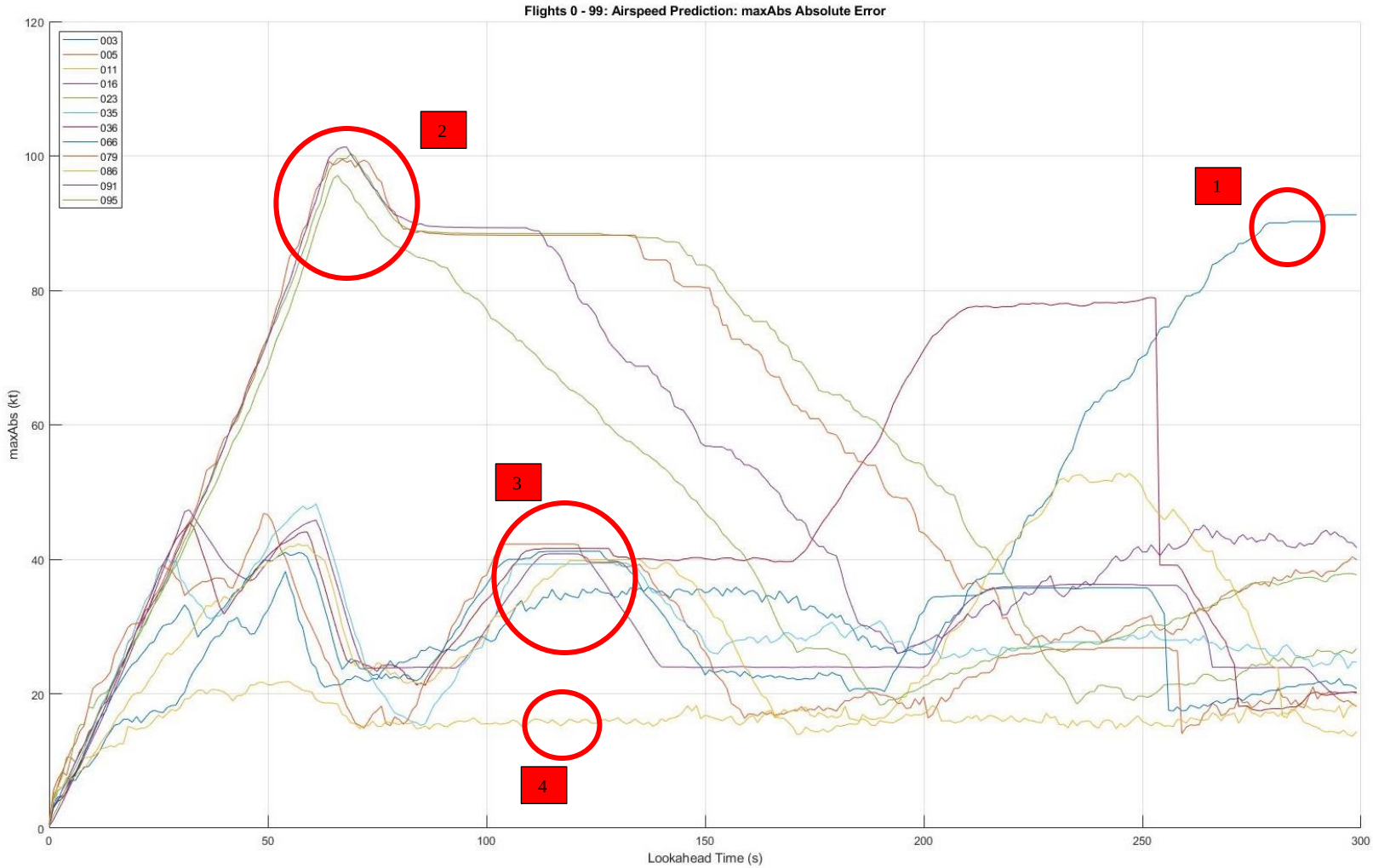

Figure 47: Outlier Test Flights: maxAbs Absolute Error of Airspeed Prediction as a Function of Look-Ahead Time

The second observation from a visual inspection of the prediction performance plots is that the outliers seem to be naturally divided into four subgroups based on visual similarities: Group 1 = {3}, Group 2 = {23, 79, 91, 95}, Group 3 = {5, 16, 35, 36, 66, 86}, and Group 4 = {11}. This grouping is shown in Figure 46 and Figure 47. Various distance analyses were performed with the goal of identifying objective criteria that define and distinguish these groups. Although that activity was not successful, several features of the outliers and the subgroup were identified.

Figure 48 shows the average values of the controlled factors for the groups of normal (i.e., not outlier) and outlier test flights. The ranges of the controlled factors are scaled to the interval ±1. The most salient differences are that, on average, the outlier flights have higher initial altitude, higher wind speed, and much higher wind gradient.

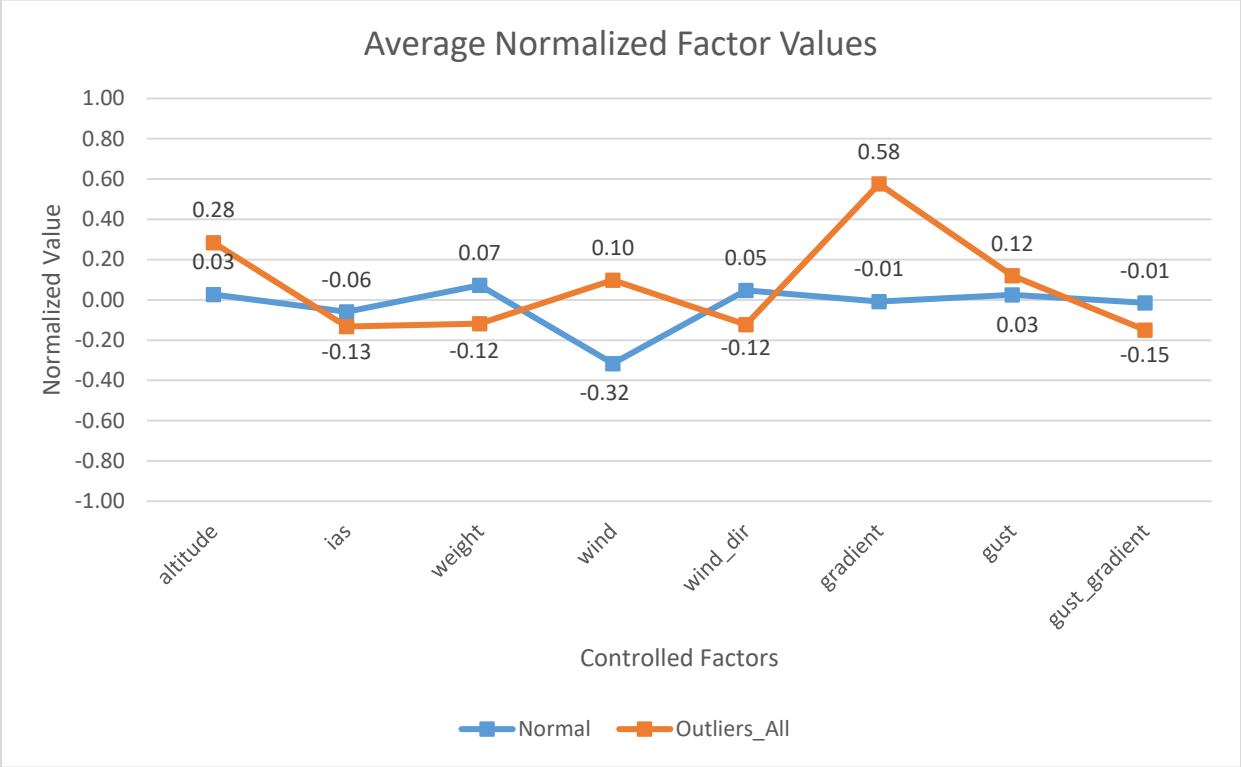

Figure 48: Average Values of the Controlled Factors for Normal and Outliers Groups of Test Flights

Figure 49 shows the values of controlled factors for outlier groups 1 and 4. These groups, which consist of flights 3 and 11, respectively, are similar in initial altitude, wind gradient, and gust intensity, but they differ significantly in all other factors. The largest differences are in airplane weight, wind speed, and wind direction.

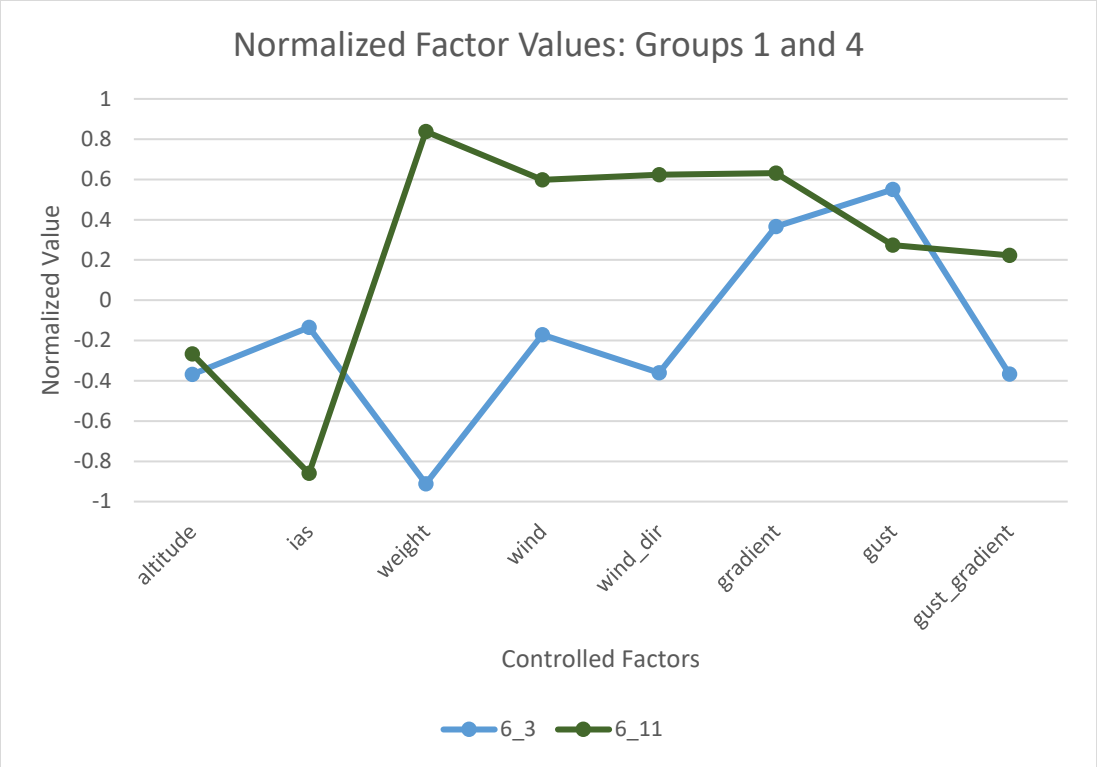

Figure 49: Values of Controlled Factors for Outlier Groups 1 and 4

Figure 50 shows the values of the controlled factors for the test flight of outlier Group 2. The flights are similar in initial altitude, weight, wind speed, wind direction, and wind gradient. Since the wind direction is in the range 0^0 to 360^0 and normalized to the range ±1, the flights in Group 2 have wind direction of around 180^0, i.e., tailwind. The wind speed is in the bottom half of its range, but the wind gradient is in the upper half of its range. The weight of the airplane is around the bottom quarter of the range.

Figure 51 shows the values of controlled factors for outlier Group 3. All the flights in Group 3 have nearly identical wind direction of approximately 0^0, i.e., headwind. Also, wind speed and wind gradient are in the upper half of their ranges.

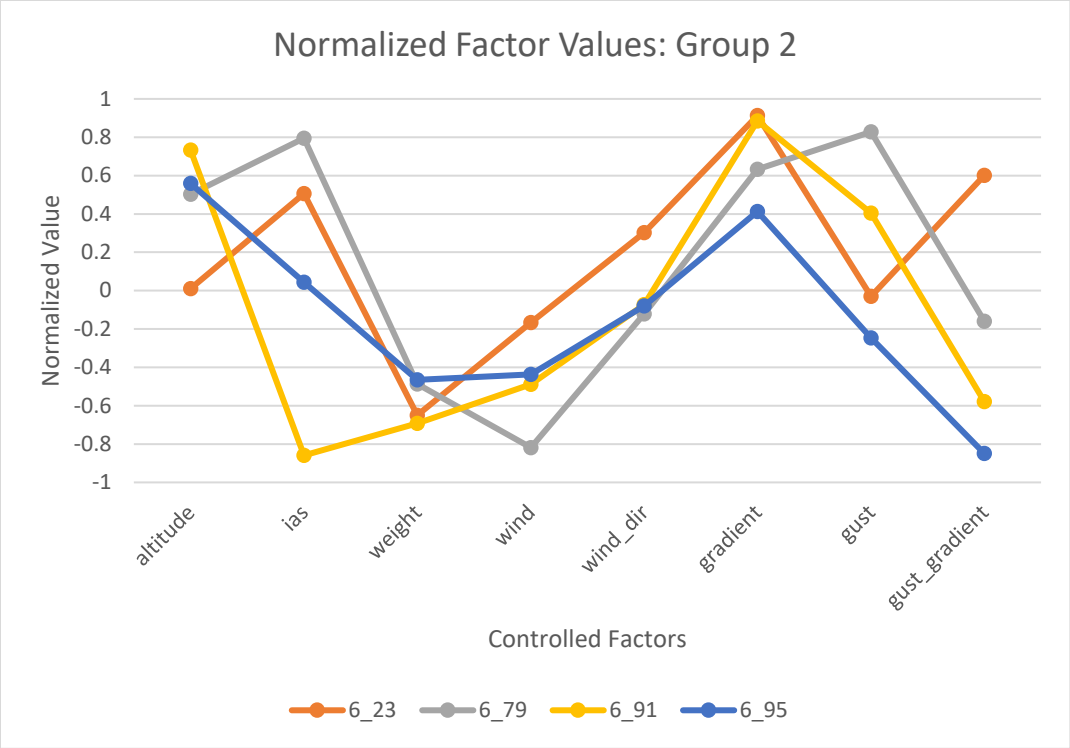

Figure 50: Values of Controlled Factors for Outlier Groups 2

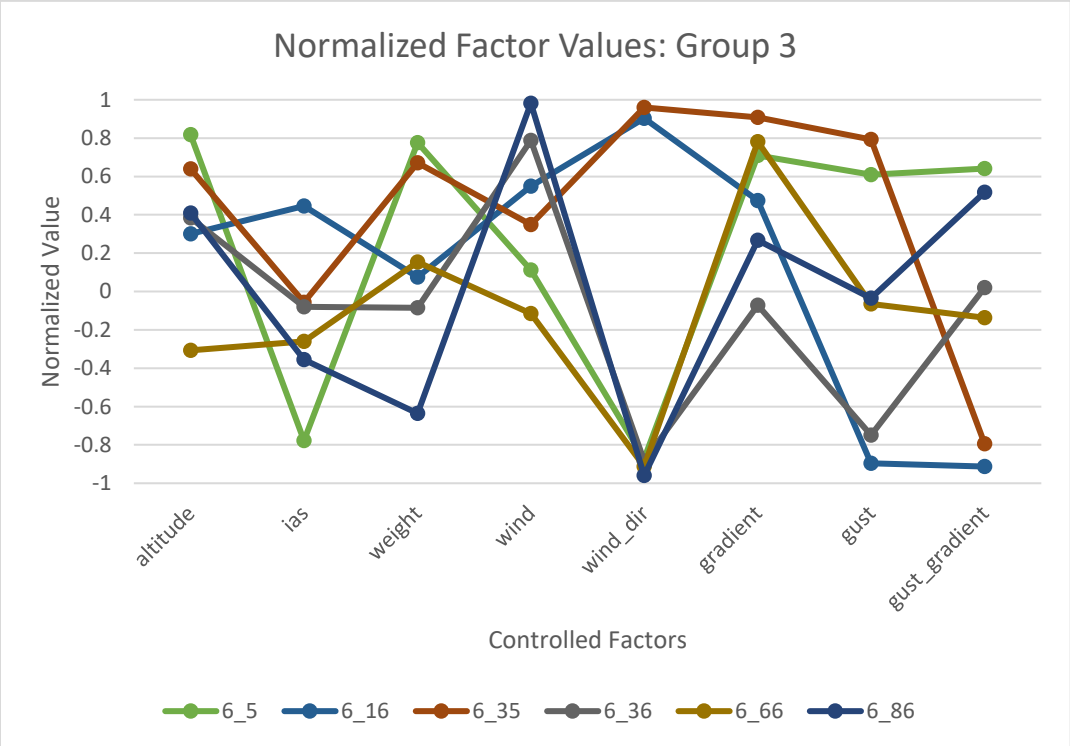

Figure 51: Values of Controlled Factors for Outlier Groups 3

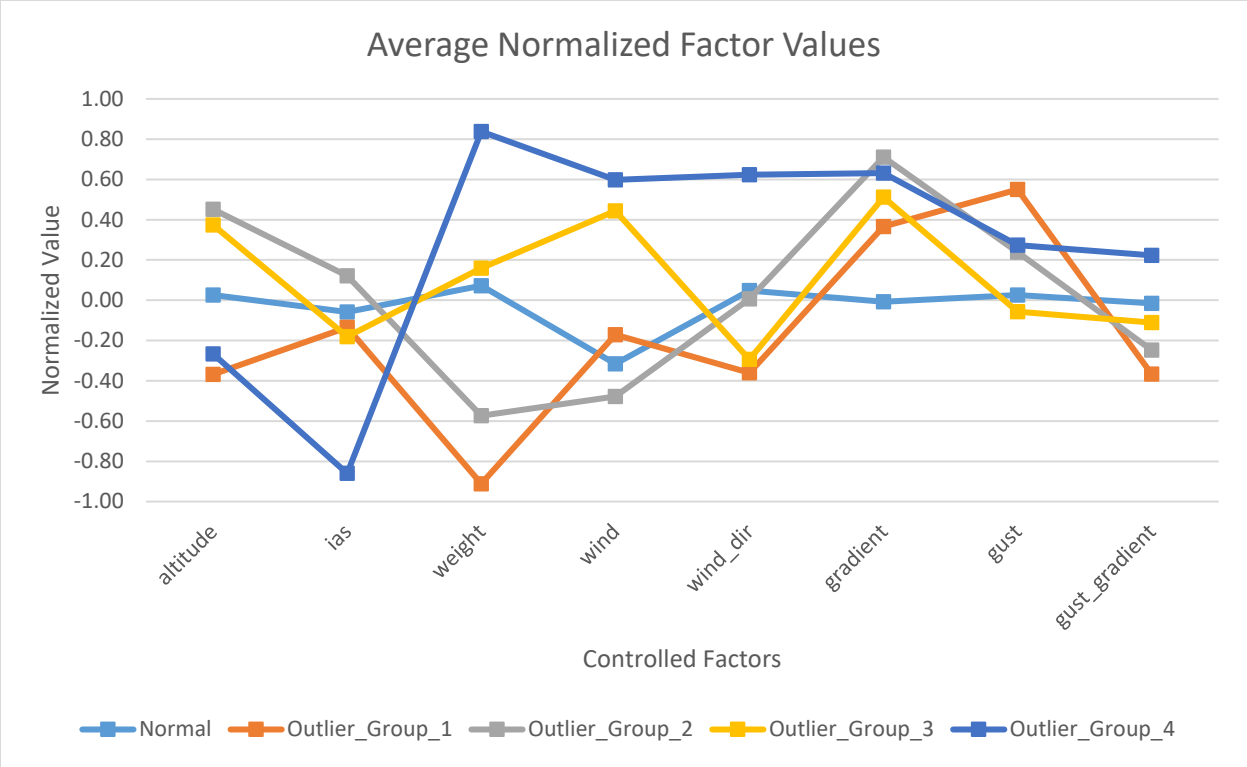

Figure 52: Average Values of the Controlled Factors for Normal and Individual Outlier Groups of Test Flights

Figure 52 shows the average factor values for the normal test flights and each subgroup of outliers. The figure shows that the outlier groups differ in most controlled factors, but they are similar in that the average wind gradient is high, the average gust intensity is in the upper half of its range, and the average gust gradient is in the middle half of its range.

Notice from Figure 49 to Figure 51 that every outlier flight has one or more controlled factors whose values are either in the bottom quarter or the top quarter of their ranges. This suggests that outlier prediction performance is probably caused by extremes in airplane energy or weather factors.

The most significant observation from examination of the prediction performance plots in Appendix E is that, for every outlier test flight, the altitude and/or airspeed predictions have discrete changes in the absolute error. This is shown in Figure 53 for outlier 36. Notice that both altitude and airspeed prediction error have discrete changes in values. These error discontinuities are probably caused by temporary incorrect predictions of the automation mode. The fact that all the outliers have this error characteristic is a strong motivation for a close examination of automation mode prediction error. This will be the topic of a future report.

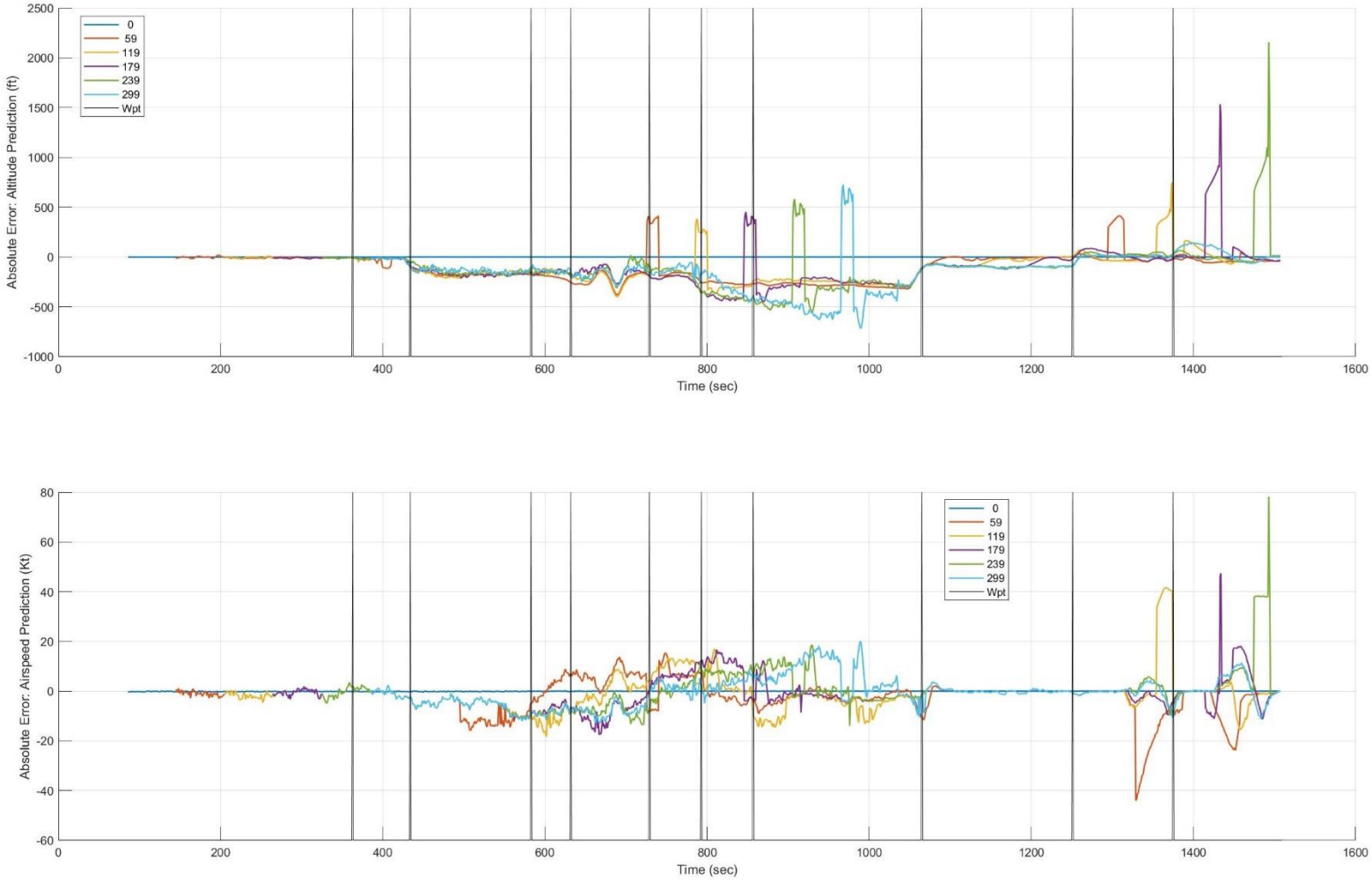

Figure 53: Test Flight 36: Absolute Error of Predicted Altitude and Airspeed as a Function of Time t

10. Summary and Final Remarks

The data analysis of CASPEr-1 Part 6 has yielded interesting results. The quantification of performance uncertainty (i.e., variability) generated plots of central tendency and dispersion with confidence intervals across the range of the look-ahead time. On average, the median absolute error for altitude prediction can be off by as much as 110 ft., or 1.3% at low altitude. The RMS absolute error for altitude is about 180 ft. at five-minute look-ahead time, or 7% at low altitude. The median airspeed can be off by 1.7 kt, or 0.75% at low airspeed. The RMS airspeed prediction error is under 7 kt or 3.5% at low airspeed.

Polynomial models of prediction performance as a function of controlled factors showed that performance depends on both the energy state of the airplane and the weather conditions. Wind speed, wind direction, and wind gradient were found to be major factors in prediction performance. Initial energy (i.e., altitude, airspeed, and weight) and gust intensity were also significant factors in airspeed prediction performance.

About 10% of the flights were deemed to be outliers with respect to prediction performance. It was observed that every outlier flight has one or more controlled factors with values in the extremes of their ranges (i.e., the bottom 25% or the top 25% of the range). This is an indication that the prediction function is not robust over the full range of operational and environmental conditions tested. It was also observed that the altitude and/or airspeed prediction error histories of every outlier flight had discrete changes of limited duration. Based on this, it was suggested that the like cause of outlier energy state prediction performance was errors in automation mode prediction.

CASPEr is an approach for performance evaluation of onboard predictive technologies using fully automated high-fidelity flight simulations. CASPEr-1 is the first application of this approach. The relation between automation mode prediction error and energy state prediction error will be examined in future analyses of data from CASPEr-1. Future analyses will also examine the effect of descent trajectories with different airplane energy profiles, the effect of weather parameters, and the effect of pilot interventions with the autoflight system to implement altitude holds and step-down descents.

The preliminary results and lessons learned from CASPEr-1 have informed the design of a second, more thorough round of performance characterization tests for the TP function called CASPEr-2. The results of CASPEr-2 will appear in future reports.

The final product from this work will be a report documenting a proposed approach to assess the goodness of onboard airplane energy state and automation mode prediction functions.

11. References

[1] Commercial Aviation Safety Team: Airplane State Awareness Joint Safety Analysis Team, "Final Report: Analysis and Results," 2014.

[2] Commercial Aviation Safety Team: Airplane State Awareness Joint Safety Analysis Team, "Final Report: Analysis and Recommendations," 2014.

[3] Commercial Aviation Safety Team, "Safety Enhancement SE 207.1 (R&D)," 2016.

[4] Commercial Aviation Safety Team, "Safety Enhancement SE 208.1 (R&D)," 2016.

[5] S. Young, T. Daniels, E. Evans, T. Etherington, K. Shish, M. Uijit de Haag, S. Schuet and D. Kiggins, "Evaluating Technologies for Improved Airplane State Awareness and Prediction," in *AIAA SciTech Forum*, San Diego, CA, January 4-8, 2016.

[6] K. Shish, J. Kaneshige, D. Acosta, S. Schuet, T. Lombaerts, L. Martin and A. N. Madavan, "Aircraft Mode and Energy-State Prediction, Assessment, and Alerting," *Journal of Guidance, Control, and Dynamics*, vol. 40, no. 4, April 2017.

[7] K. Shish, J. Kaneshige, D. Acosta, S. Schuet, T. Lombaerts, L. Martin and A. N. Madavan, "Trajectory Prediction and Alerting for Aircraft Mode and Energy State Awareness," in *AIAA SciTech Forum*, Kissimmee, Florida, 2015.

[8] P. P. Duan, M. Uijt de Haag, T. Etherington and L. Smith-Velazquez, "Energy state prediction methods for airplane state awareness," in *IEEE/AIAA 35th Digital Avionics Systems Conference (DASC)*, 2016.

[9] Federal Aviation Administration (FAA), "Instrument Flight Procedures Information Gateway," [Online]. Available: https://www.faa.gov/air_traffic/flight_info/aeronav/procedures/. [Accessed 24 October 2018].

[10] Merriam-Webster, "Dictionary by Merriam-Webster," Merriam-Webster, Incorporated, 2018. [Online]. Available: https://www.merriam-webster.com/. [Accessed 3 December 2018].

[11] Oxford, "English Dictionary, Thesaurus, & Grammar Help," Oxford University Press, 2018. [Online]. Available: https://en.oxforddictionaries.com/. [Accessed 3 December 2018].

[12] Federal Aviation Administration (FAA), "Pilot/Control Glossary," 2017. [Online]. Available: https://www.faa.gov/Air_traffic/Publications/media/PCG_10-12-17.pdf. [Accessed 25 October 2018].

[13] Eurocontrol Experimental Centre, "User Manual for the Base of Aircraft Data (BADA), Revision 3.12," Eurocontrol, 2014.

[14] A. Avizienis, J.-C. Laprie, B. Randell and C. Landwehr, "Basic Concepts and Taxonomy of Dependable and Secure Computing," *IEEE Transactions on Dependable and Secure Computing*, vol. 1, no. 1, pp. 11 - 33, January - March 2004.

[15] H. Kopetz, Real-Time Systems: Design Principles for Distributed Embedded Applications, 2nd ed., Springer Science + Business Media, 2011.

[16] A. M. Law, Simulation Modeling and Analysis, McGraw-Hill Education, 2015.

Appendix A. CASPEr-1 Test Plan

CASPEr: Characterization of Airplane State Prediction Error

Notes:

1. Airport: KMEM
2. The FMC always controls lateral navigation.
3. Normal initial altitude is 15,000 ft.
4. Normal initial speed is 280 kt.
5. Normal initial weight is 187,500 lbs. This is the mid-point of the initial weight range.
6. Range for the initial weight is 150,000 – 225,000 lbs.
7. Approach is always on an existing STAR at KMEM set back on the route at a distance corresponding to initial altitude. On BLUZZ ONE landing north, this is near the LTOWN waypoint.

Summary:

Part	**Title**	**Purpose**	**Number of Runs**
1	FMC-Controlled Energy Without Pilot Intervention: All Routes	Test arrival routes and landing directions. No weather.	28
2	FMC-Controlled Energy Without Pilot Intervention: Energy Cube Extremes	Test at end-points of energy cube defined by ranges of airplane altitude, speed, and weight. No weather.	8
3	FMC-Controlled Energy Without Pilot Intervention: Weather	Test for effects of weather conditions, including wind direction, gusts, and wind gradient. Maximum wind speed only.	29
4	FMC-Controlled Energy with Altitude Hold Intervention	Test for single altitude-hold intervention. No weather.	12
5	Stepdown Energy Management	Test descent with multiple step-downs in altitude and speed. No weather.	18
6	Uncertainty Quantification with Monte Carlo Simulations	Random sampling of controlled variables	100
		Total Number of Runs	195

Part 1: FMC-Controlled Energy without Pilot Intervention: All Routes

Description: The purpose is to exercise all the arrival routes and approach directions. The FMC controls lateral, vertical, and speed profiles. In effect, the FMC manages the energy of the airplane. No pilot inputs, except where and when required to complement FMC controls. Normal initial conditions and energy factors (altitude, speed, and weight). No weather.

Variable	**Values**	**Number of Values**
STAR	BLUZZ ONE, HYTHR ONE, BRBBQ TWO, CONDR TWO, HOBRK TWO, VANZE ONE, MONAA TWO	7
Runway	9, 18C, 27, 36C	4
Weather:		
Wind Speed	0	1
Initial Energy Factors		
Altitude	Normal	1
Speed	Normal	1
Weight	Normal	1
Descent Energy Factors		
Altitude	Per published STAR and Approach routes; Managed by FMC	1
Speed	Per published STAR and Approach routes; Managed by FMC	1
Weight	Normal for the airplane	1
Pilot Inputs	As needed	
	Number of Runs	28 See Note 1

Notes:

1. Number of runs: 7 STARs x 4 Runway Approaches = 28

Part 2: FMC-Controlled Energy without Pilot Intervention: Energy Cube End-Points

Description: The purpose is to observe the effects of extremes in the energy cube defined by the ranges of altitude, speed, and weight. No weather. No pilot inputs, except where and when required to complement FMC controls.

- This is implemented by changing the altitude and speed constraints of the waypoints.
- Horizontal locations of the waypoints remain as on published on STAR and approach charts.
- TOD is at the same horizontal along-track distance to DINKE as LTOWN on the published STAR, i.e., 55 NM.
- Altitude:
  - Initial: Min = 11,000 ft.; Max = 19,000 ft.
  - Descent: Approximately constant angle along track from TOD to DINKE
- Speed:
  - Initial: Min = 210 kt ; Max = 290 kt
  - Descent: Constant to DINKE
- Must ensure that the procedure for required pilot inputs (e.g., flap setting, landing gear) is adequate in all cases.

Variable	**Values**	**Number of Values**
STAR	BLUZZ ONE	1
Runway	36C	1
Weather:		
Wind Speed	0	1
Initial Energy Factors		
Altitude	Min, Max	2
Speed	Min, Max	2
Weight	Min, Max	2
Descent Energy Factors		
Altitude	Min and Max for STAR and Approach route; Managed by FMC	Match (min ➔ min, max ➔ max) with Initial Energy Factor: Altitude
Speed	Min and Max for STAR and Approach route; Managed by FMC	Match (min ➔ min, max ➔ max) with Initial Energy Factor: Speed
Weight	Min and Max for airplane	Match (min ➔ min, max ➔ max) with Initial Energy factor: Weight
Pilot Inputs	As needed	
	Number of Runs	8 See Note 1

Notes:

1. Number of runs: 2 altitudes x 2 speeds x 2 weights = 8

Part 3: FMC-Controlled Energy without Pilot Intervention: Weather

Description: The purpose is to observe the effects of weather variables, including wind speed, wind direction, wind gradient, gust speed, and gust gradient. No pilot inputs, except where and when required to complement FMC controls.

Variable	Values	Number of Values
STAR	BLUZZ ONE	1
Runway	36C	1
Weather:		
Wind Direction ("from")	North-East, South-West, North, South	4
Wind Speed	Max	7 See Notes 1 - 5 below
Gusts	Mid, Max	
Wind Gradient	Mid, Max	
Initial Energy Factors		
Altitude	Normal	1
Speed	Normal	1
Weight	Normal	1
Descent Energy Factors		
Altitude	Normal for STAR and Approach route; Controlled by FMC	1
Speed	Normal for STAR and Approach route; Controlled by FMC	1
Weight	Normal for airplane	1
Pilot Inputs	As needed	
	Number of Runs	28 + 1 = 29 See Notes 6 and 7

Notes:

1. Test sequence for wind speed, gusts, and gradients:

Index	Speed	Gusts	Wind Gradient
1	Max	0	0
2	Max	Mid	0
3	Max	Max	0
4	Max	0	Mid
5	Max	0	Max
6	Max	Mid	Mid
7	Max	Max	Max

2. Max wind speed at ground level is 25 knots for headwind and crosswind components, and 10 knots for tailwind component. Maximum wind speeds <u>at ground level</u> for each wind direction is as specified in the following table.

Wind Direction	Maximum Wind Speed at ground level (Kt)
North	25
North-East	25
South-East	14
South	10

3. Note that to maintain approach simplicity we are not including gust speed/strength in the wind constraint. We are assuming that this is valid since we are not simulating the final landing part of the approach.
4. Max wind gradient is 5 knots per 1,000 ft. altitude.
5. Max gusts is 6 knots RMS at 15,000 ft. and 2 knots RMS at ground level. Note that gusts always have a gradient.
6. Number of runs: 4 wind directions x 7 wind speed/gust/gradient combos = 28
7. Add one run: Max Wind, Max Gradient, No gusts (i.e., Index 5 in table of Note 1), North-East wind direction. All previously defined runs include wind forecast given to the FMC. For this extra run, wind forecast is not given to the FMC. Intended as a sample run to measure the effect on FMC and TFMS/TPS of not having a wind forecast.

Part 4: FMC-Controlled Energy with Altitude Hold Intervention

Description: The purpose is to observe the effects of simple tactical interventions. No weather.

Variable	Values	Number of Values
STAR	BLUZZ ONE	1
Runway	36C	1
Weather:		
Wind Speed	0	1
Initial Energy Factors		
Altitude	Normal	1
Speed	Normal	1
Weight	Normal	1
Descent Energy Factors		
Altitude	Normal for STAR and Approach route; Controlled by FMC, except during pilot interventions	1
Speed	Normal for STAR and Approach route; Controlled by FMC	1
Weight	Normal for airplane	1
Pilot Inputs		
Altitude Hold	11,000 ft. 9,000 ft. 7,000 ft.	3 See Note 1 below
Hold Duration	3.0, 4.0, 5.0 min at 11,000 ft. 1.0, 2.0, 3.0 min at 9,000 ft. 1.0, 1.5, 2.0 min at 7,000 ft.	3 See Note 2 below
Input Event Subsequences	{1} (No return to normal profile. Permanent hold.) {1, 2}	2 See Notes 3 and 4 below
	Number of Runs	12 See Note 5

Notes:

1. At most one hold per descent. Holding at one of the listed altitudes.
2. Hold duration options are dependent on the hold altitude. There should be one simulation run for each of these hold durations.
3. It is assumed that Pilot Input is a random variable from the point of view of the predictors. It is expected that every Pilot Input event may cause a relatively abrupt change in the predicted state of the airplane and the automation. The only way to measure the accuracy of a predictions is to allow the airplane state to evolve without additional Pilot Input events and to reach the time of the predicted state in order to make a prediction error measurement.
4. Conceptually, a full Pilot Input event sequence for an altitude hold has two events: (1) Select hold altitude, (2) Select return to normal descent. In order to measure the state prediction error, there should be one simulation run for each Pilot Input event. (See Note 3). For example, for an altitude-hold scenario there should be one run with only the first Pilot Input event (event 1) and another run with two Pilot Input events (events 1 and 2).

5. Number of runs: 3 + 9 = 12
    a. Runs with one Pilot Input event: 3 altitudes (each with indefinite hold time) = 3
    b. Runs with two Pilot Input events: 3 altitudes x 3 hold times for each altitude = 9

Part 5: Step-down Energy Management

Description: The purpose is to observe the effects of more complex Pilot Input sequences. The FMC manages the altitude and speed, except during pilot interventions. No weather.

Variable	Values	Number of Values
STAR	BLUZZ ONE	1
Runway	36C	1
Weather:		
Wind Speed	0	1
Initial Energy Factors		
Altitude	Normal	1
Speed	Normal	1
Weight	Normal	1
Descent Energy Factors		
Altitude	Managed by FMC for normal for STAR and Approach trajectory , except during pilot interventions	1
Speed	Stepped down with following speed targets: • 250 KT for altitude step at 11,000 ft. • 230 KT for altitude step at 9,000 ft. • 210 KT for altitude step at 7,000 ft.	1
Weight	Normal for airplane	1
Pilot Inputs		
Altitude Steps	Two steps = {11,000 ft.; 9,000 ft.} Three steps = {11,000 ft.; 9,000 ft.; 7,000 ft.}	2 See Note 1 below
Speed	Stepped-down	1 See Descent Energy Factors: Speed above; See Note 2 below
Vertical Descent Speed	2,000 fpm 3,000 fpm	2 See Note 3
Distance-to-reference-waypoint for stepdown transitions	Early stepdown transitions = • 30 NM for altitude step at 11,000 ft. • 20 NM for altitude step at 9,000 ft. • 10 NM for altitude step at 7,000 ft. Late stepdown transitions = • 25 NM for altitude step at 11,000 ft. • 15 NM for altitude step at 9,000 ft. • 5 NM for altitude step at 7,000 ft. Reference waypoint is DINKE	2 See Note 4 below
Input Event Subsequences	For two steps of altitude and speed: • {1}	3 for two steps, 4 for three steps

	○ Airplane remains at first step of altitude and speed • {1, 2} ○ Airplane remains at second step of altitude and speed. • {1, 2, 3} ○ Airplane returns to normal altitude and speed at the end of the second step. For three steps of altitude and speed: • {1} ○ Airplane remains at first step of altitude and speed • {1,2} ○ Airplane remains at second step of altitude and speed • {1, 2, 3} ○ Airplane remains at third step of altitude and speed • {1, 2, 3, 4} ○ Airplane returns to normal altitude and speed at the end of the third step	See Notes 5 and 6 below.
	Number of Runs : Two steps	10 See Note 7
	Number of Runs : Three steps	8 See Note 8
	Total Number of Runs	18

Notes:

1. Stepdown sequence begins with Pilot Input applied at 14,000 ft. to descend to the first altitude step. Additional Pilot Inputs are applied to descend to the next level at one of the distance-to-reference-waypoint options listed in the table.
2. Pilot Inputs for speed targets are made at the same time as Pilot Inputs for altitude transitions.
3. For a particular run, all stepdown transitions are made with the same target vertical speed.
4. For a particular run, the stepdown transitions are either all early (i.e., at the farthest listed distance to DINKE) or all late (i.e., at the closest listed distance to DINKE).
5. A two-step descent requires three Pilot Input events: (1) Select descent to first level, (2) Select descent to second level, and (3) Select descent back to normal altitude
6. A three-step descent requires four Pilot Input events: (1) Select descent to first level, (2) Select descent to second level, (3) Select descent to third level, and (3) Select descent back to normal altitude.
7. Number of runs for two stepdown levels for altitude and speed:

Number of Pilot Input events	Number of Vertical Descent Speeds for Transitions (2000 or 3000 fpm)	Number of Timings for Stepdown Transitions (Early or Late)	Total Number of Runs	Comment
1	2	Not applicable	2	Initial transition is from 14,000 ft. to the first step; Airplane remains at first step of altitude and speed; There is no stepdown transition from this level.
2	2	2	4	Airplane remains at second step of altitude and speed; Stepdown transitions are at the end of each step.
3	2	2	4	Airplane returns to normal altitude and speed at the end of the second step; Stepdown transitions are at the end of each step.
		Total	10	

8. Number of runs for three stepdown levels for altitude and speed:

Number of Pilot Input events	Number of Vertical Descent Speeds for Transitions (2000 or 3000 fpm)	Number of Timings for Stepdown Transitions (Early or Late)	Total Number of Runs	Comments
1	2	Not applicable	2	Transition is from 14,000 ft. to the first step; Airplane remains at first step of altitude and speed; There is no stepdown transition from this level. These runs are the same as the runs in the first row of the table in Note 7 for two stepdown levels. It is not necessary to re-redo these runs.

2	2	2	4	Airplane remains at second step of altitude and speed; Stepdown transitions are at the end of each step. These runs are the same as the runs in the second row of the table in Note 7 for two stepdown levels. It is not necessary to redo these runs.
3	2	2	4	Airplane remains at third step of altitude and speed; Stepdown transitions are at the end of each step.
4	2	2	4	Airplane returns to normal altitude and speed at the end of the third step; Stepdown transitions are at the end of each step.
		Total	14 – 6 = 8	

Part 6: Uncertainty Quantification with Monte Carlo Simulation

Description: The purpose is to quantify the state prediction uncertainty. This is a Monte Carlo simulation experiment for low confidence estimation of uncertainty in state prediction error. No Pilot Inputs.

- Altitude:
  - Initial: Min = 14,000 ft.; Max = 16,000 ft.
  - Descent: Normal
- Speed:
  - Initial: Min = 250 kt; Max = 310 kt.
  - Descent: Normal

Variable	**Values**	**Number of Values**
STAR	BLUZZ ONE	1
Runway	36C	1
Weather:		
Wind Speed	0 to Max, Uniform Distribution	Sampled See Note 1
Wind Direction ("from")	0 to 360 degrees, Uniform Distribution	Sampled
Gusts	0 to Max, Uniform Distribution	Sampled
Wind Gradient	0 to Max, Uniform Distribution	Sampled
Initial Energy Factors		
Altitude	Min to Max, Uniform Distribution	Sampled
Speed	Min to Max, Uniform Distribution	Sampled
Weight	Min to Max, Uniform Distribution	Sampled
Descent Energy Factors		
Altitude	Normal for STAR and Approach route; Managed by FMC	1
Speed	Normal for STAR and Approach route; Managed by FMC	1
Weight	Normal for airplane	Sampled
	Number of Runs	100

Notes:

1. To satisfy the wind speed limitations for landing, the range of wind speed at ground level must depend on wind direction. The Max wind speed is set as follows:
   a. For wind direction within ±66 degrees of the landing direction (i.e., North for runway 36C): Max = 10 / cos(θ) knots, where θ is the angle between the landing direction and the wind direction.
   b. Otherwise: Max wind speed = 25 knots

Appendix B. Test Points for Part 6

The following table contains the test points for initial energy and weather. IAS denotes indicated airspeed.

	Initial Airplane Energy			Weather				
ID	Altitude (ft)	IAS (kt)	Weight (lbs)	Wind Speed (kt, Ground Altitude)	Wind Direction (deg)	Wind Gradient (kt / 1,000 ft)	Gust (kt RMS, Ground Altitude)	Gust Gradient (kt RMS / 1,000 ft)
0	15,001.50	277.68	188,215.00	4.26	317.35	0.59	1.94	0.07
1	14,705.80	257.78	188,667.00	7.78	258.32	1.03	1.40	0.01
2	15,866.70	258.14	184,564.00	16.62	88.24	3.65	0.81	0.20
3	14,632.10	275.94	153,332.00	10.36	115.00	3.42	1.55	0.08
4	14,234.30	294.17	196,489.00	19.48	114.76	0.47	0.65	0.12
5	15,817.50	256.69	216,581.00	13.89	22.96	4.27	1.61	0.22
6	15,262.80	286.50	185,399.00	3.79	290.48	2.19	1.31	0.07
7	15,661.70	269.28	154,061.00	12.14	250.19	4.51	0.00	0.24
8	14,047.10	253.34	191,772.00	2.52	140.79	3.89	0.58	0.26
9	15,940.80	263.89	220,519.00	10.99	118.01	0.27	1.74	0.24
10	15,890.40	290.78	215,163.00	14.45	286.16	0.03	1.35	0.26
11	14,733.60	254.20	218,917.00	19.98	292.26	4.08	1.27	0.16
12	15,826.30	305.01	223,703.00	13.53	108.69	4.66	1.36	0.22
13	15,051.80	282.84	169,267.00	20.03	279.16	1.13	0.18	0.17
14	15,533.40	299.45	196,128.00	1.79	100.45	0.02	0.11	0.07
15	15,864.50	277.39	187,511.00	9.66	299.23	1.18	1.50	0.19
16	15,300.10	293.39	190,297.00	19.37	342.63	3.69	0.10	0.01
17	14,987.10	276.20	193,240.00	17.42	83.06	0.45	1.50	0.12
18	15,090.00	278.64	207,569.00	5.52	304.41	4.31	1.65	0.24
19	14,335.90	270.28	160,978.00	7.51	215.22	0.04	0.56	0.26
20	15,690.90	262.96	203,653.00	7.31	166.20	0.13	1.76	0.07
21	15,120.70	274.98	204,012.00	3.26	156.71	3.57	1.75	0.12
22	14,019.10	258.63	211,023.00	3.57	216.33	1.26	0.62	0.01
23	15,011.30	295.19	163,135.00	10.43	234.38	4.78	0.97	0.21
24	14,761.70	282.82	223,440.00	7.57	169.24	4.94	0.50	0.12
25	14,069.20	261.43	152,439.00	0.80	159.82	1.21	2.00	0.15
26	14,949.40	269.03	203,457.00	0.07	196.95	1.01	0.61	0.14
27	14,483.90	278.37	214,275.00	6.65	248.21	2.26	1.79	0.15
28	15,366.50	296.73	176,446.00	1.09	260.40	4.89	1.10	0.14
29	14,629.10	263.68	223,856.00	9.11	296.46	4.06	0.10	0.24
30	15,269.70	254.12	207,738.00	3.00	239.44	4.70	2.00	0.18

31	14,903.80	302.40	162,248.00	18.44	41.92	2.96	0.71	0.07
32	15,598.10	273.34	157,289.00	21.95	269.15	4.38	0.32	0.23
33	15,568.30	263.05	194,428.00	5.55	199.82	0.00	0.15	0.08
34	14,768.20	290.76	195,129.00	10.09	204.76	1.55	1.31	0.06
35	15,639.60	278.32	212,683.00	16.87	352.80	4.77	1.79	0.03
36	15,384.00	277.62	184,285.00	22.35	20.91	2.32	0.25	0.14
37	14,618.90	265.80	193,190.00	12.16	268.73	4.31	1.40	0.06
38	15,300.40	285.07	201,681.00	8.43	157.60	2.89	0.30	0.23
39	15,774.40	254.07	180,213.00	13.94	318.33	2.62	1.88	0.25
40	14,196.90	298.86	209,808.00	9.47	57.05	2.97	1.09	0.08
41	15,755.40	253.38	184,419.00	10.44	331.85	2.20	1.93	0.23
42	15,519.20	304.00	193,788.00	9.92	189.16	1.12	1.08	0.00
43	14,586.90	275.36	211,138.00	1.55	186.97	3.06	1.93	0.10
44	14,573.60	294.42	173,685.00	17.18	268.55	1.73	0.11	0.10
45	14,947.00	267.66	216,273.00	3.30	259.12	3.37	1.02	0.08
46	14,967.90	303.03	182,406.00	12.74	131.39	3.65	0.72	0.07
47	14,467.60	258.06	154,409.00	0.44	47.75	1.44	0.94	0.21
48	15,076.80	262.09	205,911.00	24.02	84.17	3.19	0.78	0.25
49	14,021.40	262.24	176,532.00	3.27	231.59	1.57	0.47	0.21
50	15,243.10	302.59	177,659.00	5.68	339.19	2.96	1.41	0.21
51	15,926.80	278.97	201,542.00	5.34	264.79	4.30	0.80	0.22
52	15,549.90	292.18	171,508.00	2.83	1.74	3.05	1.95	0.07
53	14,228.60	258.83	223,463.00	2.62	69.18	3.27	0.66	0.08
54	14,771.20	257.86	203,788.00	7.43	211.02	4.56	0.96	0.15
55	14,440.50	268.80	204,865.00	23.59	105.40	3.93	0.39	0.04
56	15,108.60	255.41	202,743.00	9.57	44.43	0.72	0.52	0.16
57	14,386.10	306.59	215,028.00	13.78	288.10	2.85	0.99	0.17
58	14,468.80	292.42	202,590.00	14.01	327.30	3.78	1.67	0.01
59	15,162.30	295.77	193,520.00	15.15	87.62	2.21	1.50	0.13
60	15,393.70	291.46	206,207.00	2.95	173.27	3.36	0.72	0.09
61	15,726.80	305.41	209,485.00	0.07	196.22	0.18	0.34	0.12
62	15,327.20	267.07	156,526.00	2.01	331.39	4.54	0.32	0.11
63	15,494.80	258.94	175,366.00	4.07	266.58	4.92	1.49	0.11
64	15,844.30	269.85	200,799.00	10.59	151.78	2.15	1.38	0.11
65	15,978.20	255.86	203,564.00	10.50	17.71	3.73	0.20	0.18
66	14,692.60	272.21	193,292.00	11.07	15.75	4.45	0.93	0.12
67	14,085.60	258.75	158,033.00	11.54	108.95	4.58	1.88	0.10
68	15,834.20	299.97	165,773.00	16.22	66.47	3.04	1.90	0.09
69	15,935.00	306.52	188,584.00	1.73	284.67	3.04	1.22	0.01
70	15,500.70	289.93	178,053.00	2.39	278.19	2.22	1.54	0.24
71	14,133.10	284.19	176,873.00	2.68	218.00	3.72	1.94	0.06

72	14,630.20	308.71	159,847.00	3.78	95.26	4.96	1.81	0.23
73	15,764.80	274.83	208,976.00	19.04	243.78	1.24	0.37	0.17
74	14,043.00	302.12	183,898.00	21.44	114.82	1.86	1.02	0.11
75	14,030.10	280.71	152,200.00	5.27	324.52	2.96	0.49	0.06
76	15,899.40	289.89	202,781.00	9.51	35.99	0.88	0.20	0.20
77	15,148.90	282.38	194,221.00	1.48	36.05	2.72	1.62	0.08
78	14,108.00	274.54	186,804.00	11.55	31.86	0.20	0.96	0.08
79	15,502.50	303.85	169,256.00	2.27	158.08	4.08	1.83	0.11
80	14,991.10	250.91	174,648.00	10.21	112.38	2.49	0.06	0.05
81	14,275.70	260.08	191,362.00	3.09	133.77	2.65	1.86	0.06
82	15,978.60	253.21	170,959.00	15.37	236.85	2.99	1.43	0.06
83	14,197.80	309.53	198,613.00	7.01	307.95	0.69	0.40	0.02
84	15,010.60	296.49	163,736.00	6.55	292.72	4.42	1.59	0.04
85	14,709.60	279.48	201,699.00	8.76	150.24	2.76	0.28	0.23
86	15,408.90	269.35	163,662.00	24.77	7.29	3.17	0.96	0.20
87	15,823.50	306.11	158,780.00	2.50	22.25	3.99	0.28	0.21
88	15,649.10	281.67	200,764.00	5.14	351.43	2.06	0.01	0.19
89	14,420.50	309.68	199,940.00	7.60	323.56	0.90	1.04	0.05
90	15,534.00	288.03	176,496.00	3.74	359.18	1.04	0.39	0.11
91	15,732.80	254.23	161,560.00	6.39	166.75	4.71	1.40	0.06
92	15,210.80	257.02	172,467.00	17.23	355.57	1.25	0.84	0.08
93	14,758.00	253.79	176,236.00	2.08	16.10	1.18	1.74	0.09
94	15,884.20	259.63	160,712.00	6.17	9.47	1.99	1.01	0.22
95	15,558.80	281.29	170,030.00	7.04	165.56	3.53	0.75	0.02
96	14,587.60	291.89	215,807.00	0.55	135.73	1.29	0.37	0.01
97	14,267.30	286.96	190,982.00	0.36	34.48	3.24	0.53	0.11
98	14,002.80	261.78	206,544.00	7.62	318.85	0.24	0.48	0.07
99	14,178.40	295.01	208,963.00	11.74	345.73	1.02	1.56	0.18

Appendix C. Prediction Performance and Outlier Candidates for All Flights

The following figures show the altitude and airspeed prediction performance results for all the flights in Part 6 of CASPEr-1. The figures also identify performance curves that were considered as candidates for detailed analysis of outliers.

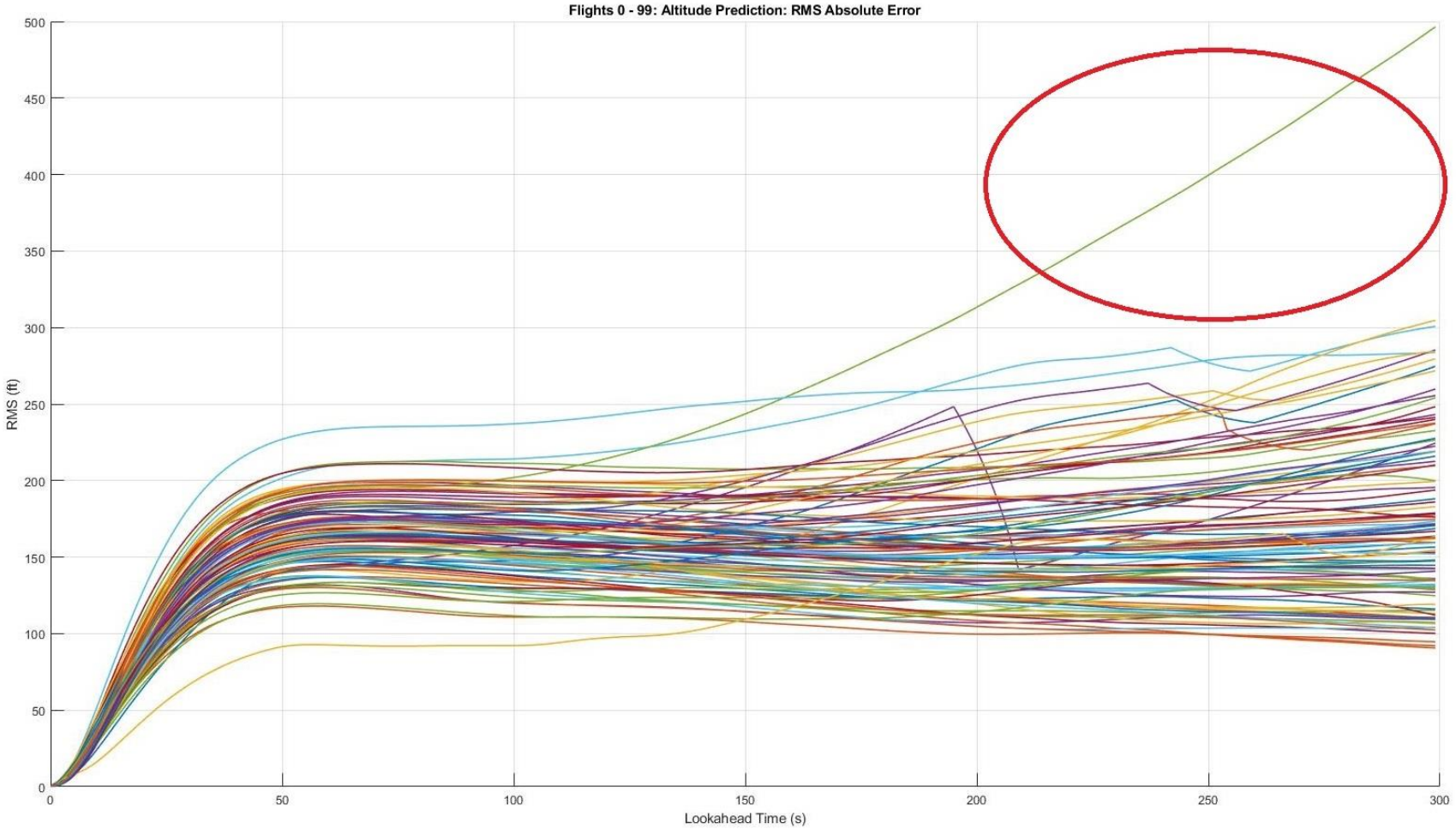

Figure C. 1: Flights 0 - 99: RMS Absolute Error of Altitude Prediction as a Function of Look-Ahead Time (with circled candidate outliers)

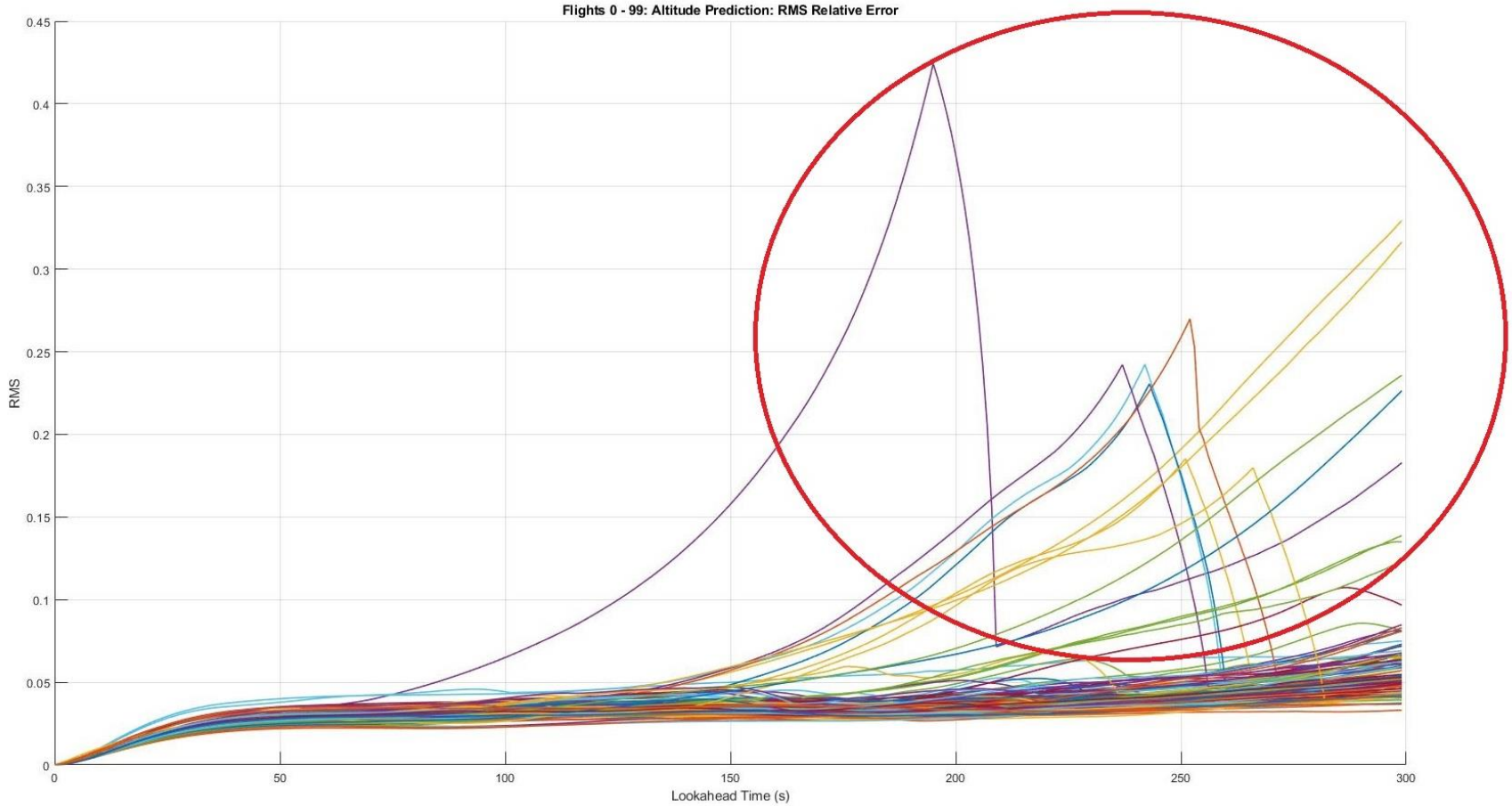

Figure C. 2: Flights 0 - 99: RMS Relative Error of Altitude Prediction as a Function of Look-Ahead Time (with circled candidate outliers)

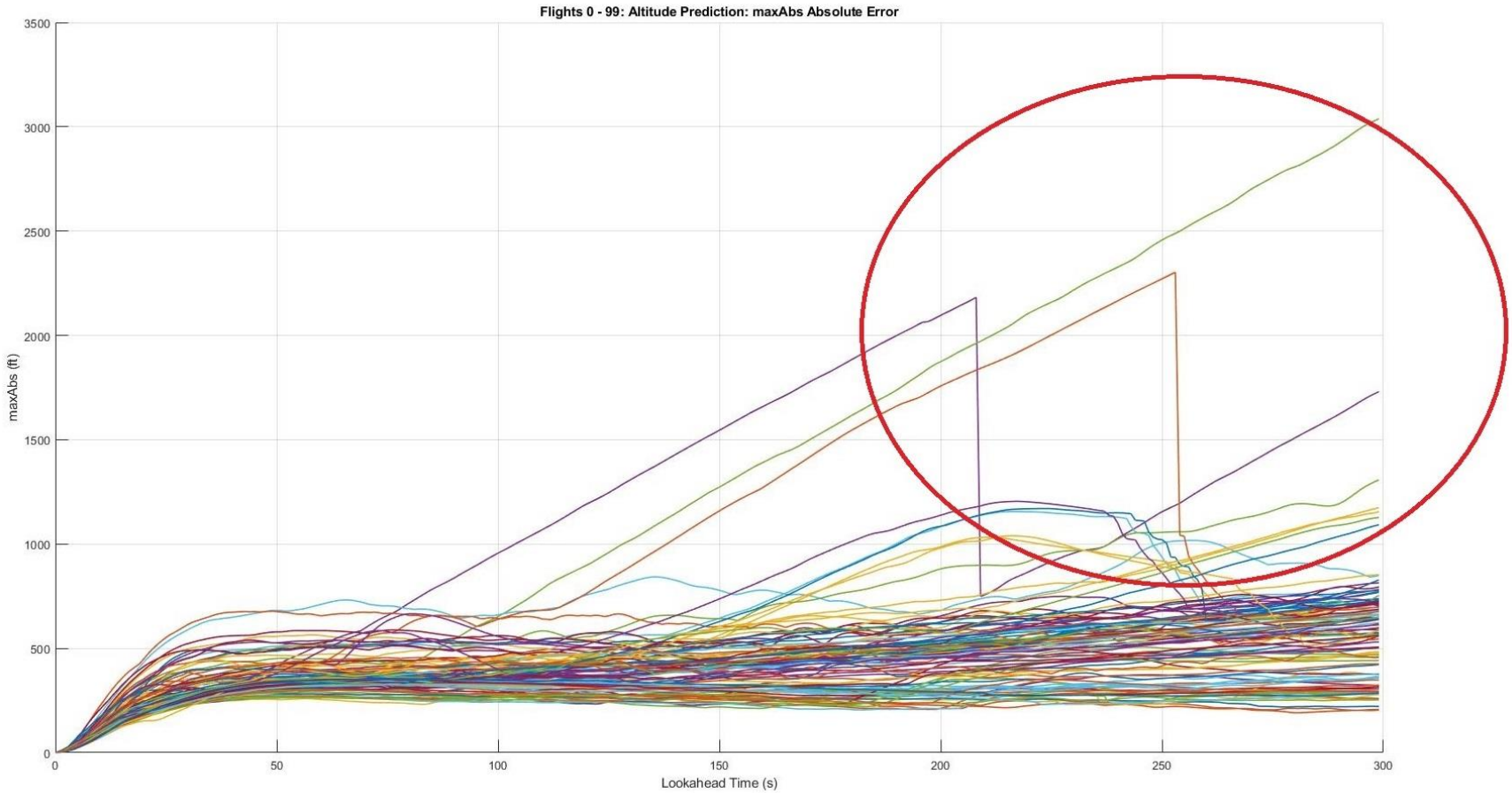

Figure C. 3: Flights 0 - 99: maxAbs Absolute Error of Altitude Prediction as a Function of Look-Ahead Time (with circled candidate outliers)

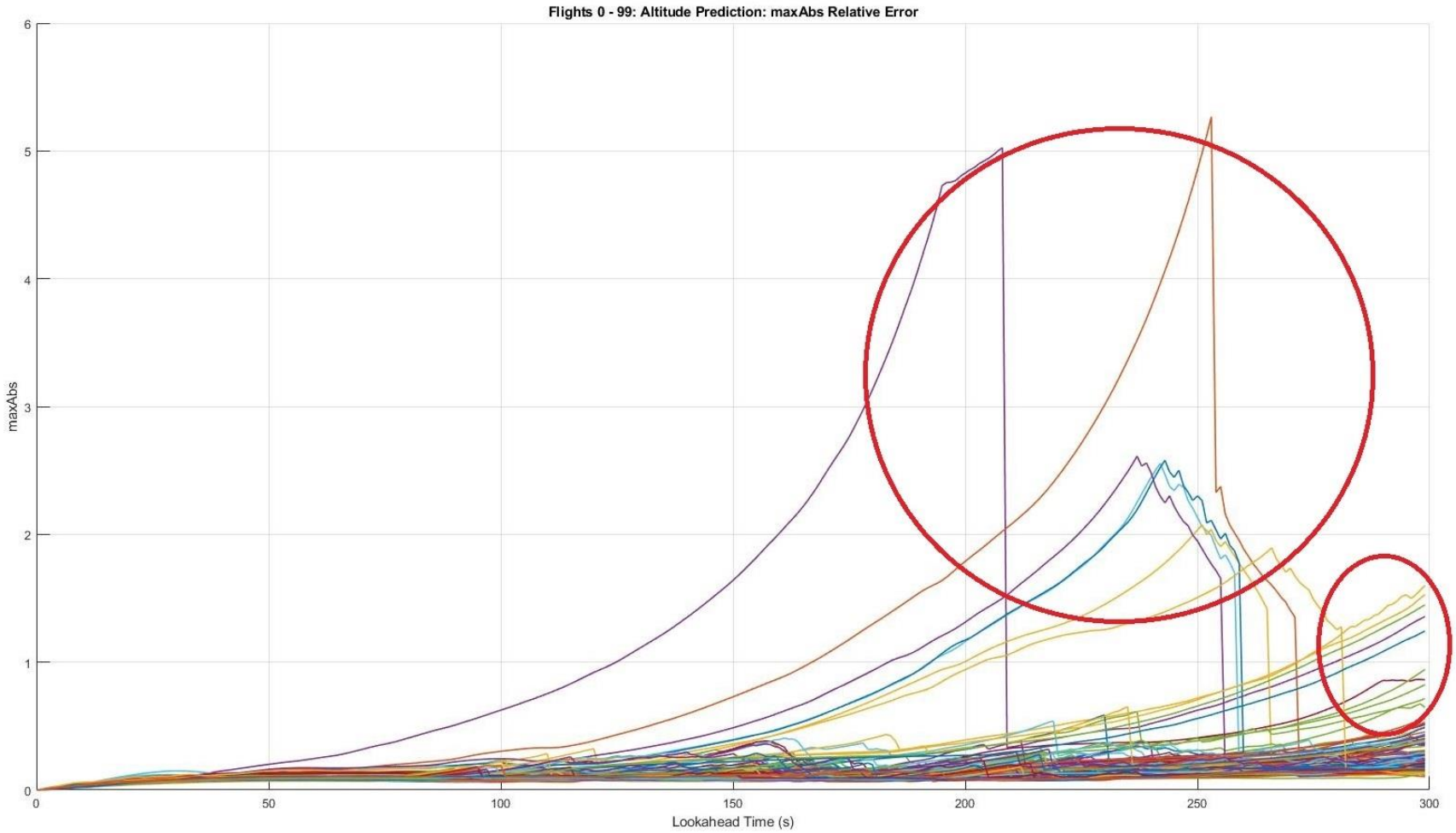

Figure C. 4: Flights 0 - 99: maxAbs Relative Error of Altitude Prediction as a Function of Look-Ahead Time (with circled candidate outliers)

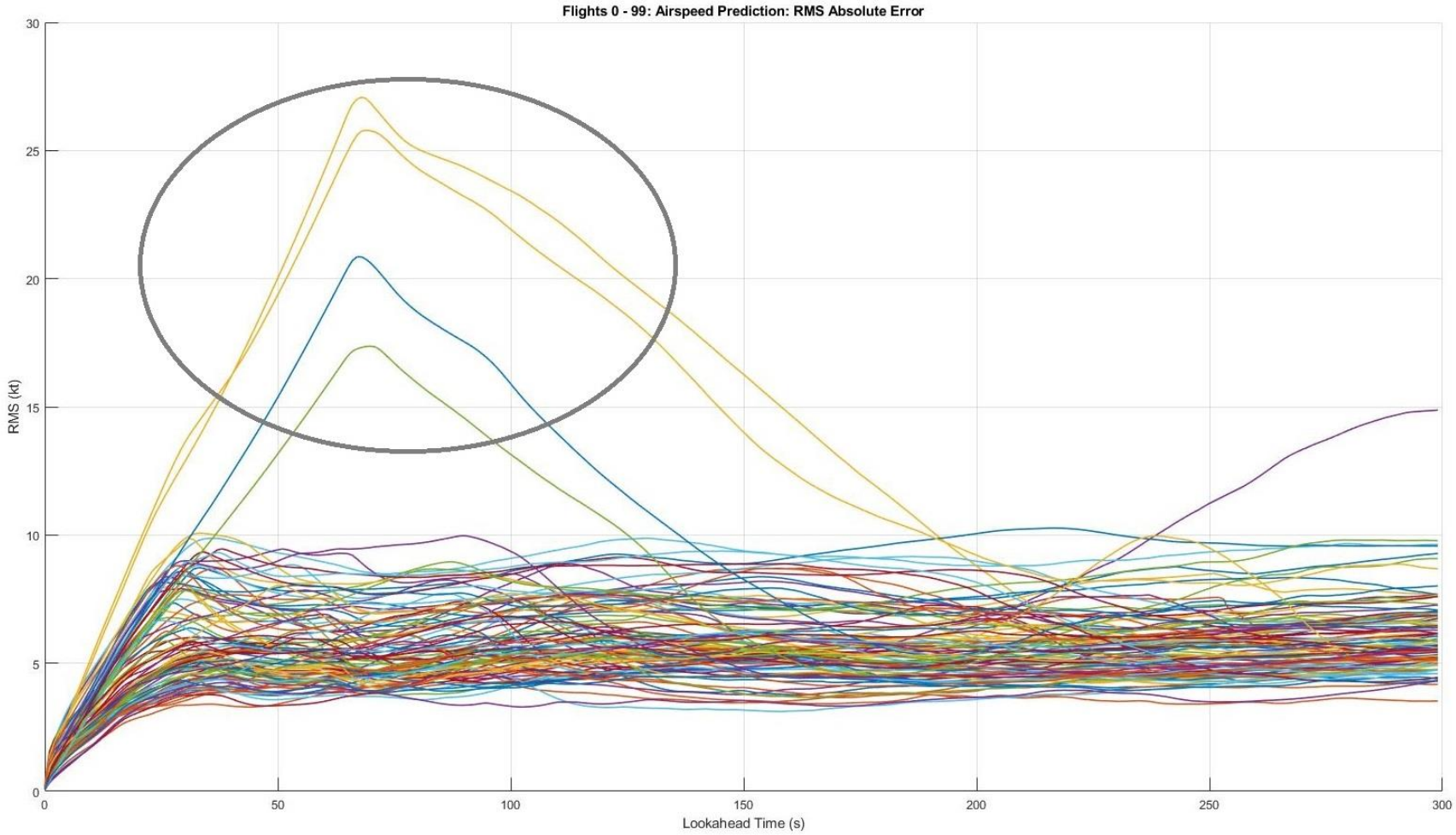

Figure C. 5: Flights 0 - 99: RMS Absolute Error of Airspeed Prediction as a Function of Look-Ahead Time (with circled candidate outliers)

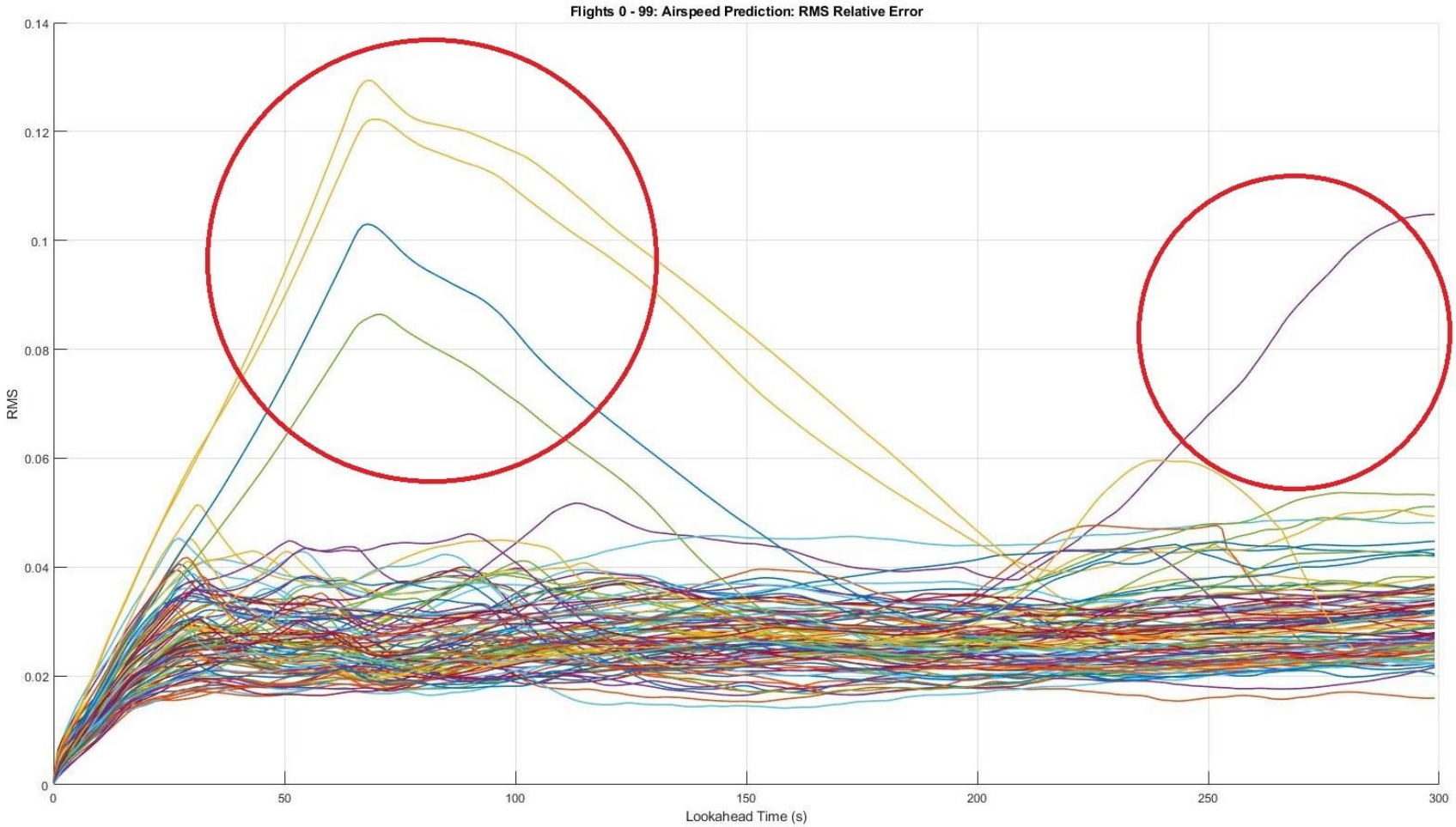

Figure C. 6: Flights 0 - 99: RMS Relative Error of Airspeed Prediction as a Function of Look-Ahead Time (with circled candidate outliers)

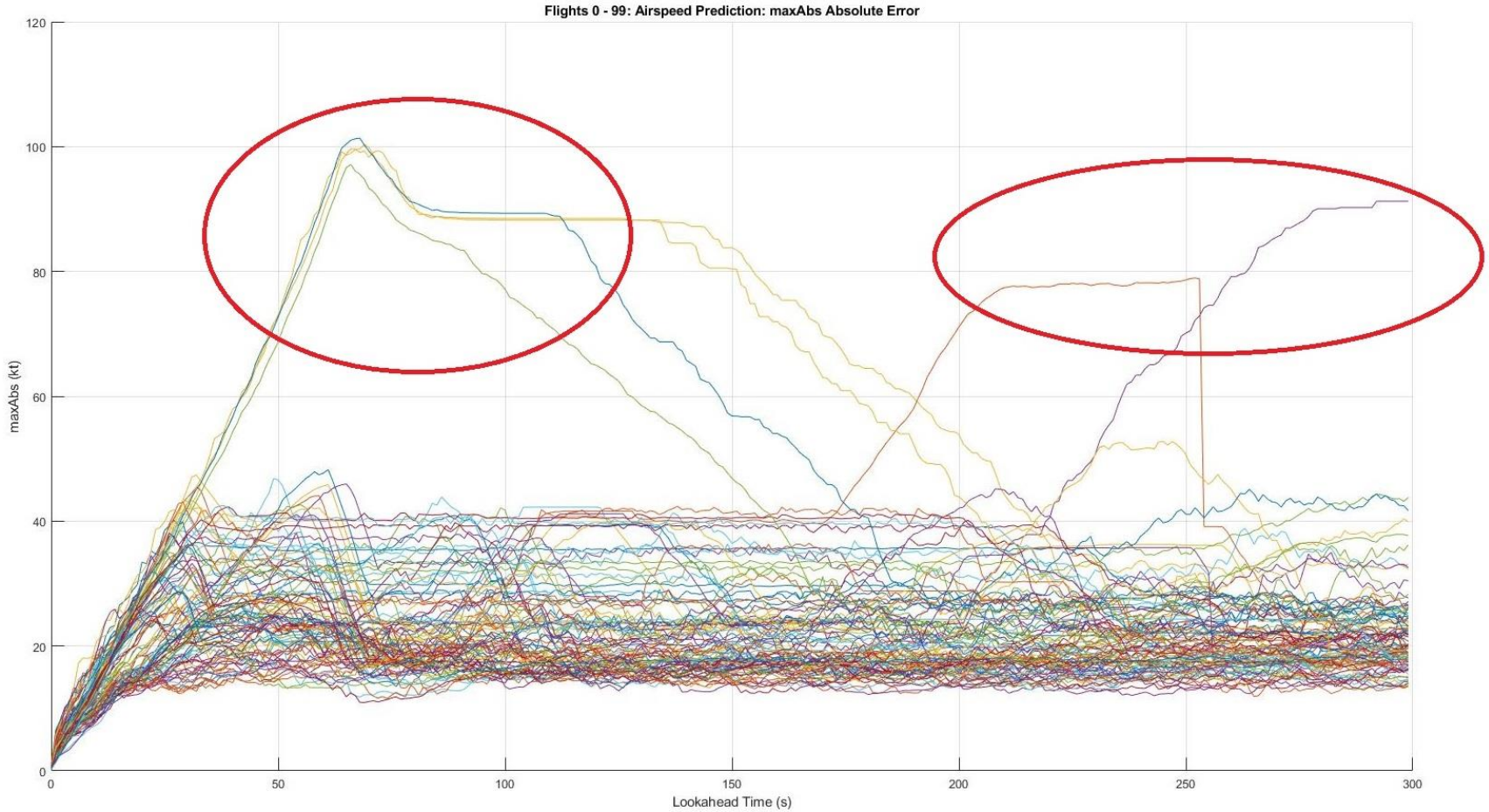

Figure C. 7: Flights 0 - 99: maxAbs Absolute Error of Airspeed Prediction as a Function of Look-Ahead Time (with circled candidate outliers)

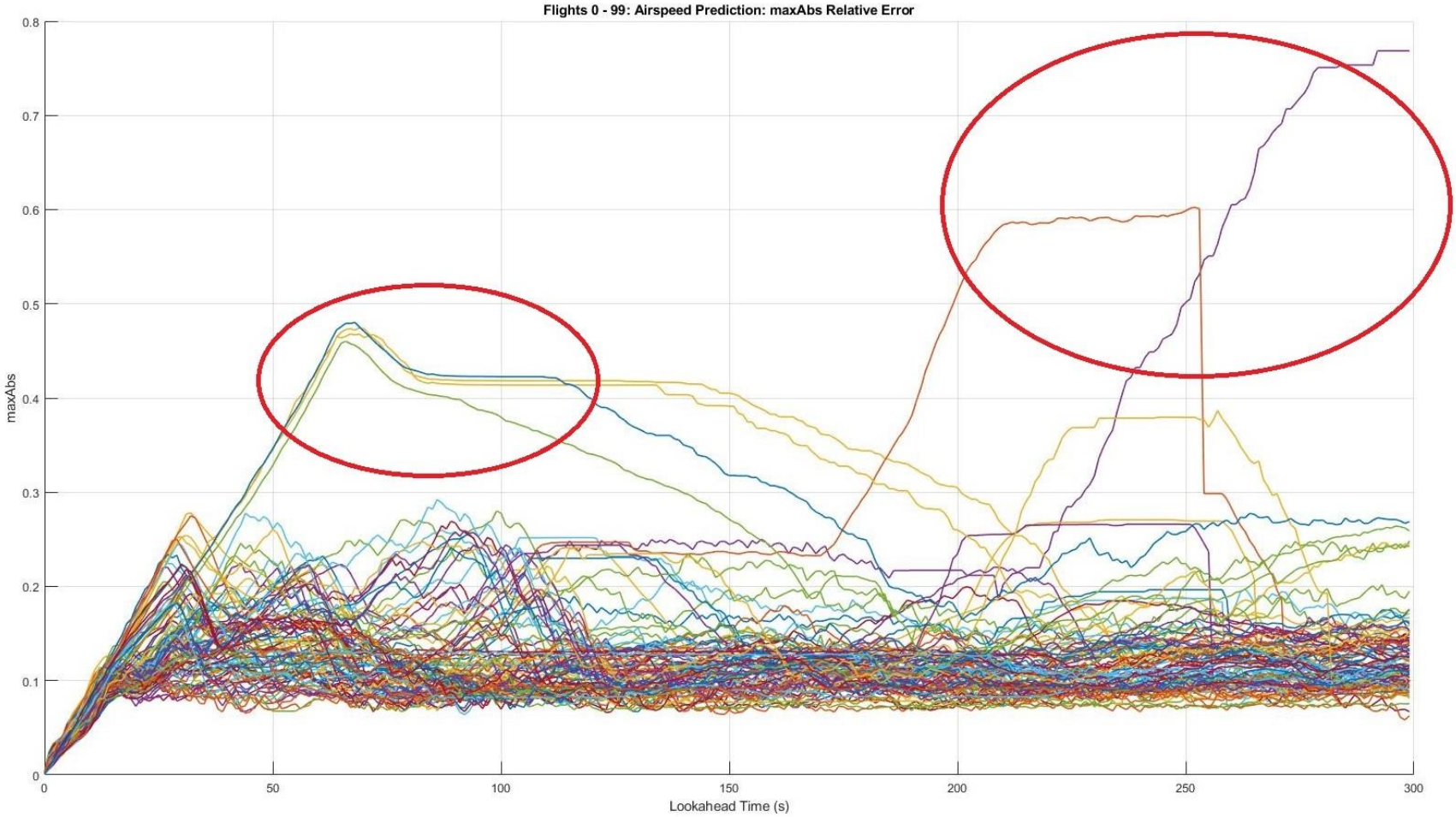

Figure C. 8: Flights 0 - 99: maxAbs Relative Error of Airspeed Prediction as a Function of Look-Ahead Time (with circled candidate outliers)

Appendix D. Prediction Performance for Selected Set of Outlier Test Flights

The following figures show the prediction performance plots for the selected set of test flights with outlier prediction performance. The plots are for RMS and maxAbs statistics of absolute and relative prediction errors for altitude and airspeed.

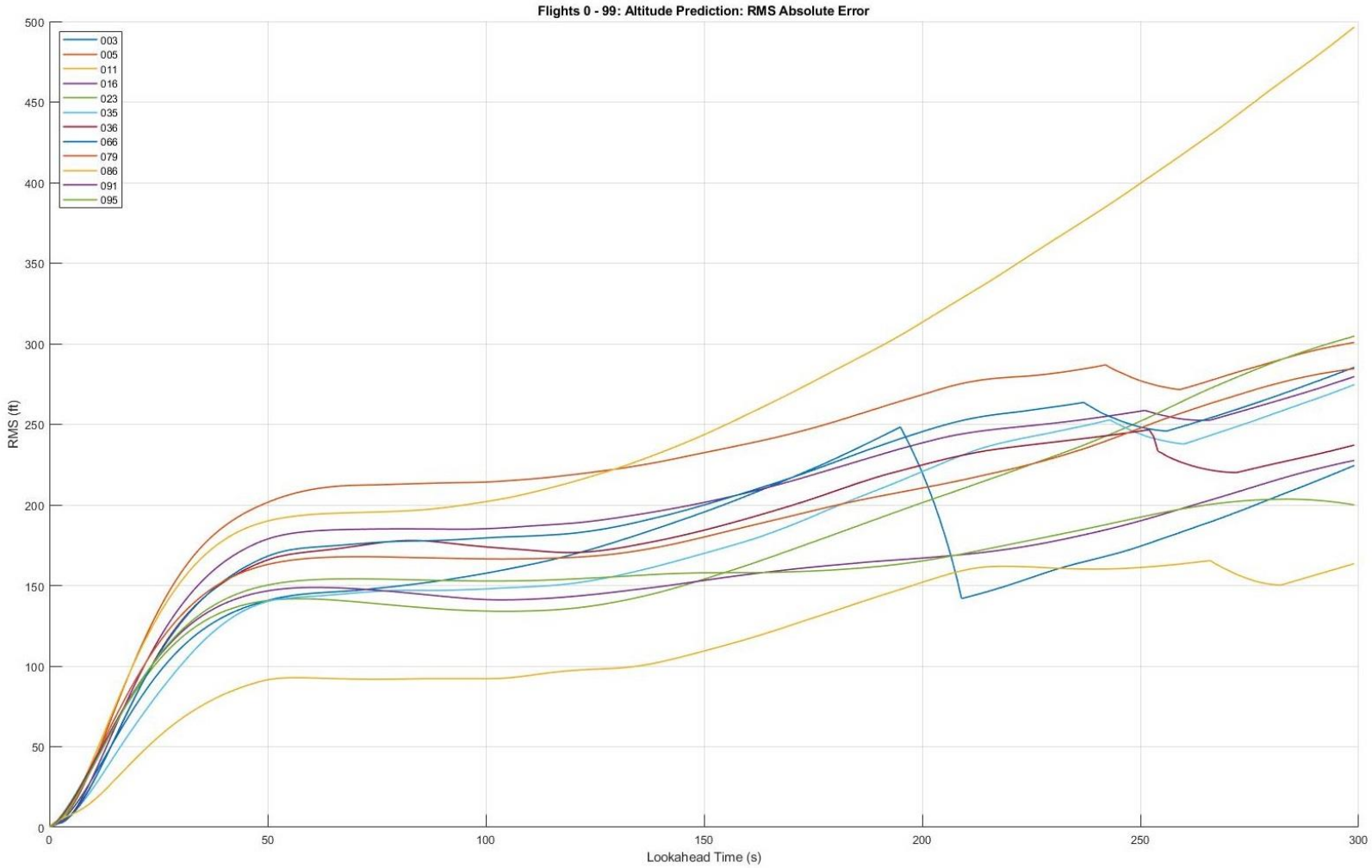

Figure D. 1: Outlier Test Flights: RMS Absolute Error of Altitude Prediction as a Function of Look-Ahead Time

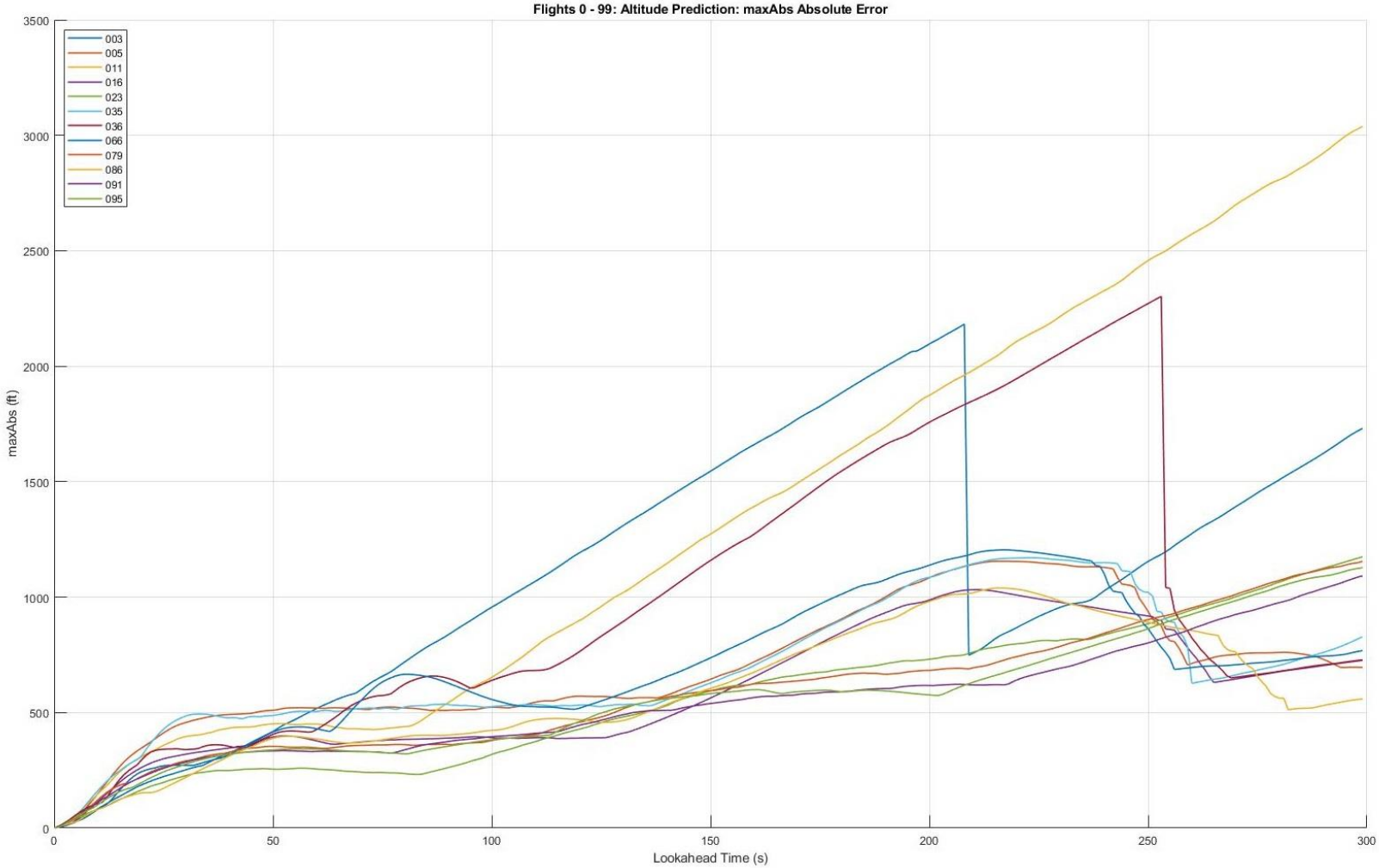

Figure D. 2: Outlier Test Flights: maxAbs Absolute Error of Altitude Prediction as a Function of Look-Ahead Time

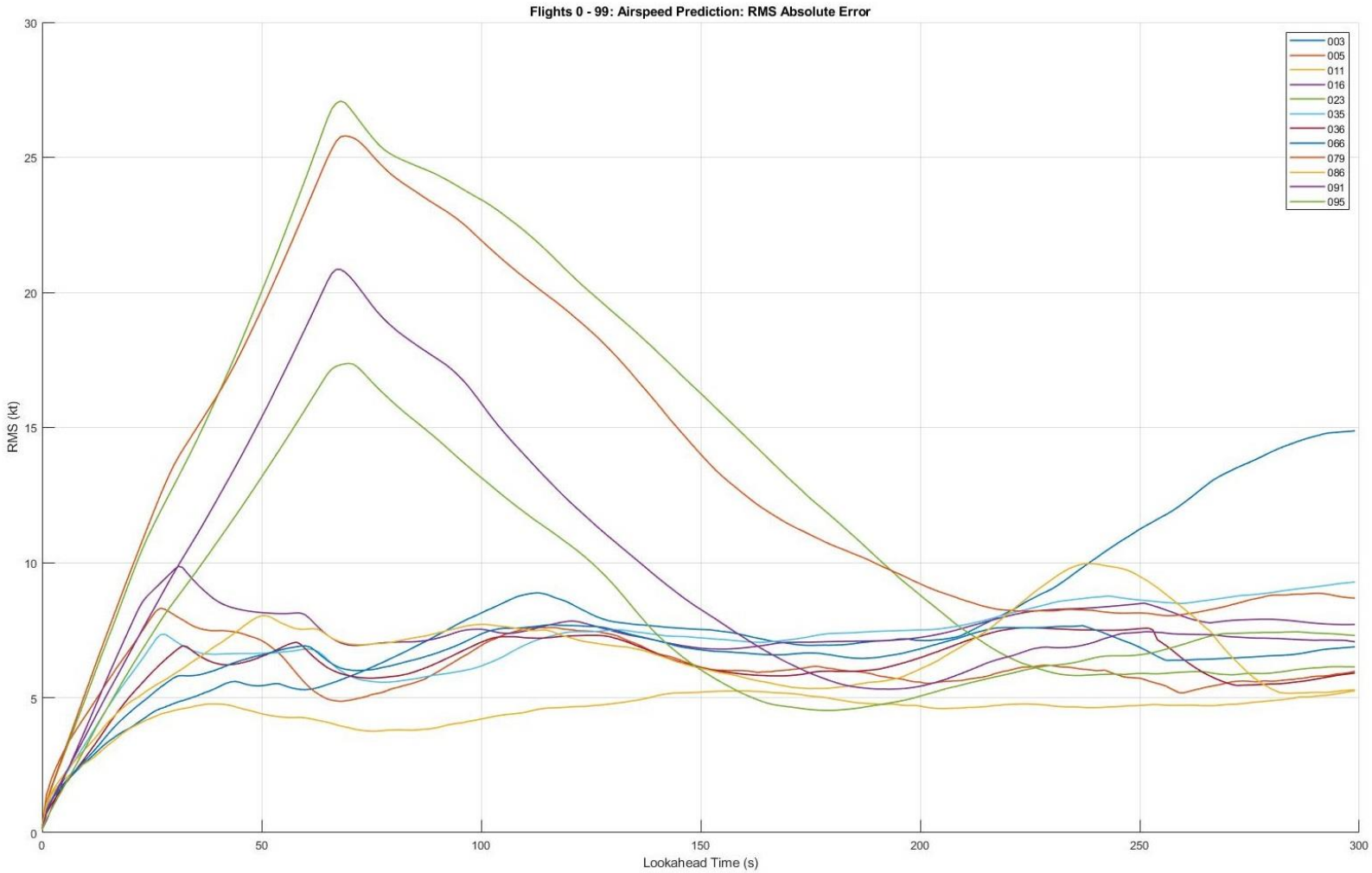

Figure D. 3: Outlier Test Flights: RMS Absolute Error of Airspeed Prediction as a Function of Look-Ahead Time

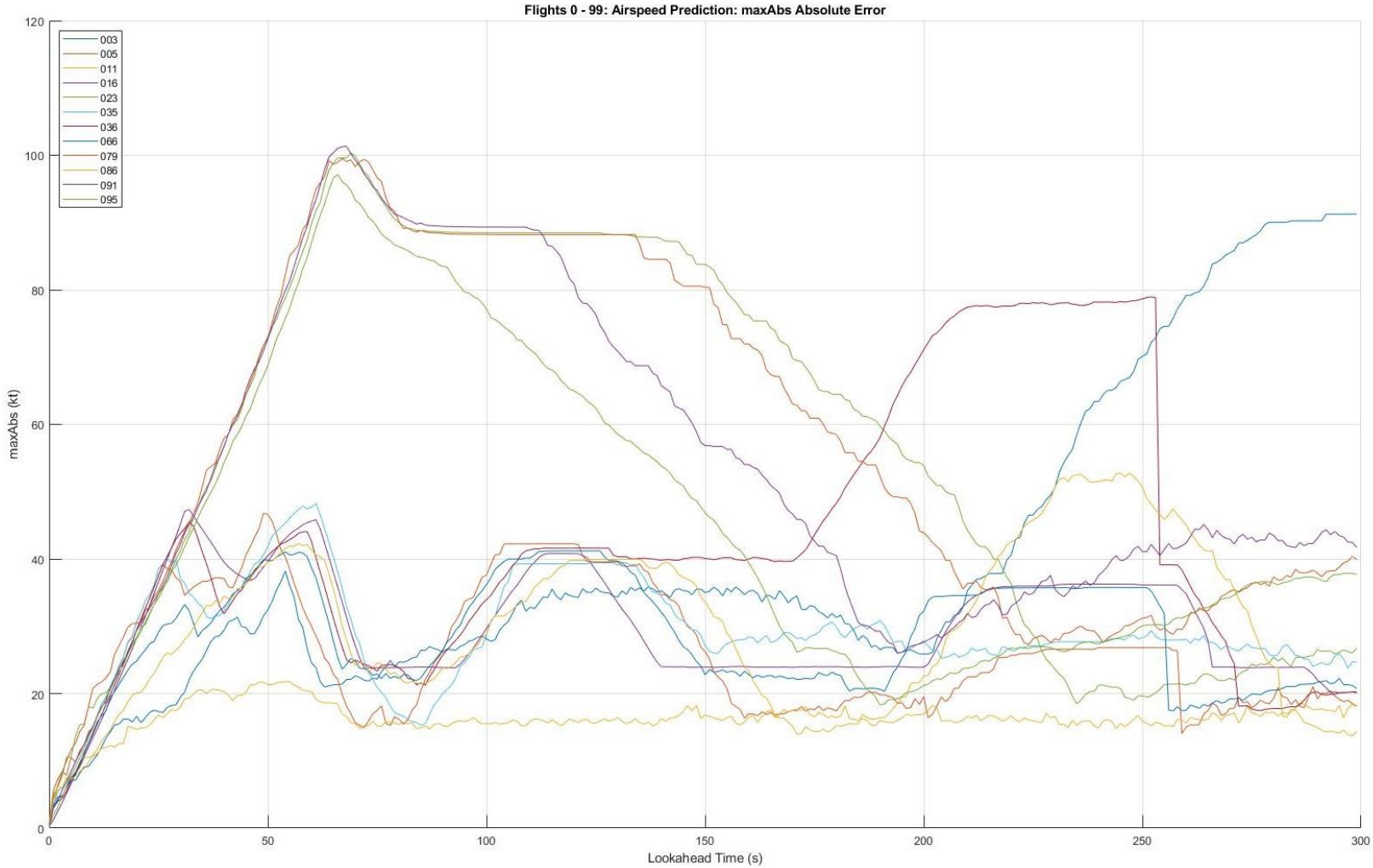

Figure D. 4: Outlier Test Flights: maxAbs Absolute Error of Airspeed Prediction as a Function of Look-Ahead Time

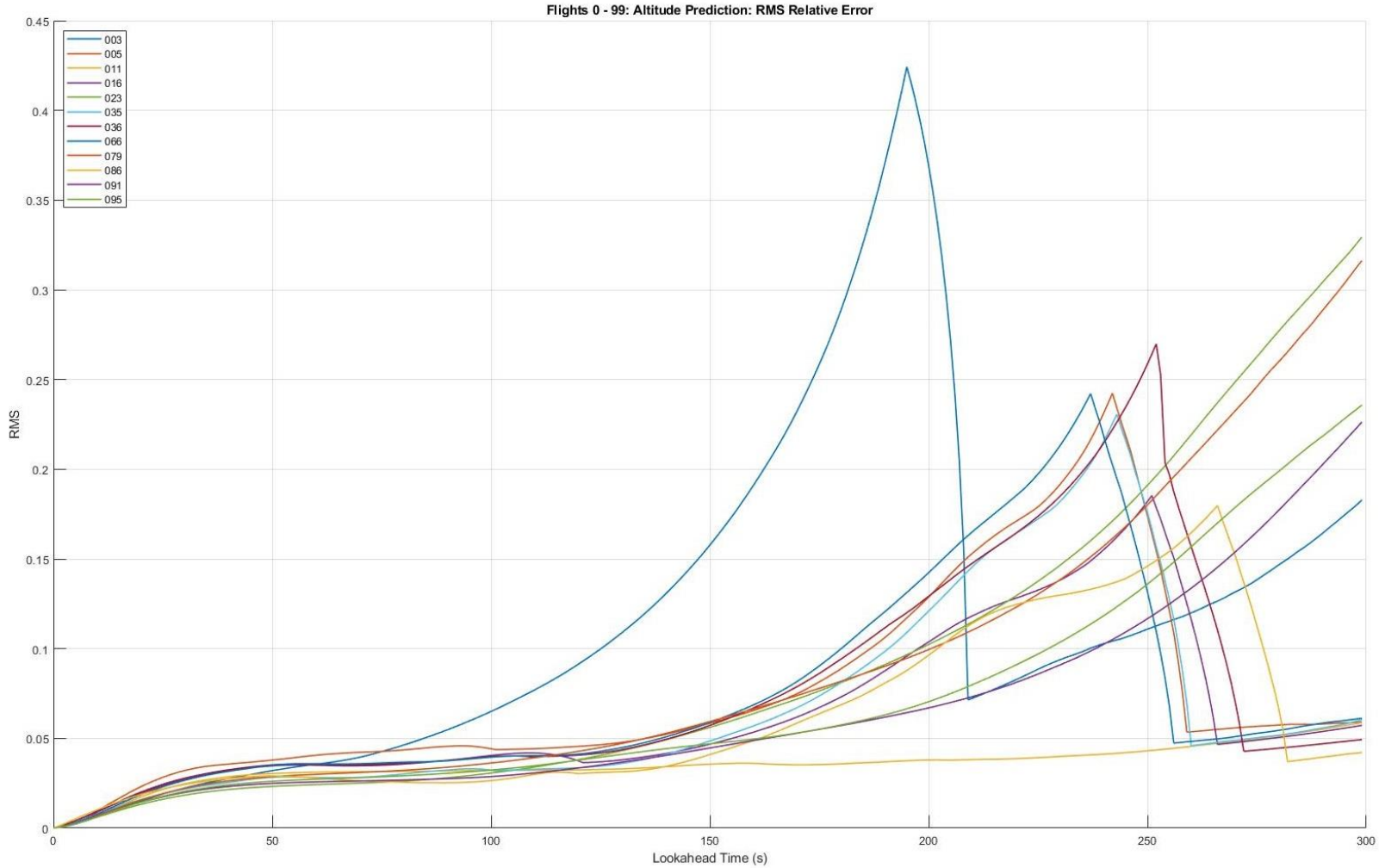

Figure D. 5: Outlier Test Flights: RMS Relative Error of Altitude Prediction as a Function of Look-Ahead Time

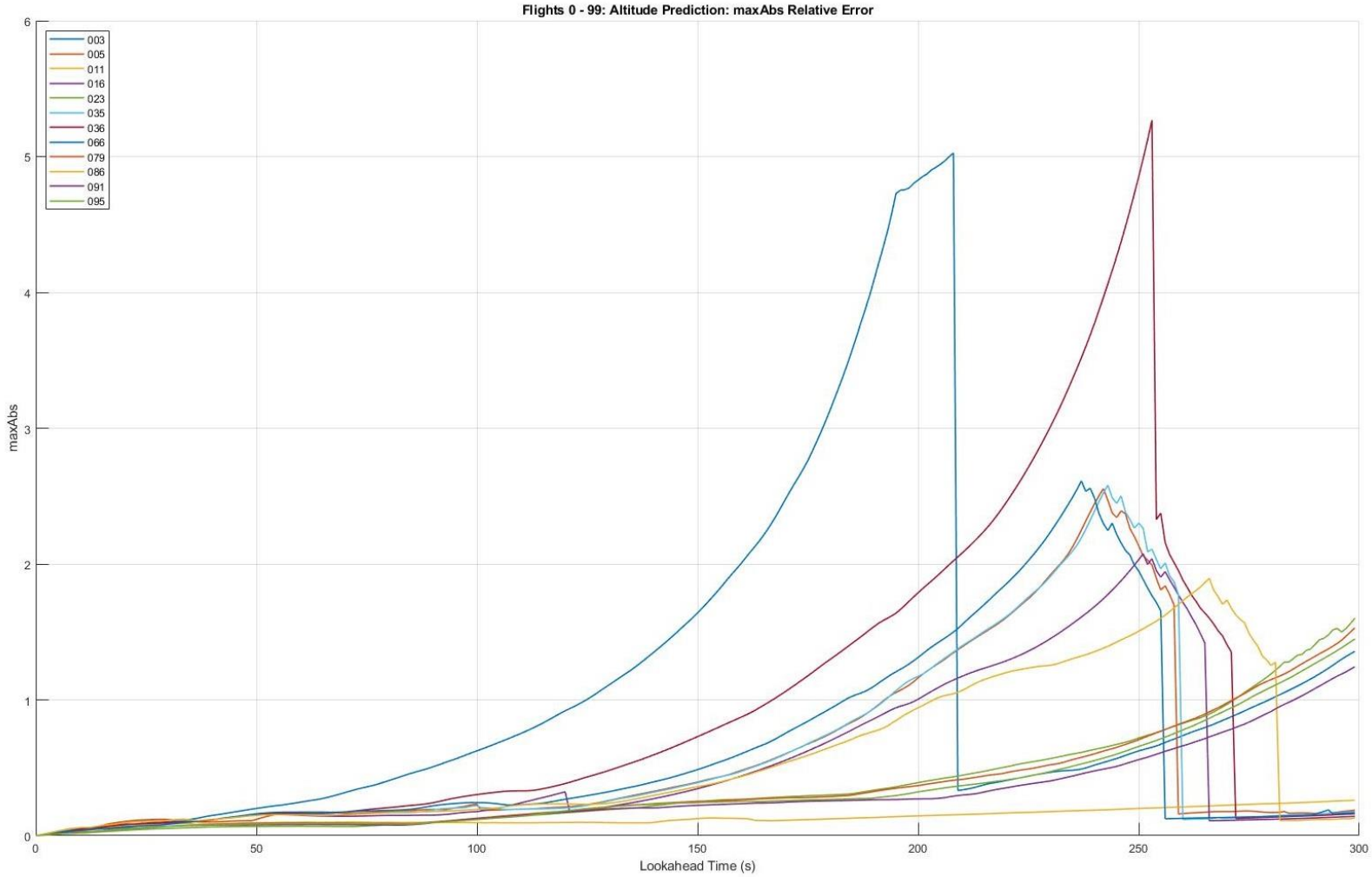

Figure D. 6: Outlier Test Flights: maxAbs Relative Error of Altitude Prediction as a Function of Look-Ahead Time

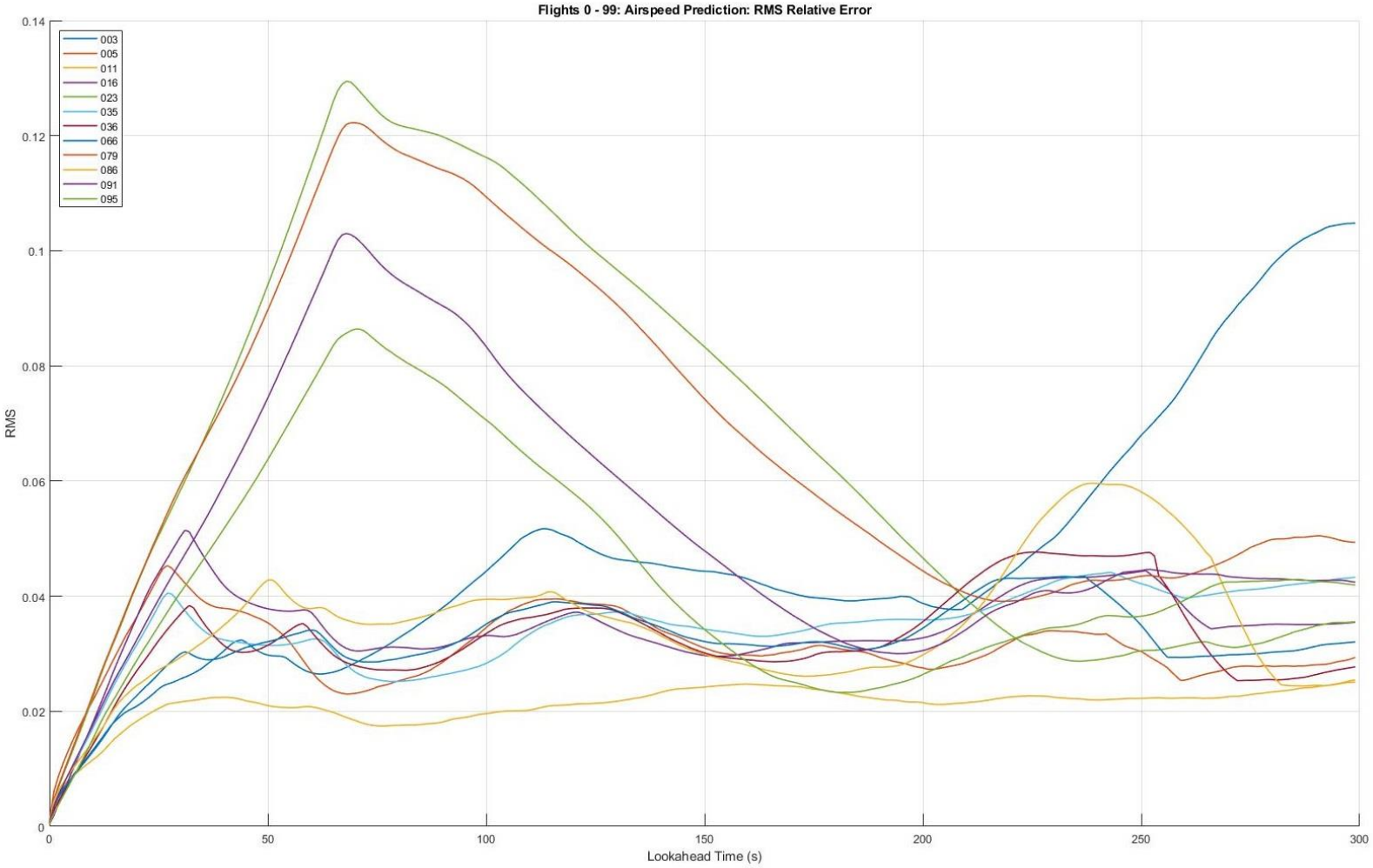

Figure D. 7: Outlier Test Flights: RMS Relative Error of Airspeed Prediction as a Function of Look-Ahead Time

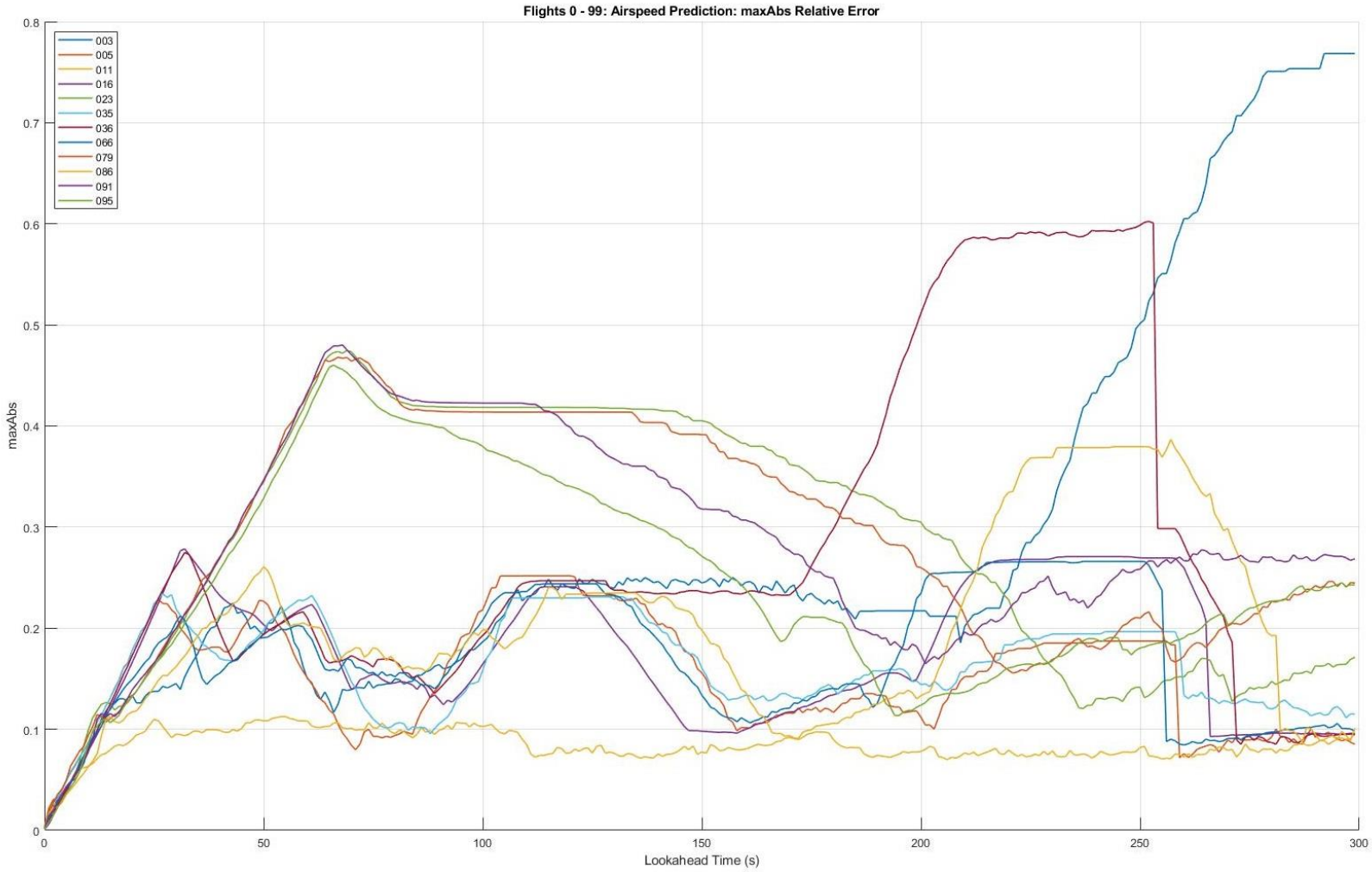

Figure D. 8: Outlier Test Flights: maxAbs Relative Error of Airspeed Prediction as a Function of Look-Ahead Time

Appendix E. Prediction Performance for Individual Outlier Test Flights

This appendix gives a sample of the results for test flights with outlier prediction performance.

E.1: Test Flight 3

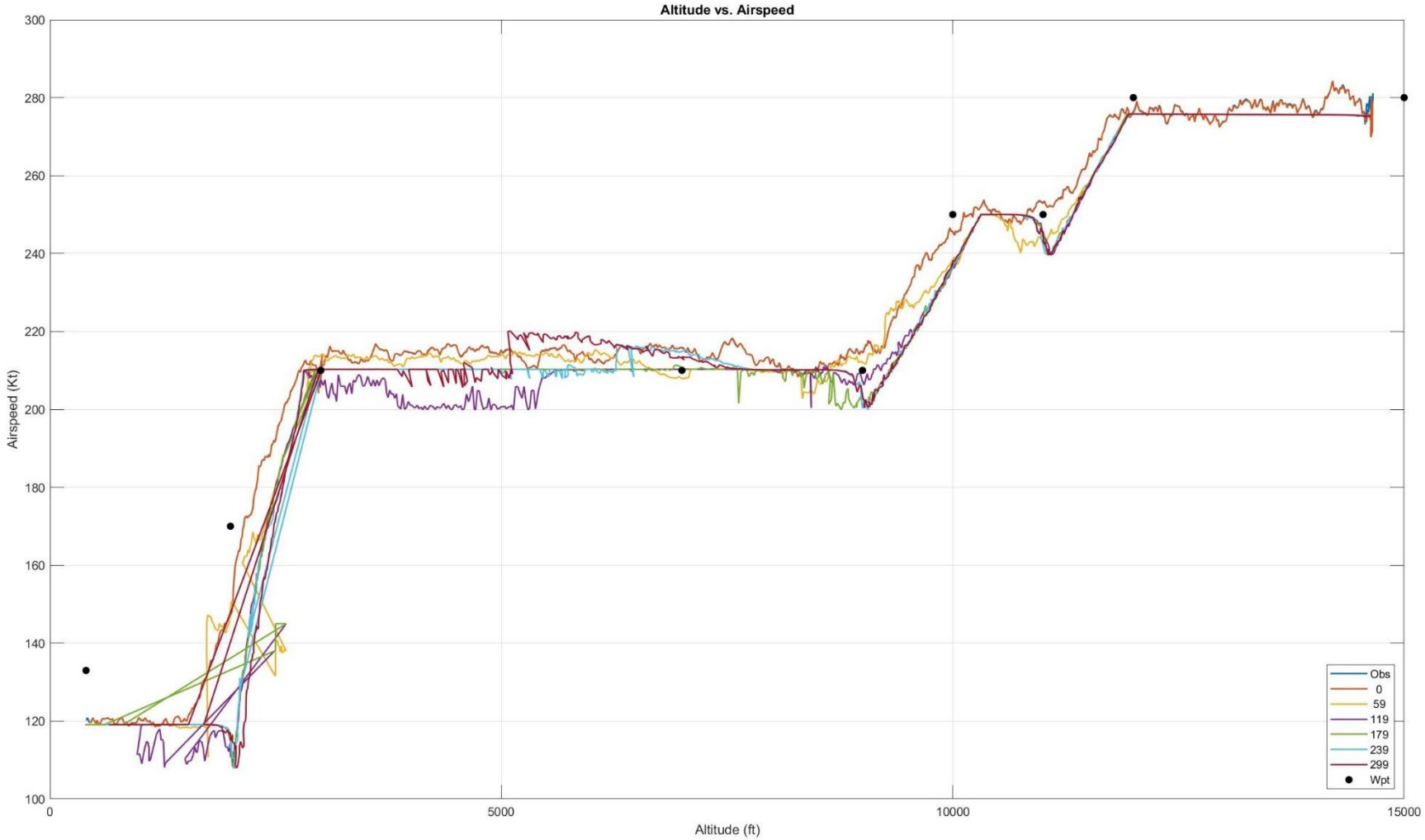

Figure E. 1: Test Flight 3: Observed and Predicted Altitude vs. Airspeed

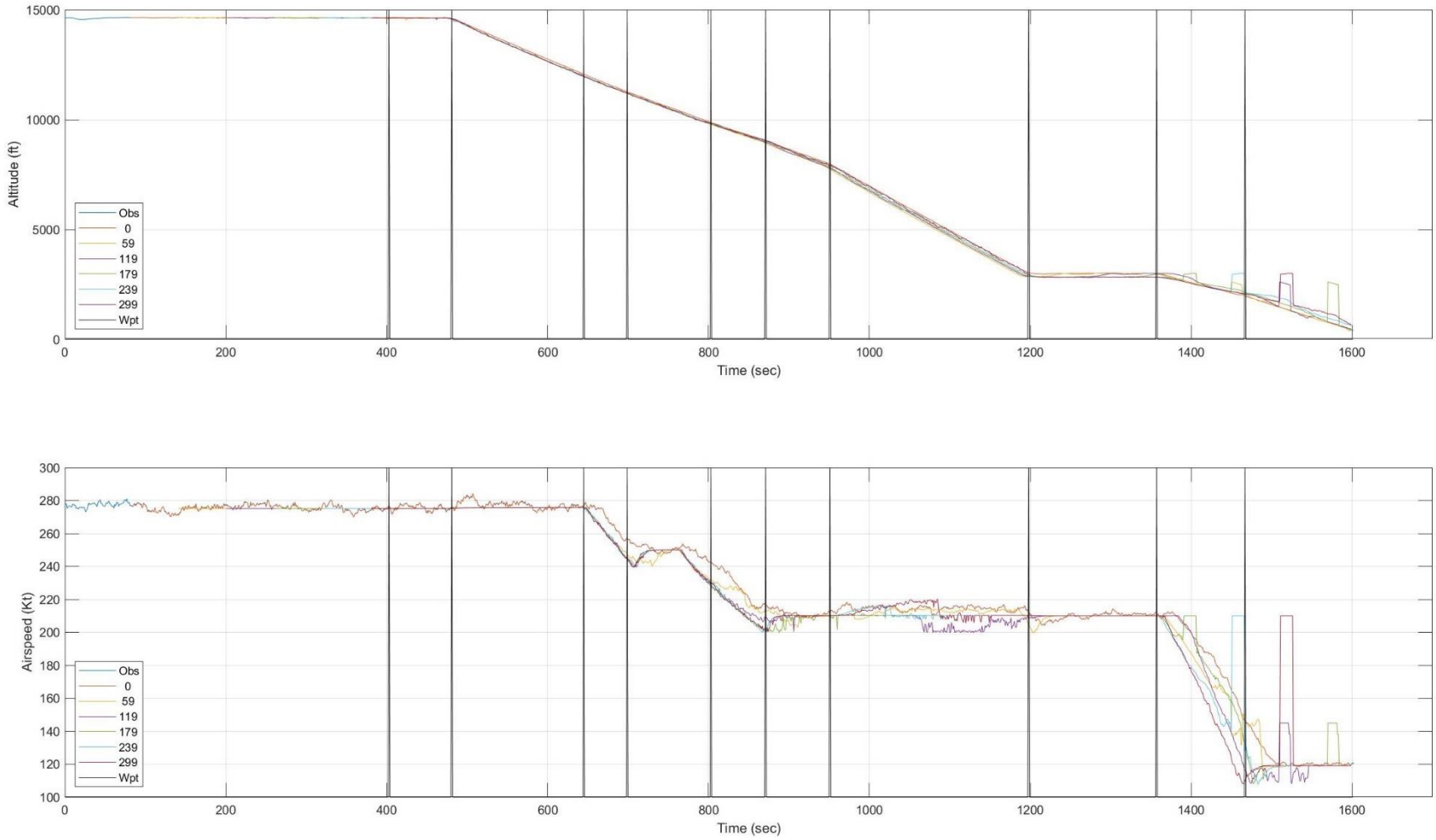

Figure E. 2: Test Flight 3: Observed and Predicted Altitude and Airspeed as a Function of Time t

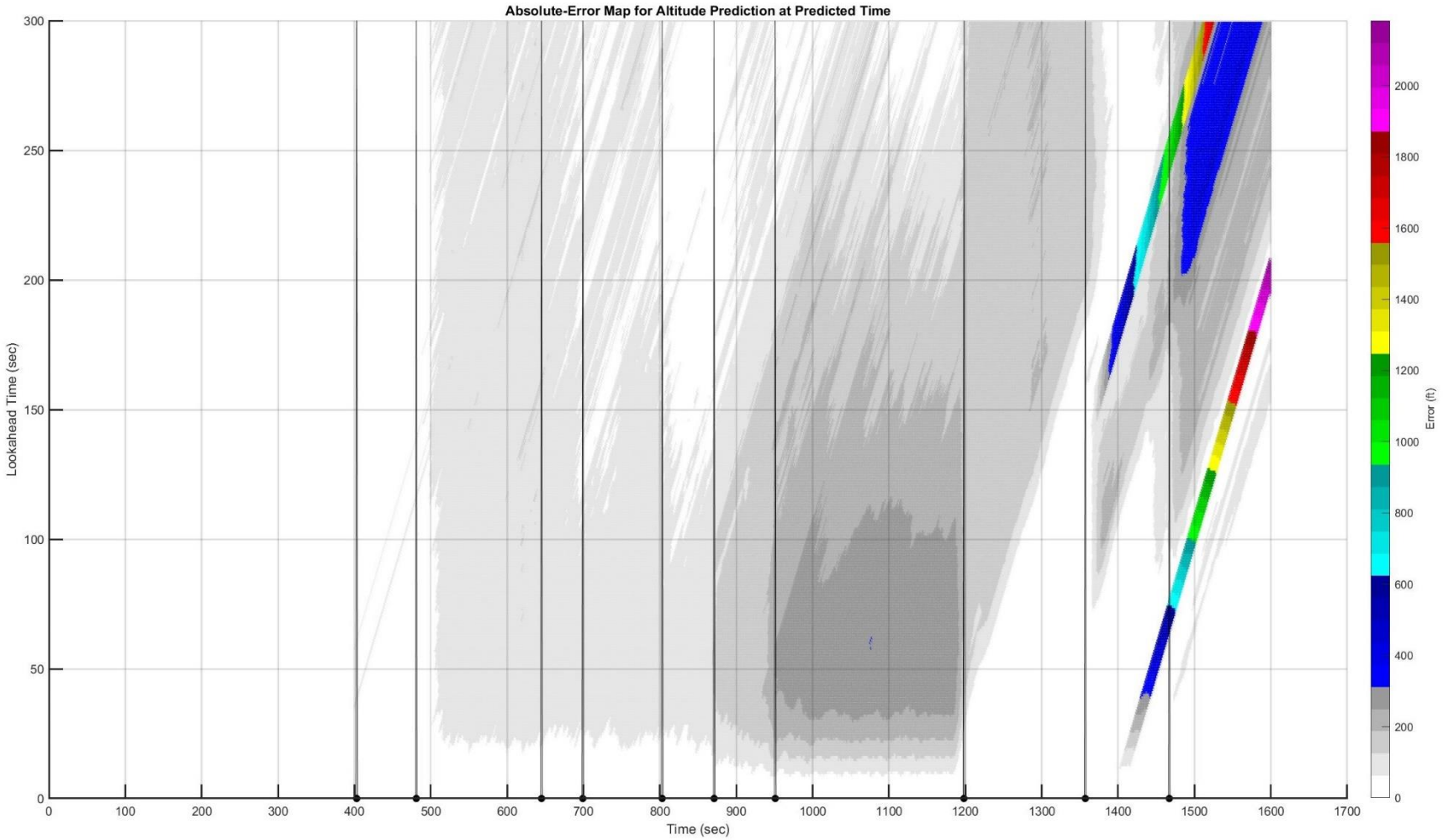

Figure E. 3: Test Flight 3: Heatmap of Absolute Error for Altitude Prediction as a Function of Predicted Time $t + \tau$

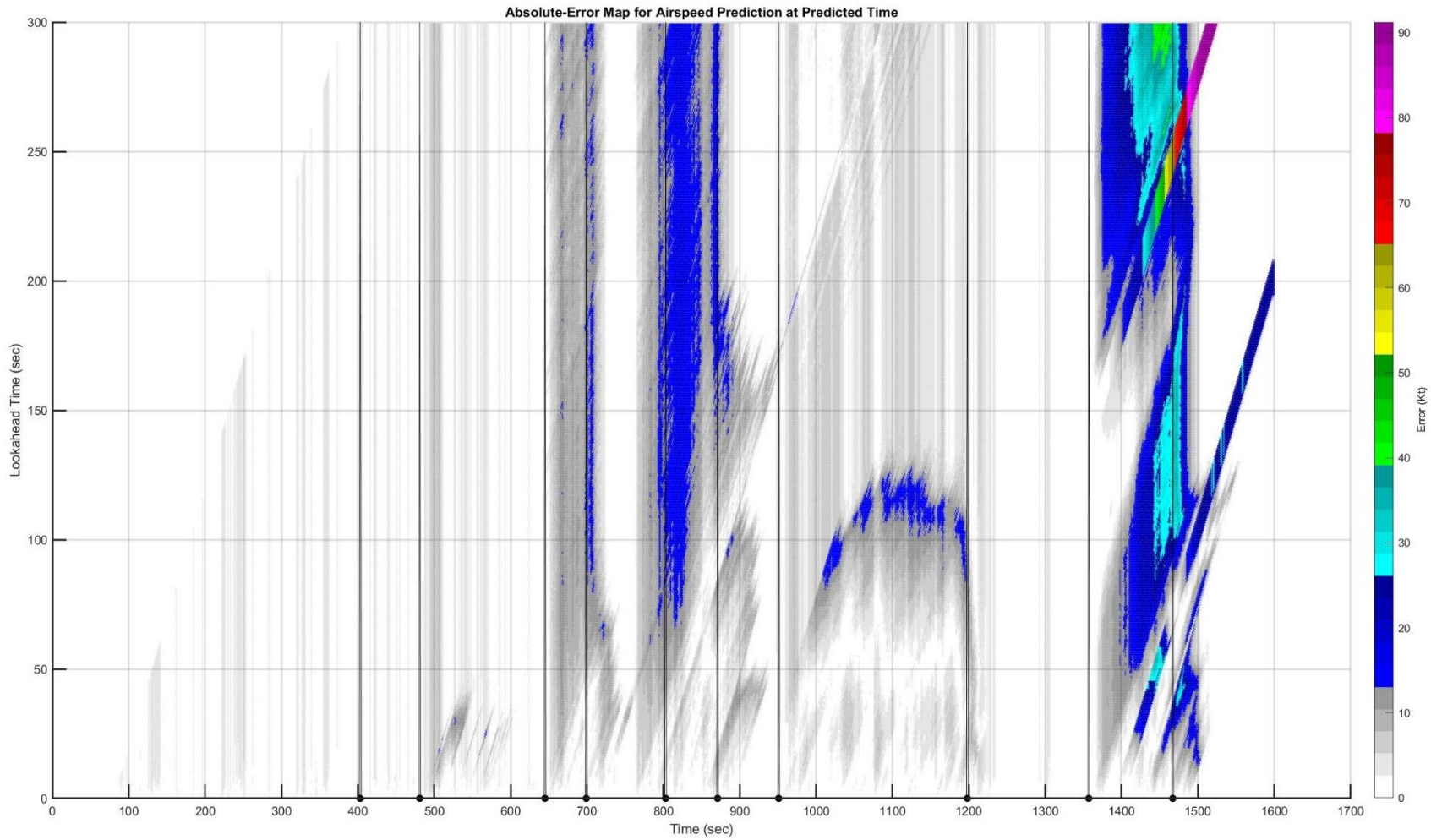

Figure E. 4: Test Flight 3: Heatmap of Absolute Error for Airspeed Prediction as a Function of Predicted Time $t + \tau$

E.2: Test Flight 5

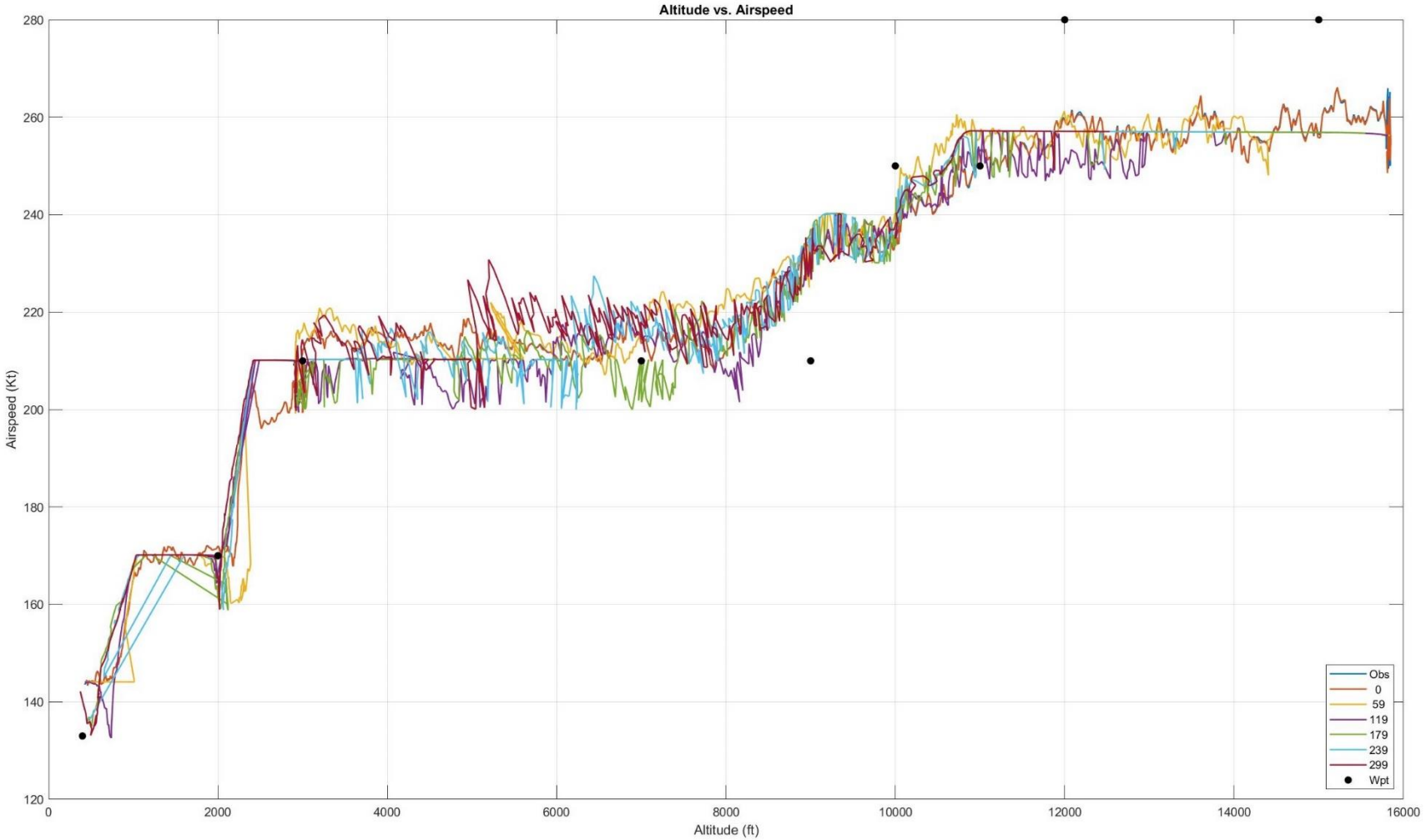

Figure E. 5: Test Flight 5: Observed and Predicted Altitude vs. Airspeed

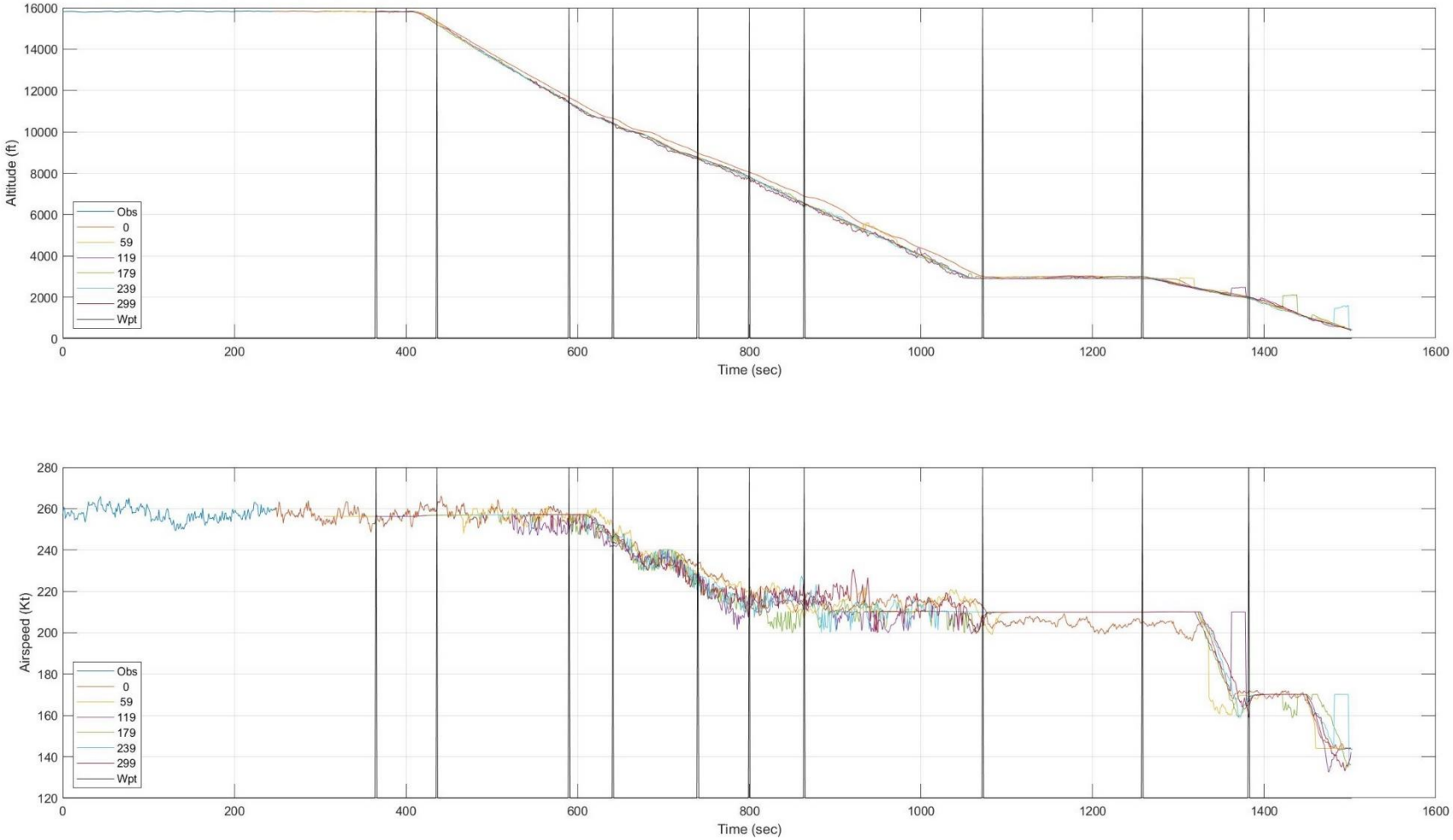

Figure E. 6: Test Flight 5: Observed and Predicted Altitude and Airspeed as a Function of Time t

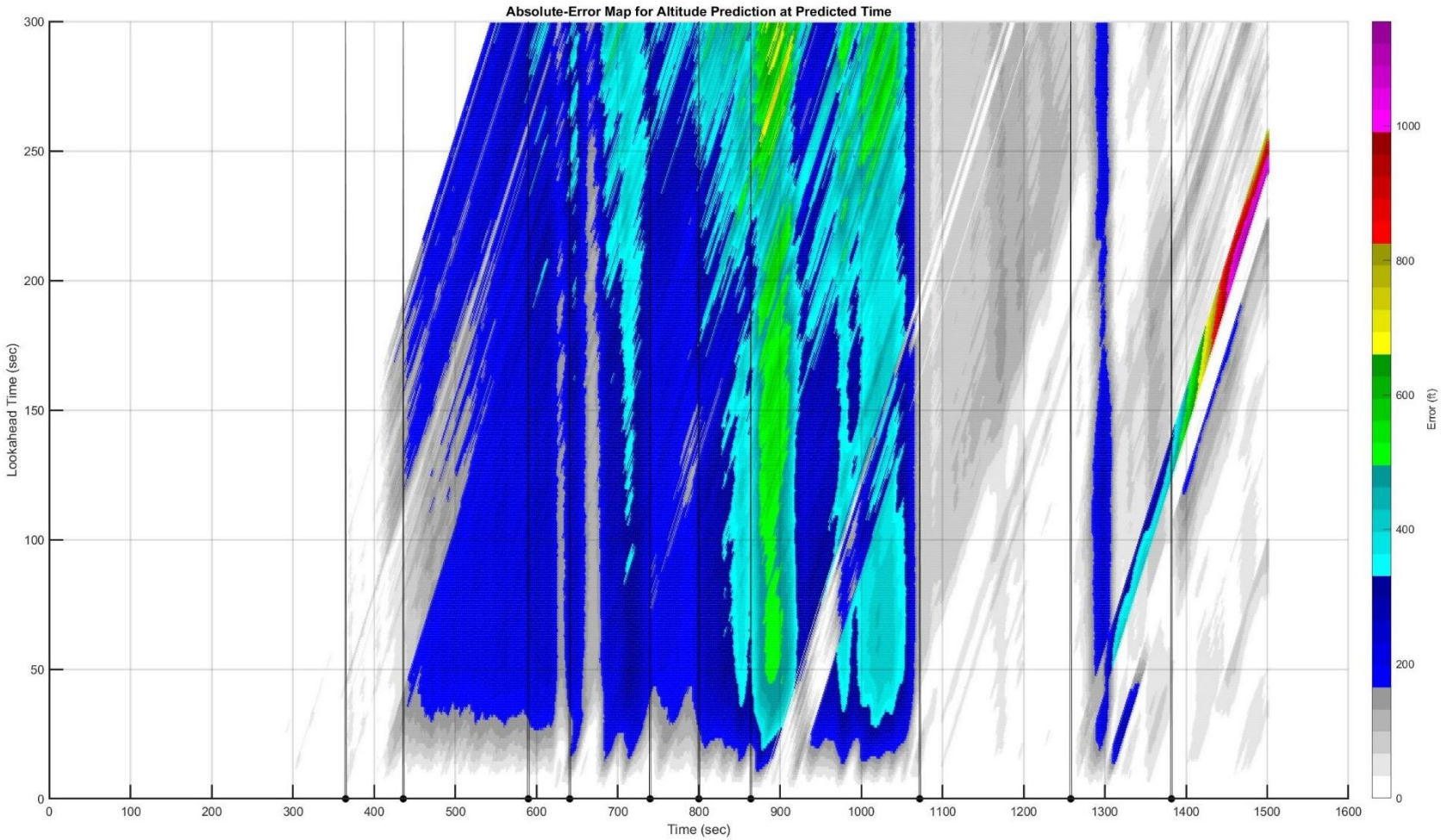

Figure E. 7: Test Flight 5: Heatmap of Absolute Error for Altitude Prediction as a Function of Predicted Time $t + \tau$

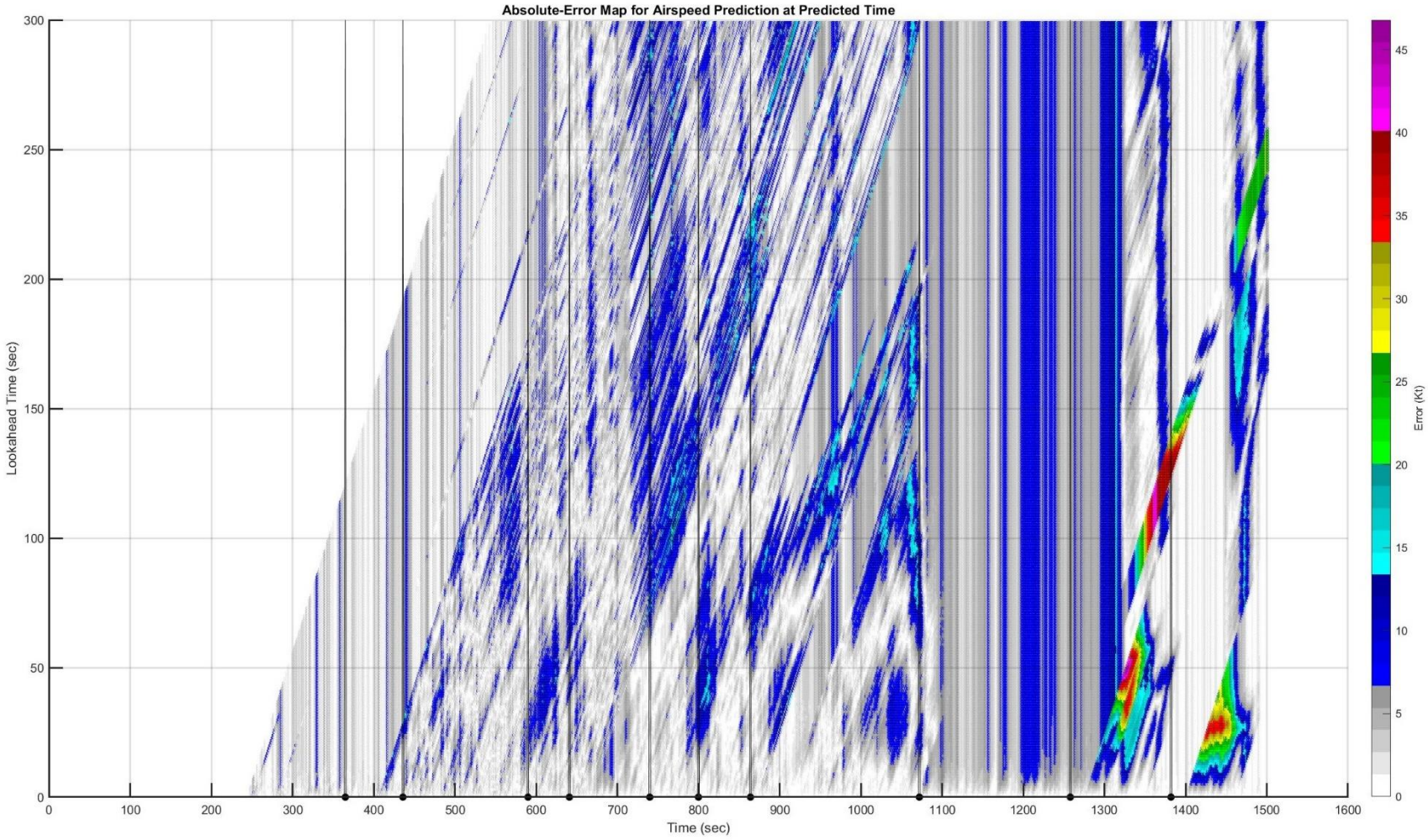

Figure E. 8: Test Flight 5: Heatmap of Absolute Error for Airspeed Prediction as a Function of Predicted Time $t + \tau$

E.3: Test Flight 11

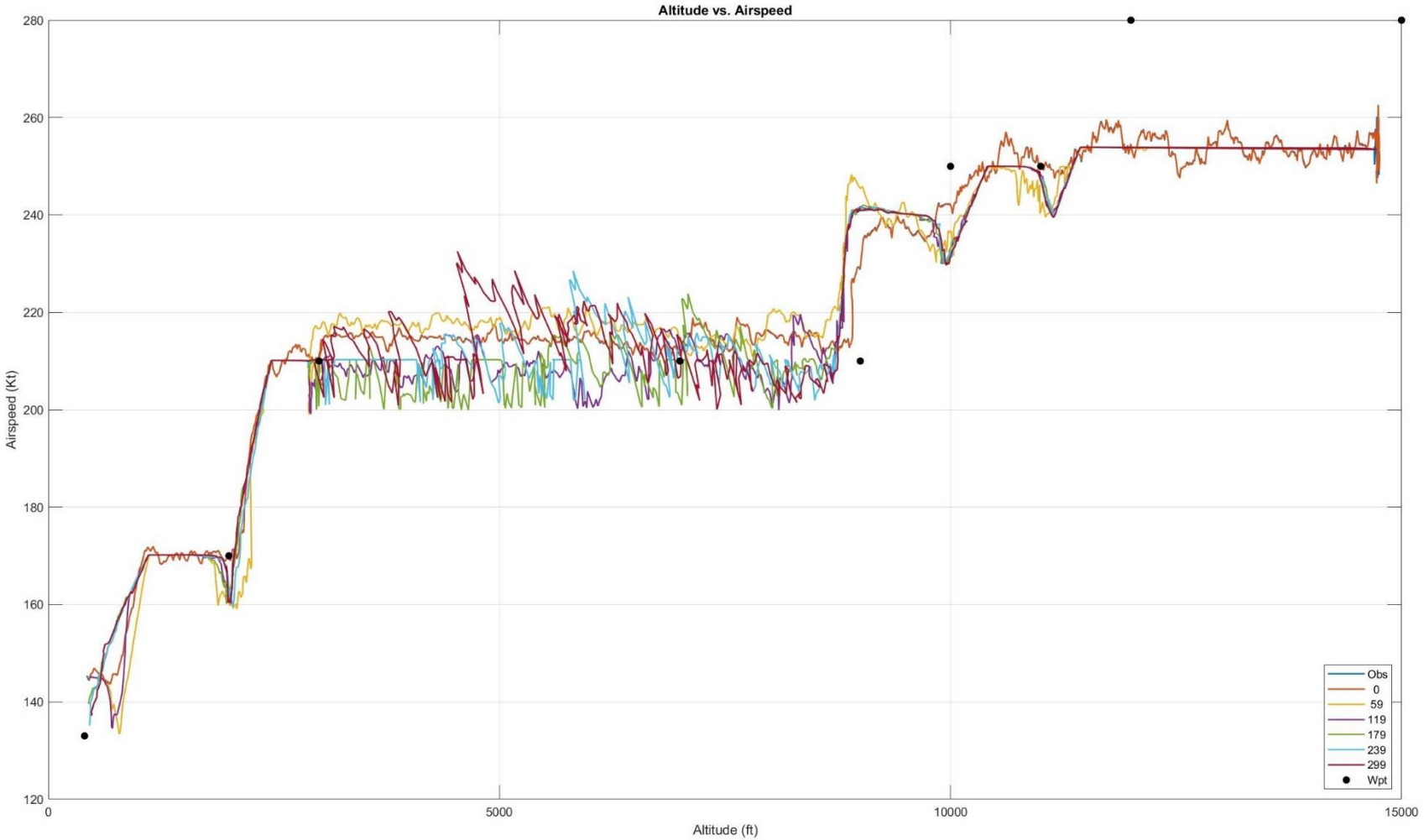

Figure E. 9: Test Flight 11: Observed and Predicted Altitude vs. Airspeed

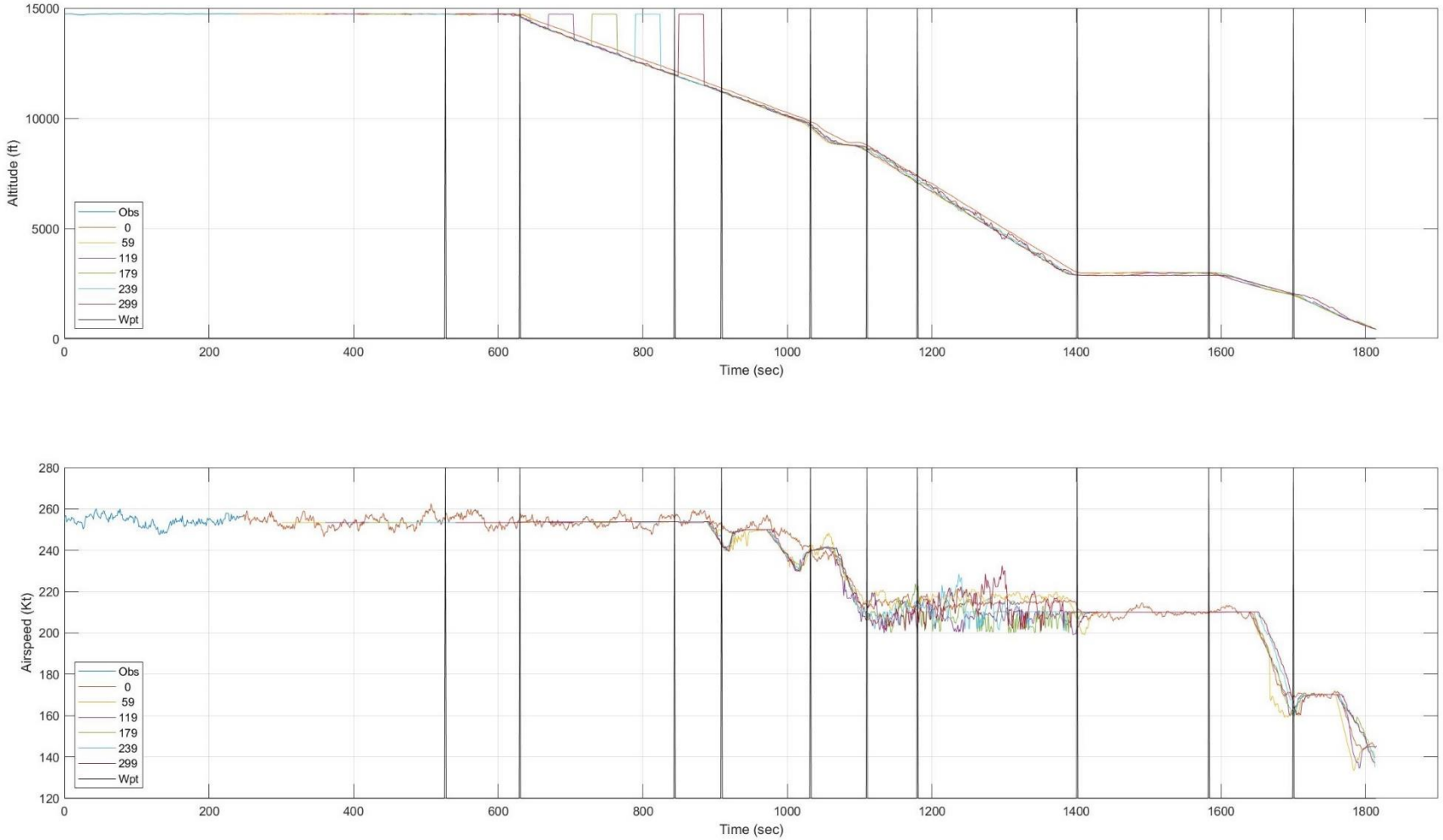

Figure E. 10: Test Flight 11: Observed and Predicted Altitude and Airspeed as a Function of Time t

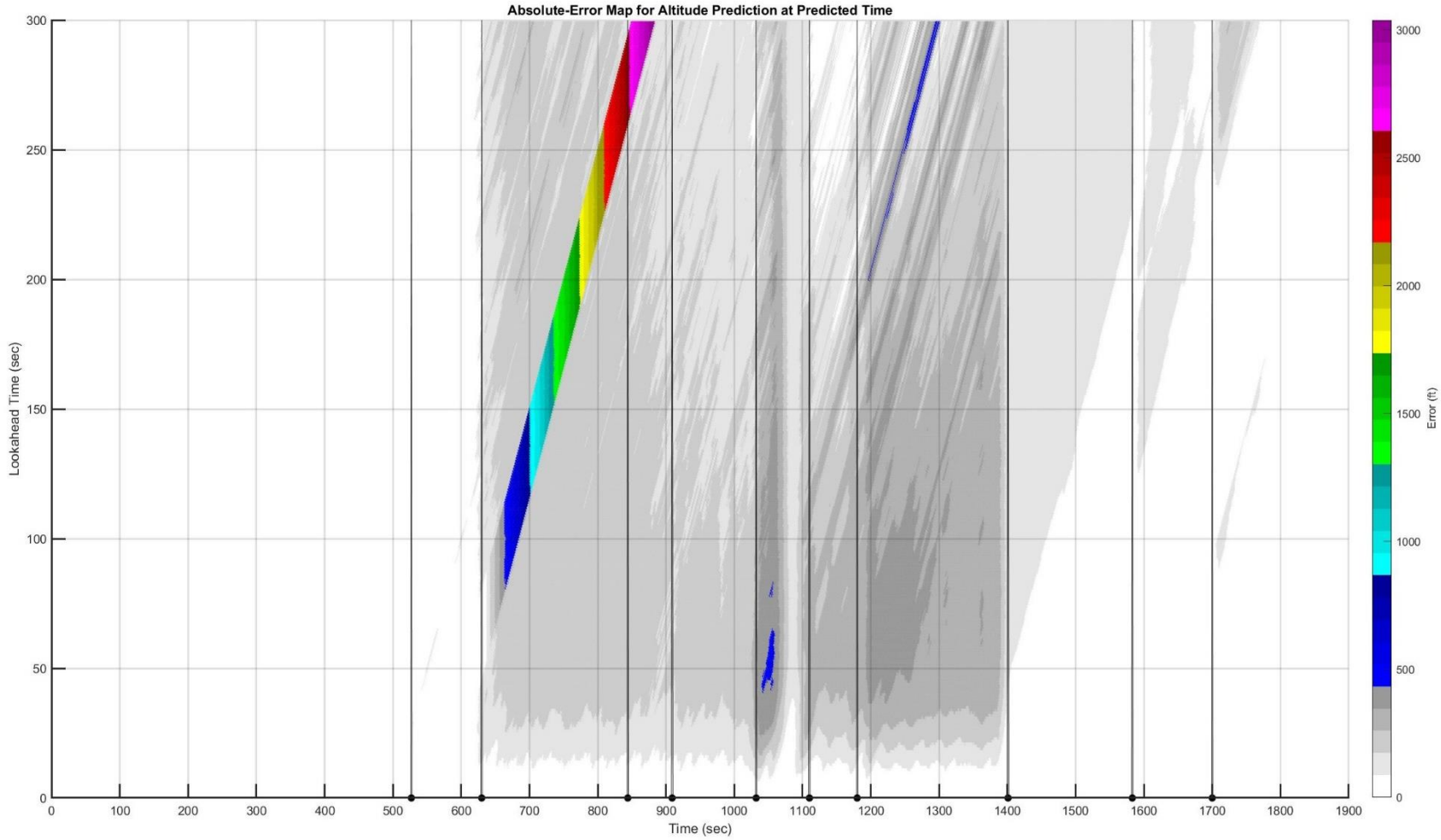

Figure E. 11: Test Flight 11: Heatmap of Absolute Error for Altitude Prediction as a Function of Predicted Time $t + \tau$

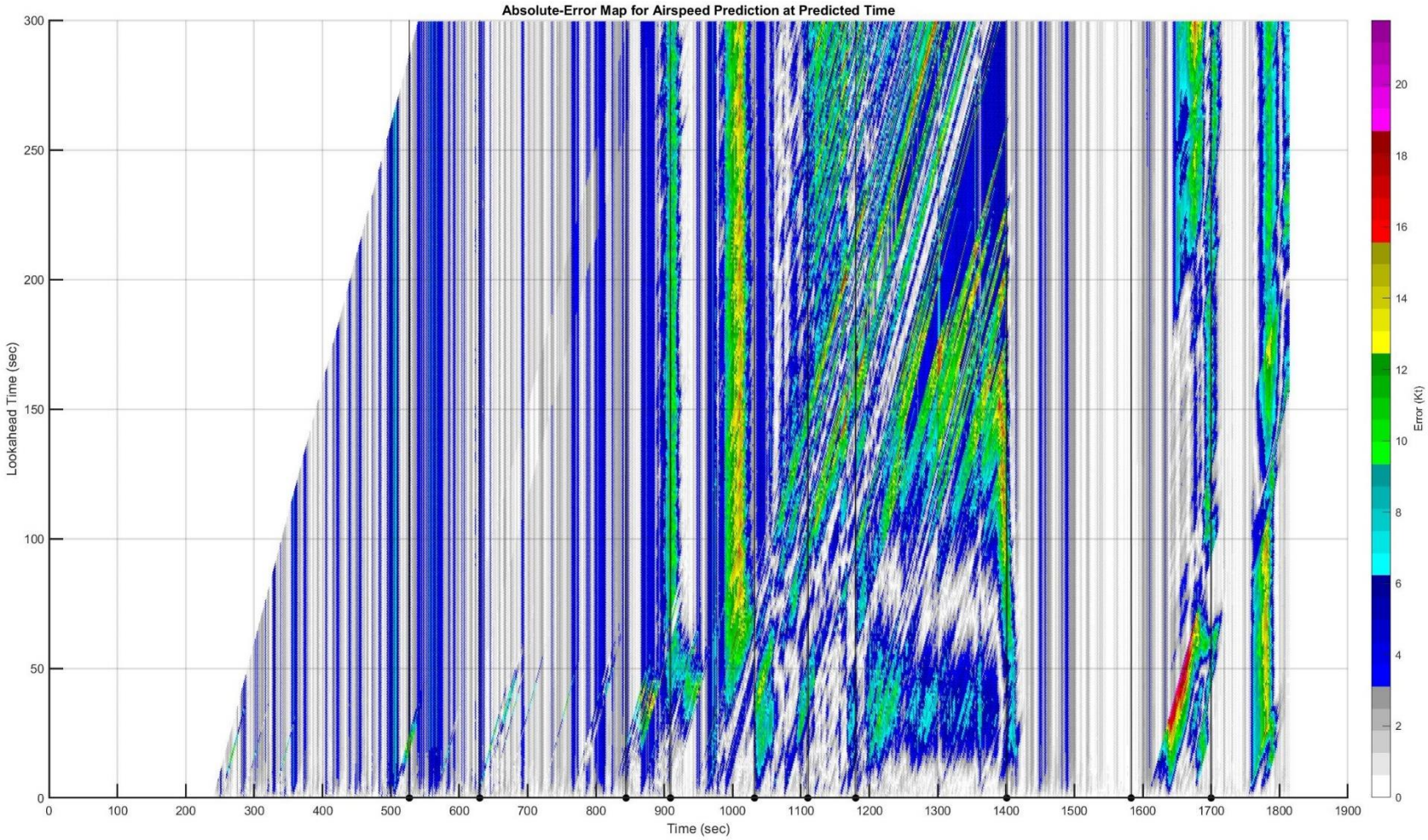

Figure E. 12: Test Flight 11: Heatmap of Absolute Error for Airspeed Prediction as a Function of Predicted Time $t + \tau$

E.4: Test Flight 16

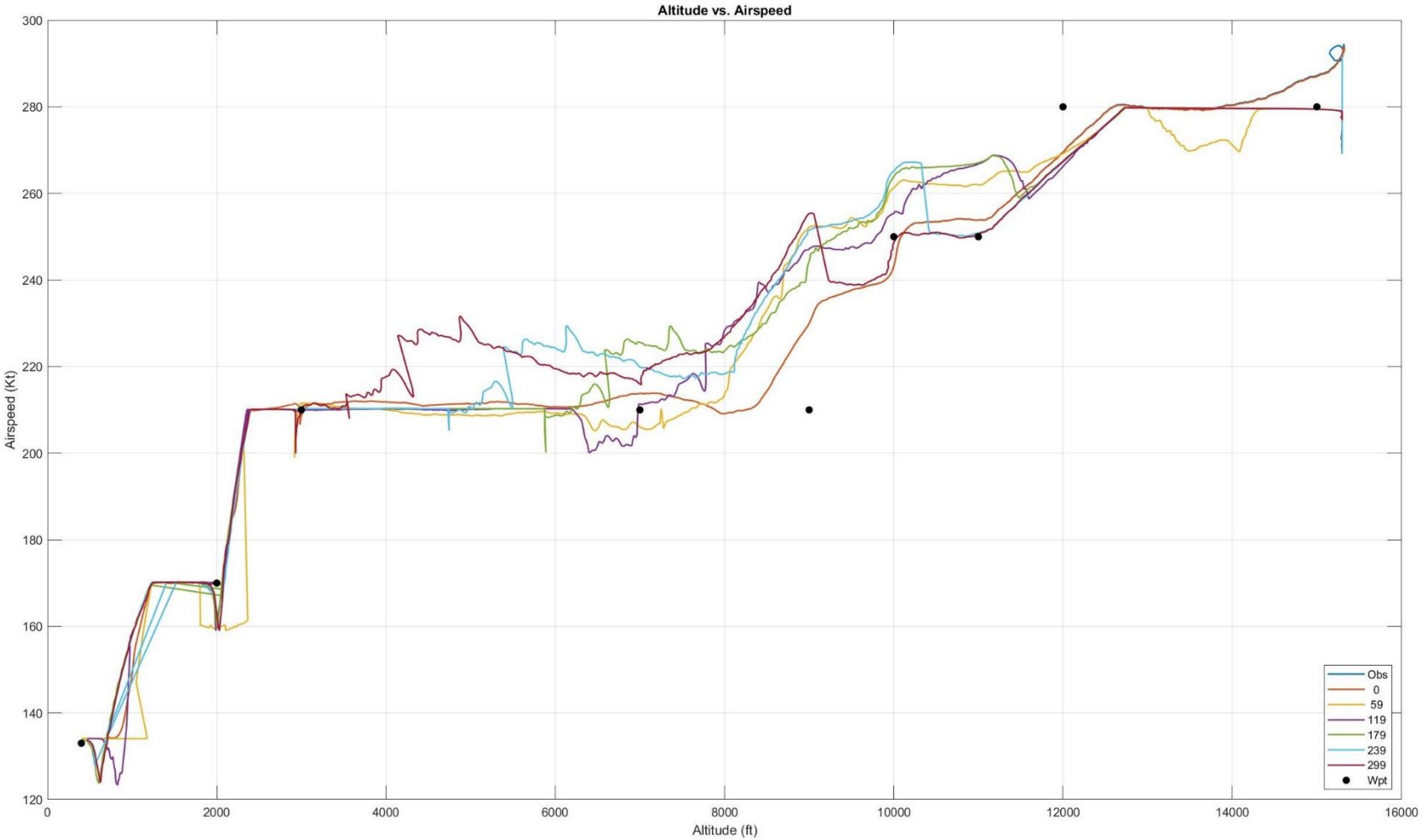

Figure E. 13: Test Flight 16: Observed and Predicted Altitude vs. Airspeed

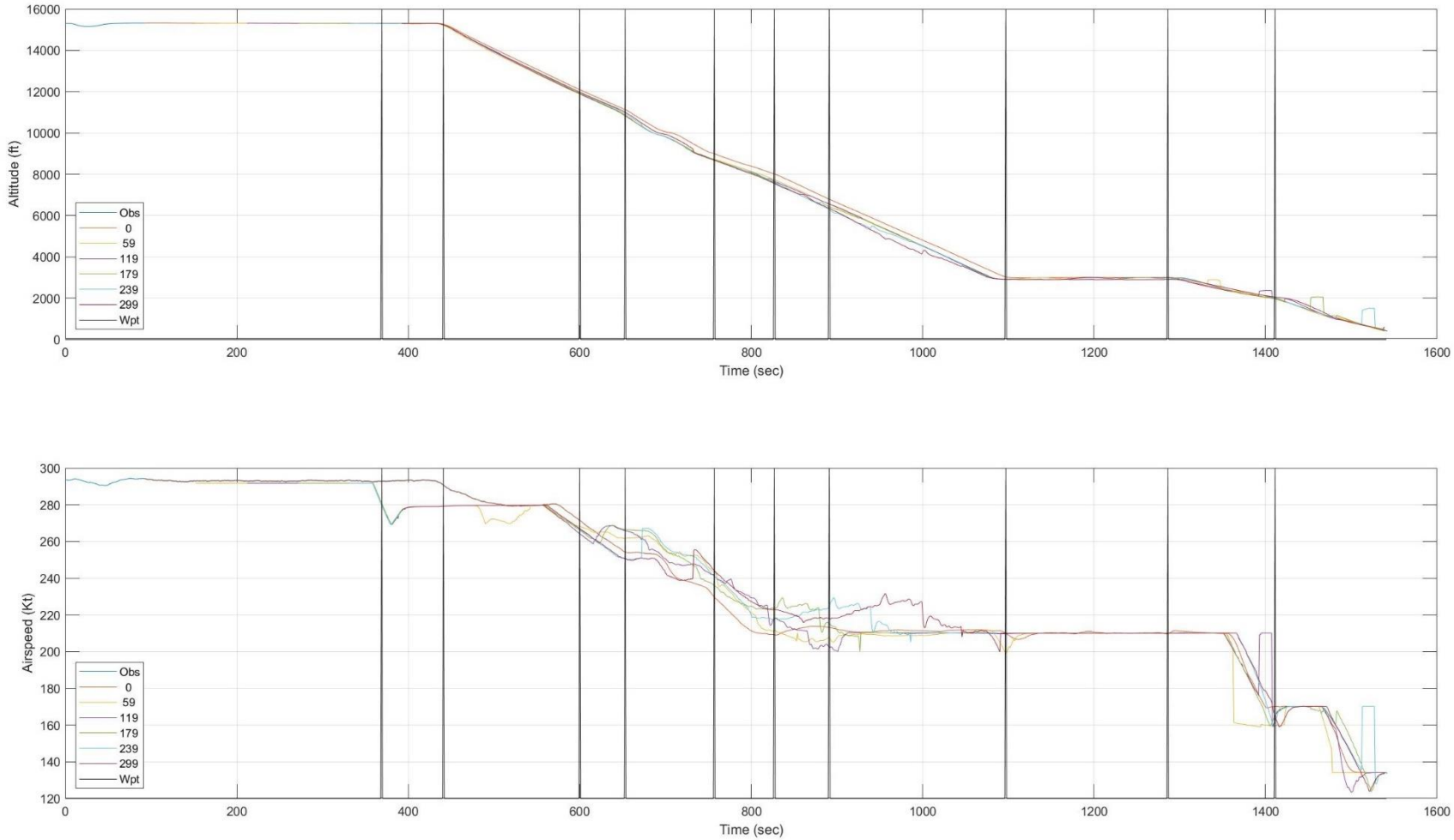

Figure E. 14: Test Flight 16: Observed and Predicted Altitude and Airspeed as a Function of Time t

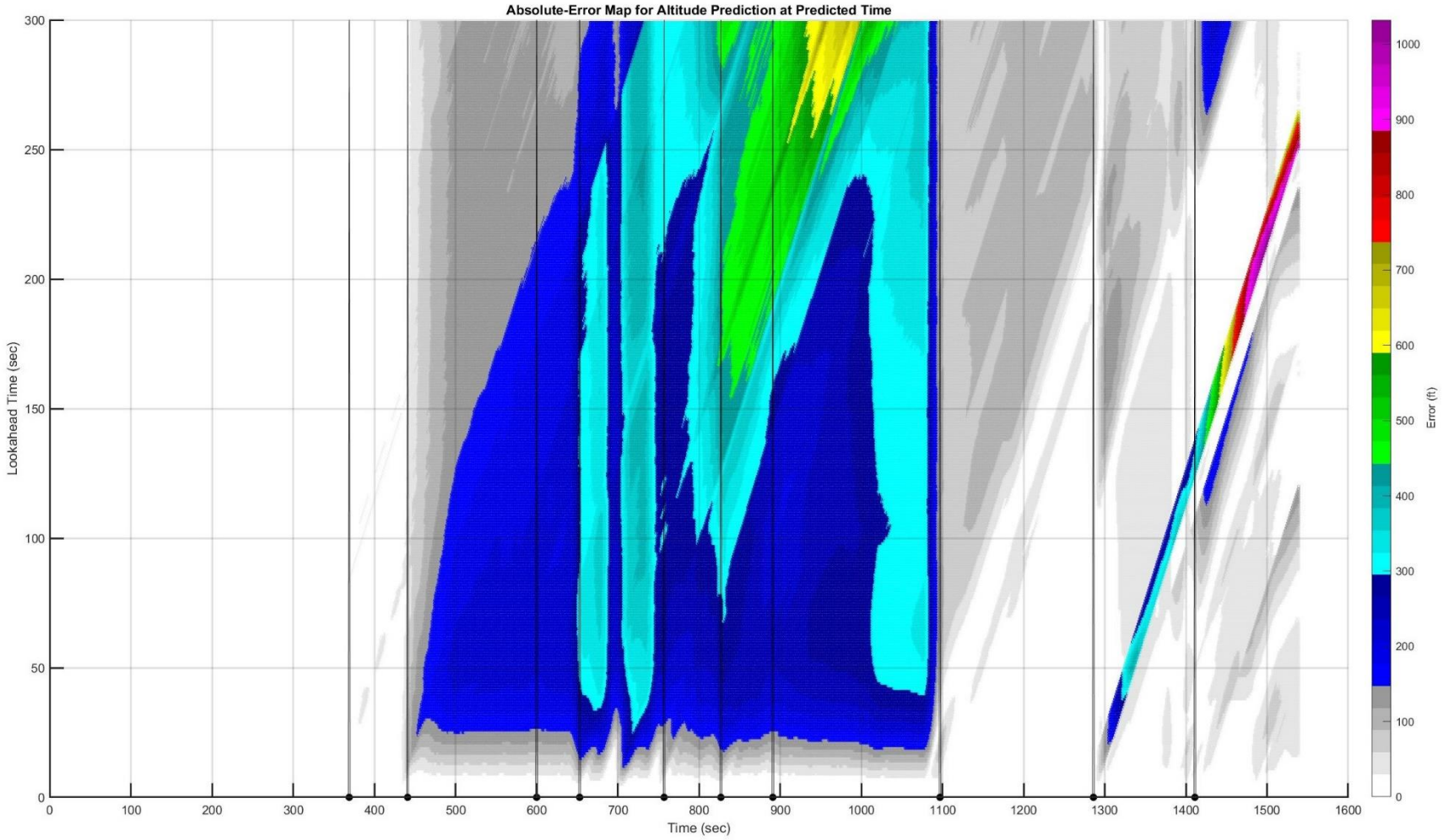

Figure E. 15: Test Flight 16: Heatmap of Absolute Error for Altitude Prediction as a Function of Predicted Time $t + \tau$

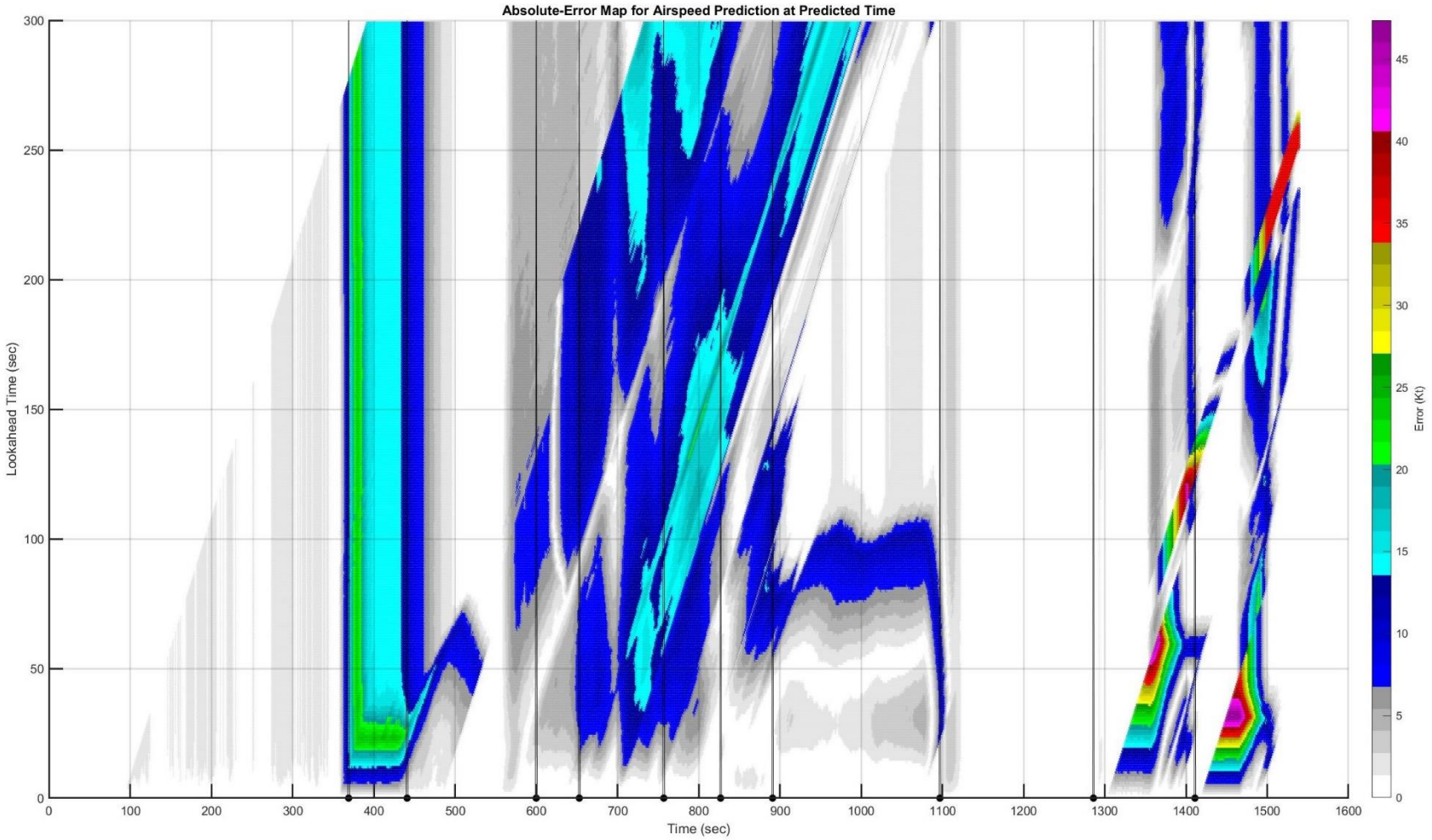

Figure E. 16: Test Flight 16: Heatmap of Absolute Error for Airspeed Prediction as a Function of Predicted Time $t + \tau$

E.5: Test Flight 23

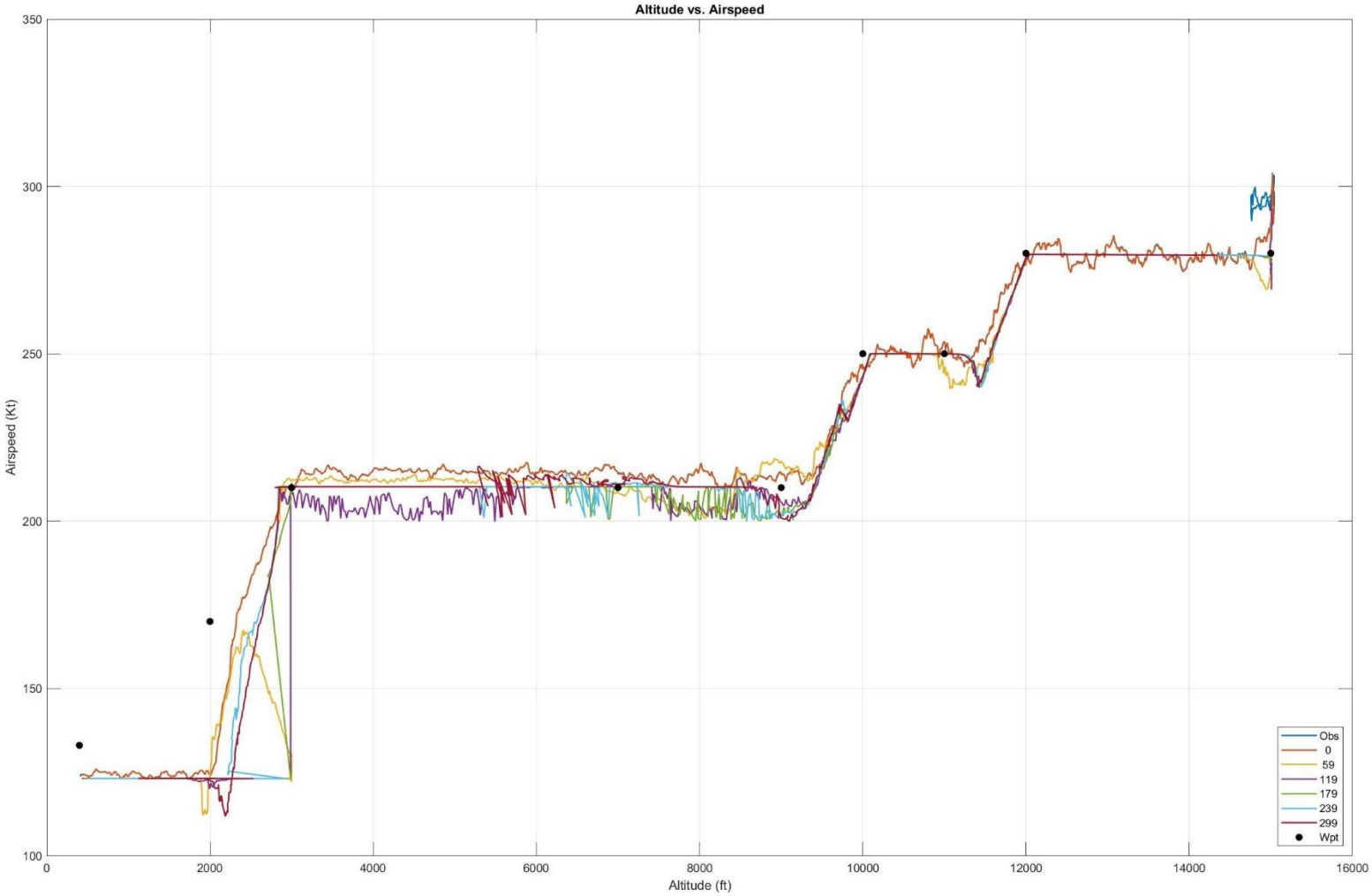

Figure E. 17: Test Flight 23: Observed and Predicted Altitude vs. Airspeed

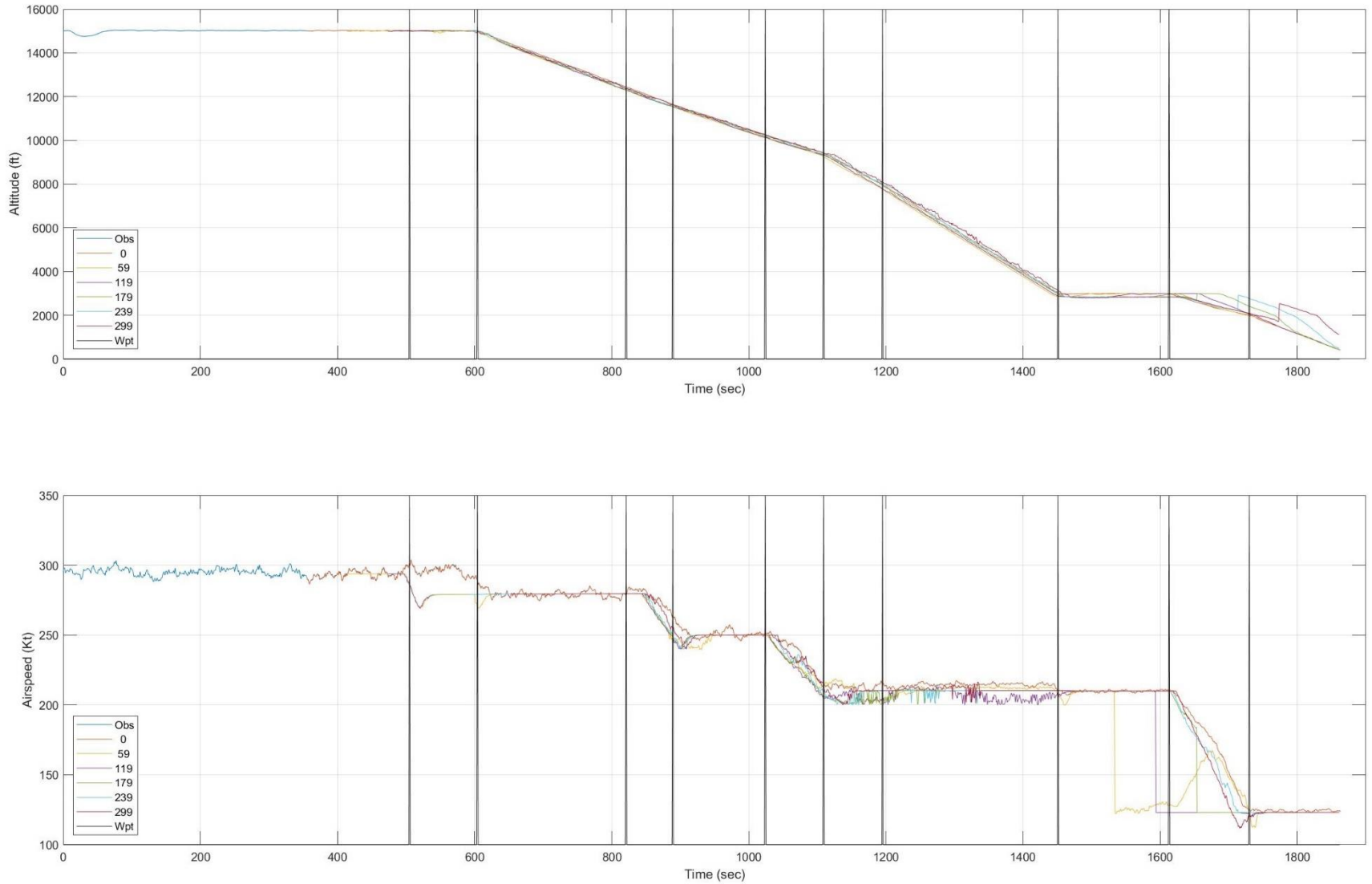

Figure E. 18: Test Flight 23: Observed and Predicted Altitude and Airspeed as a Function of Time t

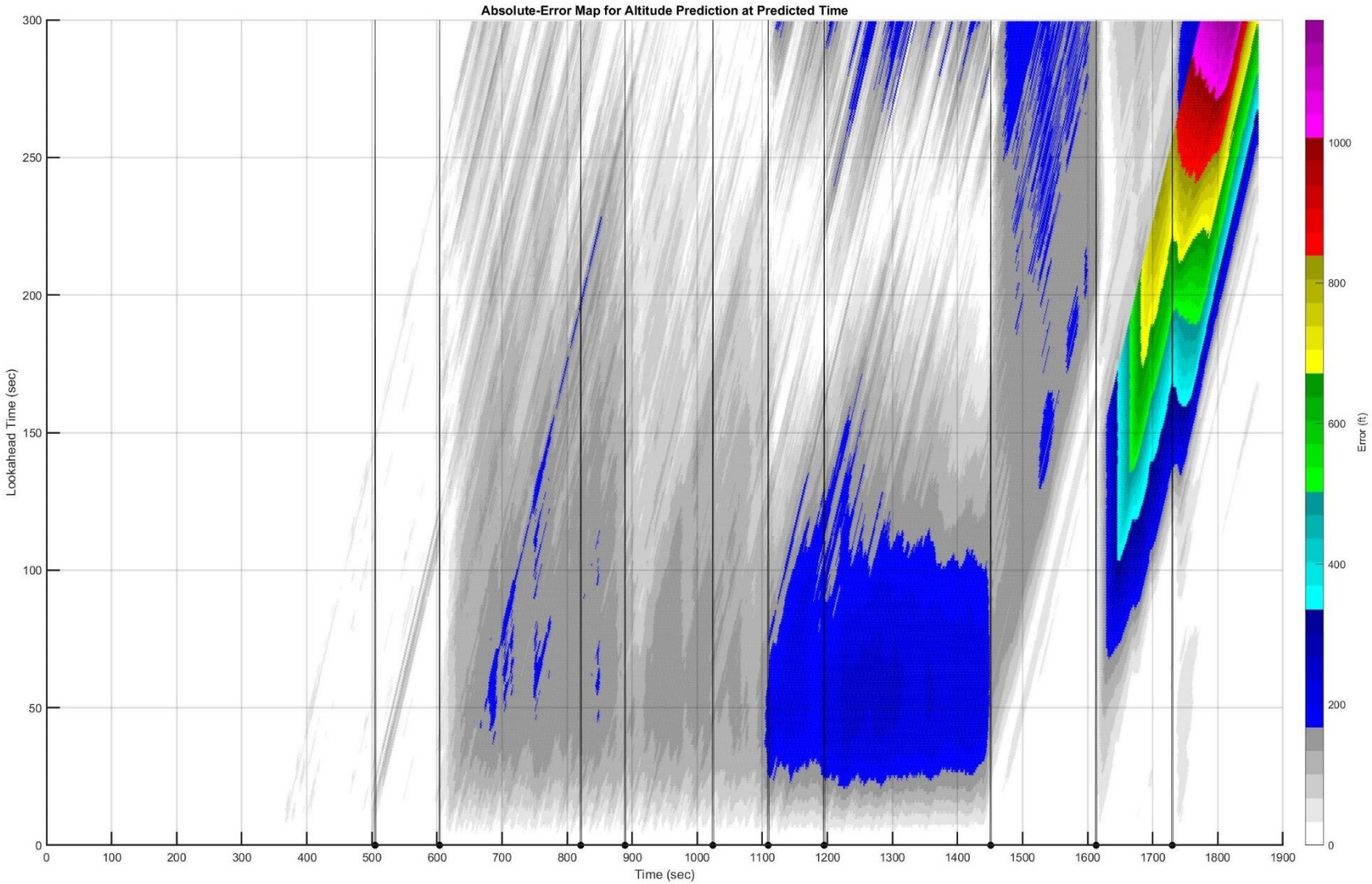

Figure E. 19: Test Flight 23: Heatmap of Absolute Error for Altitude Prediction as a Function of Predicted Time $t + \tau$

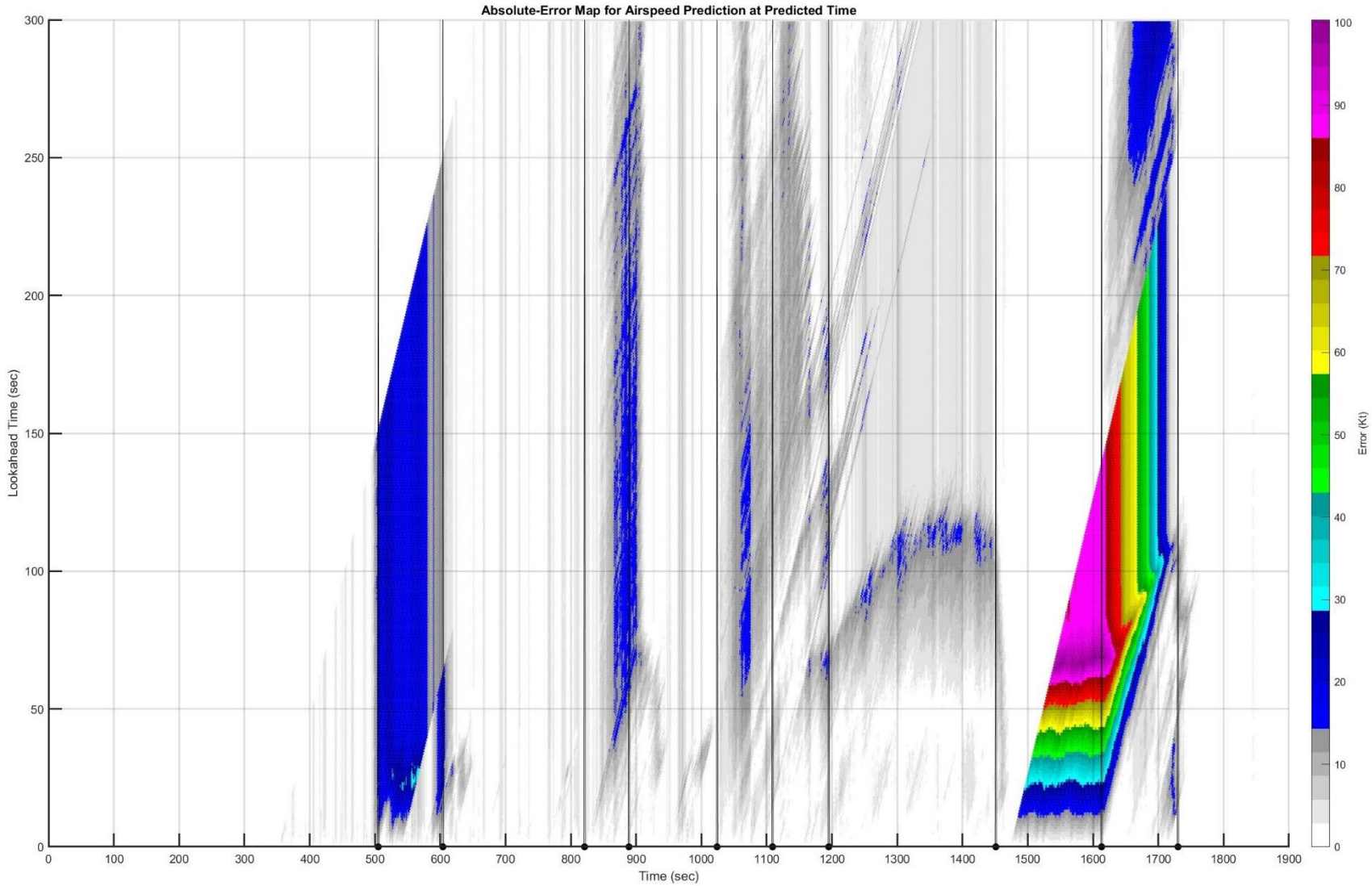

Figure E. 20: Test Flight 23: Heatmap of Absolute Error for Airspeed Prediction as a Function of Predicted Time $t + \tau$

E.6: Test Flight 35

Figure E. 21: Test Flight 35: Observed and Predicted Altitude vs. Airspeed

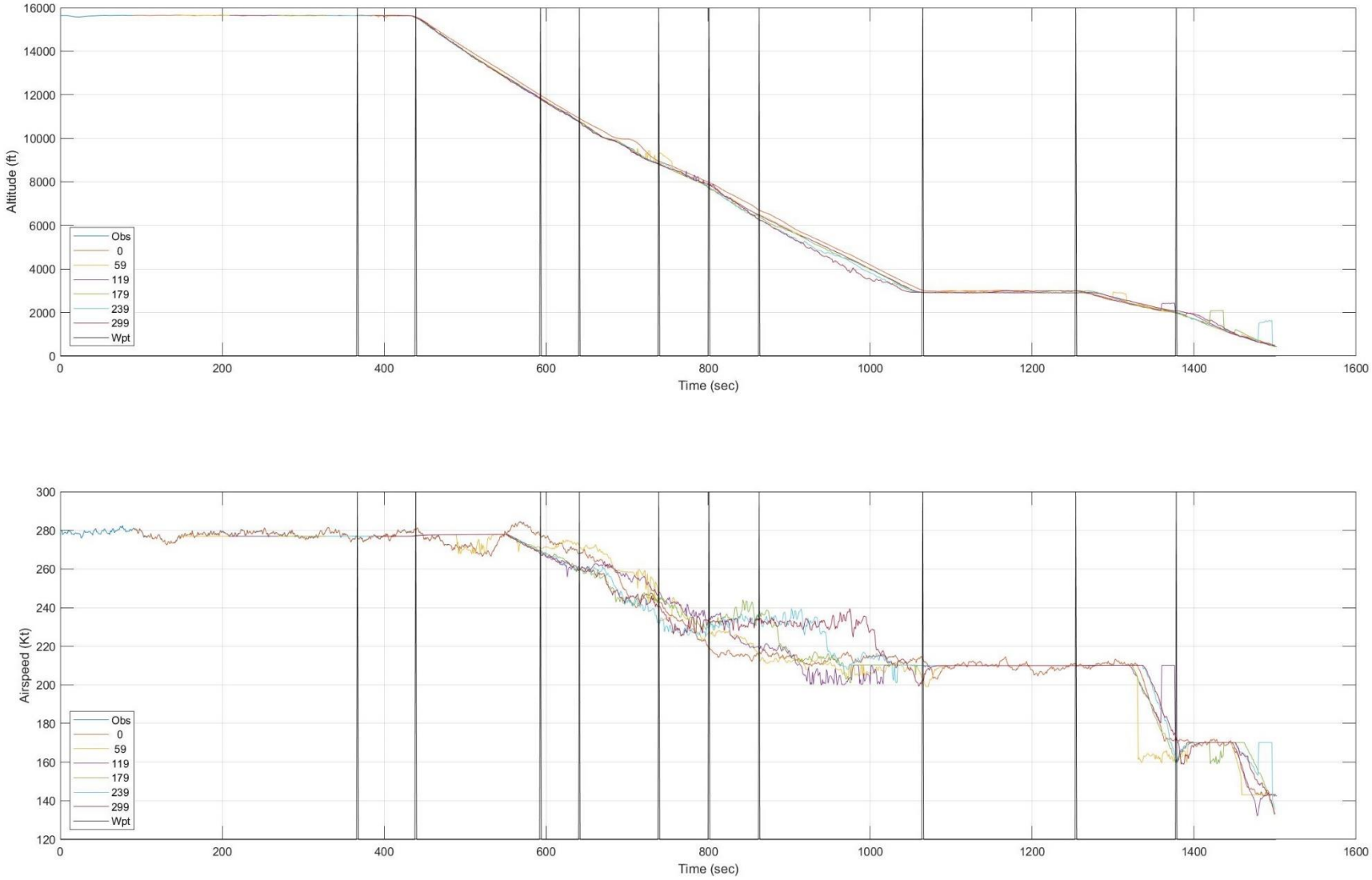

Figure E. 22: Test Flight 35: Observed and Predicted Altitude and Airspeed as a Function of Time t

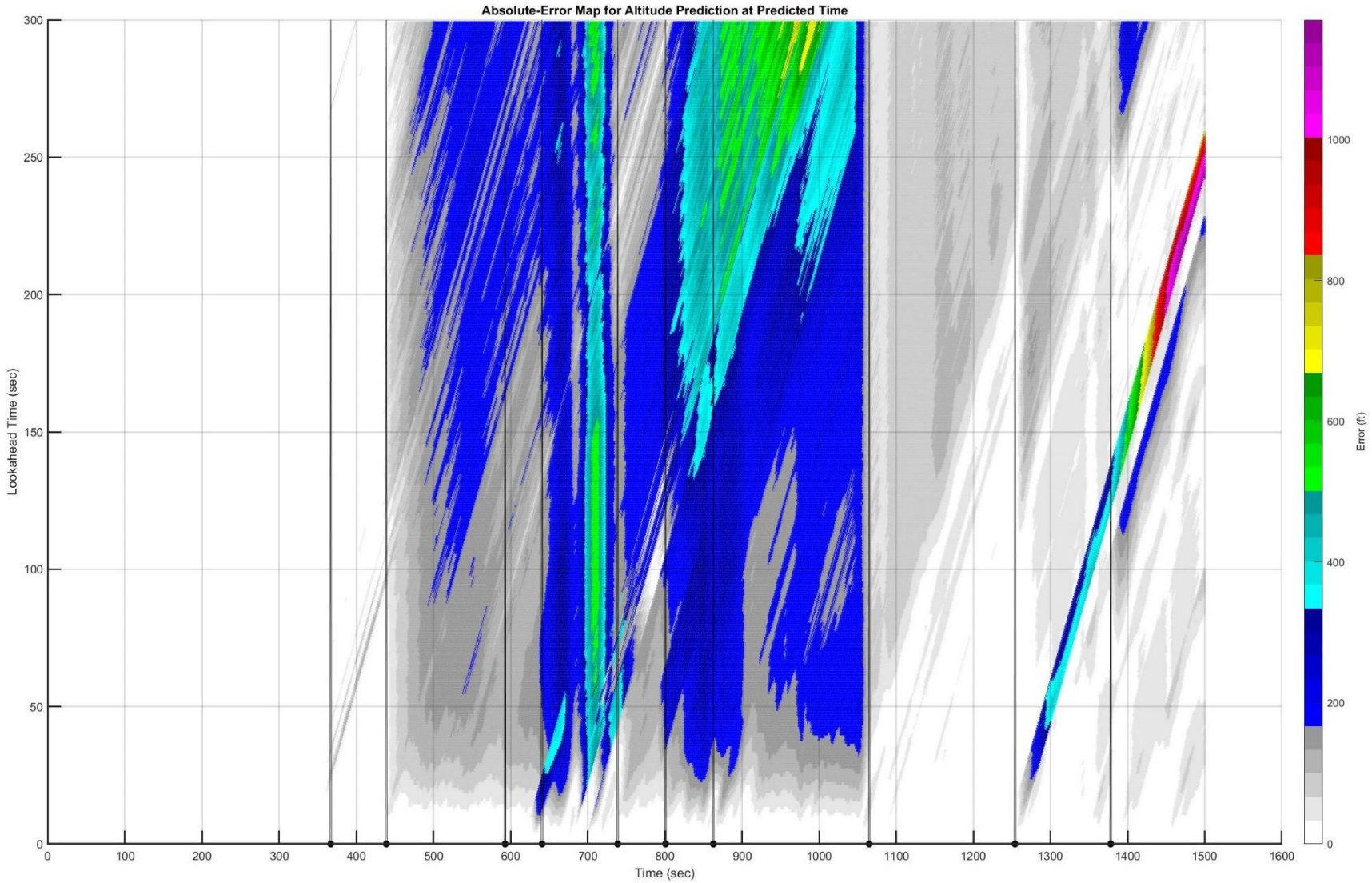

Figure E. 23: Test Flight 35: Heatmap of Absolute Error for Altitude Prediction as a Function of Predicted Time $t + \tau$

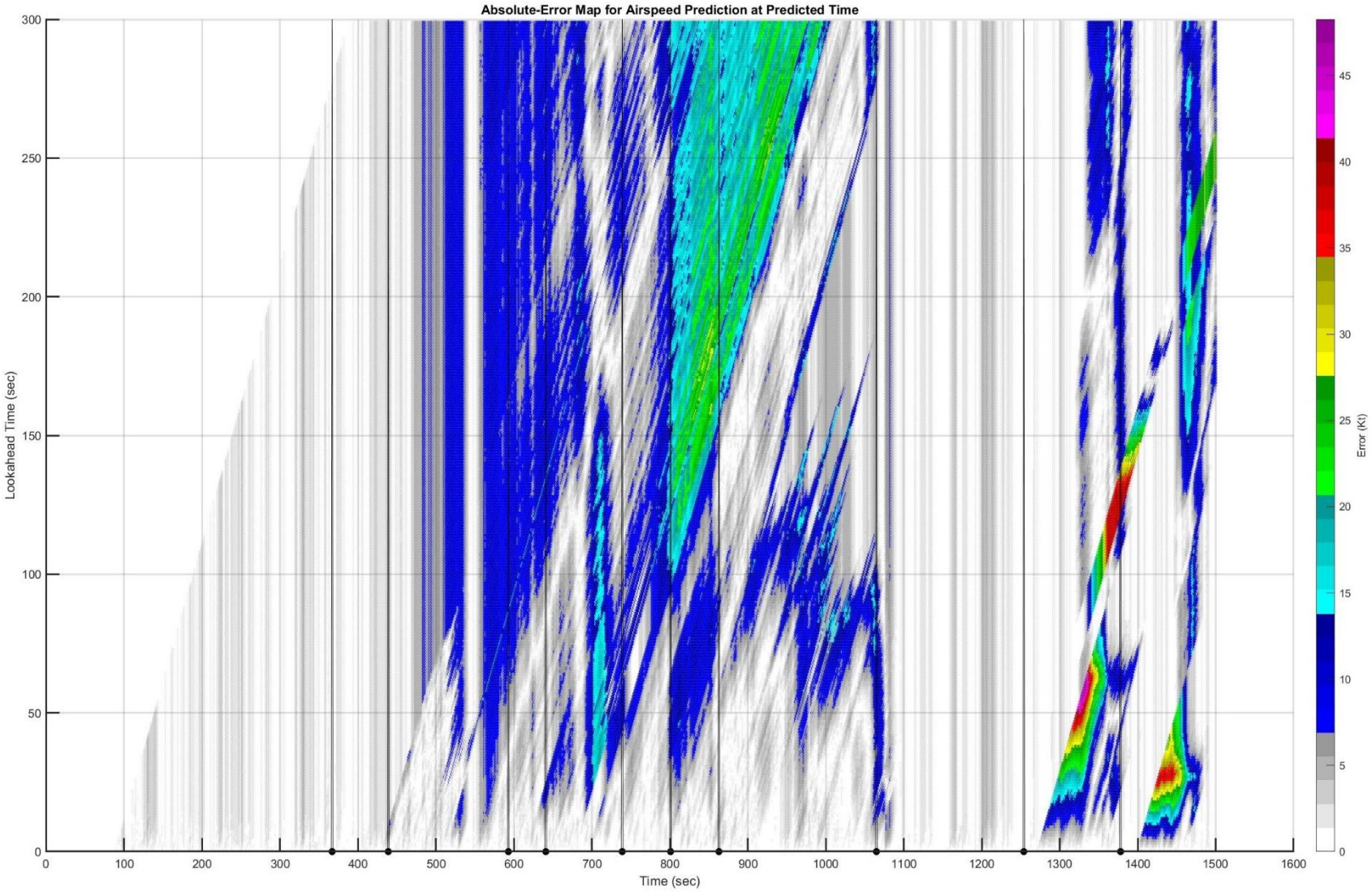

Figure E. 24: Test Flight 35: Heatmap of Absolute Error for Airspeed Prediction as a Function of Predicted Time $t + \tau$

E.7: Test Flight 36

Figure E. 25: Test Flight 36: Observed and Predicted Altitude vs. Airspeed

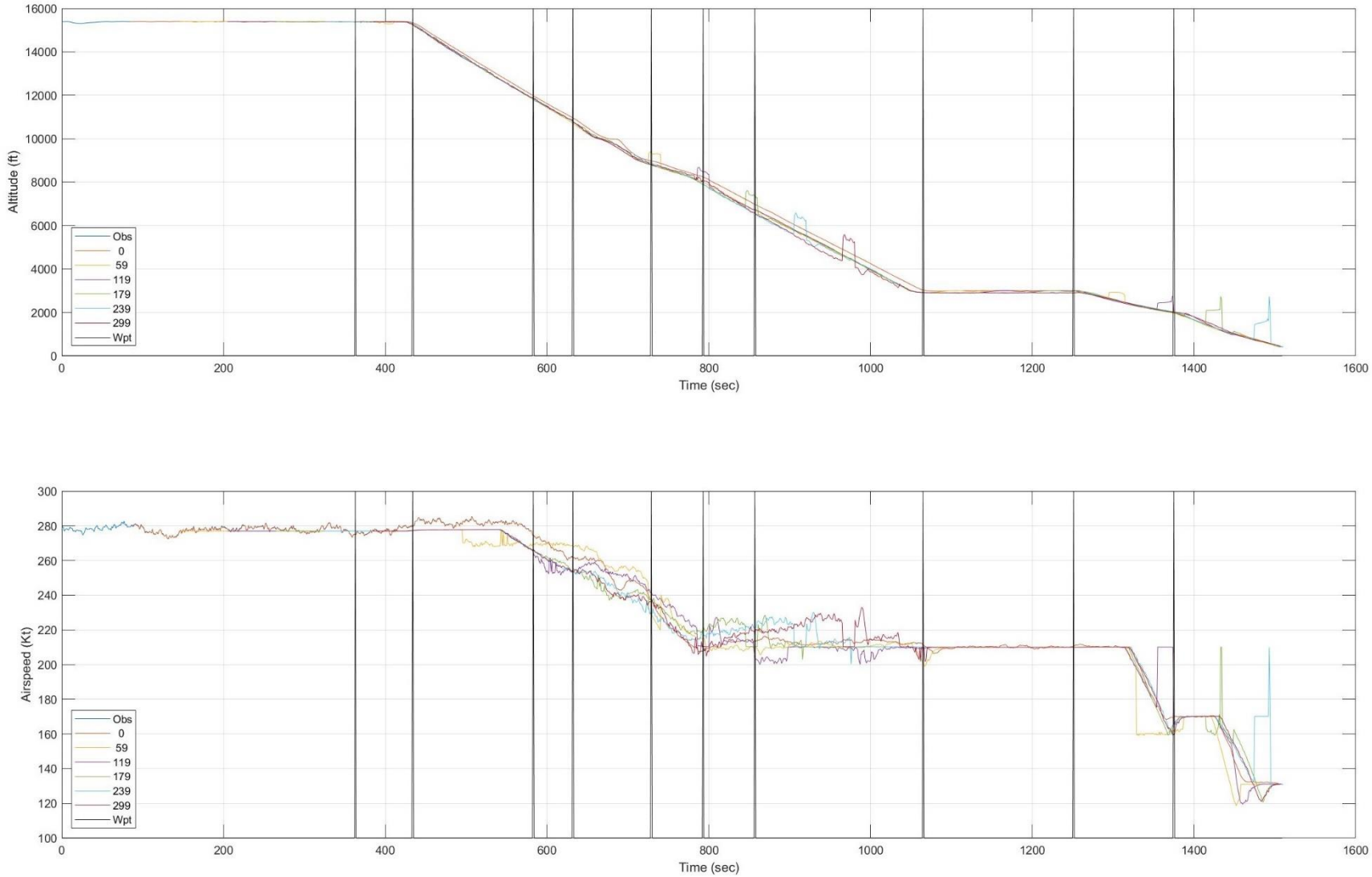

Figure E. 26: Test Flight 36: Observed and Predicted Altitude and Airspeed as a Function of Time t

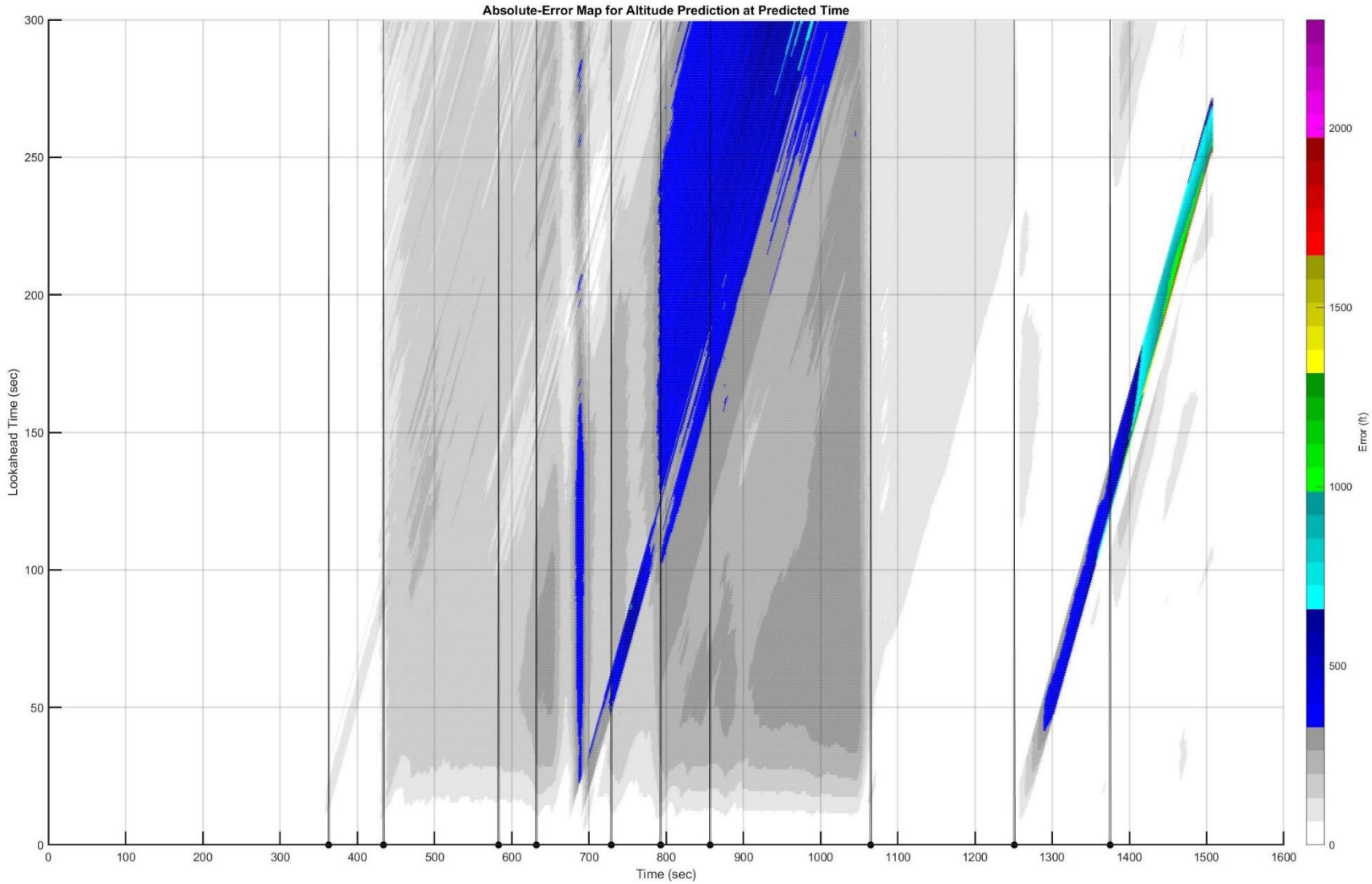

Figure E. 27: Test Flight 36: Heatmap of Absolute Error for Altitude Prediction as a Function of Predicted Time $t + \tau$

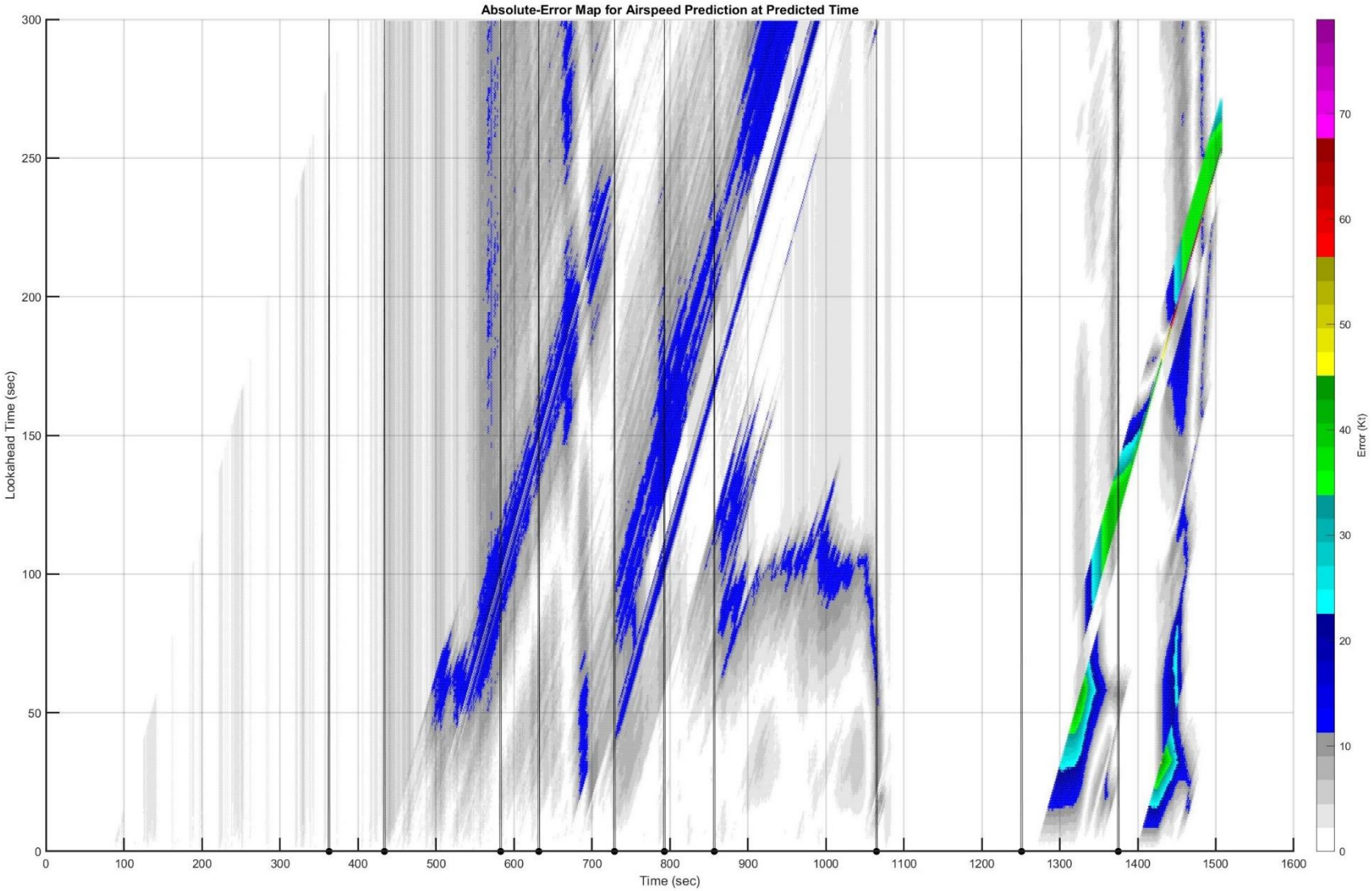

Figure E. 28: Test Flight 36: Heatmap of Absolute Error for Airspeed Prediction as a Function of Predicted Time $t + \tau$

E.8: Test Flight 66

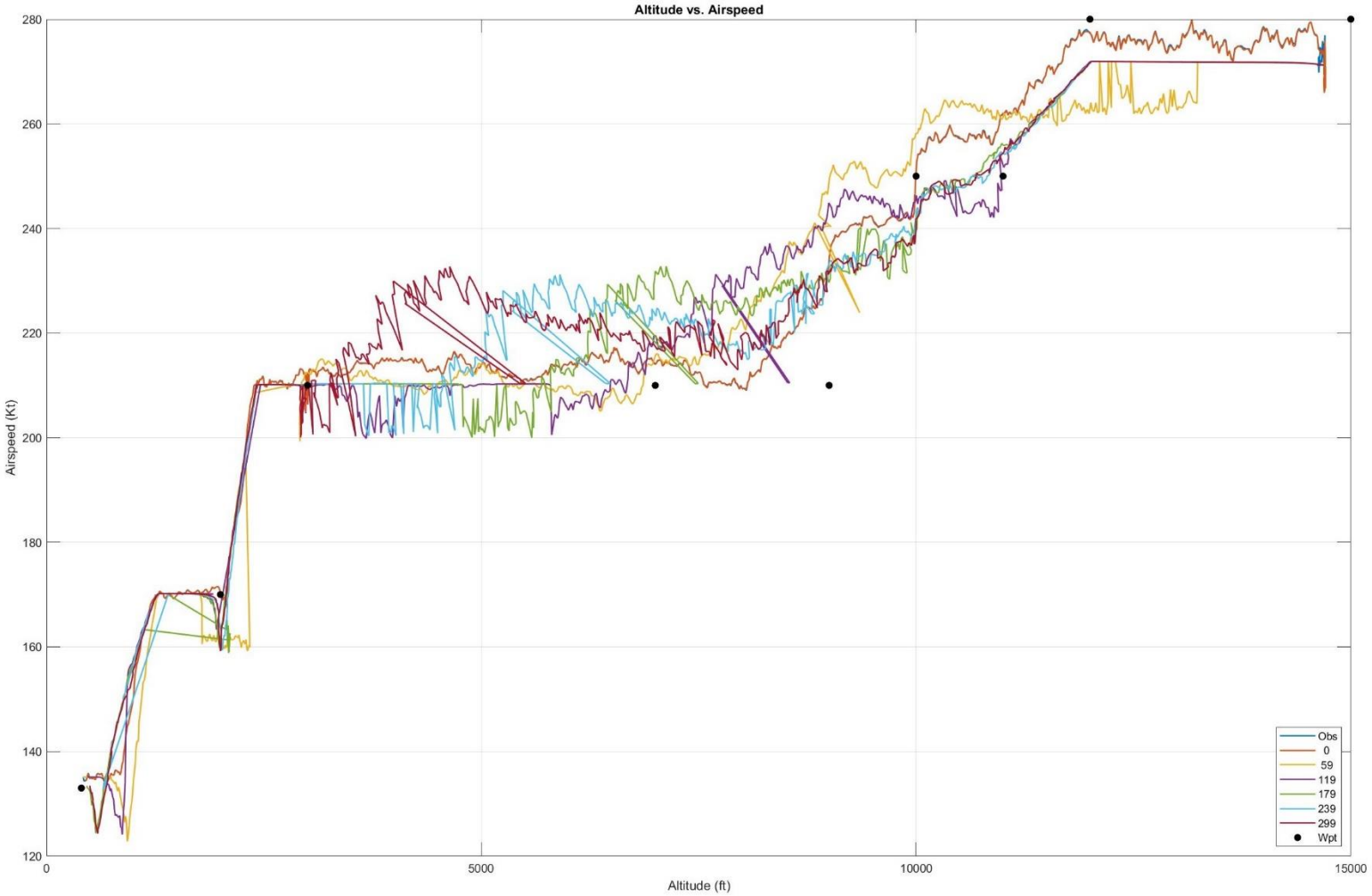

Figure E. 29: Test Flight 66: Observed and Predicted Altitude vs. Airspeed

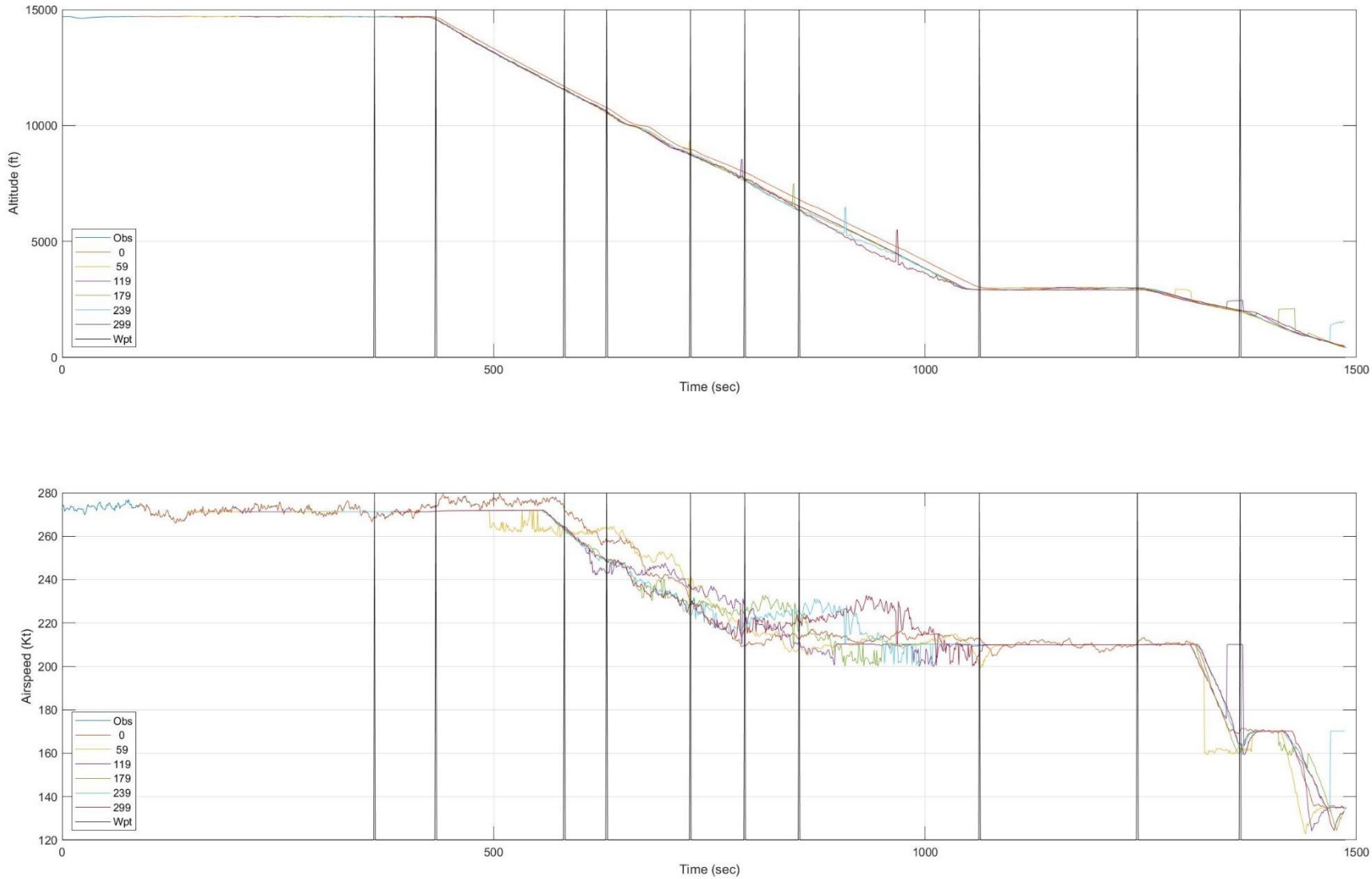

Figure E. 30: Test Flight 66: Observed and Predicted Altitude and Airspeed as a Function of Time t

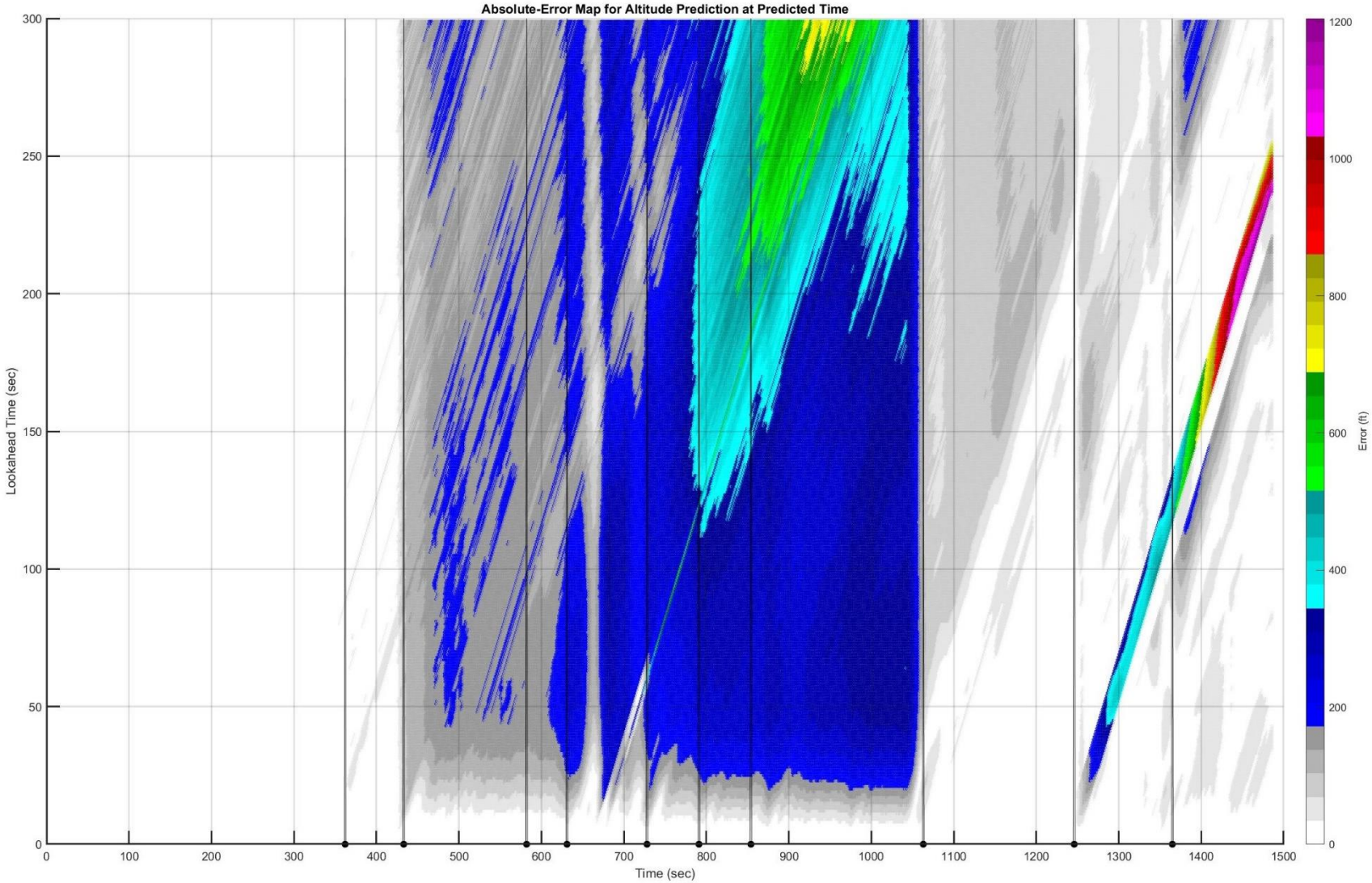

Figure E. 31: Test Flight 66: Heatmap of Absolute Error for Altitude Prediction as a Function of Predicted Time $t + \tau$

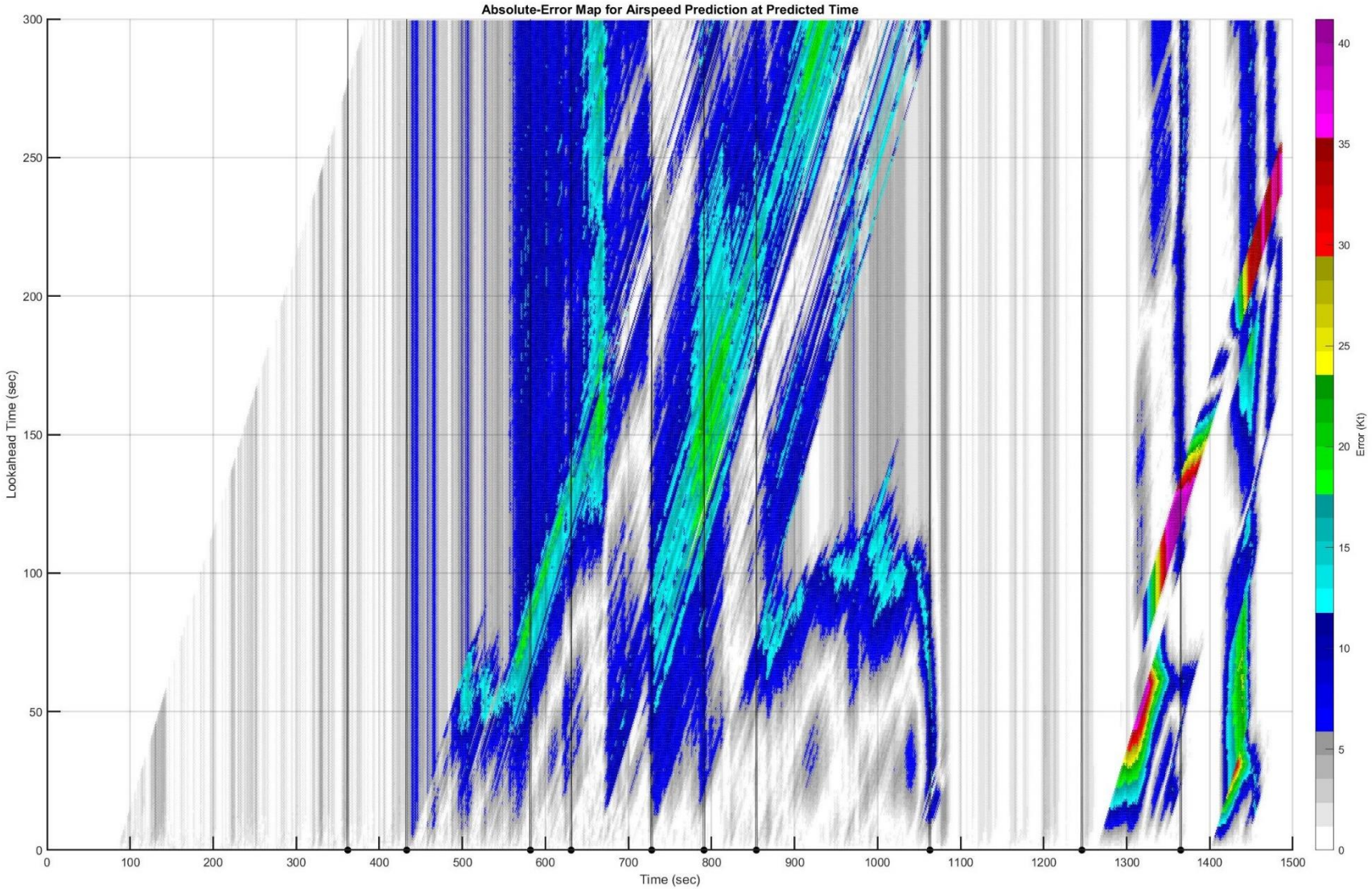

Figure E. 32: Test Flight 66: Heatmap of Absolute Error for Airspeed Prediction as a Function of Predicted Time $t + \tau$

E.9: Test Flight 79

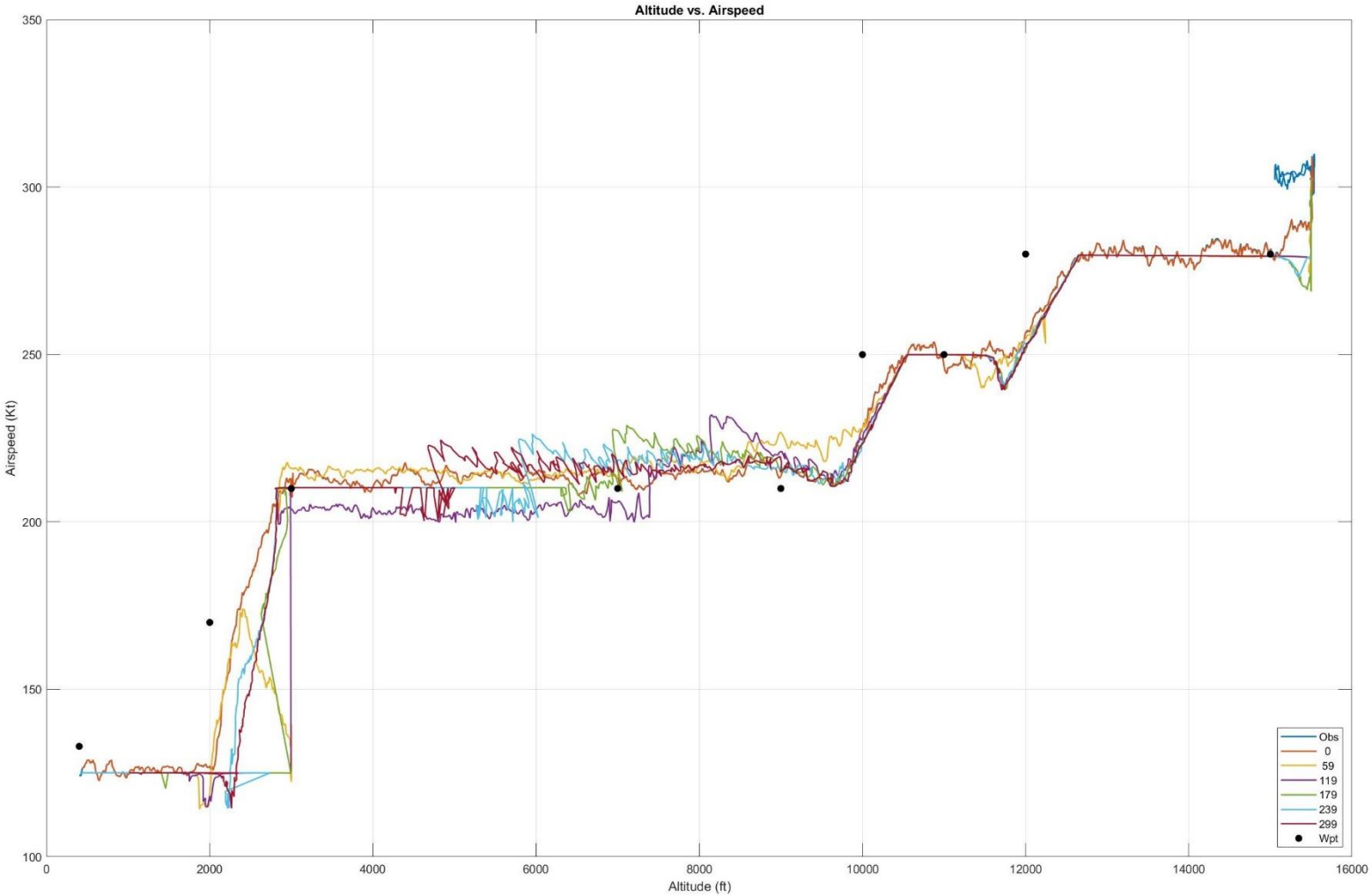

Figure E. 33: Test Flight 79: Observed and Predicted Altitude vs. Airspeed

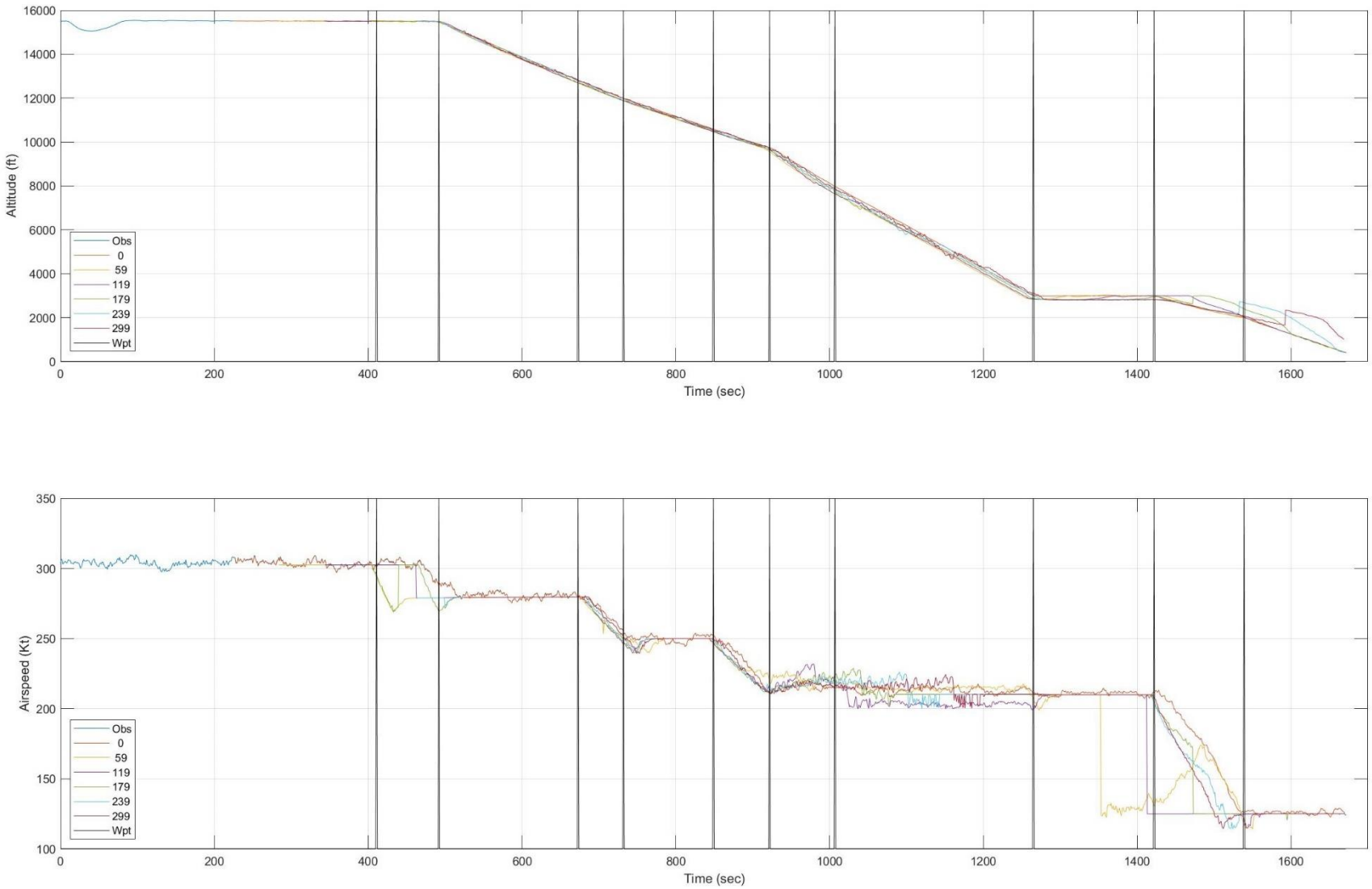

Figure E. 34: Test Flight 79: Observed and Predicted Altitude and Airspeed as a Function of Time t

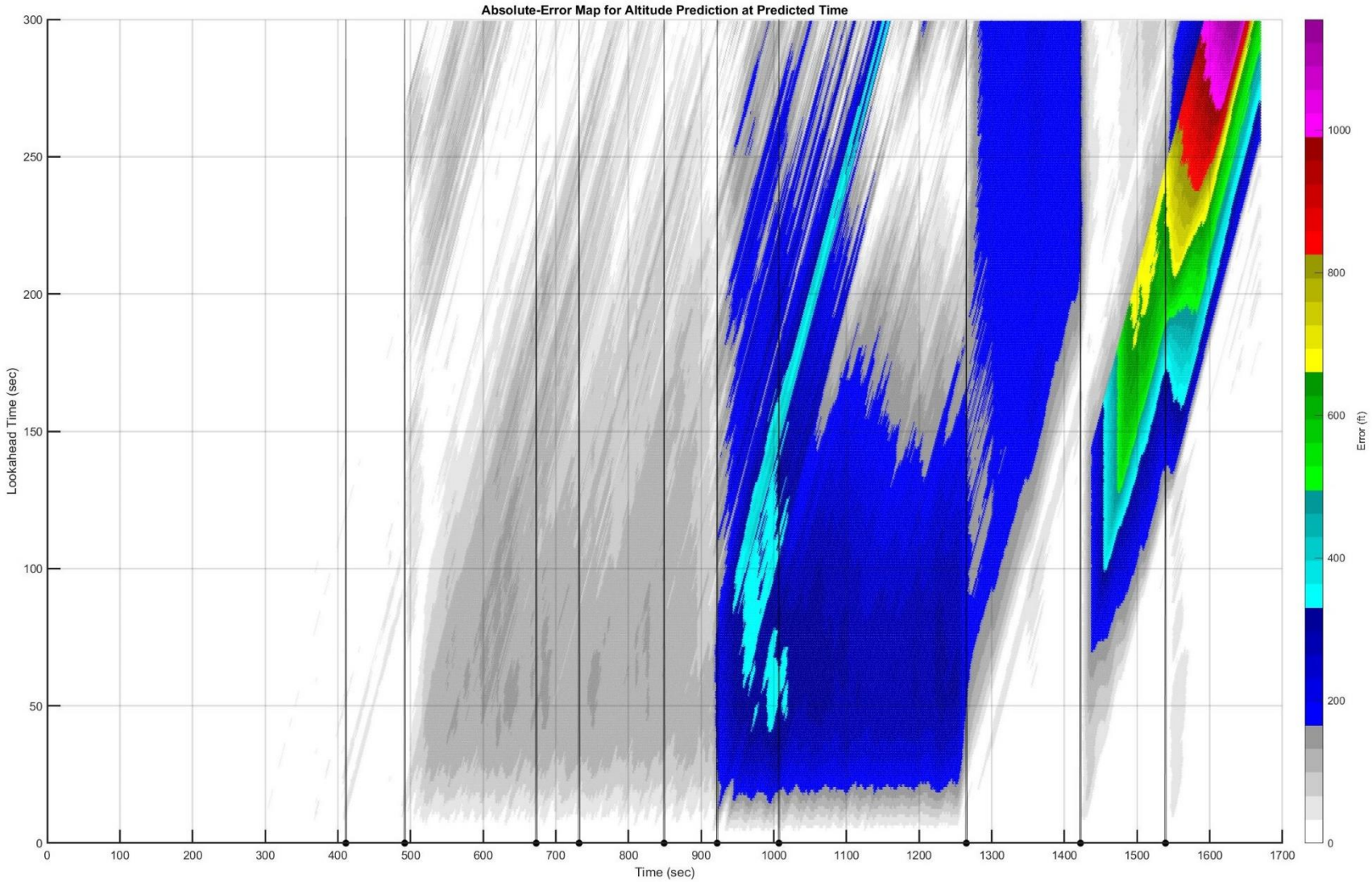

Figure E. 35: Test Flight 79: Heatmap of Absolute Error for Altitude Prediction as a Function of Predicted Time $t + \tau$

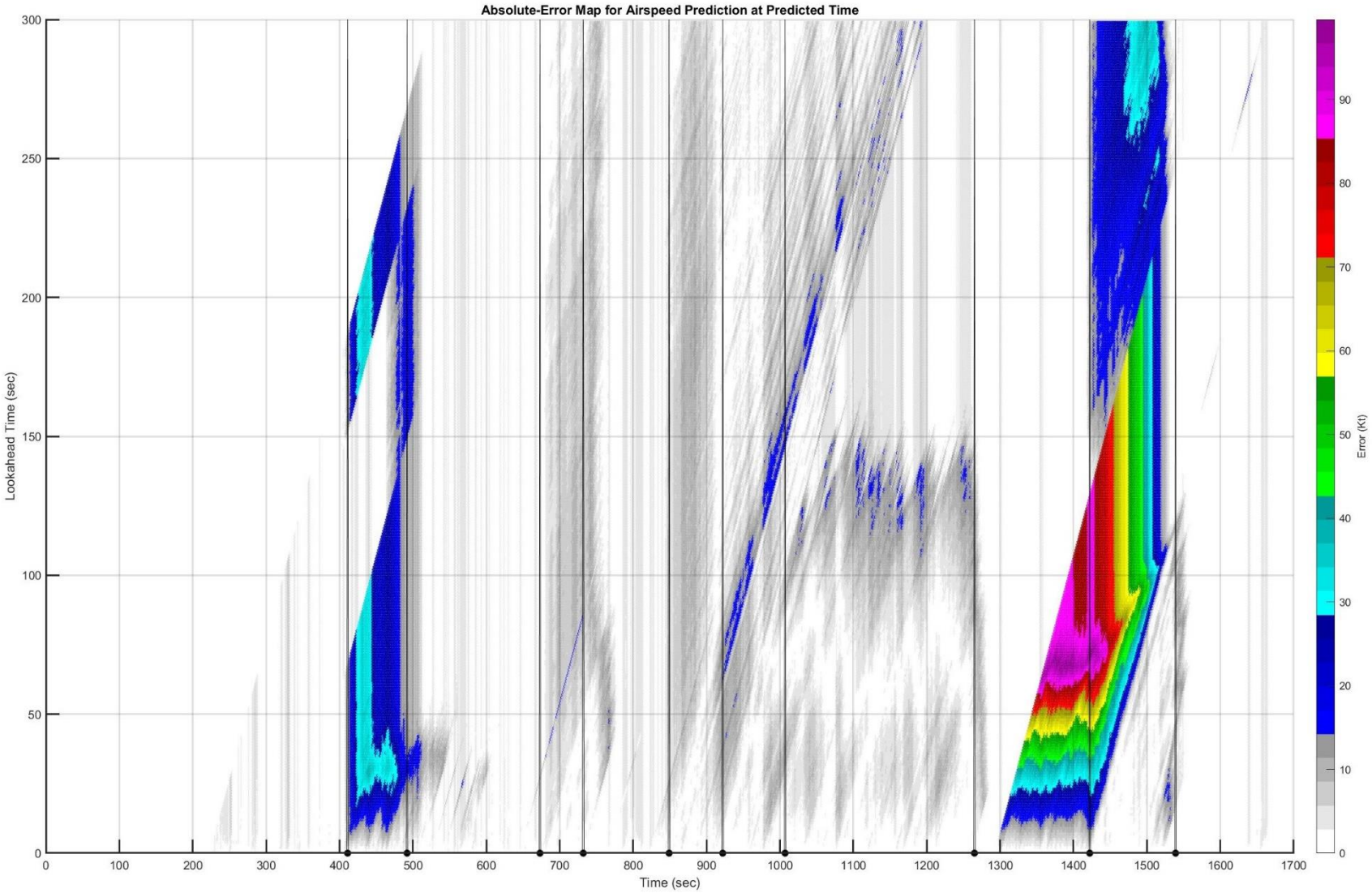

Figure E. 36: Test Flight 79: Heatmap of Absolute Error for Airspeed Prediction as a Function of Predicted Time $t + \tau$

E.10: Test Flight 86

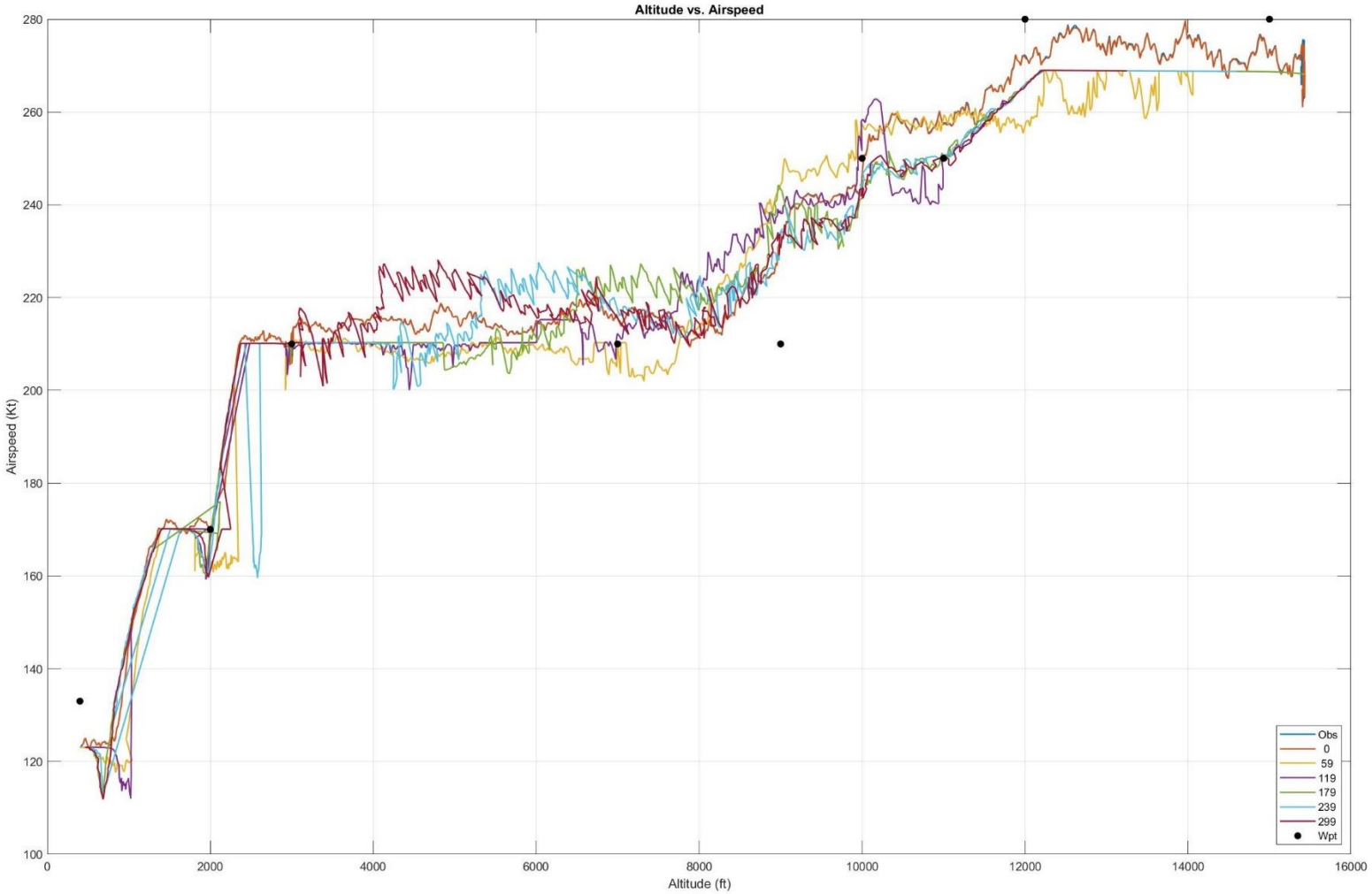

Figure E. 37: Test Flight 86: Observed and Predicted Altitude vs. Airspeed

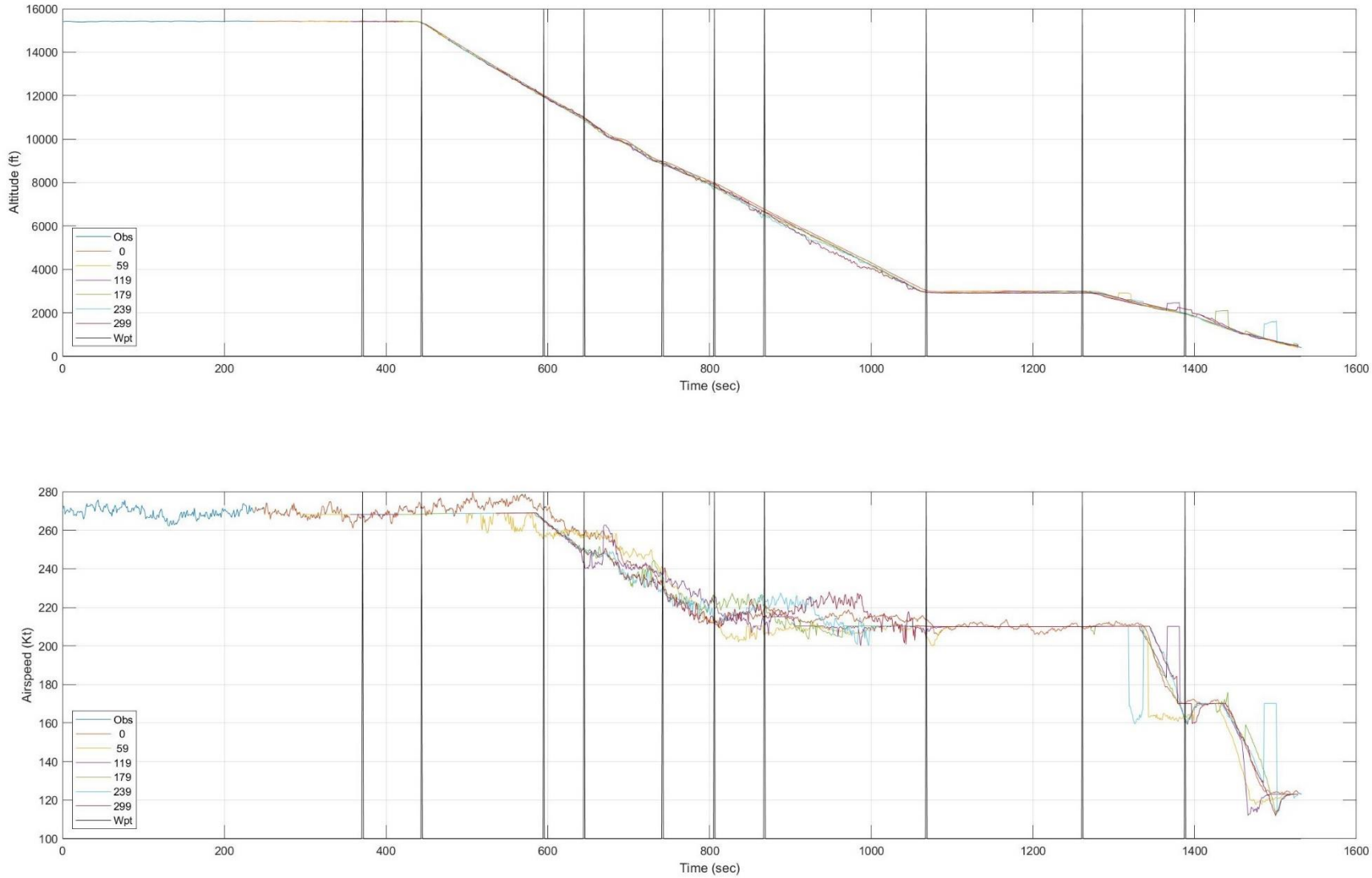

Figure E. 38: Test Flight 86: Observed and Predicted Altitude and Airspeed as a Function of Time t

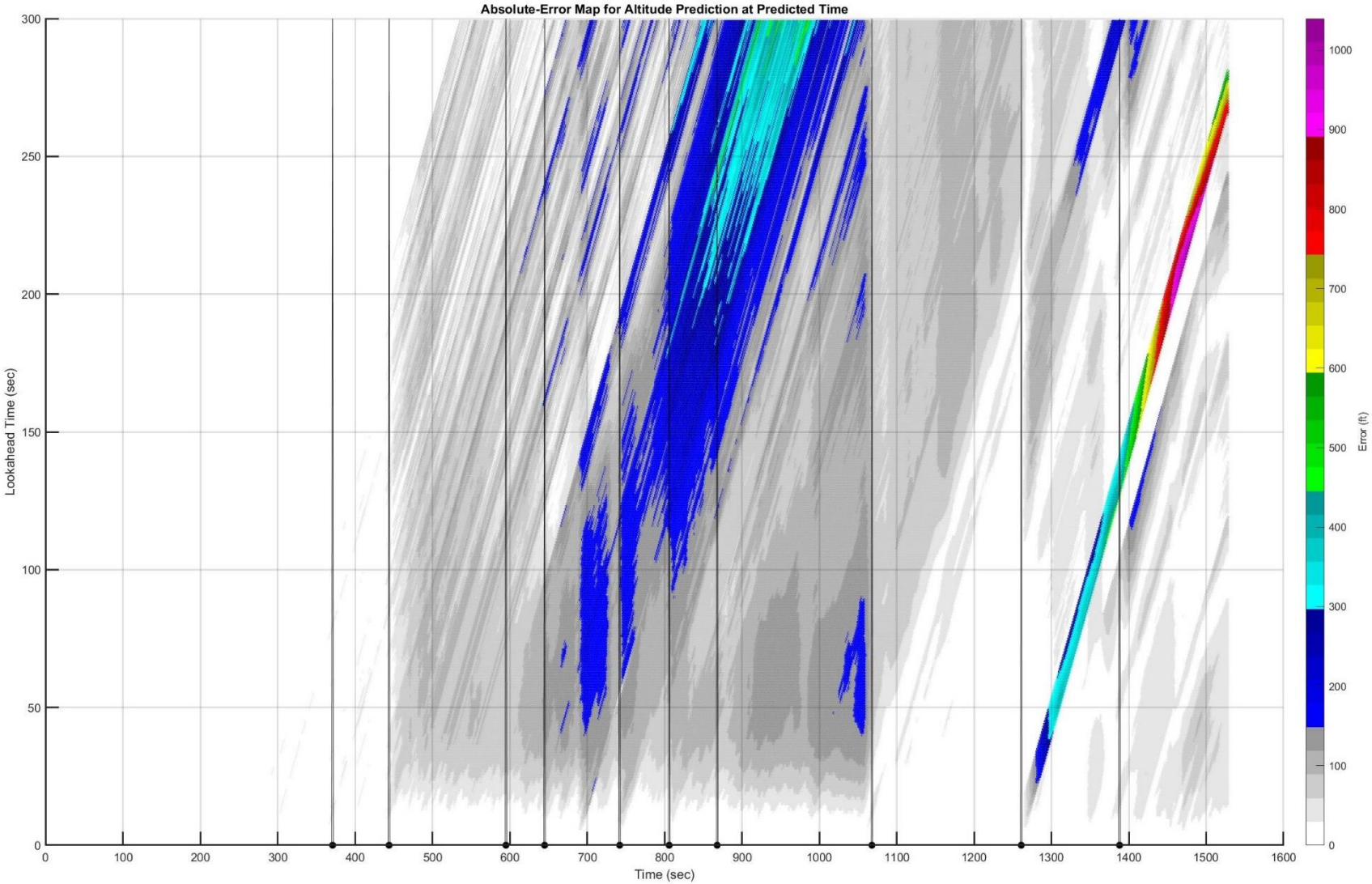

Figure E. 39: Test Flight 86: Heatmap of Absolute Error for Altitude Prediction as a Function of Predicted Time $t + \tau$

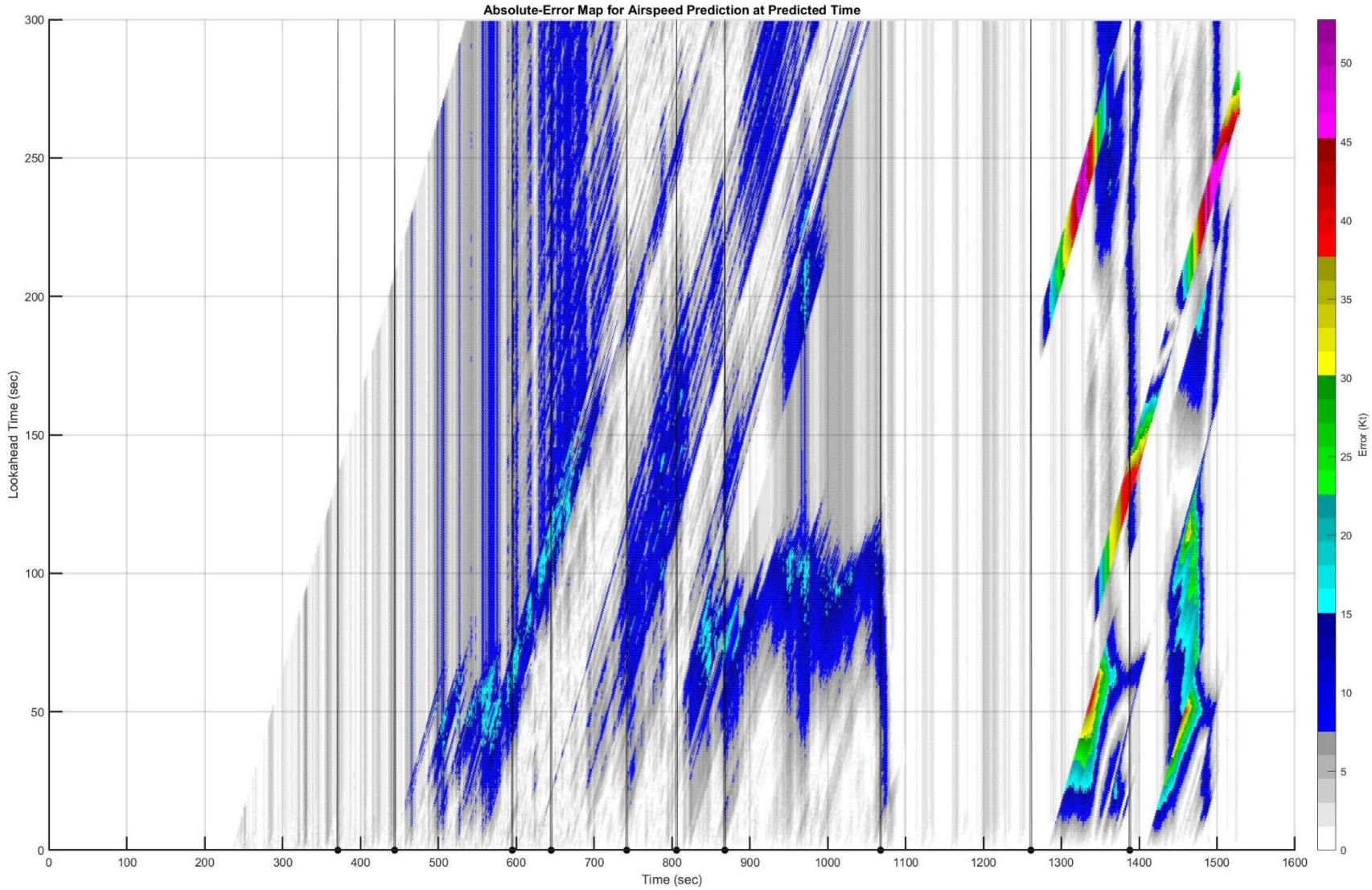

Figure E. 40: Test Flight 86: Heatmap of Absolute Error for Airspeed Prediction as a Function of Predicted Time $t + \tau$

E.11: Test Flight 91

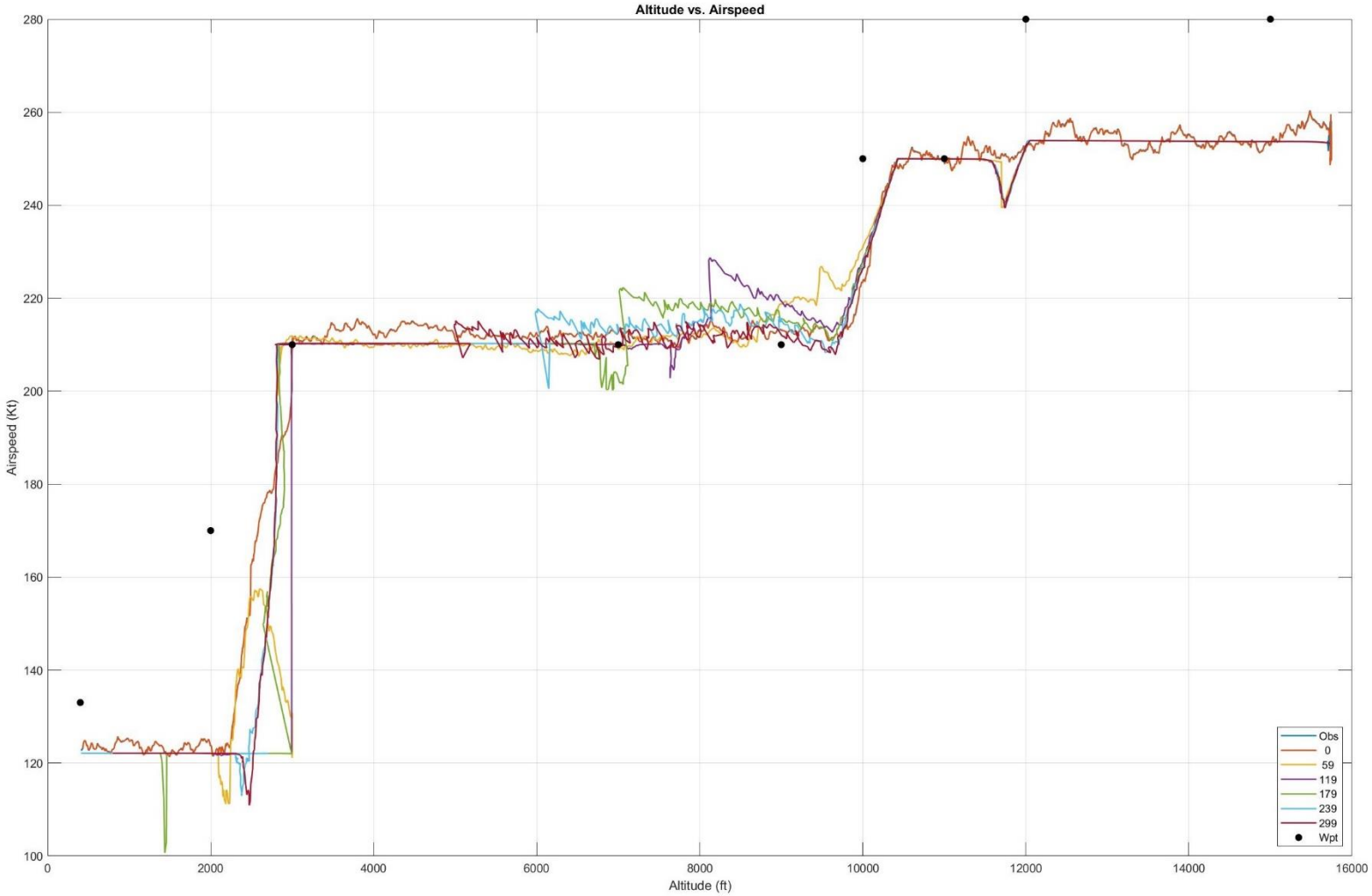

Figure E. 41: Test Flight 91: Observed and Predicted Altitude vs. Airspeed

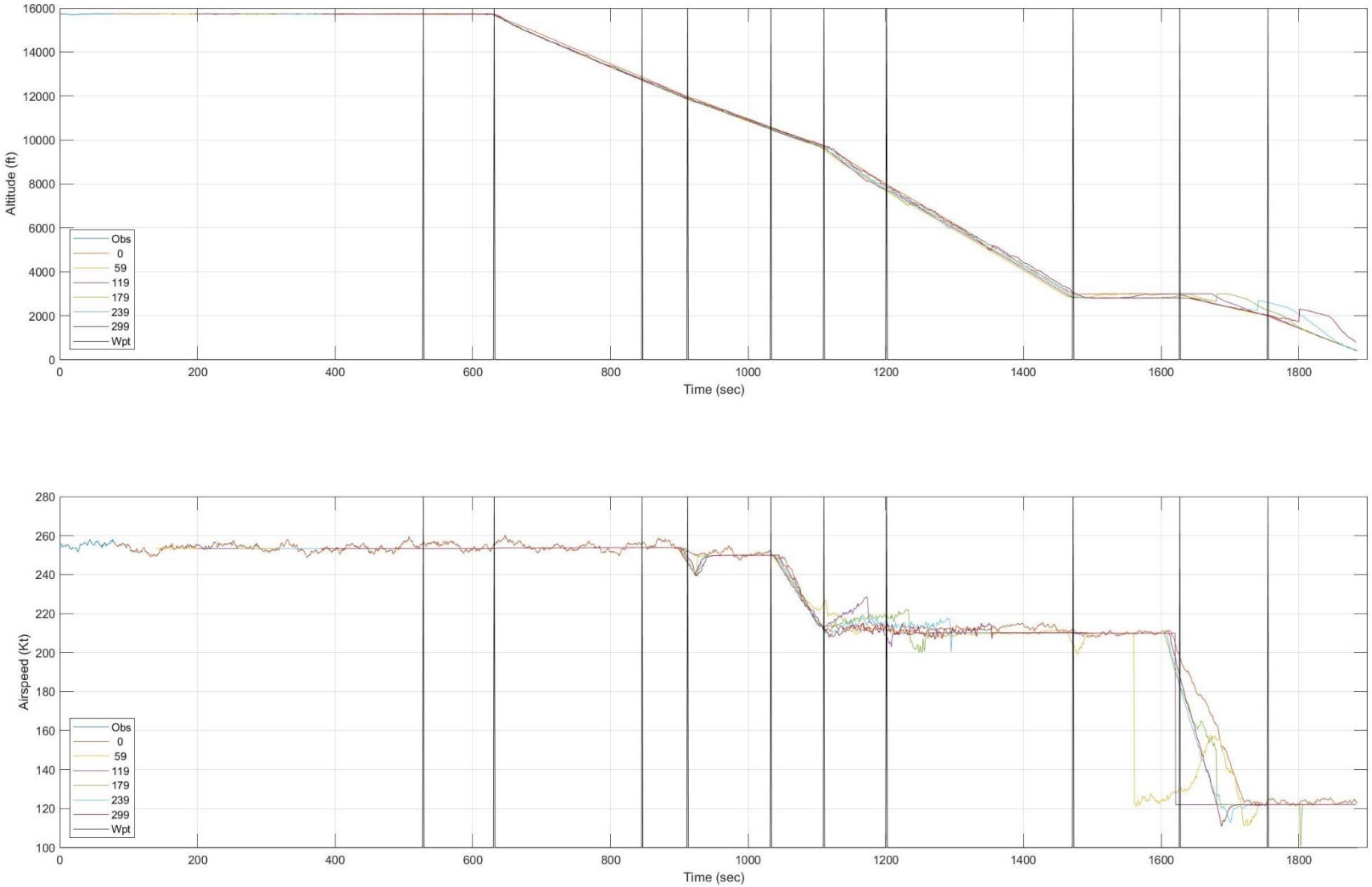

Figure E. 42: Test Flight 91: Observed and Predicted Altitude and Airspeed as a Function of Time t

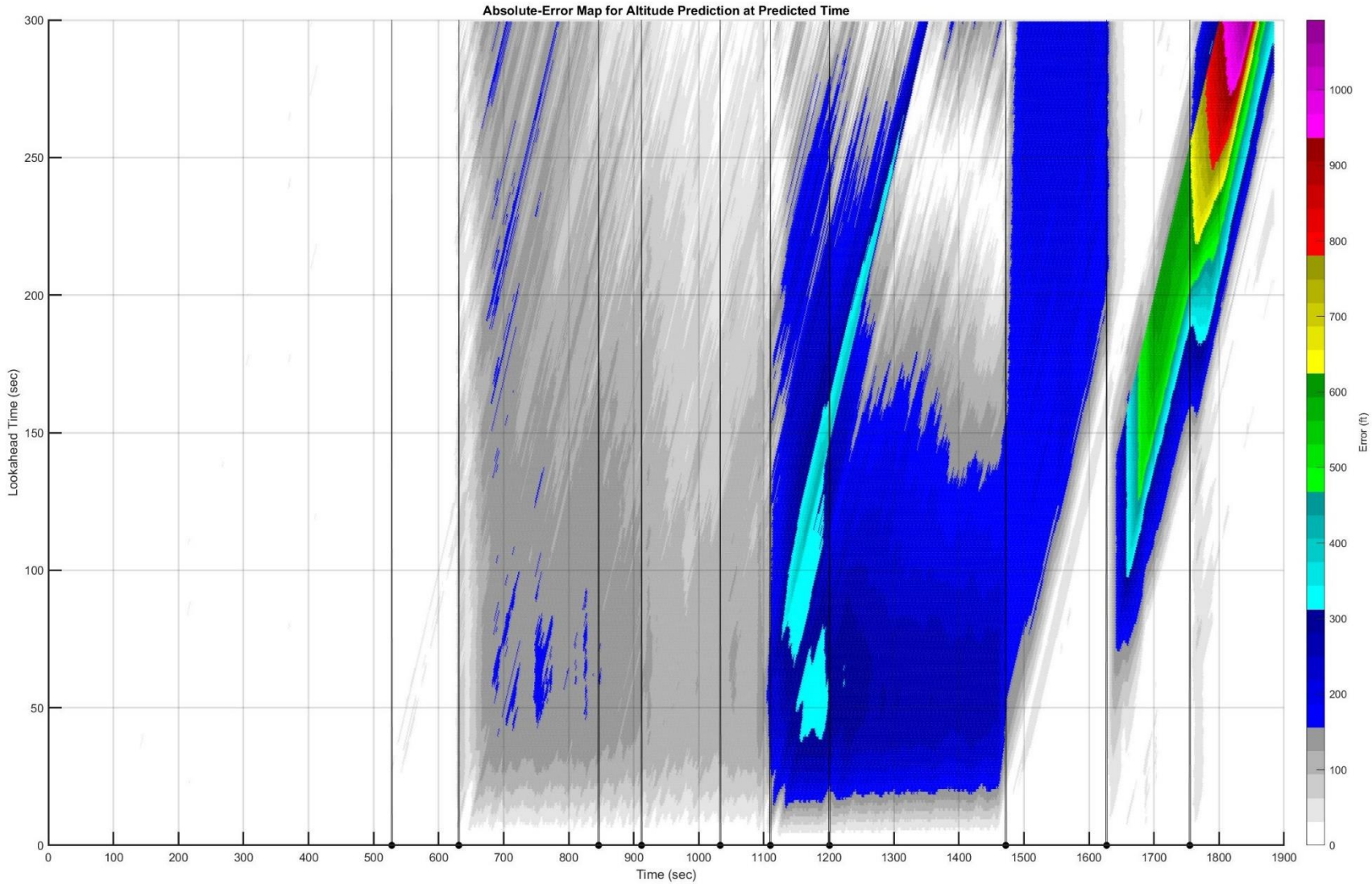

Figure E. 43: Test Flight 91: Heatmap of Absolute Error for Altitude Prediction as a Function of Predicted Time $t + \tau$

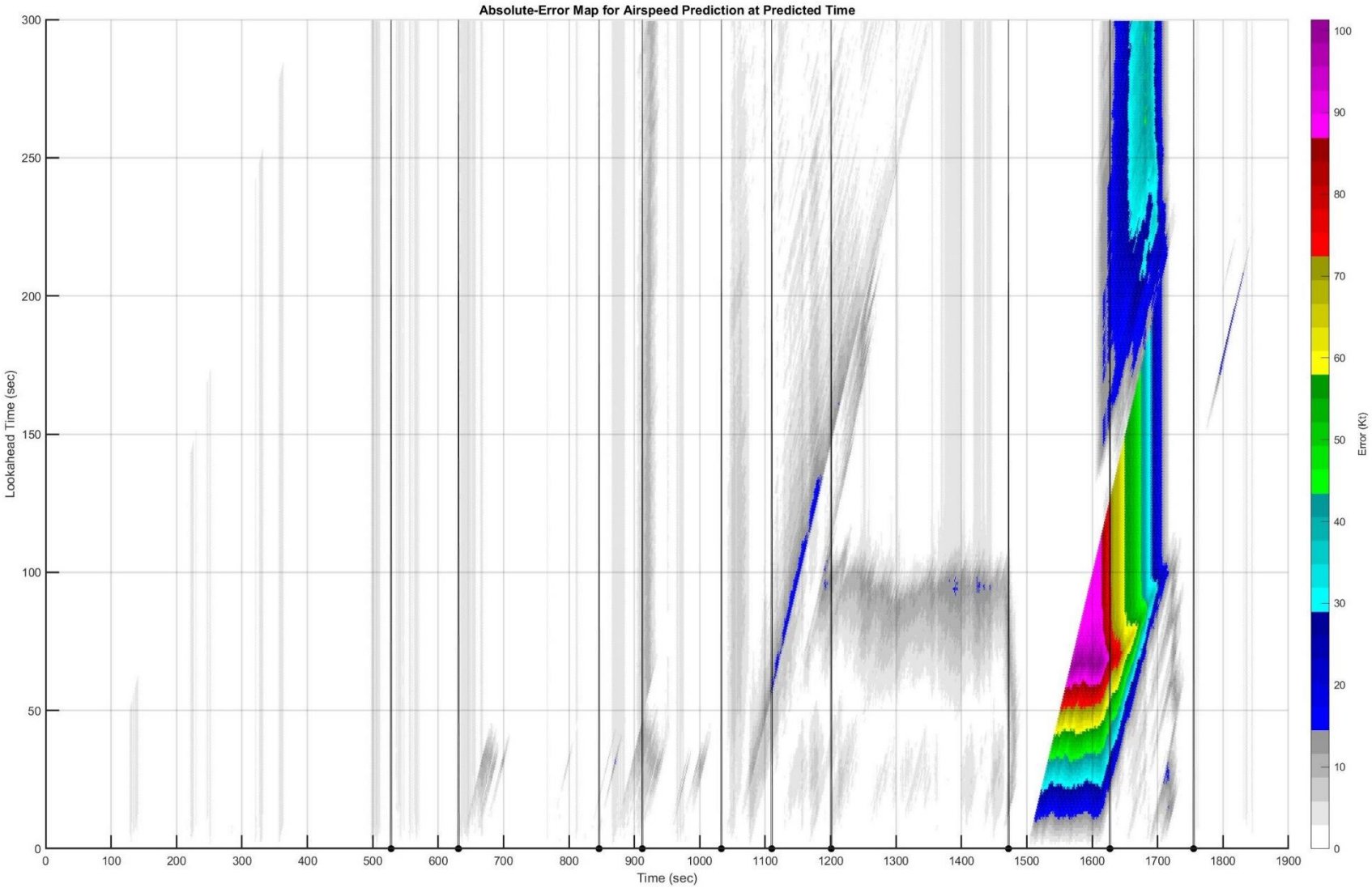

Figure E. 44: Test Flight 91: Heatmap of Absolute Error for Airspeed Prediction as a Function of Predicted Time $t + \tau$

E.12: Test Flight 95

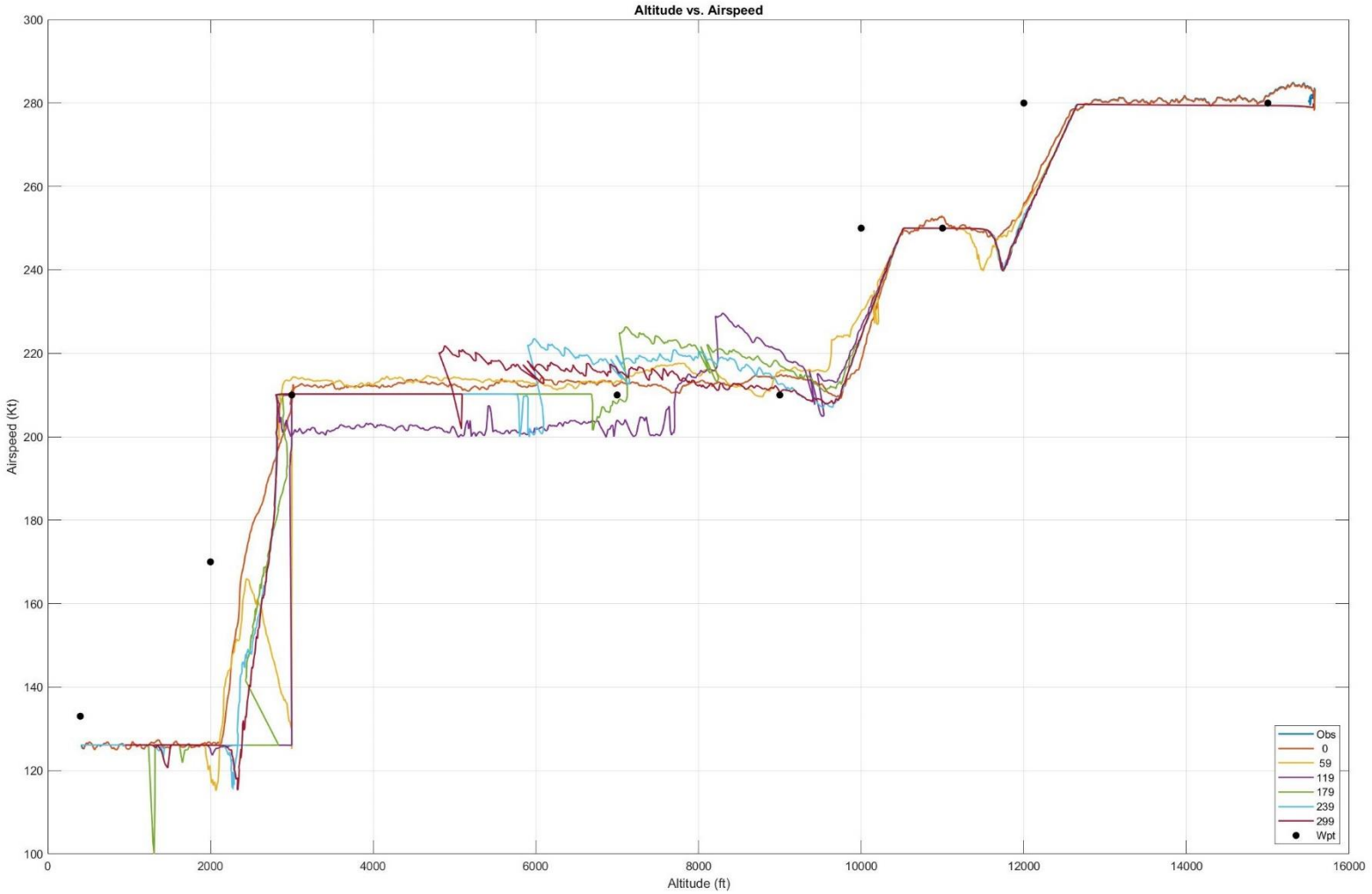

Figure E. 45: Test Flight 95: Observed and Predicted Altitude vs. Airspeed

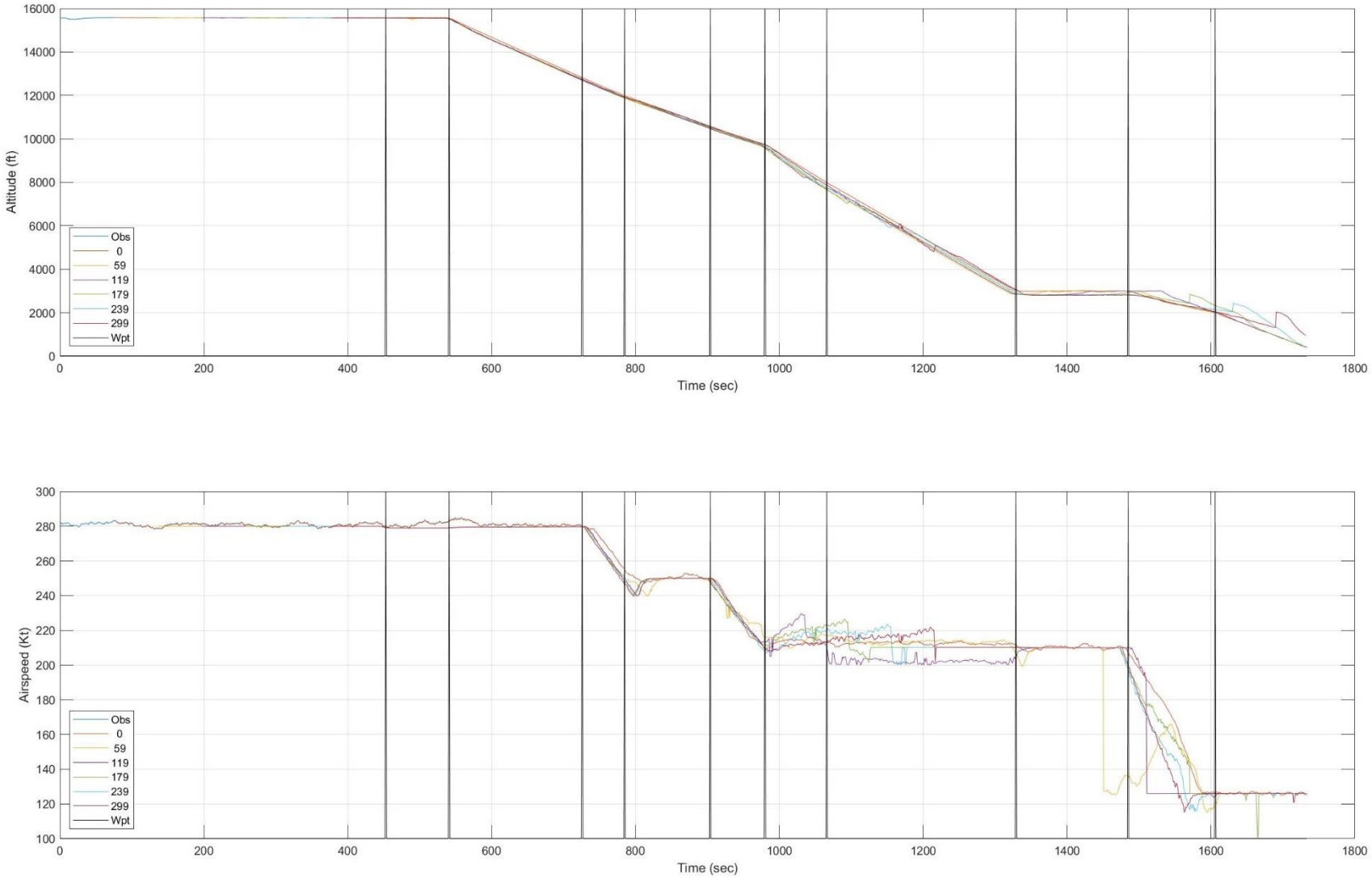

Figure E. 46: Test Flight 95: Observed and Predicted Altitude and Airspeed as a Function of Time t

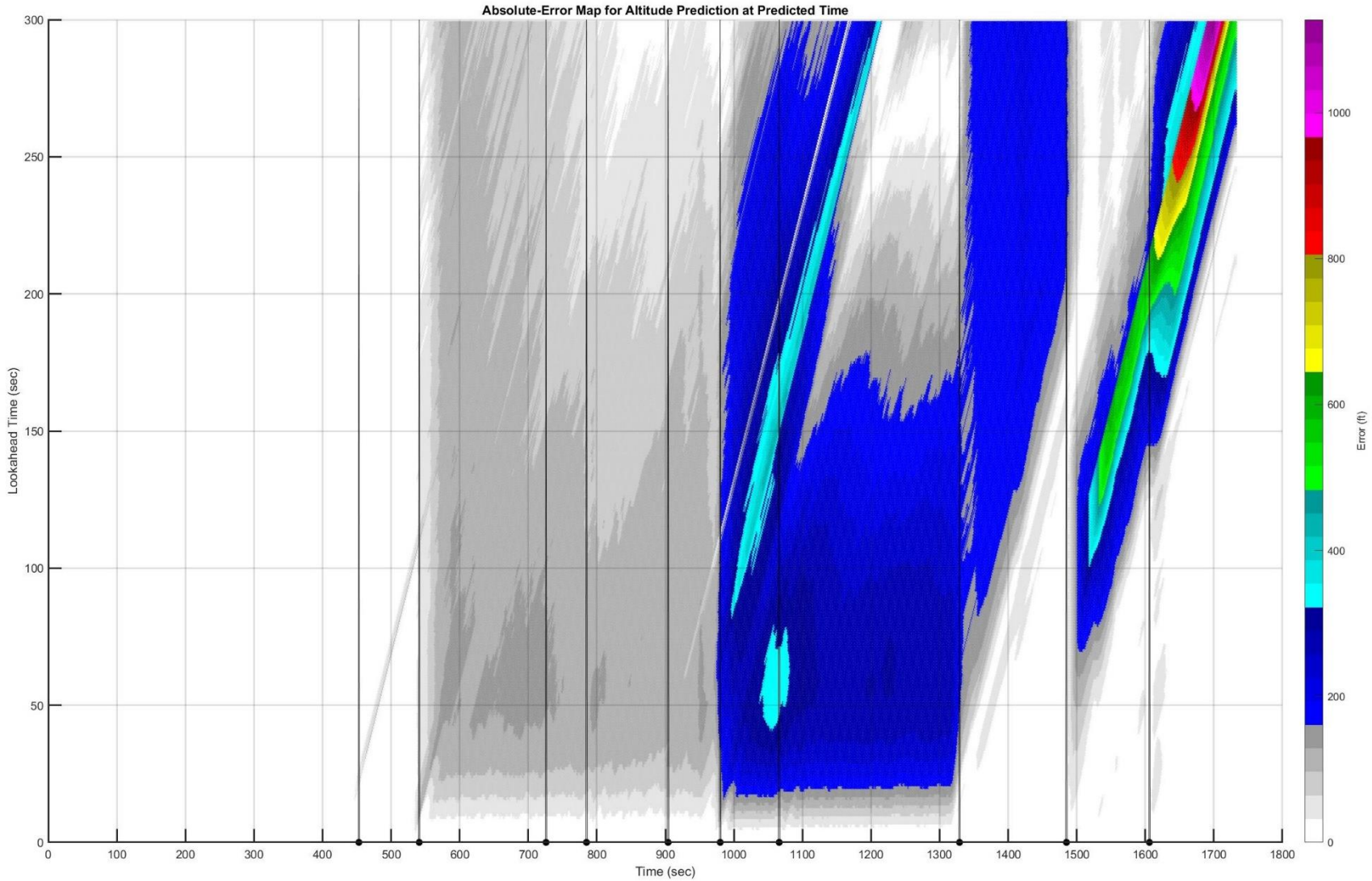

Figure E. 47: Test Flight 95: Heatmap of Absolute Error for Altitude Prediction as a Function of Predicted Time $t + \tau$

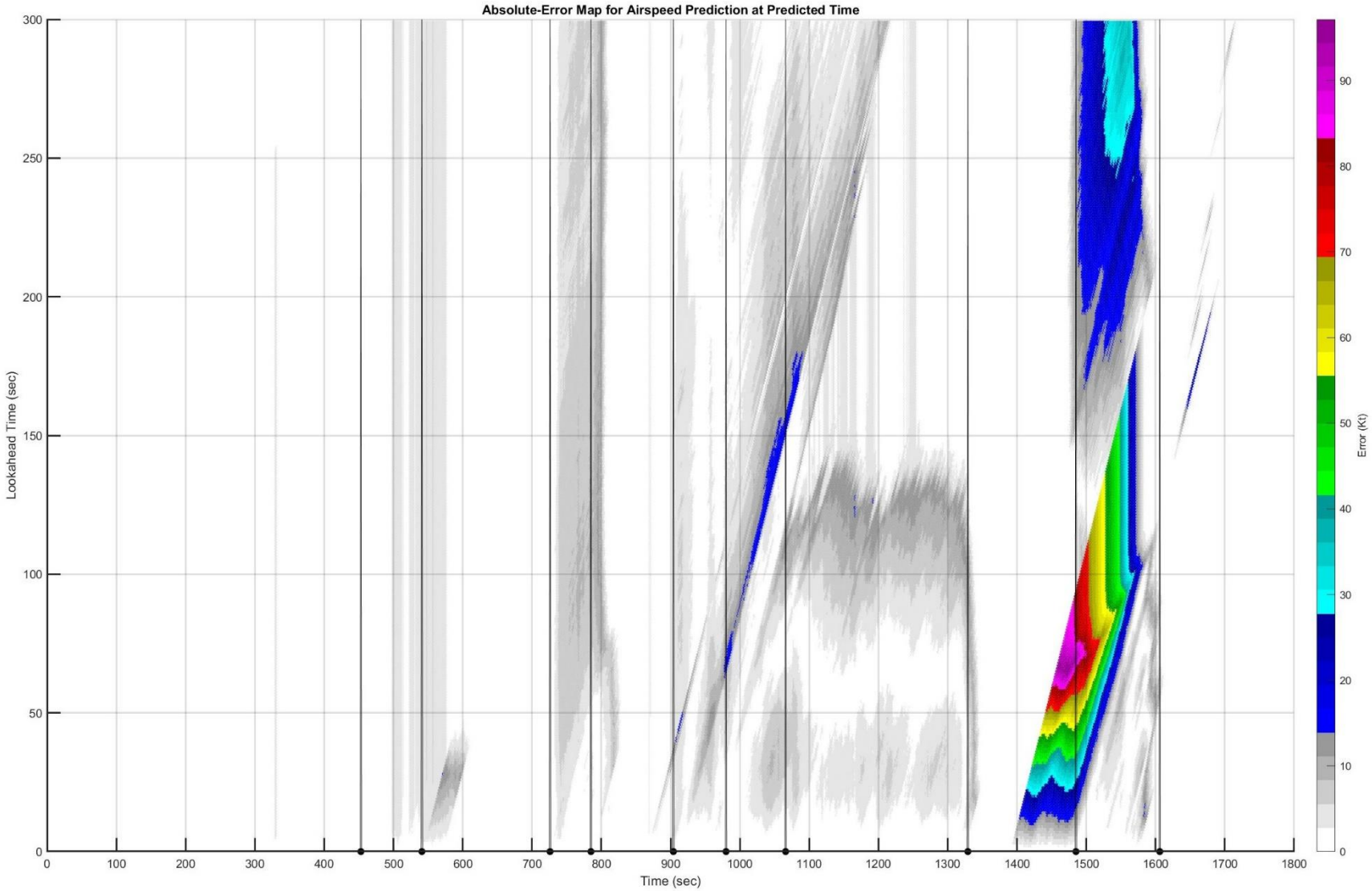

Figure E. 48: Test Flight 95: Heatmap of Absolute Error for Airspeed Prediction as a Function of Predicted Time $t + \tau$

REPORT DOCUMENTATION PAGE

Form Approved
OMB No. 0704-0188

1. REPORT DATE *(DD-MM-YYYY)*
1-07-2019

2. REPORT TYPE
Technical Memorandum

3. DATES COVERED *(From - To)*

4. TITLE AND SUBTITLE

CASPEr-1, Part 6: Uncertainty Quantification, Factor Effects, and Outlier Analysis for an On-board Airplane Trajectory Prediction Function

5a. CONTRACT NUMBER

5b. GRANT NUMBER

5c. PROGRAM ELEMENT NUMBER

6. AUTHOR(S)

Torres-Pomales, Wilfredo

5d. PROJECT NUMBER

5e. TASK NUMBER

5f. WORK UNIT NUMBER
340428.04.90.07.07

7. PERFORMING ORGANIZATION NAME(S) AND ADDRESS(ES)

NASA Langley Research Center
Hampton, VA 23681-2199

8. PERFORMING ORGANIZATION REPORT NUMBER
L-21037

9. SPONSORING/MONITORING AGENCY NAME(S) AND ADDRESS(ES)

National Aeronautics and Space Administration
Washington, DC 20546-0001

10. SPONSOR/MONITOR'S ACRONYM(S)
NASA

11. SPONSOR/MONITOR'S REPORT NUMBER(S)
NASA-TM-2019-220291

12. DISTRIBUTION/AVAILABILITY STATEMENT

Unclassified-
Subject Category 03
Availability: NASA STI Program (757) 864-9658

13. SUPPLEMENTARY NOTES

14. ABSTRACT

This report presents data analysis results for a simulation-based approach named CASPEr (Characterization of Airplane State Prediction Error) to characterize the performance of onboard energy state and automation mode prediction functions for terminal area arrival and approach phases of flight over a wide range of conditions. In particular, the results include quantification of energy state (i.e., altitude and airspeed) prediction performance, models for prediction performance as a function of initial energy state (i.e., initial altitude, airspeed, and weight) and weather factors, and analysis of outlier prediction performance. Wind speed, wind direction, and wind gradient were found to be major factors in energy state prediction performance. Initial energy and gust intensity were also significant factors in airspeed prediction performance. Furthermore, the results suggest that errors in automation mode prediction may be a major contributor to outlier prediction performance.

15. SUBJECT TERMS

Airplane Trajectory; Prediction Performance; Simulation; Situational Awareness; State Prediction

16. SECURITY CLASSIFICATION OF:			17. LIMITATION OF ABSTRACT	18. NUMBER OF PAGES	19a. NAME OF RESPONSIBLE PERSON
a. REPORT	b. ABSTRACT	c. THIS PAGE			STI Help Desk (email: help@sti.nasa.gov)
U	U	U	UU	163	19b. TELEPHONE NUMBER *(Include area code)* (757) 864-9658